JUSTUS-LIEBIG-
UNIVERSITÄT
GIESSEN

Dynamic critical behavior of hot and dense QCD matter from the real-time functional renormalization group

Dissertation
submitted to Fachbereich 07
- Mathematik und Informatik, Physik, Geographie -
of the Justus-Liebig-Universität in Gießen, Germany

for the degree of
Doctor of Natural Sciences

put forward by
M.Sc. Johannes Roth

08.07.2025

Referees: Prof. Dr. Lorenz von Smekal
Prof. Dr. Christian Fischer

Abstract

In this work, we study dynamic critical behavior of hot and dense QCD matter near second-order phase transitions. We consider the chiral phase transition for two flavors of massless quarks, as well as the conjectured critical point at physical quark masses and finite baryon chemical potential. These are plausibly in the same dynamic universality classes as a four-component Heisenberg antiferromagnet and the liquid-gas critical point of a pure fluid, respectively, whose critical dynamics are described by Models G and H in the Halperin-Hohenberg classification.

Our central tool in this work is a real-time generalization of the functional renormalization group (FRG) based on the Schwinger-Keldysh contour. Starting with Model G, we develop a novel formulation of the real-time FRG which preserves all relevant symmetries of dynamical systems with reversible mode couplings. We show that associated Ward identities imply exact statements about the FRG flow, including the non-renormalization of the mode-coupling constant, and the independence of the static free energy on the dynamics. We show that the formalism reproduces the non-trivial value $z = d/2$ for the dynamic critical exponent in d spatial dimensions, and we compute a novel scaling function which describes the universal temperature and momentum dependence of the iso-vector and iso-axial-vector charge diffusion coefficient in the chiral limit.

As a next step, we adapt this novel FRG technique to Model H. We derive analytical expressions for dynamic critical exponents that describe the universal power-law divergence of the heat conductivity and the shear viscosity near the QCD critical point. As a central result, we find that the critical exponent of the shear viscosity as a function of d exhibits a maximum in the range $2 < d < 4$ and approaches zero for $d = 2$ spatial dimensions. We verify the robustness of this result by considering improved truncations of the static free energy. In parallel, we emphasize the structural similarities and differences with Model G by comparing the fixed-point structures of both models and discuss the presence/absence of weak and strong dynamic scaling relations.

While the leading universal scaling behavior can be described by Models G and H, non-universal corrections require a real-time description of the microscopic dynamics. In this regard, we consider a real-time formulation of the quark-meson model as a particular low-energy effective theory for QCD. As a first application, we study the influence of bosonic dissipation on the phase diagram and the excitation spectrum. We find that dissipation has a non-vanishing but quantitatively small effect on equilibrium observables. The influence on the excitation spectrum, on the other hand, can be drastic, as (over-)damping potentially turns weakly-damped quasiparticles into purely relaxational excitations.

Zusammenfassung

In dieser Arbeit wird das dynamische kritische Verhalten von heißer und dichter QCD-Materie in der Nähe von Phasenübergängen zweiter Ordnung untersucht. Betrachtet werden der chirale Phasenübergang für zwei masselose Quark-Flavors sowie der vermutete kritische Punkt bei physikalischen Quarkmassen und endlichem baryonischem chemischen Potential. Es wird vermutet, dass diese denselben dynamischen Universalitätsklassen zuzuordnen sind wie ein vierkomponentiger Heisenberg-Antiferromagnet bzw. der kritische Punkt eines fluiden Reinstoffs. Deren jeweilige kritische Dynamik wird in der Klassifikation von Halperin und Hohenberg durch die Modelle G und H beschrieben.

Unser zentrales Werkzeug in dieser Arbeit ist eine Realzeit-Verallgemeinerung der funktionalen Renormierungsgruppe (FRG), basierend auf der Schwinger-Keldysh-Kontur. Zunächst entwicklen wir anhand von Modell G eine neuartige Formulierung der Realzeit-FRG welche alle relevanten Symmetrien von dynamischen Systemen mit reversiblen Modenkopplungen erhält. Wir zeigen, dass zugehörige Ward-Identitäten exakte Aussagen über den FRG-Fluss erlauben, einschließlich der Nicht-Renormierung der Modenkopplungskonstante und der Unabhängigkeit der statischen freien Energie von der Dynamik. Wir zeigen, dass der Formalismus den nichttrivialen Wert von $z = d/2$ für den dynamischen kritischen Exponenten in d räumlichen Dimensionen reproduziert, und berechnen eine neuartige Skalierungsfunktion, die die universelle Temperatur- und Impulsabhängigkeit des Diffusionskoeffizienten der Isovektor- und Isoaxialvektorladungen im chiralen Limes beschreibt.

Im nächsten Schritt wenden wir diese neuartige Realzeit-Formulierung der FRG auf Modell H an. Wir leiten analytische Ausdrücke für dynamische kritische Exponenten, welche das universelle Potenzgesetzverhalten der Wärmeleitfähigkeit und der Scherviskosität in der Nähe des kritischen Punkts der QCD beschreiben, her. Ein zentrales Resultat des FRG-Flusses ist, dass der kritische Exponent der Scherviskosität als Funktion von d ein Maximum im Bereich $2 < d < 4$ aufweist und für $d = 2$ räumliche Dimensionen gegen Null geht. Weiterhin betonen wir strukturelle Ähnlichkeiten und Unterschiede zu Modell G, indem wir die resultierenden Fixpunkte beider Modelle vergleichen und diskutieren, inwieweit schwache und starke dynamische Skalengesetze gelten.

Während das führende Skalenverhalten durch die Modelle G und H beschrieben wird, erfordern nicht-universelle Korrekturen hingegen eine Realzeit-Beschreibung der mikroskopischen Dynamik. In dieser Hinsicht betrachten wir eine Realzeit-Formulierung des Quark-Meson-Modells als effektive Theorie der QCD bei niedrigen Energien. Als erste Anwendung untersuchen wir den Einfluss bosonischer Dissipation auf das Phasendiagramm und das Anregungsspektrum. Wir finden, dass Dissipation einen nicht-verschwindenden aber quantitativ kleinen Einfluss auf Gleichgewichtsgrößen hat, jedoch das Anregungsspektrum insofern drastisch beeinflussen kann, dass eine hinreichend große Dämpfung schwach gedämpfte Quasiteilchen in rein relaxierende Anregungen überführen kann.

Contents

1 Introduction **1**

1.1 Motivation . . . 1

1.2 Outline of this work . . . 5

2 Theoretical foundation **9**

2.1 Non-equilibrium quantum field theory . . . 9

2.2 Dynamic universality classes . . . 22

2.3 Functional renormalization group . . . 46

3 Critical dynamics near the chiral phase transition **59**

3.1 Martin-Siggia-Rose path-integral formulation . . . 60

3.2 FRG for dynamical systems with reversible mode couplings . . . 73

3.3 Truncation and flow equations . . . 79

3.4 Results for dynamic critical behavior of $O(4)$ Model G . . . 88

3.5 Discussion . . . 98

4 Critical dynamics near the QCD critical point **101**

4.1 MSR path-integral formulation of Model H . . . 102

4.2 Truncation and flow equations . . . 104

4.3 Dynamic critical behavior of Model H and G . . . 111

4.4 Discussion . . . 114

5 Real-time dynamics of the quark-meson model **117**

5.1 The quark-meson model on the closed-time path . . . 119

5.2 Real-time FRG with fermions . . . 126

5.3 Results for phase diagram with dissipation . . . 135

5.4 Discussion . . . 141

6 Conclusion & Outlook **145**

A Causality and Kramers-Kronig relations **151**

B Details on the MSR path-integral formulation of Model G **153**
B.1 Continuum formulation of the Ito discretization 153
B.2 Jacobians and ghosts 154
B.3 Traditional approach of constructing generating functionals 158

C Thermal-equilibrium symmetry in systems with reversible mode couplings **159**

D Details on the FRG for systems with reversible mode couplings **163**
D.1 Derivation of the flow equation 163
D.2 Convergence towards the bare action in the UV limit $k \to \Lambda$ 165
D.3 Regulators for ghosts 166

E 1PI vertex functions of Model G **167**

F Extraction of the dynamic critical exponent in Model G **169**

G Details on the real-time FRG for the quark-meson model **173**
G.1 Effective Keldysh action 173
G.2 Infinite damping calculation 174

H Temperature dependence of the pion damping **175**

Bibliography **177**

Chapter 1

Introduction

1.1 Motivation

The Standard Model of particle physics is currently the best description of the microscopic structure of the world, classifying all known elementary particles and describing the electromagnetic, weak, and strong interaction between them. In particular, the strong interaction as described by the theory of quantum chromodynamics (QCD) is responsible for the binding of quarks and gluons into hadrons such as protons and neutrons and, in a second step, for the binding of protons and neutrons into atomic nuclei via the residual strong force.

One of the most characteristic properties of QCD is asymptotic freedom [5,6], which implies that at higher energies the interaction between quarks and gluons gets weaker. As a consequence, at a temperature around 155 MeV [7] (corresponding to $\sim 1.8\times10^{12}$ K) ordinary hadronic matter undergoes a transition to the quark-gluon plasma (QGP), where the quarks and gluons are no longer confined into colorless hadrons but remain strongly interacting. It is believed that the QGP filled the early universe a few microseconds after the Big Bang. Another example of a form of matter which is dominated by the strong interaction is the highly compressed baryonic matter found in neutron stars, where the central densities reach several times the nuclear saturation density of $\sim 2.8 \times 10^{14}$ g/cm^3 [8]. Understanding corresponding phases of QCD and the nature of the transitions between them under these extreme conditions is an active area of current research. For instance, one popular conjecture for the QCD phase diagram as a function of temperature T and baryon chemical potential μ_B is visualized on the left-hand side of Fig. 1.1.

One central difficulty in computing the phase structure of QCD at larger baryon chemical potential is that one of the first-principle tools, lattice QCD, is practically restricted to small baryon chemical potential due to the notorious sign problem. Hence, at present, larger baryon chemical potential requires different methods, including calculations within effective models and functional approaches to QCD. In particular, many low-energy effective theories for QCD predict a first-order phase transition at higher baryon chemical potential [12–15]. Assuming that such a first-order phase transition indeed exists in QCD, and given the known crossover at zero baryon chemical potential [7, 16], thermodynamic arguments suggest (if not require) the existence of a critical point in which the first-order transition line ends [9, 10]. Functional approaches to QCD such as the functional renormalization group or Dyson-Schwinger equations can estimate the location of the critical point [17–20] without any additional parameters other than the ones already appearing in the microscopic QCD Lagrangian. However, they require

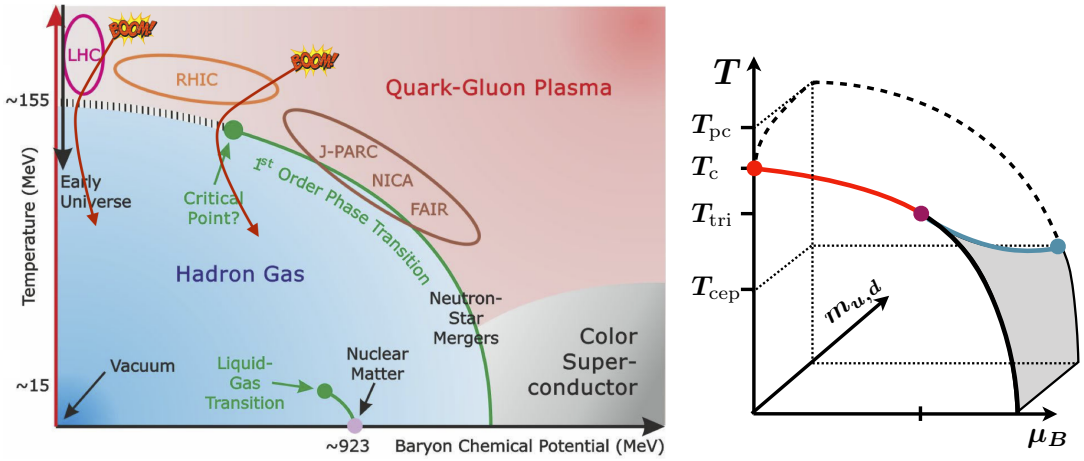

Figure 1.1: (Left) Schematic illustration of the conjectured QCD phase diagram as a function of baryon chemical potential μ_B and temperature T for physical values of up and down quark masses. In addition, we have sketched typical (approximately isentropic) trajectories realized during the hydrodynamic evolution of a heavy-ion collision after the fireball has thermalized at some initial values of μ_B and T. Figure adapted from the CRC-TR 211. (Right) Illustration of the conjectured dependence of the phase boundaries on the (degenerate) up and down quark masses $m_{u,d}$. The second-order line of Z_2 critical points (blue) is connected via a tricritical point (purple) to a second-order chiral phase transition line (red) in the chiral limit $m_{u,d} \to 0$ [9, 10]. Figure taken from Ref. [11].

truncations of the infinite tower of equations, which makes a reliable error estimate rather difficult. Other approaches for locating the critical point include the determination of Yang-Lee edge singularities in the complex baryon chemical potential plane from lattice-QCD data [21, 22] and the gauge/gravity duality [23, 24].

Experimentally, the phase structure of QCD can be probed in relativistic heavy-ion collisions, which are performed at particle accelerators such as the Relativistic Heavy Ion Collider (RHIC) at Brookhaven National Laboratory, the Large Hadron Collider at CERN, and at the heavy-ion synchrotron SIS 18 (and in the future also SIS 100) at the Facility for Antiproton and Ion Research (FAIR). The standard picture of a relativistic heavy-ion collision is as follows: After the initial collision and the fast subsequent thermalization, the locally-equilibrated fireball expands and cools down until it reaches a temperature of about 155 MeV where it passes the crossover transition and hadronizes again. Then, after kinetic freezeout, the hadrons stream freely to the detectors. Remarkably, a modelling of the fireball in terms of relativistic viscous hydrodynamics with an equation of state from lattice QCD yields a tremendously successful description of the experimental data [25]. In particular, a fit of the transport coefficients to experimental observables yields a shear viscosity to entropy density ratio η/s in a range which is remarkably close to the conjectured lower bound of $\eta/s = 1/4\pi$ [26], making the QGP the 'most perfect liquid' on earth [27–30]. The success of the hydrodynamic description also means that the fireball created in a relativistic heavy-ion collision is in a state close to local thermal equilibrium, which allows one to use the terms 'temperature' and 'baryon chemical potential' in the first place. As such, the hydrodynamic evolution in the intermediate stage of a relativistic heavy-ion collision can be imagined as an (approximately isentropic) trajectory through the QCD phase diagram, as sketched on the left-hand side of Fig. 1.1.

Lowering the beam energy in a heavy-ion collision introduces a non-zero net baryon number into the QGP. This shifts the trajectories shown on the left-hand side of Fig. 1.1 to higher baryon chemical potentials, bringing the fireball closer to the conjectured critical point. To identify a critical point in the experimental observables, one would search for characteristic signatures that reflect the associated thermodynamic singularity. Universality and the scaling hypothesis at the critical point entail that the non-analytic (critical) part of the equation of state is fully determined by a universal scaling function from the Z_2 universality class [31]. Here, the power of universality is that a universal scaling function may be computed using a simpler model from the same universality class (by performing, e.g., Monte-Carlo simulations of the $3d$ Ising model [32]) and then mapped back to QCD [33, 34], whereas lattice-QCD simulations in this region of the phase diagram are prohibited due to the sign problem. For example, Z_2 universality implies that higher-order cumulants of the critical mode diverge more strongly with the correlation length [35], and are thus conjectured to be a sensitive probe of criticality. In particular, one common observable is the kurtosis, which, by Z_2 universality, is expected to switch sign as the critical point is passed [36]. As a proxy for net-baryon number [37], cumulants of net-proton number have been measured as a function of beam energy $\sqrt{s}$ at the Beam Energy Scan program at RHIC, and although there are tantalizing hints for non-monotonous behavior of the quartic cumulant [38–40], the results do not allow for strong conclusions about the (non-)existence of a critical point yet. Reaching even lower beam energies and thus even larger baryon chemical potentials with sufficiently high interaction rate is one of the motivations for the future Compressed Baryonic Matter experiment at FAIR [41].

Close to a potential critical point one encounters problems with the standard hydrodynamic description. Due to the general phenomenon of critical slowing down near a critical point, the critical modes are guaranteed to fall out of local thermal equilibrium [42]. Hence, strong conclusions about the (non-)existence of a critical point from possible imprints of critical fluctuations in experimental observables require proper understanding of non-equilibrium effects [43–45]. Luckily, just as the singular behavior of thermodynamic quantities near a critical point is determined by the corresponding static universality class, the *dynamics* of critical fluctuations is determined by the *dynamic* universality class. Historically, the notion of dynamic universality classes arose in condensed-matter physics and the corresponding classification scheme into Models A–J goes back to the seminal work of Halperin and Hohenberg from the 1970s [46]. The main idea which motivates large parts of this thesis is that one may be able to understand the dynamics of critical fluctuations in hot and dense QCD matter by studying a simpler system from the same dynamic universality class, which is conjectured to be the one of Model H from the Halperin-Hohenberg classification [47]. In particular, the singular behavior of transport coefficients near the critical point, including the heat conductivity and the shear viscosity, would then be described by critical exponents and scaling functions of Model H. Moreover, a quantitative description of the critical dynamics in terms of Model H is also expected to extend to genuine non-equilibrium phase transitions. For instance, Kibble-Zurek scaling has been observed in numerical simulations of quenches through the critical point in Models A and B [48, 49], but corresponding non-equilibrium simulations have yet to be performed in Model H. For recent developments in simulating Model H and stochastic hydrodynamics, see, e.g., Refs. [50, 51] and Refs. [52–54], respectively.

A description of the dynamics of QCD matter based on universality arguments might not be limited to the Z_2 critical point. One can imagine adding another axis corresponding to the (degenerate) up and down quark masses $m_q \equiv m_{u,d}$ to the phase diagram, which is shown on

the right-hand side of Fig. 1.1. Upon reducing the quark masses m_q, it is known from lattice-QCD simulations [55, 56] and functional approaches [57, 58] that the chiral crossover transition sharpens, and is generally believed to turn into a second-order phase transition in the $O(4)$ universality class[1] in the chiral limit $m_q \to 0$ [59]. This is because QCD is then invariant under independent $SU(2)$ rotations of left and right-handed quarks, giving rise to the $SU(2)_L \times SU(2)_R$ chiral symmetry, which is locally same as the rotation group $O(4)$.

Since the physical up and down quark masses $m_u \approx 2$ MeV and $m_d \approx 5$ MeV [60] are much smaller than typical QCD scales, it is not unreasonable to expect that the fireball produced in a heavy-ion collision could be affected by dynamical effects associated with the chiral phase transition when passing the chiral crossover region [61]. An argument by Rajagopal and Wilczek [62] suggests that the relevant dynamic universality class is the one of Model G, i.e., the one of a Heisenberg antiferromagnet [46], extended to an $O(4)$ order parameter. Corresponding dynamical effects are expected to primarily affect pions, since they are the pseudo-Goldstone bosons of the chiral transition. In fact, it was suggested that an observed excess of low-p_T pions [63,64] could be attributed to dynamical effects of a second-order chiral phase transition [61, 65–69], since the latter are usually not taken into account by current hydrodynamic simulations. However, despite the apparent smallness of the quark masses, the rather large physical pion mass of $m_\pi \approx 138$ MeV in vacuum limits the correlation length at the pseudo-critical temperature in the pion channel to $m_\pi^{-1} \approx 1.4$ fm [62]. Correspondingly, it is a topic of ongoing research to determine the size of the true scaling region around the chiral phase transition and whether (or not) it includes the physical point, see, e.g., Refs. [55,58,70,71]. Luckily, to observe scaling in the dynamics, it is not a priori necessary for the physical point to lie strictly within the potentially small static scaling region.

With these motivations in mind, one main objective of the present work is to describe the dynamic critical behavior of hot and dense QCD matter close to the chiral phase transition and the conjectured critical point, respectively, by studying the critical dynamics of Models G and H. In the relevant case of $d = 3$ spatial dimensions, non-perturbative field-theoretic methods are required due to the absence of a small expansion parameter. For static critical phenomena, the functional renormalization group (FRG) [72–74] is a well-approved non-perturbative framework for the quantitative description of universal quantities such as critical exponents and amplitude ratios [75–80]. For *dynamic* critical phenomena, on the other hand, this description must be generalized, since the models of the Halperin-Hohenberg classification are defined via Langevin equations of motion and thus describe genuine real-time dynamics. Corresponding real-time formulations of the FRG have been used in the past to study critical dynamics of the relaxational Models A, B & C, see, e.g., Refs. [1, 81–84]. In this work, we take the real-time FRG to the next level by incorporating the 'reversible mode couplings' needed for Models G and H. Other genuine real-time methods are provided by classical-statistical simulations [49, 85–90] and extensions including the leading quantum corrections in a Gaussian-state approximation [90–92]. Finally, the AdS/CFT correspondence can also be used to study critical dynamics near second-order phase transitions of $\mathcal{N} = 4$ Super-Yang-Mills at finite temperature and R-charge chemical potential via a dual gravitational description [93–97].

Even though Model G and H describe the universal dynamic properties of the chiral phase transition and the critical point, a complete description of the dynamics of hot and dense QCD matter requires non-universal corrections in addition to the leading scaling behavior. The power

[1] Assuming that the axial anomaly is sufficiently strong at the critical temperature.

of the real-time FRG is that it is not limited to classical-statistical systems, but can be straightforwardly extended to full quantum field theories using a description based on the Schwinger-Keldysh closed-time path (CTP) [98]. As a first step in this direction, we formulate a real-time FRG flow for the quark-meson model, the latter being a well approved low-energy effective theory for QCD [14, 99]. As a concrete application, we introduce dissipation to the dynamics by attaching an external heat bath to the mesons (which effectively turns the model into an open quantum system), and study the influence on the phase diagram and the bosonic excitation spectrum.

1.2 Outline of this work

In this work, we study dynamic critical behavior of hot and dense QCD matter near the chiral transition and the conjectured critical point by developing a novel formulation of the real-time FRG for dynamical systems with reversible mode couplings, as needed for Models G and H. Moreover, as a first step towards non-universal corrections to the leading universal scaling behavior, we study a real-time formulation of the quark-meson model with the FRG on the CTP.

In Chapter 2 we introduce some theoretical background as a basis for our developments in the subsequent chapters. In Sec. 2.1 we start by reviewing the Schwinger-Keldysh formalism of real-time quantum field theory, and discuss how the Martin-Siggia-Rose-Janssen-De Dominicis (MSRJD or often simply MSR) formalism [100–102] is recovered in the classical-statistical limit. In Sec. 2.2 we review the concept of dynamic critical phenomena [46, 103, 104], discuss the dynamic universality classes represented by Models A, B, C, G & H in the Halperin-Hohenberg classification, and put particular emphasis on their relation to QCD. In Sec. 2.3 we review the FRG [73, 74] and its real-time formulation [105, 106], with special emphasis on the issue of constructing suitable regulators that comply with the causality structure of the real-time framework.

In Chapter 3 we study universal aspects of critical dynamics near the chiral phase transition, as described by Model G [62]. In Sec. 3.1 we set up an MSR path-integral formulation for Model G and discuss the various symmetries of the associated MSR action, including the discrete symmetry of thermal equilibrium [107], and an extended temporal gauge symmetry [108, 109], which is characteristic for dynamical systems with reversible mode couplings as it reflects the underlying Poisson-bracket structure. In Sec. 3.2 we formulate an FRG flow that preserves these symmetries. Using the ansatz for the effective average action discussed in Sec. 3.3, we show in Sec. 3.4 that this novel approach reproduces the non-trivial value $z = d/2$ for the dynamic critical exponent, and we compute a scaling function which describes the universal temperature and momentum dependence of the iso-vector and iso-axial-vector charge diffusion coefficient in the chiral limit.

In Chapter 4 we study universal aspects of critical dynamics near the QCD critical point, as described by Model H in the Halperin-Hohenberg classification [47]. In Sec. 4.1 we adapt our novel FRG formalism developed in Chapter 3 to Model H, emphasizing structural similarities with Model G. In Sec. 4.2 we derive analytical expressions for the flow equations of the kinetic coefficients of Models H and G, employing a ϕ^4-truncation of the static free energy. Using these analytical expressions for the flow equations, we discuss in Sec. 4.3 similarities and differences in the resulting fixed-point structure and dynamic critical exponents between both models. This includes the weak-scaling relation which holds in either case versus the characteristic strong-

scaling relation of Model G which is absent in Model H [104]. We compute the dynamic critical exponents of both Model H and G as a function of the spatial dimension d in the range $2 < d < 4$, and compare our results to other perturbative and non-perturbative approaches to critical dynamics, including 1^{st}-order and 2^{nd}-order ϵ-expansion results for Model G [110] and Model H [111,112], respectively, as well as recent numerical simulations of Model H [50,51]. To assess the robustness of our FRG results for the dynamic critical exponents of Model H, we also consider an improved truncation of the static free energy within the extended local-potential approximation (LPA') based on two different expansion points in field space.

While Model G and H describe at least the leading universal scaling behavior exactly, at any finite 'distance' to a second-order phase transition it becomes important to quantify non-universal corrections, for which an underlying microscopic theory is needed. In this case quantum fluctuations become important, especially concerning fermions, since the latter carry a Matsubara mass πT and thus never appear in the classical limit. One of our results in Chapter 3 is that the FRG flow of the static free energy is independent of the equations of motion, at least in classical-statistical systems such as Models G and H. This raises the question to which extent similar statements hold in systems where quantum fluctuations are important.

Chapter 5 is concerned with a real-time formulation of the quark-meson model as a particular low-energy effective theory for QCD [14]. In Sec. 5.1 we review the CTP formalism for fermions and derive a Keldysh action for the quark-meson model. We generalize the symmetry of thermal equilibrium [107,113] to a Keldysh action which describes Dirac fermions. We then introduce dissipation in the spirit of the Caldeira-Leggett model by coupling the mesons to an ensemble of harmonic oscillators and integrating out the latter [114], which turns the model into an open quantum system. In particular, the dissipative interaction with the heat bath leads to a finite decay width for the mesons. Since in vacuum the sigma meson appears as a broad resonance [115], while the pions are effectively stable (at least on QCD timescales), we model the heat bath in a way which allows different decay widths for the sigma meson and the pions, while keeping the action chirally symmetric. In Sec. 5.2 we derive real-time FRG flow equations for fermions. We shall find that the dissipative dynamics indeed enters the FRG flow of the effective potential through the contribution of non-zero Matsubara modes, which is unlike classical-statistical systems. In Sec. 5.3 we study the quantitative effects of dissipation both on the phase diagram [99] and bosonic excitations by employing two phenomenological models for the pion damping, motivated by chiral perturbation theory at low temperature T [116], and by spectral-reconstruction results from lattice QCD at high T [117]. To estimate the largest possible effect on the phase diagram, we consider limits where the damping constants approach infinity.

In Chapter 6 we summarize the main results of this thesis and provide an outlook for possible future directions.

Parts of this thesis have already been published in:

[1] J. V. Roth and L. von Smekal, *Critical dynamics in a real-time formulation of the functional renormalization group*, JHEP **10**, 065 (2023), arXiv:2303.11817 [hep-ph]

[2] J. V. Roth, Y. Ye, S. Schlichting, and L. von Smekal, *Dynamic critical behavior of the chiral phase transition from the real-time functional renormalization group*, JHEP **01**, 118 (2025), arXiv:2403.04573 [hep-ph]

[3] J. V. Roth, Y. Ye, S. Schlichting, and L. von Smekal, *Universal critical dynamics near the chiral phase transition and the QCD critical point*, Phys. Rev. D **111**, L111901 (2025), arXiv:2409.14470 [hep-ph]

[4] J. V. Roth, Y. Ye, S. Schlichting, and L. von Smekal, *Effects of dissipation on phase diagram and bosonic excitations in the quark-meson model*, arXiv:2503.21746 [hep-ph] (submitted to Phys. Rev. D)

Figures and texts taken from these references are not explicitly marked again. Instead, this is indicated at the beginning of the respective sections.

Note on the author's contributions. In [1–4] the author of this thesis contributed central ideas, carried out major parts of the analytical calculations (in collaboration with Yunxin Ye in [2–4]), implemented the numerical methods (in collaboration with Yunxin Ye in [2]), and took the leading role in writing the manuscript.

Chapter 2

Theoretical foundation

In this chapter, we introduce a theoretical foundation for the subsequent developments in the following chapters. In Sec. 2.1 we start with the Schwinger-Keldysh approach to real-time quantum field theory (QFT). In particular, we discuss the dissipative Keldysh action which describes a system in contact with an external heat bath [114], the symmetry of thermal equilibrium [107], and that the MSR formalism is recovered in the limit $\hbar \to 0$. In Sec. 2.2 we review the concept of dynamic critical phenomena [103, 104], and discuss certain dynamic universality classes which are particularly relevant for QCD, as represented by Model A, B, C, H & G in the Halperin-Hohenberg classification [46]. In particular, we summarize some of our earlier real-time FRG results on the critical spectral functions of the Models A, B & C [1]. In Sec. 2.3 we introduce the FRG [73, 74] and its formulation on the CTP [105, 106]. As a peculiarity of the real-time framework, we discuss in detail which additional constraints regulators have to satisfy so as to preserve the causality structure of the Keldysh action.

2.1 Non-equilibrium quantum field theory

In this section we review the Schwinger-Keldysh approach to non-equilibrium QFT. For a more elaborate introduction see, e.g., Chapters 1–5 in the textbook by Kamenev [118].

2.1.1 Closed-time path

The partition function of a system in global thermal equilibrium at temperature $T \equiv 1/\beta$ can be expressed as a Euclidean path integral by re-interpreting the thermal density operator $e^{-\beta H}$ with Hamiltonian H as an evolution operator along a compact imaginary-time interval $[0, \beta]$.[1] This observation lays the foundation for the imaginary-time formalism [119], which allows one to apply the powerful toolbox of path integrals to finite-temperature systems. However, despite its merits, the imaginary-time formalism is, by construction, not applicable to systems which start in general non-equilibrium initial density operators, or, e.g., involve time-dependent external fields. On the contrary: in the imaginary-time formalism all changes are applied infinitely slowly (adiabatically), causing the system to remain in thermal equilibrium at all times. Hence,

[1] Throughout this work we employ natural units, $\hbar = c = k_B = 1$, unless explicitly stated otherwise.

studying time-dependent phenomena requires a generalized description.[2] This is the purpose of the CTP formalism [126–128].

We consider a general density operator $\hat{\rho}$, whose time evolution is described by the von Neumann equation

$$i\frac{d}{dt}\hat{\rho}(t) = [H(t), \hat{\rho}(t)] \tag{2.1}$$

where $H(t)$ is the (now possibly time-dependent) Hamiltonian of the quantum system. Eq. (2.1) can be formally solved with the aid of the time-evolution operator

$$U(t, t_0) = T \exp\left\{-i \int_{t_0}^{t} dt'\, H(t')\right\}, \tag{2.2}$$

where T here denotes the time-ordering operator. The time-evolution operator has the general properties

$$U^{-1}(t, t_0) = U^{\dagger}(t, t_0) = U(t_0, t)\,, \tag{2.3a}$$
$$U(t_0, t_0) = \mathbb{1}\,, \tag{2.3b}$$
$$U(t, t'') = U(t, t')U(t', t'')\,, \tag{2.3c}$$

and satisfies the time-evolution equation

$$i\frac{d}{dt}U(t, t_0) = H(t)U(t, t_0) \tag{2.4}$$

for fixed t_0, from which one can verify that the formal solution of the von Neumann equation (2.1) is given by

$$\hat{\rho}(t) = U(t, t_0)\hat{\rho}_0 U^{\dagger}(t, t_0) \tag{2.5}$$

where $\hat{\rho}_0 \equiv \hat{\rho}(t_0)$ denotes the density operator at time $t = t_0$. The expectation value of a Hermitian operator A at some time t is generally expressed as

$$\langle A(t)\rangle = \frac{\operatorname{tr}\hat{\rho}(t)A}{\operatorname{tr}\hat{\rho}(t)}\,. \tag{2.6}$$

Due to its cyclicity and with (2.5), the trace of $\hat{\rho}(t)$ is independent of time. Inserting (2.5) into (2.6) and using the relation $U(t_0, t) = U(t_0, +\infty)U(+\infty, t)$ which follows from the general property (2.3c), the expectation value (2.6) can be reformulated as

$$\langle A(t)\rangle = \frac{\operatorname{tr} U(t_0, +\infty)U(+\infty, t)AU(t, t_0)\hat{\rho}_0}{\operatorname{tr}\hat{\rho}_0}\,, \tag{2.7}$$

or equivalently

$$\langle A(t)\rangle = \frac{\operatorname{tr} U(t_0, t)AU(t, +\infty)U(+\infty, t_0)\hat{\rho}_0}{\operatorname{tr}\hat{\rho}_0}\,. \tag{2.8}$$

[2] In the special case of the time-dependent linear response of a system around thermal equilibrium, there is the possibility of analytic continuation from imaginary to real times. However, there one usually encounters the ill-posed numerical problem of analytic continuation from a finite set of noisy data points at the discrete Matsubara frequencies to continuous real frequencies (which is avoided in genuine real-time approaches). For various approaches in this direction, see e.g. Refs. [99, 120–125].

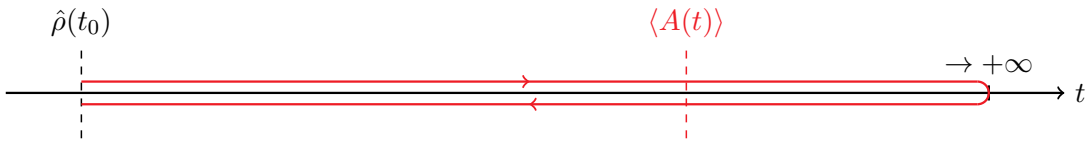

Figure 2.1: Closed-time path $\mathcal{C}$ running from the initial time $t = t_0$ to the far future $t \to +\infty$ and back, with an insertion of a Hermitian operator A at time t.

Eqs. (2.7) and (2.8) can be interpreted as evolving the system from its initial state $\hat{\rho}_0$ at $t = t_0$ first to $t = +\infty$ and back to $t = t_0$. The insertion of the operator A either on the forward branch as in (2.7), or on the backward branch as in (2.8), corresponds to measuring the observable. This resulting contour $\mathcal{C}$ in the complex-time plane shown in Fig. 2.1 is called 'closed-time path' or also 'Schwinger-Keldysh contour'. Historically, the corresponding formalism was foreshadowed by Schwinger [126] and then proposed by Keldysh [127], and, independently, by Kadanoff and Baym [128].

We can define a partition function for the non-equilibrium system as

$$Z \equiv \frac{\operatorname{tr} U_{\mathcal{C}} \hat{\rho}_0}{\operatorname{tr} \hat{\rho}_0} \tag{2.9}$$

with $U_{\mathcal{C}} = U(t_0, +\infty)U(+\infty, t_0)$. As usual, expectation values of observables A and unequal-time correlation functions can be obtained by introducing source terms to the CTP. In contrast to the thermodynamic partition function, here we have $Z = 1$ in the absence of such external sources, since the evolution along the backward branch exactly cancels the evolution along the forward branch. Indeed, even if a time-dependent source $J(t)$ for some Hermitian operator A is added to the Hamiltonian, $H \to H - J(t)A$, the resulting generating functional $Z[J] = 1$ is independent of J. We shall discuss in Sec. 3.1.2 that this is a consequence of a hidden Becchi-Rouet-Stora-Tyutin (BRST) symmetry, and that the partition function (2.9) actually computes the Witten index of a corresponding topological field theory.

Up to this point we have not specified any details about the system, other than time evolution being described by the von Neumann equation (2.1). For simplicity, we first consider a harmonic oscillator described by the 'free' Hamiltonian $H_0 = \omega_0 a^\dagger a$, with some 'bare' frequency ω_0, and with creation and annihilation operators $a^\dagger$ and a which are defined by their action on an energy eigenstate $|n\rangle$ of H_0,

$$a^\dagger |n\rangle = \sqrt{n+1}\, |n+1\rangle \quad \text{and} \quad a |n\rangle = \sqrt{n}\, |n-1\rangle \,. \tag{2.10}$$

Their commutator is given by $[a, a^\dagger] = 1$. Moreover, we define the occupation-number operator $N \equiv a^\dagger a$. In a second step, interactions V may be included in the form of sums over normally-ordered products of creation and annihilation operators, such that the full Hamiltonian H is given by $H = H_0 + V$.

The path-integral representation of the partition function (2.9) is most conveniently derived via a Suzuki-Trotter decomposition of the time-evolution operator $U_{\mathcal{C}}$ in the over-complete basis of coherent states. The latter are defined as (right) eigenstates of the annihilation operator a,

$$a |\alpha\rangle = \alpha |\alpha\rangle \,, \tag{2.11}$$

with the corresponding complex eigenvalue α. In contrast, the creation operator $a^\dagger$ only admits left eigenstates,

$$\langle\alpha| a^\dagger = \langle\alpha| \alpha^* \,. \tag{2.12}$$

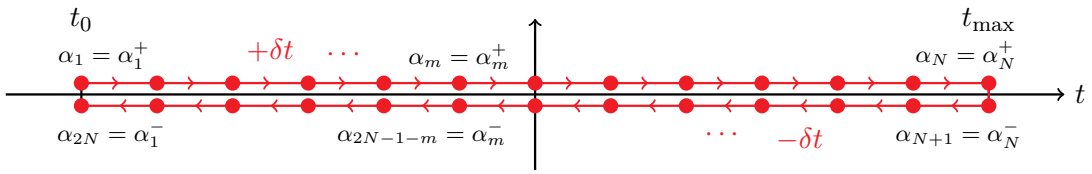

Figure 2.2: Closed-time path $\mathcal{C}$ running from the initial time t_0 to a sufficiently large but finite time $t_{\max}$ and back, discretized into $2N$ time slices which are each a time step $\delta t = (t_{\max} - t_0)/(N-1)$ apart.

To evaluate the path integral in these coherent states, we shall need two particular properties, namely the resolution of unity,

$$\mathbb{1} = \int d[\alpha^*, \alpha]\; e^{-|\alpha|^2}\; |\alpha\rangle\, \langle\alpha| \tag{2.13}$$

where the notation for the measure is defined as

$$d[\alpha^*, \alpha] \equiv \frac{d(\mathrm{Re}\,\alpha)\, d(\mathrm{Im}\,\alpha)}{\pi}\,,$$

and the trace of an operator A,

$$\mathrm{tr}\, A = \int d[\alpha^*, \alpha]\; e^{-|\alpha|^2} \langle\alpha|A|\alpha\rangle\,. \tag{2.14}$$

With (2.14), the trace in the partition function (2.9) can be expressed in coherent states according to

$$Z \equiv \frac{1}{\mathrm{tr}\,\hat{\rho}_0} \int d[\alpha^*, \alpha]\; e^{-|\alpha|^2}\; \langle\alpha|\, U_{\mathcal{C}}\, \hat{\rho}_0\, |\alpha\rangle \tag{2.15}$$

We assume that at the initial time t_0 the interactions in V are switched off, and the system is in a thermal equilibrium state (thus with respect to H_0),

$$\hat{\rho}_0 = e^{-\beta(H_0 - \mu N)} \tag{2.16}$$

with the inverse temperature $\beta \equiv 1/T$ and the chemical potential μ.[3] Using the geometrical series, the trace of the initial density operator (2.16) can be evaluated according to $\mathrm{tr}\,\hat{\rho}_0 = 1/(1 - e^{-\beta(\omega_0 - \mu)}) = 1/(1-\rho_0)$ with $\rho_0 = e^{-\beta(\omega_0 - \mu)}$.

To perform the Suzuki-Trotter decomposition of $U_{\mathcal{C}}$, we regularize the CTP to go from t_0 to some sufficiently large time $t_{\max}$ (with the limit $t_{\max} \to \infty$ taken at the end), and discretize the time variable to assume $2N$ discrete values in steps $\delta t = (t_{\max} - t_0)/(N-1)$. This is visualized in Fig. 2.2. Inserting the resolution of unity (2.13) at each time slice, the final result for the partition function is [118]

$$Z = \underbrace{\frac{1}{\mathrm{tr}\,\hat{\rho}_0} \int \left(\prod_{i=1}^{2N} d[\alpha_i^*, \alpha_i]\right) \exp\Big\{ - \sum_{i,j=1}^{2N} \alpha_i^* (iG_{0,ij}^{-1}) \alpha_j}_{\text{free theory in thermal equilibrium}} \underbrace{- i\delta t \sum_{j=1}^{N-1} V(\alpha_{j+1}^*, \alpha_j) + i\delta t \sum_{j=N+1}^{2N-1} V(\alpha_{j+1}^*, \alpha_j) \Big\}}_{\text{interactions}} \tag{2.17}$$

[3] The chemical potential μ is well-defined as long as the Hamiltonian H is such that $[N, H] = 0$.

where the $2N \times 2N$-matrix $iG^{-1}_{0,mn}$ represents the discretized (free) inverse propagator,

$$\left(iG^{-1}_{0,mn}\right) = \left(\begin{array}{ccccc|ccccc} 1 & & & & & & & & & -\rho_0 \\ -u^+ & 1 & & & & & & & & \\ & \ddots & \ddots & & & & & & & \\ & & & -u^+ & 1 & & & & & \\ \hline & & & & -1 & 1 & & & & \\ & & & & & -u^- & 1 & & & \\ & & & & & & \ddots & \ddots & & \\ & & & & & & & & -u^- & 1 \end{array}\right) \tag{2.18}$$

with $u^\pm \equiv e^{\mp i\omega_0 \delta t}$. The equilibrium initial conditions (2.16) enter through the off-diagonal matrix element $-\rho_0$ in the upper right corner.

As an important side remark, we mention that to ensure thermal equilibrium in the presence of interactions V at all times, while still using the *free* density operator (2.16) as the initial state, requires the interactions V to be switched on adiabatically while evolving the system from the distant past $t_0 \to -\infty$ [127]. In this way, energy levels are adjusted 'infinitely slowly' without causing transitions [129]. However, in contrast to zero-temperature QFT, the interactions remain active in the distant future $t \to \infty$, and are only adiabatically switched off again in the distant past $t \to -\infty$ on the backward branch [118].

In the continuum limit $N \to \infty$ with $N\,\delta t = \text{const.}$, the partition function (2.17) becomes

$$Z = \int \mathcal{D}[\alpha^*, \alpha]\, e^{iS}\,, \tag{2.19}$$

where S denotes the (naive) continuum limit of the contour action,

$$S = \int_{\mathcal{C}} dt\, \left(-\alpha^* G_0^{-1} \alpha - V(\alpha^*, \alpha)\right)\,, \tag{2.20}$$

with the operator $-G_0^{-1} = i\partial_t - \omega_0$. The time integral in (2.20) runs along the closed contour $\mathcal{C}$. The problem with (2.20) is that the boundary conditions, which were encoded in the upper-right elements of the lower-left and upper-right blocks of the discrete matrix (2.18), have disappeared. As such, the inverse of G_0^{-1} is not unique.[4] Hence, finding an appropriate continuum formulation of (2.17) is one of the goals in the remaining part of this section.

For simplicity, we relabel the $2N$ variables α_m around the contour according to Fig. 2.2,

$$\alpha_m \equiv \begin{cases} \alpha^+_m & \text{for } m = 1, \ldots, N\,, \\ \alpha^-_{2N-m+1} & \text{for } m = N+1, \ldots, 2N\,. \end{cases} \tag{2.21}$$

The advantage of this relabelling is that only forward time evolution remains, but at the cost of doubling the number of field components. The partition function (2.17) becomes

$$\begin{aligned} Z = \frac{1}{\operatorname{tr} \hat{\rho}_0} \int \left(\prod_{i=1}^{N} d[\alpha_i^{+*}, \alpha_i^+]\, d[\alpha_i^{-*}, \alpha_i^-]\right) \exp\Bigg\{ &- \sum_{m,n=1}^{2N} (\alpha_m^{+*}, \alpha_m^{-*}) \begin{pmatrix} iG^{-1,++}_{0,mn} & iG^{-1,+-}_{0,mn} \\ iG^{-1,-+}_{0,mn} & iG^{-1,--}_{0,mn} \end{pmatrix} \begin{pmatrix} \alpha_n^+ \\ \alpha_n^- \end{pmatrix} \\ &- i\delta t \sum_{m=1}^{N-1} V(\alpha_{m+1}^{+*}, \alpha_m^+) + i\delta t \sum_{m=1}^{N-1} V(\alpha_m^{-*}, \alpha_{m+1}^-) \Bigg\} \end{aligned} \tag{2.22}$$

[4] Indeed, G_0^{-1} possesses a zero mode of the form $e^{-i\omega_0 t}$.

with $(iG_0^{-1})^{\pm\pm}$ denoting the matrices that result from applying the relabelling (2.21) to (2.18),

$$\begin{aligned}
\left(iG_0^{-1}\right)^{++} &= \begin{pmatrix} 1 & & & \\ -u^+ & 1 & & \\ & \ddots & \ddots & \\ & & -u^+ & 1 \end{pmatrix}, \quad \left(iG_0^{-1}\right)^{+-} = \begin{pmatrix} -\rho_0 & & & \\ & 0 & & \\ & & \ddots & \\ & & & 0 \end{pmatrix}, \\
\left(iG_0^{-1}\right)^{-+} &= \begin{pmatrix} 0 & & & \\ & \ddots & & \\ & & 0 & \\ & & & -1 \end{pmatrix}, \quad \left(iG_0^{-1}\right)^{--} = \begin{pmatrix} 1 & -u^- & & \\ & \ddots & \ddots & \\ & & 1 & -u^- \\ & & & 1 \end{pmatrix}.
\end{aligned} \tag{2.23}$$

By inverting these, we find the discretized free propagators,

$$\langle \alpha_m^+ \alpha_n^{+*} \rangle_0 = -iG_{0,mn}^{++} = \frac{1}{1-\rho_0}(u^+)^{m-n} \times \begin{cases} 1 & \text{for } m \geq n\,, \\ \rho_0 & \text{for } n > m\,, \end{cases} \tag{2.24a}$$

$$\langle \alpha_m^- \alpha_n^{-*} \rangle_0 = -iG_{0,mn}^{--} = \frac{1}{1-\rho_0}(u^+)^{m-n} \times \begin{cases} \rho_0 & \text{for } m > n\,, \\ 1 & \text{for } n \geq m\,, \end{cases} \tag{2.24b}$$

$$\langle \alpha_m^+ \alpha_n^{-*} \rangle_0 = -iG_{0,mn}^{+-} = \frac{\rho_0}{1-\rho_0}(u^+)^{m-n}\,, \tag{2.24c}$$

$$\langle \alpha_m^- \alpha_n^{+*} \rangle_0 = -iG_{0,mn}^{-+} = \frac{1}{1-\rho_0}(u^+)^{m-n}\,. \tag{2.24d}$$

In the continuum limit $N \to \infty$ with $N\,\delta t = \text{const.}$, we obtain

$$\langle \alpha_m^+ \alpha_n^{-*} \rangle_0 \to \langle \alpha^+(t)\alpha^{-*}(t') \rangle_0 = n_B(\omega_0) e^{-i\omega_0(t-t')}\,, \tag{2.25a}$$

$$\langle \alpha_m^- \alpha_n^{+*} \rangle_0 \to \langle \alpha^-(t)\alpha^{+*}(t') \rangle_0 = (n_B(\omega_0)+1) e^{-i\omega_0(t-t')}\,, \tag{2.25b}$$

$$\langle \alpha_m^+ \alpha_n^{+*} \rangle_0 \to \langle \alpha^+(t)\alpha^{+*}(t') \rangle_0 = \left[\theta(t-t')(n_B(\omega_0)+1) + \theta(t'-t) n_B(\omega_0)\right] e^{-i\omega_0(t-t')}\,, \tag{2.25c}$$

$$\langle \alpha_m^- \alpha_n^{-*} \rangle_0 \to \langle \alpha^-(t)\alpha^{-*}(t') \rangle_0 = \left[\theta(t'-t)(n_B(\omega_0)+1) + \theta(t-t') n_B(\omega_0)\right] e^{-i\omega_0(t-t')}\,, \tag{2.25d}$$

where $n_B(\omega) = 1/(e^{\beta(\omega-\mu)}-1) = \rho_0/(1-\rho_0)$ denotes the Bose-Einstein distribution, and $\theta(t)$ the Heaviside step function. In both (2.25c) and (2.25d) the first θ-function is regularized according to $\theta(0) = 1$, and the second one according to $\theta(0) = 0$, which is slightly inconvenient and originates from the discretization (2.24). It is more convenient to use $\theta(0) = 1/2$ for both θ-functions, which can be required without harm here since it merely affects the value of the time-ordered and anti-time-ordered propagators on the diagonal $t = t'$, which is a set of measure zero.[5]

In general, after the relabelling (2.21), one encounters four different Green functions,

$$\langle \alpha^+(t)\alpha^{+*}(t') \rangle = -iG^{++}(t,t') = -iG^T(t,t') = \langle T\{a(t)a^\dagger(t')\} \rangle\,, \tag{2.26a}$$

$$\langle \alpha^+(t)\alpha^{-*}(t') \rangle = -iG^{+-}(t,t') = -iG^<(t,t') = \langle a^\dagger(t')a(t) \rangle\,, \tag{2.26b}$$

$$\langle \alpha^-(t)\alpha^{+*}(t') \rangle = -iG^{-+}(t,t') = -iG^>(t,t') = \langle a(t)a^\dagger(t') \rangle\,, \tag{2.26c}$$

$$\langle \alpha^-(t)\alpha^{-*}(t') \rangle = -iG^{--}(t,t') = -iG^{\tilde{T}}(t,t') = \langle \tilde{T}\{a(t)a^\dagger(t')\} \rangle\,, \tag{2.26d}$$

[5] This convention corresponds to defining the (anti-)time-ordering of (non-commuting) operators A and B at equal times as $T\{A(t)B(t)\} \equiv \tilde{T}\{A(t)B(t)\} \equiv (A(t)B(t) + B(t)A(t))/2$.

with the superscripts denoting the time-ordered (T), lesser ($<$), greater ($>$), and anti-time-ordered ($\tilde{T}$) Green functions, respectively. One can directly verify that the correlators on the left-hand sides of (2.26) are indeed given by the operator expressions from the right-hand sides of (2.26): First, (anti-)time ordering in (2.26a) and (2.26d) implies that the field operators inside the expectation value are sorted such that t is (after) before t', which corresponds to the cases where the fields are both on the $(+)$ or the $(-)$ branch, respectively. The lesser ($<$) and greater ($>$) superscripts in (2.26b) and (2.26c) indicate that the first field is evaluated before the second field in the ($<$) case and vice versa in the greater ($>$) case, which corresponds to the two possibilities of placing the fields on different branches of the CTP, since the field on the forward $(+)$ branch is always evaluated before the field on the backward $(-)$ branch.

The time-ordered and anti-time-ordered Green functions are related to the lesser and greater Green functions via [118]

$$G^T(t,t') = \theta(t-t')G^>(t,t') + \theta(t'-t)G^<(t,t')\,, \tag{2.27}$$

$$G^{\tilde{T}}(t,t') = \theta(t'-t)G^>(t,t') + \theta(t-t')G^<(t,t')\,, \tag{2.28}$$

where the regularization of $\theta(0)$ here depends on the underlying discretization and can be different for both θ-functions in each of the equations. However, at coinciding times $t = t'$ time ordering and anti-time ordering are equivalent, and we have $G^T(t,t) = G^{\tilde{T}}(t,t)$.

An important observation is that the Green functions in (2.26) satisfy the exact relation

$$G^T(t,t') + G^{\tilde{T}}(t,t') - G^<(t,t') - G^>(t,t') = 0 \tag{2.29}$$

for all $t \neq t'$,[6] which can be directly verified by evaluating the expression (2.29) with the operator expressions from the right-hand sides of (2.26). Eq. (2.29) suggests to perform a linear transformation which sets one of the Green functions identically to zero. This is achieved by the Keldysh rotation, where one defines the 'classical' field α^c and the 'quantum' field α^q as

$$\alpha^c \equiv \frac{1}{\sqrt{2}}(\alpha^+ + \alpha^-)\,, \qquad \alpha^q \equiv \frac{1}{\sqrt{2}}(\alpha^+ - \alpha^-)\,, \tag{2.30}$$

and analogously for their complex conjugates α^{c*} and α^{q*}. With this linear transformation, the Green functions (2.26) from the $(+,-)$ basis are transformed into

$$G^{cq}(t,t') = i\langle\alpha^c(t)\alpha^{q*}(t')\rangle = \frac{1}{2}\big(G^T - G^{\tilde{T}} + G^> - G^<\big)\,, \tag{2.31a}$$

$$G^{qc}(t,t') = i\langle\alpha^q(t)\alpha^{c*}(t')\rangle = \frac{1}{2}\big(G^T - G^{\tilde{T}} - G^> + G^<\big)\,, \tag{2.31b}$$

$$G^{cc}(t,t') = i\langle\alpha^c(t)\alpha^{c*}(t')\rangle = \frac{1}{2}\big(G^T + G^{\tilde{T}} + G^> + G^<\big)\,, \tag{2.31c}$$

$$G^{qq}(t,t') = i\langle\alpha^q(t)\alpha^{q*}(t')\rangle = \frac{1}{2}\big(G^T + G^{\tilde{T}} - G^> - G^<\big) = 0\,. \tag{2.31d}$$

Note that the anomalous qq Green function vanishes identically, which is a direct consequence of (2.29). Moreover, by virtue of the identity (2.29), the propagators in (2.31) can be shown to be related to the operator expectation values

$$G^{cq}(t,t') = G^T(t,t') - G^<(t,t') = \quad i\theta(t-t')\langle[a(t),a^\dagger(t')]\rangle = G^R(t,t')\,, \tag{2.32a}$$

$$G^{qc}(t,t') = G^>(t,t') - G^{\tilde{T}}(t,t') = -i\theta(t'-t)\langle[a(t),a^\dagger(t')]\rangle = G^A(t,t')\,, \tag{2.32b}$$

$$G^{cc}(t,t') = G^>(t,t') + G^<(t,t') = \quad i\langle\{a(t),a^\dagger(t')\}\rangle = G^K(t,t')\,. \tag{2.32c}$$

[6] At coinciding times $t = t'$ the right-hand side is not necessarily zero, since the precise value depends on the underlying discretization. Nevertheless, even if it is non-zero it only acquires a finite ($< \infty$) value, and since the line $t = t'$ is a set of measure zero, relation (2.29) may be safely required also on the diagonal $t = t'$.

These denote the retarded (R), advanced (A), and Keldysh[7] (K) Green functions. At coinciding times $t = t'$ time ordering and anti-time ordering are equivalent, which implies

$$G^R(t,t) + G^A(t,t) = G^T(t,t) - G^{\tilde{T}}(t,t) = 0\,. \tag{2.33}$$

The last equality in (2.32a) can be understood as a prototypical Kubo formula [130], which here expresses that the time-dependent linear response of the operator a at time t with respect to an external source coupled to $a^\dagger$ at time t' (i.e., the retarded propagator $G^R(t,t')$) is essentially given by the commutator $[a(t), a^\dagger(t')]$. Hence, $G^R(t,t')$ has the general interpretation of encoding the spectrum of excitations in the system. Indeed, it is related to the spectral function $\rho(t,t') = \frac{1}{2\pi}\langle[a(t), a^\dagger(t')]\rangle$ via

$$G^R(t,t') = 2\pi i\theta(t-t')\rho(t,t')\,. \tag{2.34}$$

For time-translation invariant systems, their Fourier transforms $G^R(\omega)$ and $\rho(\omega)$ are related via

$$\rho(\omega) = \frac{1}{\pi}\,\mathrm{Im}\,G^R(\omega)\,. \tag{2.35}$$

Causality entails that there can not be a response for $t < t'$, which means that we generally have

$$G^R(t,t') = 0 \quad \text{for} \quad t < t'\,, \tag{2.36}$$

and thus also that the Fourier transform $G^R(\omega)$ (assuming time-translation invariance) is an analytic function in the upper half of the complex ω-plane.[8] Eq. (2.36) is only one aspect of the more general 'causality structure' of the Keldysh action, cf. Chapter 2.7 of Ref. [118]. We shall review the causality structure in more detail in Sec. 2.3.2, since its preservation is one of the main obstacles in devising suitable bilinear regulator terms for real-time FRG flows [1, 90].

Since our system is in a thermal equilibrium state, correlation functions satisfy the Kubo-Martin-Schwinger (KMS) condition [130, 131]

$$\langle A(t)B(t')\rangle_{\beta,\mu} = \langle B(t')e^{\mu\beta N}A(t+i\beta)e^{-\mu\beta N}\rangle_{\beta,\mu}\,, \tag{2.37}$$

where $A(t)$ and $B(t')$ are Heisenberg operators, and the subscript $_{\beta,\mu}$ indicates a thermal density operator with temperature $1/\beta$ and chemical potential μ. In particular, the KMS condition (2.37) implies the fluctuation-dissipation relation (FDR)

$$\begin{aligned} G^K(\omega) &= \coth\left(\frac{\omega-\mu}{2T}\right)\left(G^R(\omega) - G^A(\omega)\right) \\ &= \coth\left(\frac{\omega-\mu}{2T}\right) 2\pi i\,\rho(\omega) \end{aligned} \tag{2.38}$$

between the Keldysh Green function $G^K(\omega)$ and the spectral function $\rho(\omega)$. In other words, $G^K(\omega)$ essentially encodes how the spectrum of states given by $\rho(\omega)$ is thermally occupied.

By applying the Keldysh rotation (2.30) to the free Green functions (2.25) in the $(+,-)$ basis, we obtain their counterparts in the (c,q) basis,

$$G_0^R(t,t') = i\theta(t-t')\,e^{-i\omega_0(t-t')}\,, \tag{2.39a}$$

$$G_0^A(t,t') = -i\theta(t'-t)\,e^{-i\omega_0(t-t')}\,, \tag{2.39b}$$

$$G_0^K(t,t') = i\coth\left(\frac{\omega_0-\mu}{2T}\right)\,e^{-i\omega_0(t-t')}\,, \tag{2.39c}$$

[7] Sometimes the Keldysh Green function is also called the statistical function.

[8] For the advanced propagator similar statements hold, namely that $G^A(t,t') = 0$ for $t' < t$ and that $G^A(\omega)$ is analytic in the lower half of the complex ω-plane.

where we used that $1+2n_B(\omega_0)=\coth((\omega_0-\mu)/2T)$. After Fourier transform, we obtain

$$G_0^{R/A}(\omega)=-\frac{1}{\omega\pm i\varepsilon-\omega_0}\,,\qquad G_0^K(\omega)=2\pi i\coth\left(\frac{\omega_0-\mu}{2T}\right)\delta(\omega-\omega_0)\,, \tag{2.40}$$

from which we can directly verify the FDR (2.38).

The strategy for setting up a proper continuum formulation for the discretized partition function (2.22) is to write down an action S which reproduces the free Green functions (2.39) through the rules of Gaussian integration in the absence of interactions [118]. This is achieved by the Keldysh action

$$S=\int_{-\infty}^{\infty}dt\,(\alpha^{c*}(t),\alpha^{q*}(t))\begin{pmatrix}0 & i\partial_t-\omega_0-i\varepsilon\\ i\partial_t-\omega_0+i\varepsilon & 2i\varepsilon\coth((\omega_0-\mu)/2T)\end{pmatrix}\begin{pmatrix}\alpha^c(t)\\ \alpha^q(t)\end{pmatrix}+ \int_{-\infty}^{\infty}dt\,\{-V(\alpha^{+*},\alpha^+)+V(\alpha^{-*},\alpha^-)\} \tag{2.41}$$

where we have introduced the interaction terms V again, assuming that the latter are adiabatically switched on from $t_0=-\infty$, and with α^+ and α^- and their complex conjugates given by inverting (2.30). The Keldysh action enters the continuum partition function as

$$Z=\int\mathcal{D}[\alpha^{c*},\alpha^c]\,\mathcal{D}[\alpha^{q*},\alpha^q]\,e^{iS}\,. \tag{2.42}$$

The infinitesimal $\varepsilon\to 0^+$ in (2.41) ensures that the inverse of the operator in the bilinear form is unique, and specifically that the free propagators (2.39) are reproduced.

Eq. (2.41) represents the 1$^{\text{st}}$-order form of the Keldysh action. In certain circumstances, especially in the context of real scalar fields, it is useful to employ the corresponding 2$^{\text{nd}}$-order form. In this regard, one first parameterizes the complex eigenvalues α according to

$$\alpha=\frac{1}{\sqrt{2\omega_0}}(\pi-i\omega_0\phi)\quad\text{ and }\quad\alpha^*=\frac{1}{\sqrt{2\omega_0}}(\pi+i\omega_0\phi) \tag{2.43}$$

with real ϕ and π. If the Hamiltonian H is at most quadratic in the momenta π, the non-linear interactions terms V can only depend on the specific combination $\phi=i(\alpha-\alpha^*)/\sqrt{2\omega_0}$. In this parameterization the contour action (2.20) acquires the form

$$S=\int_{\mathcal{C}}dt\,\left\{\pi\dot{\phi}-\frac{1}{2}\pi^2-\frac{\omega_0^2}{2}\phi^2-V(\phi)\right\} \tag{2.44}$$

with $\dot{\phi}\equiv\partial_t\phi$. The integral over π is Gaussian and can therefore be performed explicitly, which leads to

$$S=\int_{\mathcal{C}}dt\,\left\{\frac{1}{2}\dot{\phi}^2-\frac{\omega_0^2}{2}\phi^2-V(\phi)\right\}\,. \tag{2.45}$$

Splitting the field ϕ again into ϕ^+ and ϕ^- parts, performing the Keldysh rotation according to

$$\phi^c=\frac{1}{\sqrt{2}}(\phi^++\phi^-)\quad\text{ and }\quad\phi^q=\frac{1}{\sqrt{2}}(\phi^+-\phi^-)\,, \tag{2.46}$$

and reintroducing infinitesimal ε-terms such that the correct free Green functions are reproduced, leads to the Keldysh action in its 2$^{\text{nd}}$-order form [118],

$$S=\frac{1}{2}\int_{-\infty}^{\infty}\frac{d\omega}{2\pi}\,(\phi^c(-\omega),\phi^q(-\omega))\begin{pmatrix}0 & (\omega-i\varepsilon)^2-\omega_0^2\\ (\omega+i\varepsilon)^2-\omega_0^2 & 4i\varepsilon\omega\coth(\omega/2T)\end{pmatrix}\begin{pmatrix}\phi^c(\omega)\\ \phi^q(\omega)\end{pmatrix}+ \int_{-\infty}^{\infty}dt\left\{-V\left(\frac{\phi^c+\phi^q}{\sqrt{2}}\right)+V\left(\frac{\phi^c-\phi^q}{\sqrt{2}}\right)\right\} \tag{2.47}$$

where we have expressed the quadratic part in frequency space for simplicity,[9] with the associated partition function

$$Z = \int \mathcal{D}\phi^c \, \mathcal{D}\phi^q \, e^{iS} = 1 \,. \tag{2.48}$$

2.1.2 Caldeira-Leggett heat bath

By coupling our system particle to an external bath consisting of an ensemble of harmonic oscillators and integrating out the latter, the Keldysh action becomes dissipative. This is the idea of the Caldeira-Leggett model [114], see Refs. [132, 133] for pedagogical introductions. The external bath can be characterized by its spectral density $J(\omega)$, which essentially encodes the frequencies that can be excited in the ensemble. For a physical external bath it is antisymmetric, $J(-\omega) = -J(\omega)$, positive semi-definite $J(\omega) \geq 0$ for $\omega > 0$, but not necessarily normalizable.

With the spectral density $J(\omega)$, the retarded/advanced components $\Sigma^{R/A}_{HB}(\omega)$ of the self-energy which our system particle acquires due to the interactions with the bath oscillators, can be written in the form of spectral integrals,

$$\Sigma^{R/A}(\omega) = -\int_0^\infty \frac{d\omega'}{2\pi} \frac{2\omega' J(\omega')}{(\omega \pm i\varepsilon)^2 - \omega'^2} \,. \tag{2.49}$$

The Keldysh component $\Sigma^K(\omega) = \coth(2T/\omega)(\Sigma^R(\omega) - \Sigma^A(\omega))$ is set by the FDR, assuming that the external bath is in thermal equilibrium at temperature T (but not necessarily the system particle). The self-energy modifies the free inverse propagator in accordance with Dyson's equation on the CTP, $G^{-1} = G_0^{-1} - \Sigma$, expanded in the (c, q) basis [118],

$$\begin{pmatrix} 0 & G_0^{-1\,A} \\ G_0^{-1\,R} & G_0^{-1\,K} \end{pmatrix} \to \begin{pmatrix} 0 & G_0^{-1\,A} \\ G_0^{-1\,R} & G_0^{-1\,K} \end{pmatrix} - \begin{pmatrix} 0 & \Sigma^A \\ \Sigma^R & \Sigma^K \end{pmatrix} \,. \tag{2.50}$$

In particular, self-energies on the CTP generally inherit the causality structure of the Keldysh action [118], as reflected by (2.50).

For an 'Ohmic' spectral density of the form $J(\omega) = 2\gamma\omega$ the retarded part of the self-energy in (2.49) becomes $\Sigma^R(\omega) = \text{const.} + i\gamma\omega$, and the resulting Keldysh action reads (absorbing the infinite constant in the bare frequency ω_0^2)

$$S = \frac{1}{2}\int_{-\infty}^{\infty} \frac{d\omega}{2\pi} \left(\phi^c(-\omega), \phi^q(-\omega)\right) \begin{pmatrix} 0 & \omega^2 - i\gamma\omega - \omega_0^2 \\ \omega^2 + i\gamma\omega - \omega_0^2 & 2i\gamma\omega\coth(\omega/2T) \end{pmatrix} \begin{pmatrix} \phi^c(\omega) \\ \phi^q(\omega) \end{pmatrix} + \int_{-\infty}^{\infty} dt \left\{ -V\left(\frac{\phi^c + \phi^q}{\sqrt{2}}\right) + V\left(\frac{\phi^c - \phi^q}{\sqrt{2}}\right) \right\} \tag{2.51}$$

In comparison with (2.47) one can see that the infinitesimal ε-terms can be dropped as soon as a finite damping constant γ is introduced. In fact, by taking the limit of an infinitesimally small damping constant $\gamma \to 0^+$ one recovers the ε-prescription from (2.47). In other words, the ε-terms in (2.47) can be interpreted as an infinitesimal coupling to an external (Ohmic) heat bath at temperature T.

[9] We have dropped the chemical potential μ here since it is not meaningful if particle number N is not conserved, which is generally the case for real scalar fields.

2.1.3 Thermal equilibrium as a symmetry of the Keldysh action

By construction, the CTP formalism is not limited to systems in thermal equilibrium. Hence, given an arbitrary Keldysh action S, it would be desirable to be able to tell whether the system is in or out of equilibrium. It was put forward in Ref. [107] that the state of thermal equilibrium is reflected by the presence of a certain discrete symmetry of S. Since, as part of the present work, we will generalize this statement to relativistic Dirac fermions in Chapter 5 below, it is instructive to briefly review a simplified form of their argument here.

Consider the two-point correlation function from (2.26c),

$$-iG^{>}(t,t') = \langle \alpha^{-}(t)\alpha^{+*}(t')\rangle_{S}\,, \tag{2.52}$$

where the subscript $_S$ denotes the action that enters the path integral (2.19). Following (2.26c), we can express (2.52) equivalently in terms of creation and annihilation operators,

$$-iG^{>}(t,t') = \langle a(t)a^{\dagger}(t')\rangle_{\beta}\,, \tag{2.53}$$

where the subscript $_\beta$ indicates that the expectation value is taken with respect to the thermal density operator $e^{-\beta H}$. (For simplicity, we set $\mu = 0$ here.) By applying the symmetrized KMS condition (2.37) to the right-hand side of (2.53), it can be equivalently expressed as

$$-iG^{>}(t,t') = \langle a^{\dagger}(t' - i\beta/2)a(t + i\beta/2)\rangle_{\beta}\,. \tag{2.54}$$

Notice that the time ordering has changed when going from (2.53) to (2.54). This is problematic for general multi-time correlation functions, since the resulting time ordering is inconsistent with the time ordering around the CTP, preventing a Keldysh path-integral formulation [107]. To remedy this, one inserts identity operators $\mathbb{1}$ in the form of two consecutive time-reversal transformations T to the right-hand side of (2.54), which here yields

$$-iG^{>}(t,t') = \langle \tilde{a}^{\dagger}(-t' - i\beta/2)\tilde{a}(-t + i\beta/2)\rangle^{*}_{\tilde{\beta}}\,. \tag{2.55}$$

(Since the time-reversal operator T is antiunitary, inner products become their complex conjugates.) The subscript $_{\tilde\beta}$ indicates that the expectation value is taken with respect to the time-reversed density operator $\hat{\tilde\rho}_\beta = T\hat\rho_\beta T^\dagger$. The tilde in $\tilde a$ and $\tilde a^\dagger$ indicates that time evolution is understood with respect to the time-reversed Hamiltonian $\tilde H = THT^\dagger$.

The complex conjugation in (2.55) reverses the ordering of operators yet again,

$$-iG^{>}(t,t') = \langle \tilde{a}^{\dagger}(-t - i\beta/2)\tilde{a}(-t' + i\beta/2)\rangle_{\tilde{\beta}}\,, \tag{2.56}$$

but now the resulting expression is consistent with time ordering around the CTP, especially in the case of multi-time correlation functions which involve more than two time arguments [107]. As such, we can generally express (2.56) as a Keldysh path integral, which here yields

$$-iG^{>}(t,t') = \langle \alpha^{-*}(-t - i\beta/2)\alpha^{+}(-t' + i\beta/2)\rangle_{\tilde{S}}\,, \tag{2.57}$$

where $\tilde S$ is the time-reversed Keldysh action, which is obtained by repeating the procedure of Sec. 2.1.1 for the time-reversed density operator $\hat{\tilde\rho}_\beta$ and the time-reversed Hamiltonian $\tilde H$. In many cases (unless there are, e.g., external magnetic fields which change sign under time reversal) one has $\hat{\tilde\rho}_\beta = \rho_\beta$ and $\tilde H = H$, and thus $\tilde S = S$.

Hence, comparing (2.52) and (2.57), we have

$$\langle \alpha^-(t)\alpha^{+*}(t')\rangle_S = \langle \alpha^{-*}(-t-i\beta/2)\alpha^+(-t'+i\beta/2)\rangle_{\tilde{S}}\,. \tag{2.58a}$$

Analogously, we can derive a similar equality for the lesser Green function (2.26b),

$$\langle \alpha^+(t)\alpha^{-*}(t')\rangle_S = \langle \alpha^-(-t'-i\beta/2)\alpha^{+*}(-t+i\beta/2)\rangle_{\tilde{S}}\,. \tag{2.58b}$$

A sufficient condition for the equalities in (2.58) to hold is

$$\tilde{S}[\boldsymbol{\alpha}] = S[\mathcal{T}_\beta \boldsymbol{\alpha}]\,, \tag{2.59}$$

with $\boldsymbol{\alpha} \equiv (\alpha^+, \alpha^-, \alpha^{+*}, \alpha^{-*})^T$, and with the discrete transformation

$$\mathcal{T}_\beta \begin{pmatrix} \alpha^\pm\ (t) \\ \alpha^{\pm *}(t) \end{pmatrix} = \begin{pmatrix} \alpha^{\pm *}(-t \pm i\beta/2) \\ \alpha^\pm\ (-t \pm i\beta/2) \end{pmatrix}. \tag{2.60}$$

As we have seen above, $\mathcal{T}_\beta$ can be regarded as a combination of the KMS condition (2.37) and time reversal. In particular, $\mathcal{T}_\beta$ is measure-preserving [107]. In fact, it was proven in Ref. [107] that the relation (2.59) is not only a sufficient criterion for thermal equilibrium, but also necessary. Moreover, in the absence of any external fields which change sign under time reversal we have $\tilde{S} = S$, such that the condition (2.59) reduces to an invariance of S under $\mathcal{T}_\beta$ in this case.

In frequency space, after Fourier transform and Keldysh rotation (2.30), the corresponding transformation is given by (here generalized to $\mu \neq 0$ [107])

$$\begin{aligned}
\mathcal{T}_\beta \begin{pmatrix} \alpha^c\ (\omega) \\ \alpha^q\ (\omega) \end{pmatrix} &= \begin{pmatrix} \cosh\left(\beta(\omega-\mu)/2\right) & -\sinh\left(\beta(\omega-\mu)/2\right) \\ -\sinh\left(\beta(\omega-\mu)/2\right) & \cosh\left(\beta(\omega-\mu)/2\right) \end{pmatrix} \begin{pmatrix} \alpha^{c*}(-\omega) \\ \alpha^{q*}(-\omega) \end{pmatrix}, \\
\mathcal{T}_\beta \begin{pmatrix} \alpha^{c*}(\omega) \\ \alpha^{q*}(\omega) \end{pmatrix} &= \begin{pmatrix} \cosh\left(\beta(\omega-\mu)/2\right) & -\sinh\left(\beta(\omega-\mu)/2\right) \\ -\sinh\left(\beta(\omega-\mu)/2\right) & \cosh\left(\beta(\omega-\mu)/2\right) \end{pmatrix} \begin{pmatrix} \alpha^c\ (-\omega) \\ \alpha^q\ (-\omega) \end{pmatrix}.
\end{aligned} \tag{2.61}$$

In particular, one may explicitly verify that an invariance of the Keldysh action S under this transformation implies the FDR (2.38). For completeness, we note that in case of the 2^{nd}-order form (2.47) of the Keldysh action, the corresponding transformation is given by [107]

$$\mathcal{T}_\beta \begin{pmatrix} \phi^c(\omega,\boldsymbol{p}) \\ \phi^q(\omega,\boldsymbol{p}) \end{pmatrix} = \begin{pmatrix} \cosh\left(\beta\omega/2\right) & -\sinh\left(\beta\omega/2\right) \\ -\sinh\left(\beta\omega/2\right) & \cosh\left(\beta\omega/2\right) \end{pmatrix} \begin{pmatrix} \phi^c(-\omega,\boldsymbol{p}) \\ \phi^q(-\omega,\boldsymbol{p}) \end{pmatrix}. \tag{2.62}$$

2.1.4 Classical-statistical limit: recovering the Martin-Siggia-Rose formalism

To perform the classical limit of the dissipative Keldysh action (2.51) it is convenient to employ a different convention for the Keldysh rotation,

$$\phi = \frac{1}{2}(\phi^+ + \phi^-)\,, \qquad \tilde{\phi} = \phi^+ - \phi^-\,, \tag{2.63}$$

which is still measure-preserving, but no longer orthogonal. The variables ϕ and $\tilde{\phi}$ are related to ϕ^c and ϕ^q from (2.46) via $\phi = \phi^c/\sqrt{2}$ and $\tilde{\phi} = \sqrt{2}\,\phi^q$. We now re-introduce $\hbar$ using (i) dimensional analysis, and (ii) the rule that every quantum field $\tilde{\phi} \to \hbar\tilde{\phi}$ acquires an additional

factor of $\hbar$ [118]. The potential $V(\phi^{\pm})$ and the equilibrium distribution function $\coth(\omega/2T)$ in the Keldysh action (2.51) become, to leading order in $\hbar$,

$$V(\phi^+) - V(\phi^-) = V\big(\phi + \tfrac{\hbar}{2}\,\tilde{\phi}\big) - V\big(\phi - \tfrac{\hbar}{2}\,\tilde{\phi}\big) = \hbar\tilde{\phi}V'(\phi) + \mathcal{O}(\hbar^2) \tag{2.64}$$

and, with $T \to T/\hbar$,

$$\coth\left(\frac{\hbar\omega}{2T}\right) = \frac{2T}{\hbar\omega} + \mathcal{O}(\hbar)\,. \tag{2.65}$$

Inserting (2.64) and (2.65) into (2.51), and replacing $S \to S/\hbar$, we obtain for the Keldysh action

$$\begin{aligned} S = \frac{1}{2\hbar}\int_{-\infty}^{\infty}\frac{d\omega}{2\pi}\left(\phi(-\omega), \hbar\tilde{\phi}(-\omega)\right)\begin{pmatrix} 0 & \omega^2 - i\gamma\omega - \omega_0^2 \\ \omega^2 + i\gamma\omega - \omega_0^2 & 2i\gamma T/\hbar + \mathcal{O}(\hbar)\end{pmatrix}\begin{pmatrix}\phi(\omega)\\ \hbar\tilde{\phi}(\omega)\end{pmatrix} + \\ \frac{1}{\hbar}\int_{-\infty}^{\infty} dt\left\{-V\big(\phi + \tfrac{\hbar}{2}\,\tilde{\phi}\big) + V\big(\phi - \tfrac{\hbar}{2}\,\tilde{\phi}\big)\right\} \\ \xrightarrow{\hbar\to 0} \int_{-\infty}^{\infty} dt\left\{-\tilde{\phi}\left(\ddot{\phi} + \gamma\dot{\phi} + V'(\phi)\right) + i\gamma T\tilde{\phi}^2\right\}\,. \end{aligned} \tag{2.66}$$

This is the classical MSR action [100] for a real degree of freedom ϕ moving in a potential $V(\phi)$ and coupled to an external heat bath with Ohmic spectral distribution. To see this, one recognizes that the response field $\tilde{\phi}$ only appears quadratically in (2.66), which allows one to linearize the action in $\tilde{\phi}$ via a Hubbard-Stratonovich transformation,

$$\exp\left\{-\int_{-\infty}^{\infty} dt\,\gamma T\tilde{\phi}^2\right\} = \int \mathcal{D}\xi\,\exp\left\{-\int_{-\infty}^{\infty} dt\big[\,\frac{1}{2\gamma T}\xi^2 - i\xi\tilde{\phi}\big]\right\}\,. \tag{2.67}$$

After applying this transformation to the partition function (2.48), the exponent becomes linear in $\tilde{\phi}$ and thus the corresponding functional integral evaluates to a δ-functional,

$$Z = \int \mathcal{D}\xi\, e^{-\int \xi^2/2\gamma T}\int \mathcal{D}\phi\,\delta\left[\ddot{\phi} + \gamma\dot{\phi} + V'(\phi) - \xi\right]\,, \tag{2.68}$$

enforcing the Langevin equation of motion

$$\ddot{\phi} + \gamma\dot{\phi} + V'(\phi) = \xi\,, \tag{2.69a}$$

in which the Gaussian noise ξ is fully specified by its first two moments,

$$\langle\xi(t)\rangle = 0\,, \qquad \langle\xi(t)\xi(t')\rangle = 2\gamma T\delta(t-t')\,. \tag{2.69b}$$

Indeed, by running the steps from Eq. (2.66) to Eq. (2.69) backwards, one can always convert a Langevin equation into a corresponding path integral. This is the essence of MSR formalism [100–102]. We shall use this approach multiple times in this thesis to convert stochastic equations of motion into corresponding path integrals, which then forms the basis for an analysis using the real-time FRG.

Towards the end of this subsection, we remark the following observation: From the point of view of the Keldysh formalism, non-equilibrium QFT and classical-statistical field theory [85] are virtually indistinguishable, since both are described by an action $S[\phi, \tilde{\phi}]$ which depends on both ϕ and $\tilde{\phi}$. In particular, as we have seen, the MSR action (2.66) is effectively obtained from the Keldysh action (2.47) by simply replacing the Bose-Einstein distribution $\frac{1}{2}\coth(\omega/2T)$ with the Rayleigh-Jeans distribution T/ω (cf. (2.65)) and removing all 'quantum' vertices, i.e., interaction

terms that involve more than one quantum field $\tilde{\phi}$. For instance, this observation allows one to benchmark non-perturbative truncation schemes for real-time QFT applications by comparing their classical limit $\hbar \to 0$ with ab-initio results from classical-statistical simulations [90, 98]. The latter can be performed, e.g., on high-performance computing clusters to solve many-body generalizations of Langevin equation such as (2.69a) numerically. In particular, the critical dynamics close to a second-order phase transition is governed by the slow (infrared) modes $\omega \ll T$ of the system, such that the classical-statistical limit captures the universal critical properties *exactly*. Hence, classical-statistical simulations are an ab-initio tool to study dynamic critical phenomena [48–51, 66, 67, 86–89, 134]. To take into account at least the leading-order quantum corrections to the classical-statistical limit, a 'Gaussian-state approximation' was proposed in Refs. [91, 92] where one propagates Gaussian states in time. These various real-time methods listed in the present paragraph were quantitatively compared in Ref. [90] by computing the spectral function of the dissipative quartic oscillator as a simple quantum-mechanical testbed system, which one can solve by exact diagonalization of the Hamiltonian.

2.2 Dynamic universality classes

In this section, we review the basics of dynamic critical phenomena with particular emphasis on their realization in QCD. For a pedagogical introduction see the textbooks by Täuber [104] and Onuki [103], and also the original review article by Halperin and Hohenberg [46].

Generally speaking, *dynamic* critical phenomena refer to the presence of universal scaling behavior in time-dependent quantities such as transport coefficients, relaxation rates, spectral functions, or general unequal-time correlation functions. In this sense, they generalize the notion of static critical phenomena [31, 135–137] to time-dependent processes. Before we discuss these dynamic critical phenomena in more detail, let us briefly review some important aspects of static critical phenomena. A central quantity is the correlation length ξ of order-parameter fluctuations. For instance, assuming that the system is described by an N-component order parameter ϕ_a, the correlation length ξ can be defined as the exponential decay of the two-point correlation function at large distances (assuming translational invariance), i.e.,

$$G_{ab}(\boldsymbol{x}) \equiv \langle \phi_a(\boldsymbol{x}) \phi_b(0) \rangle - \langle \phi_a \rangle \langle \phi_b \rangle \sim \delta_{ab} \, \frac{e^{-|\boldsymbol{x}|/\xi}}{|\boldsymbol{x}|^{d-2}} \,, \qquad |\boldsymbol{x}| \to \infty \,. \tag{2.70}$$

It is well-known that ξ diverges as the second-order phase transition is approached (assuming that no external symmetry-breaking fields are applied),

$$\xi \sim |\tau|^{-\nu} \quad \text{for } |\tau| \to 0 \,, \tag{2.71}$$

where $\tau = (T - T_c)/T_c$ denotes the reduced temperature, and ν is a critical exponent characterizing the power-law divergence. It is well-known that ν assumes the same value in all systems from the same static universality class. The latter, in turn, only depends on few macroscopic properties such as the number of spatial dimensions d and the number of components N of the order parameter, but generally not on the details of the microscopic interactions. Historically, the theoretical explanation for universality of the critical exponents came from Wilson's renormalization group and the ϵ-expansion by Wilson and Fisher [138], building on Kadanoff's earlier work on the block-spin renormalization group [139].

There are several other critical exponents. For example, $\eta_\perp$ describes the anomalous dimension of the order parameter, i.e., the power-law decay of order-parameter correlations precisely

at $T = T_c$ where the theory exhibits scale invariance,

$$G_{ab}(\boldsymbol{x}) \sim \frac{\delta_{ab}}{|\boldsymbol{x}|^{d-2+\eta_\perp}} \quad \text{for } |\boldsymbol{x}| \to \infty\,, \tag{2.72}$$

or, after Fourier transform,

$$G_{ab}(\boldsymbol{p}) \sim \delta_{ab}\,|\boldsymbol{p}|^{2-\eta_\perp} \quad \text{for } |\boldsymbol{p}| \to 0\,. \tag{2.73}$$

The critical exponent β is defined via the behavior of the order parameter as the critical temperature is approached from below,

$$\langle\phi\rangle \sim (-\tau)^\beta \quad \text{for } \tau \to 0^-\,. \tag{2.74}$$

The critical exponent α characterizes the power-law behavior of the specific heat capacity C,

$$C \sim |\tau|^{-\alpha} \quad \text{for } \tau \to 0\,. \tag{2.75}$$

A useful observation is that C shows the same power-law divergence as the two-point correlation function of the composite operator $\phi^2(\boldsymbol{x})$ at zero momentum (for $\alpha > 0$),

$$C \sim \int d^dx\,\langle\phi^2(\boldsymbol{x})\phi^2(0)\rangle \sim |\tau|^{-\alpha}\,, \tag{2.76}$$

which is because $\phi^2(\boldsymbol{x})$ is the most singular part of the canonical energy density T^{00} in the corresponding ϕ^4-theory [137]. The susceptibility exponent γ in the symmetric phase $T > T_c$ is defined via

$$\int d^dx\,\langle\phi_a(\boldsymbol{x})\phi_b(0)\rangle = G_{ab}(\boldsymbol{p}\to 0) \sim \delta_{ab}\,\tau^{-\gamma} \quad \text{for } \tau \to 0^+\,. \tag{2.77}$$

Finally, to define the critical exponent δ, we need to apply an external symmetry-breaking field $H > 0$ at $T = T_c$,

$$\langle\phi\rangle \sim H^{1/\delta} \quad \text{for } H \to 0^+\,. \tag{2.78}$$

The six critical exponents are related via four (hyper-)scaling relations [31],

$$\gamma = \beta(\delta-1)\,, \quad \alpha + 2\beta + \gamma = 2\,, \quad (2-\eta_\perp)\nu = \gamma\,, \quad d\nu = 2-\alpha \quad (\text{for } d \le 4)\,, \tag{2.79}$$

and thus only two are independent.

Now we turn to dynamic critical phenomena. Critical slowing down entails that the correlation time ξ_t of order-parameter fluctuations scales with its correlation length ξ as the critical point is approached,

$$\xi_t \sim \xi^z\,, \tag{2.80}$$

which defines the *dynamic* critical exponent z. As such, the correlation time shows a power-law divergence at the critical point as well.[10] However, the associated critical exponent, z, is *not* determined by the static universality class, which means that two systems in the same static universality class can have different value of z. Instead, z is specified by the *dynamic* universality class of the system. Here the idea is to group systems by the equations of motion that the critical

[10] Intuitively, a divergent correlation time means that the relaxation of a system back to thermal equilibrium becomes self-similar, with universal scaling determined by the dynamic critical exponent z.

long-wavelength modes satisfy. Systems with the same equations of motion are said to be in the same dynamic universality class, and have the same value of z.

Critical slowing down (2.80) implies that the long-wavelength fluctuations of the order parameter become arbitrarily slow as the critical point is approached, which means that their equations of motion are determined by a hydrodynamic theory. In general, hydrodynamics describes the time evolution of the long-wavelength modes at long timescales. Near a second-order phase transition the relevant modes potentially include, e.g., densities of conserved charges whose relaxation is slow due to the conservation law, Goldstone modes associated with the spontaneous breaking of a continuous symmetry, but also, as a novel ingredient as compared to standard hydrodynamics, possibly the order parameter itself, due to critical slowing down (2.80) [47]. Hence, to determine the dynamic universality class, it is necessary to specify whether or not the order parameter is conserved, whether there are other conserved densities in the system, and how the latter interact with the order parameter. Moreover, the large fluctuations near a thermal second-order phase transition appear in the equations of motion as Langevin noise terms whose variances are set by fluctuation-dissipation relations.

In their seminal work [46] from the 1970s, Halperin and Hohenberg defined a set of abstract models, each being a representative of a dynamic universality class. For instance, Model A describes a system with no conservation laws, Model B describes a system with a conserved order parameter but no other conserved quantities, and Model C describes a non-conserved order parameter which couples to a conserved (energy) density. On the other hand, in Model G and H the order parameter couples to the conserved quantities only dynamically in the form of *reversible mode couplings*. In principle, all of these models exist in a pure abstract way without reference to a concrete physical system. However, given the motivation for the present work, we want to particularly emphasize their potential realization in QCD in the following subsections.

Before we discuss the relevant models in detail, we review the general structure of the equations of motion [104]. Deriving the equations of motion for the long-wavelength modes rigorously from the microscopic theory is usually unfeasible in practice, in the same way as it is usually unfeasible to carry out an explicit derivation of the Landau-Ginzburg free energy from the microscopic theory in the context of static critical phenomena. Luckily, such a first-principle derivation is not necessary concerning universal properties, since these are, per definition, largely independent of the microscopic interactions. Instead, one follows the spirit of the Landau-Ginzburg free energy and postulates the form of the equations of motion on the basis of general principles, including, e.g., global symmetries, the presence/absence of conservation laws, and, as we shall see, Poisson-bracket relations between the order parameter and the conserved densities.

Assume that the Landau-Ginzburg free energy (or effective Hamiltonian) $F[\psi]$ is known, and that it depends on a set of fields $\psi = (\psi_A(\boldsymbol{x}))$ which are enumerated by the superfield index A. The equilibrium distribution for the fields in ψ at temperature T is given by the Boltzmann distribution $e^{-F[\psi]/T}$. Hence, in the absence of external time-dependent sources, the equations of motion must be such that the probability distribution relaxes to $e^{-F[\psi]/T}$ for long times, as determined by the corresponding Fokker-Planck equation. In the simplest case this requirement is fulfilled by a Langevin equation of the form

$$\frac{\partial \psi_A(t,\boldsymbol{x})}{\partial t} = -\hat{\gamma}_{AB}(\boldsymbol{\nabla}) \frac{\delta F[\psi]}{\delta \psi_B(\boldsymbol{x})} + \xi_A(t,\boldsymbol{x})\,, \tag{2.81}$$

where the functional derivative is understood at fixed time t, and the kinetic coefficients $\hat{\gamma}_{AB} = \hat{\gamma}_{AB}(\boldsymbol{\nabla})$ are local operators that may involve spatial gradients. The Gaussian noise $\xi_A(t,\boldsymbol{x})$ is

characterized by its first two moments set by the FDR in thermal equilibrium,

$$\langle \xi_A(t,\boldsymbol{x})\rangle = 0\,, \qquad \langle \xi_A(t,\boldsymbol{x})\xi_B(t',\boldsymbol{x}')\rangle = 2\hat{\gamma}_{AB}T\delta(t-t')\delta(\boldsymbol{x}-\boldsymbol{x}')\,, \tag{2.82}$$

which can be shown with the associated Fokker-Planck equation, see e.g. Chapter 4 in Ref. [118]. Apart from Onsager's principle $\hat{\gamma}_{AB} = \hat{\gamma}_{BA}$,[11] the kinetic coefficients $\hat{\gamma}_{AB}$ depend on whether or not ψ_A is a density of a conserved charge. If it is, then the Fourier transform $\gamma_{AB}(\boldsymbol{p})$ must vanish in the limit $\boldsymbol{p}\to 0$, since a homogeneous field configuration $\psi_A(\boldsymbol{x}) = \text{const.}$ can not dissipate in this case. In particular, whether or not the order parameter is conserved distinguishes, for example, Model B from Model A, as we shall see below.

There is additional freedom in writing down the equations of motion. Namely, one may add non-linear *reversible mode couplings* $f_a^{\text{rev}}(\boldsymbol{x})$ between the fields ψ to the right-hand side of (2.81),

$$\frac{\partial\psi_A(t,\boldsymbol{x})}{\partial t} = -\hat{\gamma}_{AB}\frac{\delta F[\psi]}{\delta\psi_B(\boldsymbol{x})} + \xi_A(t,\boldsymbol{x}) + f_A^{\text{rev}}(\boldsymbol{x})\,, \tag{2.83}$$

without affecting the equilibrium distribution, and thus without affecting the static critical behavior. One can explicitly verify that the Boltzmann distribution $e^{-F[\psi]/T}$ is still a stationary solution of the Fokker-Planck equation as long as the reversible terms f_A^{rev} are divergence-free with respect to $e^{-F[\psi]/T}$ [104, 110],

$$\int d^dx\,\frac{\delta}{\delta\psi_A(\boldsymbol{x})}\left(f_A^{\text{rev}}(\boldsymbol{x})\,e^{-F[\psi]/T}\right) = 0\,. \tag{2.84}$$

A particularly convenient parameterization of the reversible terms f_A^{rev} can be achieved with the rather elegant Poisson-bracket technique [140, 141]. Here one assumes that the fields in ψ admit a set of Poisson-bracket relations $\{\psi_A(\boldsymbol{x}),\psi_B(\boldsymbol{x}')\}$. In this case, the contribution from ideal (Hamiltonian) dynamics to the time evolution of ψ_a is given by[12]

$$f_A^{\text{rev}} = g\{\psi_A(\boldsymbol{x}),F\} = g\int d^dx'\,\{\psi_A(\boldsymbol{x}),\psi_B(\boldsymbol{x}')\}\frac{\delta F[\psi]}{\delta\psi_B(\boldsymbol{x}')}\,, \tag{2.85}$$

where the integral in the second equality is commonly suppressed since the Poisson-bracket is usually local, i.e., given by some local operators acting on $\delta(\boldsymbol{x}-\boldsymbol{x}')$, such that one simply writes

$$f_A^{\text{rev}} = g\{\psi_A,\psi_B\}\frac{\delta F}{\delta\psi_B}\,. \tag{2.86}$$

The strength of the reversible mode couplings is controlled by the mode-coupling constant g. In particular, the form (2.85) guarantees the exact conservation of F during infinitesimal ideal time steps, to wit

$$\left.\frac{dF}{dt}\right|^{\text{rev}} = \int d^dx\,\frac{\delta F[\psi]}{\delta\psi_A(\boldsymbol{x})}\,f_A^{\text{rev}} = g\int d^dx\,d^dx'\,\{\psi_A(\boldsymbol{x}),\psi_B(\boldsymbol{x}')\}\frac{\delta F[\psi]}{\delta\psi_A(\boldsymbol{x})}\frac{\delta F[\psi]}{\delta\psi_B(\boldsymbol{x}')} = 0\,, \tag{2.87}$$

which immediately follows from the anti-symmetry $\{\psi_A(\boldsymbol{x}),\psi_B(\boldsymbol{x}')\} = -\{\psi_B(\boldsymbol{x}'),\psi_A(\boldsymbol{x})\}$ of the Poisson bracket.

[11] Assuming that ψ_A and ψ_B have the same parity under time reversal.

[12] In general, at finite temperature T additional terms are needed to ensure (2.84), as can be shown from the Zwanzig-Mori projector formalism [142, 143]. In the present work we consider only systems where such terms are not needed, which is the case if the Poisson brackets satisfy the additional condition $\delta\{\psi_A(\boldsymbol{x}),\psi_B(\boldsymbol{x}')\}/\delta\psi_B(\boldsymbol{x}') = 0$.

The kinetic coefficients $\hat{\gamma}_{AB}$ as well as the reversible mode couplings f_A^{rev} are *not* determined by the Landau-Ginzburg free energy F, and thus not by the static universality class. Indeed, one needs the dynamic universality class to determine the form of $\hat{\gamma}_{AB}$ and f_A^{rev}.[13] As such, the Langevin equations (2.83), possibly together with non-vanishing reversible mode couplings of the form (2.85), are the basis of all the dynamic universality classes which we discuss in the following subsections.

2.2.1 Model A

This subsection presents results which have already been published in Ref. [1].

Consider a Landau-Ginzburg-Wilson (LGW) free energy F for a single-component real scalar field ϕ in d spatial dimensions of the form

$$F = \int d^d x \left\{ \frac{1}{2}(\boldsymbol{\nabla}\phi)^2 + \frac{m^2}{2}\phi^2 + \frac{\lambda}{4!}\phi^4 \right\} \tag{2.88}$$

with $m^2 < 0$ to spontaneously break the Z_2 symmetry, and a positive quartic coupling $\lambda > 0$. As usual, the equilibrium partition function Z_{eq} is given by

$$Z_{eq} = \int \mathcal{D}\phi \, e^{-F/T} \,, \tag{2.89}$$

from which, e.g., the universal scaling of the free-energy density near the critical point may be extracted.

Regarding the equations of motion, the arguably simplest case is a system in which the order parameter ϕ is not conserved, and there are no other slow modes which interact with ϕ. For small deviations from the equilibrium state, one can take the equation of motion to be of Langevin form[14]

$$\frac{\partial \phi}{\partial t} = -\Gamma^{\phi} \frac{\delta F}{\delta \phi} + \xi \,, \tag{2.90}$$

where ξ is a Gaussian noise whose variance is set by the Einstein relation (as a classic example of the FDR)

$$\langle \xi(t, \boldsymbol{x}) \rangle = 0 \,, \quad \langle \xi(t, \boldsymbol{x}) \xi(t', \boldsymbol{x}') \rangle = 2\Gamma^{\phi} T \, \delta(t - t') \delta(\boldsymbol{x} - \boldsymbol{x}') \,. \tag{2.91}$$

The kinetic (Onsager) coefficient Γ^{ϕ} is a measure for how 'fast' the system relaxes back to its equilibrium state, i.e., to the minimum of the free energy. In contrast, the noise term ξ models the effects of thermal fluctuations and can be thought of as causing Brownian motion, with the excitations experiencing random forces from the surrounding heat bath that is in thermal equilibrium at temperature T. One can verify from the corresponding Fokker-Planck equation that the probability distribution for ϕ indeed converges to the Boltzmann distribution $e^{-F/T}$ [118]. Eqs. (2.88), (2.90), and (2.91) define Model A. The dynamic critical exponent z is usually parameterized as $z = 2 + c\eta_{\perp}$ with the anomalous dimension $\eta_{\perp}$ of the order-parameter field and a positive constant c of order one. In the ϵ-expansion (with $\epsilon = 4 - d$) around the upper critical dimension $d = 4$ one has, at leading order, $c = 6\ln(4/3) - 1 + \mathcal{O}(\epsilon)$ [46].

[13] As a practical application, the freedom of choosing the kinetic coefficients can be used to optimize real-time simulations of complex-Langevin equations [144].

[14] This corresponds to taking the overdamped limit of the Langevin equation (2.69) and replacing the potential $V(\phi)$ with the LGW free energy $F[\phi]$.

We can directly conclude from Sec. 2.1.2 that, microscopically, Model-A dynamics can be realized by replacing the potential $V(\phi)$ in (2.69a) with the LGW free energy (2.88), which corresponds to coupling a standard ϕ^4-theory to an external Caldeira-Leggett heat bath [114] with Ohmic spectral distribution. The emergence of Model-A dynamics at the critical point of this theory has been explicitly demonstrated using classical-statistical lattice simulations in Ref. [88].

Dynamic critical behavior is reflected in the spectral function $\rho(\omega, \boldsymbol{p})$ of the order parameter, which is given by the imaginary part of the retarded propagator (cf. Eq. (2.35)),

$$\rho(\omega, \boldsymbol{p}) = \frac{1}{\pi} \operatorname{Im} G^R(\omega, \boldsymbol{p}) \,. \tag{2.92}$$

The retarded propagator G^R can be determined by applying an external source H in the free energy,

$$F \to F - \int d^d x \, H(t, \boldsymbol{x}) \phi(\boldsymbol{x}) \,,$$

and measuring the time-dependent linear response,

$$G^R(t - t', \boldsymbol{x} - \boldsymbol{x}') = \left. \frac{\delta \langle \phi(t, \boldsymbol{x}) \rangle_H}{\delta H(t', \boldsymbol{x}')} \right|_{H=0} . \tag{2.93}$$

After Fourier transform, the critical part of the spectral function satisfies the dynamic scaling hypothesis [86]

$$s^{2-\eta_\perp} \rho(s^z \omega, s\boldsymbol{p}, s^{1/\nu} \tau) = \rho(\omega, \boldsymbol{p}, \tau) \tag{2.94}$$

for $s > 0$, where the third argument here indicates the dependence on the reduced temperature $\tau \equiv (T - T_c)/T_c$. Introducing dimensionless frequency and momentum variables $\bar{\omega} = f_t^+ \omega$ and $\bar{p} = f^+ |\boldsymbol{p}|$, where f^+ and f_t^+ are the non-universal amplitudes of the static correlation length ξ and the correlation time ξ_t at $T > T_c$, the critical spectral function can therefore be expressed in terms of universal dynamic scaling functions [88], e.g.,

$$\rho(\omega, \boldsymbol{p}, \tau) = \bar{\omega}^{-(2-\eta^\perp)/z} f_\omega(x, y) \tag{2.95}$$

$$= \bar{p}^{-(2-\eta^\perp)} f_p(1/x, y/x^{1/\nu z}) \,, \tag{2.96}$$

where $x = \bar{p}^z/\bar{\omega}$ and $y = \tau/\bar{\omega}^{1/\nu z}$. These are not independent, of course, but chosen as convenient for the specific purpose and related by $f_\omega(x, y) = x^{-(2-\eta^\perp)/z} f_p(1/x, y/x^{1/\nu z})$. Whenever the dynamic frequency scaling function $f_\omega(x, y)$ is regular in the origin, with $f_\omega \equiv f_\omega(0, 0) > 0$, we immediately obtain for $\boldsymbol{p} = 0$, $\tau = 0$, i.e., in the long-wavelength limit at criticality, the infrared power-law,

$$\rho(\omega, \boldsymbol{0}, 0) = f_\omega \, \bar{\omega}^{-\sigma} \,, \quad \text{with} \quad \sigma = (2 - \eta^\perp)/z \,, \tag{2.97}$$

as it is the case for Model A.

Critical spectral functions of Model A were computed in Ref. [1] using the real-time FRG. The truncation was inspired from the earlier study of Ref. [90] on the spectral functions of the quantum-mechanical quartic ('anharmonic') oscillator, and is based on an expansion of the effective average action in one-particle irreducible vertex functions, combined with an expansion in the number of loop structures on the right-hand sides of the corresponding flow equations. Two different field expansion points were considered in Ref. [1], namely (*i*) the scale-dependent

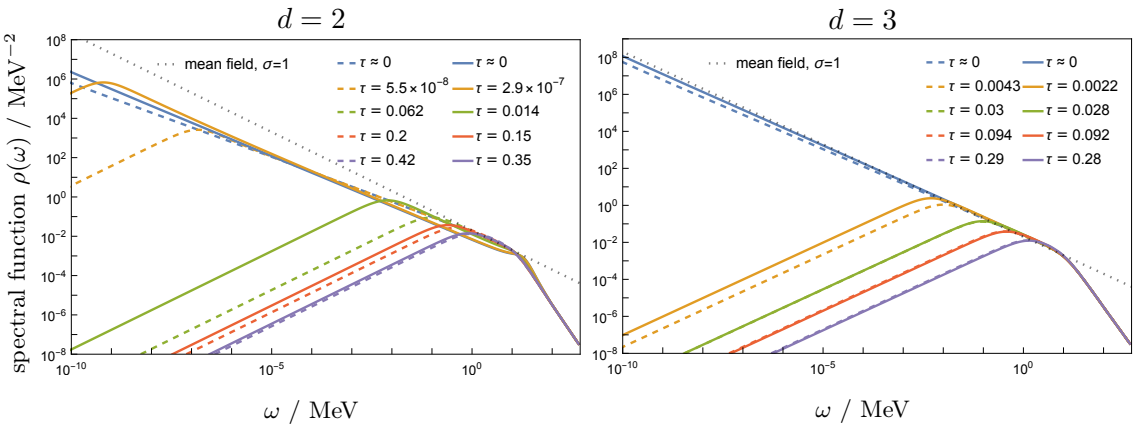

Figure 2.3: Critical infrared power-law (2.97) in the spectral functions of Model A in $d = 2$ (left) and $d = 3$ (right) spatial dimensions at vanishing momentum gradually builds up for $T \to T_c$, when approaching the critical temperature from above. Mean-field results are shown as dotted gray lines for comparison. Solid lines represent the results from the symmetric expansion scheme (*ii*), and dashed lines the results from the comoving expansion (*i*). For details on the respective truncations we refer to Secs. 3.1.1 and 3.1.2 of Ref. [1].

('comoving') minimum including one-loop structures in the two-point function, and (*ii*) the fixed field expansion point $\phi = 0$, including two-loop structures in the two-point function, and one-loop structures in the four-point function. The results are shown in Fig. 2.3 for various reduced temperatures τ. One can clearly see that for $\tau \to 0$ the expected power law (2.97) emerges in the infrared (IR), from which one can read off the associated dynamic critical exponent.

There is a slight tension in the literature on Model A in two spatial dimensions, as different results seem to converge to two slightly different values (although within about 2.5 standard deviations, see the discussion in [88]). The lower one, see e.g. Refs. [88, 145], is close to the experimental value of $z = 2.09(6)$ from Ref. [146], while most simulations tend to settle around $z = 2.17(3)$, cf. Ref. [147], which is close to the original Monte-Carlo estimate of Nightingale and Blöte [148] and also agrees with other calculations, e.g. see Refs. [84, 149, 150]. With all due appreciation of the systematic uncertainties of the FRG computation behind the spectral functions in Fig. 2.3 discussed in Ref. [1], especially in two spatial dimensions, the result for this dynamic critical exponent z seems to be in favor of the experimental value of 2.09(6) in both expansions.

In three spatial dimensions, the situation is somewhat more settled, and most precision results from the literature collectively find $z \approx 2.024$, see, e.g., Refs. [84, 149–152] and the references therein. The real-time FRG results of $z = 2.042$ and $z = 2.035$ for the comoving (*i*) and symmetric expansion (*ii*) [1], respectively, are in reasonable agreement, given that the error induced by the truncation of the FRG flow is at least of the same order as the discrepancy between the two schemes. For comparison, various results for the anomalous dimension $\eta_\perp$ and the dynamic critical exponent z of Model A are collected in Table 2.1.

$d = 2$	$\eta_\perp$	z	Reference
FRG	0.43	2.15 (LPA), 2.17 (UZA)	[149]
	0.29	2.16, 2.15, and 2.14	[84]
	$0.446^{(i)}$, $0.244^{(ii)}$	$2.094^{(i)}$, $2.073^{(ii)}$	[1] (This work.)
MC		2.1667(5)	[148]
PFT		2.093	[145]
CS		2.10(4)	[88]
ϵ-expansion		2.14(2)	[150]
Experiment		2.09(6)	[146]
Exact	1/4		[153]
$d = 3$			
FRG	0.11	2.05 (LPA), 2.14 (UZA)	[149]
	0.055	2.025	[151]
	0.0443	2.024, 2.024, and 2.023	[84]
	$0.0988^{(i)}$, $0.0427^{(ii)}$	$2.042^{(i)}$, $2.035^{(ii)}$	[1] (This work.)
	0	2.011	[154]
	0.0443 (∂^2), 0.033 (∂^4)		[155, 156]
	0.0361(11) (∂^6)		[78]
MC		2.0245(15)	[152]
CS		1.92(11)	[88]
ϵ-expansion		2.0235(8)	[150]
CB	0.036298		[157, 158]

Table 2.1: Comparison of results for the critical exponents $\eta_\perp$ and z with Ising universality and Model A dynamics in $d = 2, 3$ spatial dimensions: These include Monte-Carlo (MC) simulations [148, 152], FRG calculations [1, 84, 149, 151, 154], perturbative field theory (PFT) methods [145], classical-statistical lattice simulations [88], and five-loop ϵ-expansion [150]. In two spatial dimensions, one furthermore has the exact value for $\eta_\perp$ from Onsager's solution [153] and the experimental value for z from Ref. [146]. In three spatial dimensions, high-precision results are available from conformal bootstrap (CB) [157, 158]. The FRG results of Ref. [84] were obtained for three different 'frequency regulators'. The results from Refs. [155, 156] are understood as second $\mathcal{O}(\partial^2)$ and fourth $\mathcal{O}(\partial^4)$ order in the gradient expansion, and the more recent one of Ref. [78] as sixth order $\mathcal{O}(\partial^6)$ together with a novel error estimate. The superscripts on the results of Ref. [1] indicate: (i) comoving expansion, and (ii) symmetric expansion, as discussed in the main text.

2.2.2 Model B

This subsection presents results which have already been published in Ref. [1].

We consider the LGW free energy (2.88), which means that the static critical properties are the same as in Model A. In Model B, on the other hand, the order parameter ϕ is locally conserved, so it satisfies a continuity equation,

$$\frac{\partial \phi}{\partial t} + \boldsymbol{\nabla} \cdot \boldsymbol{j}_\phi = 0 \,. \tag{2.98}$$

For small deviations from the equilibrium state, the constitutive relation for the current $\boldsymbol{j}_\phi$ can be taken as

$$\boldsymbol{j}_\phi = -\sigma \boldsymbol{\nabla} \frac{\delta F}{\delta \phi} - \boldsymbol{\zeta} \,, \tag{2.99}$$

where σ denotes the order-parameter mobility, and $\boldsymbol{\zeta}$ is a Gaussian noise characterized by

$$\langle \zeta^i(t, \boldsymbol{x}) \rangle = 0 \,, \quad \langle \zeta^i(t, \boldsymbol{x}) \zeta^j(t', \boldsymbol{x}') \rangle = 2\sigma T \, \delta^{ij} \delta(t - t') \delta(\boldsymbol{x} - \boldsymbol{x}') \,, \tag{2.100}$$

which ensures that the system relaxes to the equilibrium distribution $e^{-F/T}$. With (2.99), the continuity equation (2.98) becomes

$$\frac{\partial \phi}{\partial t} = \sigma \boldsymbol{\nabla}^2 \frac{\delta F}{\delta \phi} + \boldsymbol{\nabla} \cdot \boldsymbol{\zeta} \,. \tag{2.101}$$

This is the original formulation of Model B [46]. The dynamic critical exponent is fixed to be exactly $z = 4 - \eta_\perp$ in this case, since the order-parameter mobility σ turns out to be protected from renormalization due to the diffusive structure of the vertices in the associated MSR action. The dynamic critical exponent thus aligns with the prediction of the 'conventional theory' of critical slowing down here [46], in which the divergence of kinetic coefficients is neglected.

A microscopic realization of Model B was simulated in Ref. [89], and a dynamic critical exponent close to $z = 4 - \eta_\perp$ was indeed observed in the infrared part of the spectral functions near the critical point. Moreover, the authors were able to extract scaling functions which describe the universal frequency, momentum and temperature dependence of the critical spectral functions, in accordance with the dynamic scaling hypothesis (2.94).

Model B can be realized in another way which is particularly relevant for QCD, as was shown by Son and Stephanov [47], which we review in the remainder of this subsection. In QCD, the chiral order parameter $\phi \sim \bar{q}q - \langle \bar{q}q \rangle_c$ is not conserved,[15] but there are other conserved densities such as the baryon density $n \sim \bar{q}\gamma^0 q - \langle \bar{q}\gamma^0 q \rangle_c$.[16] Hence, in the absence of the baryon density and any other conserved densities, one would write down the relaxational equation of motion (2.90) for ϕ, with the LGW free energy (2.88), leading to Model-A dynamics. In QCD, however, there is the conserved baryon density n, and based on the general discussion from the beginning of this section, we have to take into account the interactions of ϕ with n. How does the interaction look like? At finite baryon chemical potential and quark masses there is no symmetry that forbids

[15] Here the subscript $_c$ denotes the (finite) value at the critical point.

[16] For the purpose of this subsection we neglect any other conserved quantities, in particular, energy and momentum. On the other hand, the conserved iso-vector current associated with the $SU(2)_V$ symmetry turns out to be RG irrelevant [37, 47].

mixing of ϕ and n, see e.g. Ref. [159] for a recent discussion. As such, we can imagine that (2.88) is the result of integrating out the conserved baryon density n in

$$F = \int d^d x \left\{ \frac{1}{2}(\boldsymbol{\nabla}\phi)^2 + \frac{\tilde{m}^2}{2}\phi^2 + \frac{\lambda}{4!}\phi^4 + B\phi n + \frac{1}{2\chi_0}n^2 \right\} \tag{2.102}$$

with real parameters $\tilde{m}^2$, B and χ_0. Here we have included the leading-order terms in an expansion of n. We have neglected terms involving gradients of n, since these will turn out to not affect the dynamic critical behavior [47]. However, the $(\boldsymbol{\nabla}\phi)^2$ and ϕ^4 terms must be kept since they are responsible for triggering the phase transition in the first place. With n added to the system, the equilibrium partition function (2.89) becomes

$$Z_{eq} = \int \mathcal{D}\phi\, \mathcal{D}n\, e^{-F/T}\,. \tag{2.103}$$

One can explicitly verify that, by evaluating the Gaussian integral over n, the standard ϕ^4 LGW free energy (2.88) is recovered, albeit with the mass parameter $m^2 = \tilde{m}^2 - B^2\chi_0$, where the finite offset $-B^2\chi_0$ comes from the mixing of ϕ with n. Hence, the static universality class (Z_2) is not altered. Moreover, due to the mixing of ϕ and n, the conserved density n is an equally good order parameter concerning static critical behavior. In particular, its expectation value $\langle n\rangle$ is discontinuous across the first-order transition, and it inherits the critical fluctuations from ϕ, which implies, e.g., $\langle n^2\rangle \sim \xi^{2-\eta_\perp}$ for its variance.

To determine the *dynamic* universality class, it is sufficient to employ the mean-field approximation (MFA) for our purposes here. Since the self-consistently determined squared mass m^2 behaves linearly with the reduced temperature $m^2 \sim \tau$ near $\tau = 0$, and with the correlation length ξ being given by $\xi \sim 1/m$ for $m^2 > 0$, we obtain $\xi \sim \tau^{-\nu}$ with the mean-field critical exponent $\nu = 1/2$ near the critical point. Moreover, as usual in mean-field theory, $\eta_\perp = 0$. Importantly, the individual parameters $\tilde{m}^2$, B, and χ_0 stay finite at the critical point, only the specific combination $m^2 = \tilde{m}^2 - B^2\chi_0$ vanishes, i.e., the determinant of the quadratic form in (2.102) in (ϕ, n) field space [47].

We now turn to the dynamics. Since n is the density of a conserved charge, it must fulfill a continuity equation of the form

$$\frac{\partial n}{\partial t} + \boldsymbol{\nabla}\cdot\boldsymbol{j}_n = 0\,. \tag{2.104}$$

For small deviations from equilibrium the current $\boldsymbol{j}_n$ is given by the constitutive relation[17]

$$\boldsymbol{j}_n = -\lambda_n \boldsymbol{\nabla}\frac{\delta F}{\delta n} - \boldsymbol{\zeta}\,, \tag{2.105}$$

in which λ_n is the baryon conductivity, and the moments of the Gaussian noise $\boldsymbol{\zeta}$ are set by the FDR, as specified in (2.107) below. The equation of motion for ϕ can be seen as a generalization of (2.90) and is given by

$$\frac{\partial \phi}{\partial t} = -\Gamma^\phi \frac{\delta F}{\delta \phi} + \xi\,, \tag{2.106}$$

[17] A priori, there is no reason for the off-diagonal kinetic coefficients to vanish, which would allow a contribution from $\delta F/\delta\phi$ here as well. However, as it turns out [47] such off-diagonal terms do not affect the dynamic universality class, and we thus neglect them here from the beginning.

The noise correlators are fixed by the FDR,

$$\langle \xi(t,\boldsymbol{x})\xi(t',\boldsymbol{x}')\rangle = 2\Gamma^{\phi}T\,\delta(t-t')\delta(\boldsymbol{x}-\boldsymbol{x}')\,, \tag{2.107a}$$

$$\langle \xi(t,\boldsymbol{x})\zeta^{i}(t',\boldsymbol{x}')\rangle = 0\,, \tag{2.107b}$$

$$\langle \zeta^{i}(t,\boldsymbol{x})\zeta^{j}(t',\boldsymbol{x}')\rangle = 2\lambda_n T\,\delta^{ij}\delta(t-t')\delta(\boldsymbol{x}-\boldsymbol{x}')\,. \tag{2.107c}$$

Upon linearization of the equations of motion (2.104) and (2.106) around $\phi = n = 0$ and an expansion to leading order in $\boldsymbol{\nabla}$ we obtain

$$\partial_t\phi = -\Gamma^{\phi}(\tilde{m}^2\phi + Bn) + \xi\,, \tag{2.108a}$$

$$\partial_t n = \lambda_n\boldsymbol{\nabla}^2(B\phi + n/\chi_0) + \boldsymbol{\nabla}\cdot\boldsymbol{\zeta}\,. \tag{2.108b}$$

The eigenfrequencies of this linear system, to leading order in $\boldsymbol{p}$ (after Fourier transform), are given by

$$\omega_1(\boldsymbol{p}) = -iD_{\text{eff}}\boldsymbol{p}^2\,, \qquad \omega_2(\boldsymbol{p}) = -i\Gamma^{\phi}\tilde{m}^2\,, \tag{2.109}$$

which correspond to a diffusion mode and a relaxational mode, respectively. In particular, for the former one finds the effective diffusion coefficient $D_{\text{eff}} = \lambda_n m^2/(\chi_0\tilde{m}^2)$ [47]. As one can see, D_{eff} is proportional to m^2, and thus vanishes at the critical point.[18] On the other hand, the damping rate Γ^{ϕ} stays finite, at least on mean-field level [1]. The modes in (2.109) can be physically interpreted by analyzing the corresponding (right) eigenvectors, which read (at $\boldsymbol{p} = 0$) [47]

$$\boldsymbol{v}_1 = \begin{pmatrix} -B \\ \tilde{m}^2 \end{pmatrix}\,, \qquad \boldsymbol{v}_2 = \begin{pmatrix} 1 \\ 0 \end{pmatrix}\,. \tag{2.110}$$

First, the eigenfrequencies (2.109) entail that at sufficiently small wavenumbers $\boldsymbol{p}$ and long timescales only the diffusive mode ω_1 survives, since it becomes much slower than the non-conserved mode ω_2. In particular, the latter has effectively died off after its relaxation time $1/(\Gamma^{\phi}\tilde{m}^2)$, which in the long-wavelength limit $\boldsymbol{p}\to 0$ is guaranteed to become much smaller than the $\boldsymbol{p}$-dependent relaxation time $1/(D_{\text{eff}}\boldsymbol{p}^2)$ of the diffusive mode. The eigenmode that is left ($\boldsymbol{v}_1$ in Eq. (2.110)) involves ϕ and n in fixed proportion, $\phi = -(B/\tilde{m}^2)n$. Hence, concerning dynamic critical behavior, one can integrate out the fast chiral order parameter ϕ and focus on the slow (diffusive) dynamics of n.[19]

In general, both these modes can reflect the singular behavior near criticality at the second-order phase transition. For the diffusive mode, the usual argument is as follows: For wavevectors $|\boldsymbol{p}| \gg \xi^{-1}$ the critical singularity is manifest, $\omega_1(\boldsymbol{p}) \sim |\boldsymbol{p}|^z$. For smaller wavevectors $|\boldsymbol{p}| \ll \xi^{-1}$, on the other hand, the dispersion relation is regular and given by (2.109). Requiring these two limits to match smoothly at $|\boldsymbol{p}| \sim \xi^{-1}$, and with $D_{\text{eff}} \sim m^2 \sim \xi^{-2}$, one finds $\omega_1 = -iD_{\text{eff}}\xi^{-2} \sim \xi^{-4}$. In contrast, $\tilde{m}^2$ and Γ^{ϕ} stay finite, which means that the relaxational mode ω_2 in (2.109) does so as well. Hence, it is the diffusive mode that becomes critical, giving rise to Model-B dynamics in the infrared, with dynamic critical exponent $z = 4 - \eta_\perp$ (with $\eta_\perp = 0$ in the MFA).

The spectral function $\rho(\omega,\boldsymbol{p})$ of the order parameter reflects dynamic critical behavior according to the dynamic scaling hypothesis (2.94). The retarded propagator (2.93) is explicitly given by (after Fourier transform and partial fraction decomposition, see Ref. [1])

$$G^R(\omega,\boldsymbol{p}) = -\frac{i\Gamma^{\phi}(\omega + iD_0\boldsymbol{p}^2)}{\omega_2(\boldsymbol{p}) - \omega_1(\boldsymbol{p})}\left(\frac{1}{\omega-\omega_1(\boldsymbol{p})} - \frac{1}{\omega-\omega_2(\boldsymbol{p})}\right)\,, \tag{2.111}$$

[18] Recall that $\tilde{m}^2$ and χ_0 stay *finite* at the critical point.

[19] In Sec. 2.2.4 we shall see that, with the energy-momentum tensor included, the ω_1 mode is better thought of as the diffusion of entropy per baryon.

with the 'bare' diffusion coefficient $D_0 \equiv \lambda_n/\chi_0$. Correspondingly, the spectral function (2.92) near the critical point is given by

$$\rho(\omega, \boldsymbol{p}) \approx \frac{1}{\pi} \frac{D_0 \boldsymbol{p}^2 \omega}{\tilde{m}^2(\omega^2 + (D_{\text{eff}}\boldsymbol{p}^2)^2)} + \frac{1}{\pi} \frac{\Gamma^\phi \omega}{\omega^2 + (\Gamma^\phi \tilde{m}^2)^2}\,, \tag{2.112}$$

where we have used that near the critical point $D_{\text{eff}} \ll D_0$, and that typical wavevectors are of order $|\boldsymbol{p}| \sim \xi^{-1}$ (or smaller) such that $D_0\boldsymbol{p}^2 \ll \Gamma^\phi \tilde{m}^2$, in addition. Here we can see that it consists of two terms, corresponding to contributions from the diffusive mode ω_1 and the relaxational mode ω_2 in (2.109), which are peaked at $\omega \sim D_{\text{eff}}\boldsymbol{p}^2$ and $\omega \sim \Gamma^\phi \tilde{m}^2$, respectively. As stated above, it is the diffusive mode which becomes critical, and thus it is the first term in (2.112) which fulfills the dynamic scaling hypothesis (2.94) and is correspondingly described by a universal scaling function such as (2.95) or (2.96) near the critical point (albeit of mean-field form here, see the discussion below).

This formulation of Model B after Son and Stephanov has been studied with the real-time FRG in Ref. [1]. In particular, the equations of motion considered in Ref. [1] are given by

$$\partial_t^2 \phi + \gamma \partial_t \phi = -\frac{\delta F}{\delta \phi} + \xi\,, \tag{2.113a}$$

$$\tau_R \partial_t^2 n + \partial_t n = \lambda_n \boldsymbol{\nabla}^2 \frac{\delta F}{\delta n} + \boldsymbol{\nabla} \cdot \boldsymbol{\zeta}\,, \tag{2.113b}$$

with the free energy (2.102), which in addition include a second-order time derivative in the equation of motion for ϕ (2.113a), and a finite Israel-Stewart-type relaxation time τ_R in the equation of motion for n (2.113b), to exclude propagation at superluminal velocities [160]. The damping constant $\gamma = 1/\Gamma^\phi$ is inversely related to the damping rate Γ^ϕ from above. The equation of motion (2.113b) for the conserved density n represents the relaxation equation for the associated baryon current $\boldsymbol{j}_n$,

$$\partial_t \boldsymbol{j}_n = -\frac{1}{\tau_R}\left(\boldsymbol{j}_n + \lambda_n \boldsymbol{\nabla} \frac{\delta F}{\delta n} + \boldsymbol{\zeta}\right), \tag{2.114}$$

so that $\partial_t n + \boldsymbol{\nabla}\cdot\boldsymbol{j}_n = 0$ as in (2.104) and the total baryon number $Q = \int d^d x\, n(\boldsymbol{x})$ in the system is conserved.

In Ref. [1] spectral functions of the order parameter ϕ were computed with the real-time FRG using the combined vertex and loop expansion (i) around the comoving minimum from above. Corresponding exemplary results are shown in Fig. 2.4 for two temperatures: somewhat below the critical temperature in Fig. 2.4 (a) on the left, and approximately at the criticality in (b) on the right. The spectral function essentially consists of two modes: First, there is the quasi-particle pole of the non-conserved but massive order-parameter fluctuations which is gapped in the long-wavelength limit, corresponding to ω_2 in (2.109). Secondly, and more interestingly, already in Fig. 2.4 (a) there is a gapless mode with diffusive dispersion relation $\omega \sim \boldsymbol{p}^2$, corresponding to ω_1 in (2.109). This is of course due to the mixing of the order parameter fluctuations with those of the conserved (baryon) density.

If we now tune the temperature very close to the critical one, as shown in Fig. 2.4 (b), we observe that in contrast to Models A (cf. Fig. 2.3) the quasi-particle ridge stays gapped here. In particular, no power-law divergence builds up for $\boldsymbol{p} \to 0$, which means that (2.97) does not apply, in contrast to Model A. As such, the $\boldsymbol{p} = 0$ part of the critical spectral function is not described by the dynamic scaling functions in Eqs. (2.95), (2.96), here. What actually does

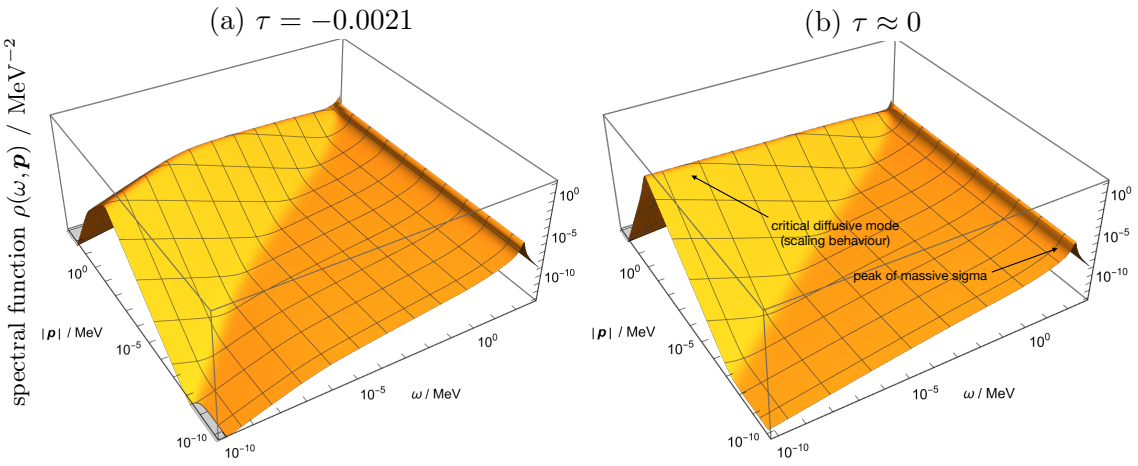

Figure 2.4: Non-critical (a) and critical (b) spectral functions of Model B in $d = 3$ spatial dimensions, realized after Son and Stephanov [47] by coupling a conserved density linearly to the non-conserved order parameter. We see that near the critical temperature in (b) the chiral order parameter stays massive. Indeed, it is instead the diffusive mode ω_1 which emerges as a mixture of fluctuations in the baryon density and fluctuations in the chiral order parameter which becomes critical, and gives rise to critical scaling behavior, as visible in (b), where the spectral function obeys the scaling hypothesis (2.94) with mean-field exponents $\eta_\perp = 0$ and $z = 4$. For details we refer to Ref. [1].

becomes critical is the part of the spectral function induced by the mixing with the conserved (baryon) density, as discussed above. We first note that the dispersion relation of the diffusive peak changes from $\omega \sim |\boldsymbol{p}|^2$ in Fig. 2.4 (a) to $\omega \sim |\boldsymbol{p}|^z$ in Fig. 2.4 (b), here with the mean-field exponent $z = 4$ because of the gradient expansion that was used in Ref. [1] for the $\boldsymbol{p}$ dependence of the 2-point function. Moreover, the $\boldsymbol{p}$ dependence of this diffusive peak is described by the dynamic scaling functions in (2.95), (2.96) (here with $\tau \approx 0$), e.g., by

$$\rho(\omega, \boldsymbol{p}, 0) = \bar{\omega}^{-\sigma} \, f_\omega(x, 0) \, . \tag{2.115}$$

This scaling function was numerically determined in Ref. [89] to be very well described by

$$f_\omega(x, 0) = \rho_0 \, \frac{x^{-\sigma}}{x^{-1} + x} \, , \quad x = \bar{p}^z / \bar{\omega} \, , \tag{2.116}$$

with some non-universal normalization ρ_0, yielding

$$\rho(\omega = \text{const.}, \boldsymbol{p}, 0) \propto \frac{\bar{p}^{-(2-\eta_\perp)}}{\bar{\omega}/\bar{p}^z + \bar{p}^z/\bar{\omega}} \, . \tag{2.117}$$

This diffusive part of the spectral function at criticality is thus exactly described by the scaling hypothesis (2.94), in the case of the spectral function in Fig. 2.4 (b) albeit with mean-field exponents $\eta_\perp = 0$ and $z = 4$, as discussed above.

In summary, the Model B spectral function in Fig. 2.4 nicely illustrates how both features discussed by Son and Stephanov in Ref. [47] as a result of the mixing of the chiral order parameter field with the baryon density fluctuations near the critical point in the phase diagram of QCD, are combined in a single spectral function: The quasi-particle peak, which represents the fast and gapped fluctuations of the chiral condensate, and which practically instantaneously adjusts to the slow diffusive critical mode representing the mixture between chiral condensate and baryon-density fluctuations that gives rise to Model B dynamics (without the coupling to the shear modes in the energy-momentum tensor in QCD).

2.2.3 Model C

This subsection presents results which have already been published in Ref. [1].

Historically, it was argued by Berdnikov and Rajagopal in Ref. [42] that the dynamic universality class of the QCD critical point should be that of Model C, when they analyzed critical slowing down and off-equilibrium phenomena in heavy-ion collisions. The question was later revisited by Son and Stephanov in Ref. [47], where they argued in favor of Model H. The original argument behind Model C in Ref. [42] was built on the assumptions that the chiral order parameter ϕ is not conserved, that there are other conserved densities in the system such as the baryon density, and that there are no Poisson brackets between the order parameter and the conserved densities. In addition, chiral symmetry would suggest an invariance of the LGW free energy under a Z_2 transformation $\phi \to -\phi$, and hence the conserved density could only couple to an invariant like the square ϕ^2 of the order-parameter field. With such a coupling to the conserved density, the LGW free energy (2.88) becomes

$$F = \int d^d x \left\{ \frac{1}{2}(\boldsymbol{\nabla}\phi)^2 + \frac{m^2}{2}\phi^2 + \frac{\lambda}{4!}\phi^4 + \frac{v}{2}\phi^2 n + \frac{n^2}{2\chi_0} \right\} . \tag{2.118}$$

and the equations of motion correspond to the prototypical formulation of Model C [46],

$$\frac{\partial \phi}{\partial t} = -\Gamma^\phi \frac{\delta F}{\delta \phi} + \xi \,, \tag{2.119a}$$

$$\frac{\partial n}{\partial t} = \lambda_n \boldsymbol{\nabla}^2 \frac{\delta F}{\delta n} + \boldsymbol{\nabla} \cdot \boldsymbol{\zeta} \,. \tag{2.119b}$$

In Model C, mixing of ϕ and n is forbidden by the reflection symmetry $\phi \to -\phi$ of the order parameter. In contrast, when such linear coupling terms appear in the free energy, as in Eq. (2.102) above, they fundamentally change the infrared structure of the theory, and subsequently the dynamic universality class to that of Model B, as we have seen explicitly in Sec. 2.2.2. Due to the non-linear coupling between ϕ^2 and n, on the other hand, compared to Model B, the interpretation of the conserved density changes: In the context of microscopic ϕ^4-theories, such a conserved density n is usually interpreted as representing the critical fluctuations in the energy density of the system, because it couples to the operator ϕ^2 which is the most singular part of the canonical energy density T^{00} (see e.g. Chapter 36 of Ref. [137]). As usual, the equilibrium fluctuations $\langle n^2 \rangle$ of the energy density are related to the specific heat $C \sim \langle n^2 \rangle$, so both admit the same critical behavior. In particular, if the specific heat exponent $\alpha > 0$ is positive (as it is the case with Ising universality in $d = 2, 3$ spatial dimensions), we have $C \sim |\tau|^{-\alpha}$ in the critical regime, and thus also a diverging susceptibility, $\langle n^2 \rangle \sim \chi_0 \sim |\tau|^{-\alpha}$.

To discuss dynamic critical behavior, one can analyze the time-dependent response of the system to external perturbations. For non-critical momenta $|\boldsymbol{p}| \ll \xi^{-1}$ the equations (2.119) may be linearized, which yields the eigenfrequencies

$$\omega_\phi = -i\Gamma^\phi m^2 \quad \text{and} \quad \omega_n = -i\lambda_n \boldsymbol{p}^2/\chi_0 \,, \tag{2.120}$$

but with renormalized parameters Γ^ϕ, m^2, λ_n, and χ_0, in the sense that fluctuations of modes with wavenumbers down to ξ^{-1} have been taken into account. Near the critical point, the eigenfrequencies are expected to behave as $\omega_\phi \sim \xi^{-z_\phi}$ and $\omega_n \sim \xi^{-z_n}$ at the characteristic momentum scale $|\boldsymbol{p}| \sim \xi^{-1}$, with the dynamic critical exponents z_ϕ and z_n. On the other hand, for $|\boldsymbol{p}| \gg \xi^{-1}$ the critical power law is already manifest, and one expects the non-analytic

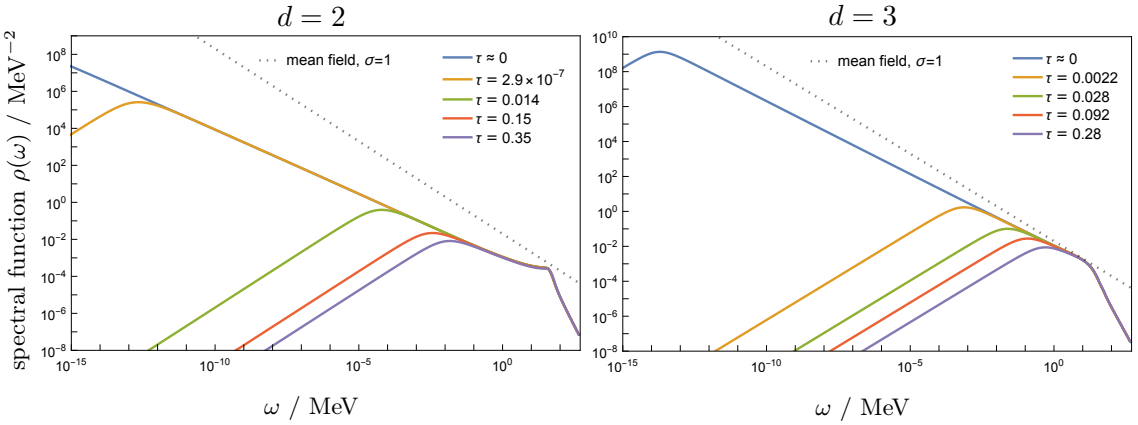

Figure 2.5: Critical infrared power-law (2.97) in the spectral function Model C in $d = 2$ (left) and $d = 3$ (right) spatial dimensions at vanishing momentum gradually builds up for $T \to T_c$, when approaching the critical temperature from above. Mean-field results are shown as dotted gray lines for comparison. For details on the truncation we refer to Sec. 3.3.1 of Ref. [1].

behavior $\omega_\phi \sim |\boldsymbol{p}|^{z_\phi}$ and $\omega_n \sim |\boldsymbol{p}|^{z_n}$. Analogous to Model B, one can verify diagrammatically that the mobility λ_n of the diffusive energy density n receives no loop corrections, and thus stays finite at the critical point [161]. Hence, using (2.120) right at its boundary of validity $|\boldsymbol{p}| \sim \xi^{-1}$, one can deduce that ω_n behaves as $\omega_n \sim \xi^{-(2+\alpha/\nu)}$, using that $\chi_0 \sim |\tau|^{-\alpha}$ and $\xi \sim |\tau|^{-\nu}$, which implies $z_n = 2 + \alpha/\nu$. Finally, to determine the dynamic critical exponent z_ϕ of the order parameter, note that in the case of a one-component order parameter Model C has a strong-scaling fixed point, which means that the dynamic critical exponents are locked to the same value, $z_\phi = z_n = 2 + \alpha/\nu$ [104]. From this result we can conclude that the dynamic critical behavior is mainly driven by the static critical behavior of the susceptibility χ_0 of n. In $d = 3$ spatial dimensions, this would imply the value $z \approx 2.17$ for the dynamic critical exponent, inserting $\alpha \approx 0.11$ and $\nu \approx 0.63$ for the $3d$ Ising model [162]. An analysis of Model C with the ϵ-expansion was later performed, e.g., in Ref. [163], and an FRG study was performed, e.g., in Ref. [83]. Moreover, scaling functions that describe the universal temperature, momentum, and frequency dependence of the order-parameter spectral function at criticality were computed by simulating a classical-statistical ϕ^4-theory with Hamiltonian dynamics in Ref. [88], following the precursor study of Ref. [86].

Here we want to particularly focus on Ref. [1], where the critical spectral functions of Model C were computed using the real-time FRG. In particular, the expected IR power-law behavior (2.97) applies to Model C as well, but of course with the Model-C exponent of $z_\phi = 2 + \alpha/\nu$. The results of Ref. [1] are shown in Fig. 2.5 for various reduced temperatures τ. The emerging IR power law is clearly visible as one approaches the critical point from above, $\tau \to 0$, and corresponds to the exponent $z = 2.56$ in two spatial dimensions, and $z = 2.31$ in three spatial dimensions, respectively. This is to be compared with the exact result $z = 2$ in two spatial dimensions (from Onsager's solution of the two-dimensional Ising model [153]), and $z = 2+\alpha/\nu \approx 2.17$ in three spatial dimensions, where for the latter one may insert the known numerical result for $\nu = 0.629971(4)$ [157, 158] and use the hyperscaling relation $\alpha = 2 - \nu d$ for the specific heat exponent. While the three-dimensional result from Ref. [1] has the qualitatively correct property of being larger than the Model-A value of $z = 2 + c\eta_\perp$ [46], such that the ordering of the two Models is captured correctly the truncations, this is not the case in two spatial dimensions. The rather large discrepancy from the exact value can be attributed to the

difficulty of reproducing the specific heat exponent α with the FRG, since α vanishes in the two-dimensional Ising model, whereas the FRG result corresponds to $\alpha/\nu \approx 0.56$. In fact, the result of Ref. [1] more closely resembles the result from 1^{st}-order ϵ-expansion (with $\epsilon = 4 - d$), where one has $z = 2 + \epsilon/3 + \mathcal{O}(\epsilon^2)$ [46]. One obtains the same result from linearizing the static FRG flow equations of Ref. [1] around the Wilson-Fisher fixed point.

We close this subsection by commenting on the realization of Model C in QCD. The issue with the original argument [42] behind Model C being the dynamic universality class of the QCD critical point was pointed out in Ref. [47]: At finite quark masses and finite baryon chemical potential, chiral symmetry and charge-conjugation symmetry are explicitly broken. The absence of these symmetries allows for mixing between the chiral order parameter and the baryon density [159], leading instead to Model B (if the fluctuations of energy and momentum are neglected, see Sec. 2.2.2 above) [47]. In contrast, in the *chiral limit* of two-flavor QCD exact chiral symmetry indeed forbids mixing between the fluctuations of chiral order parameter and baryon density, which would suggest Model C for a single component order-parameter field with Z_2 universality by this argument. However, with static $O(4)$ universality in the two-flavor chiral limit of QCD, on the other hand, the specific-heat exponent α is negative, so that the coupling to the conserved energy density turns out to be irrelevant in the sense of the renormalization group [163]. Moreover, there are then six conserved (iso-vector and iso-axial-vector) currents with non-trivial reversible mode couplings which ultimately put the $O(4)$ transition of QCD with two massless quarks in the dynamic universality class of Model G [62], which we shall discuss in more detail in Sec. 2.2.5 below.

2.2.4 Model H

In this subsection, we review the argument behind Model H [111] being the dynamic universality class of the QCD critical point [47, 164].

The full hydrodynamic theory of QCD matter at finite temperature and baryon chemical potential involves also the energy density ε and the momentum density $\boldsymbol{j}$, in addition to the baryon density n from Sec. 2.2.2. It is convenient to decompose the momentum density $\boldsymbol{j} = \boldsymbol{j}_\parallel + \boldsymbol{j}_\perp$ into longitudinal and transverse parts, denoted as $\boldsymbol{j}_\parallel$ and $\boldsymbol{j}_\perp$, respectively, fulfilling $\boldsymbol{\nabla} \times \boldsymbol{j}_\parallel = 0$ and $\boldsymbol{\nabla} \cdot \boldsymbol{j}_\perp = 0$. A linearization $\varepsilon = \varepsilon_0 + \delta\varepsilon$, $n = n_0 + \delta n$ and $\boldsymbol{j} = \delta\boldsymbol{j}$ of the hydrodynamic equations around a global equilibrium state yields five eigenmodes [165]: First, there are two modes with linear dispersion relation $\omega \sim \pm v_s|\boldsymbol{p}|$, where v_s denotes the speed of sound, which constitute the propagating sound wave. An analysis of the corresponding eigenvectors reveals that these are a mixture of fluctuations of pressure δp and fluctuations of the longitudinal component $\delta\boldsymbol{j}_\parallel$ of the momentum density [166]. Second, there is a heat mode with dispersion relation $\omega \sim D_p\boldsymbol{p}^2$ which describes the diffusion of entropy per baryon $\delta\hat{s} \equiv \delta(s/n)$ (also called the specific entropy). The associated diffusion coefficient D_p is called the 'thermal diffusivity' and is related to the heat conductivity κ via $D_p = \kappa/C_p$, where $C_p = Tn(\partial\hat{s}/\partial T)_p$ is the specific heat at constant pressure [44]. In turn, the heat conductivity κ of a charged fluid is related via $\kappa = \lambda_n w^2/(n^2 T)$ to the baryon conductivity λ_n [165]. Finally, there are two viscous shear modes with dispersion relation $\omega \sim \eta\boldsymbol{p}^2/w$, where η denotes the shear viscosity and $w \equiv \varepsilon + p$ the enthalpy density. These describe the diffusion of the two transverse components $\delta\boldsymbol{j}_\perp$ of the momentum density.

Consider the time evolution of an arbitrary perturbation $\delta\varepsilon$, δn, and $\delta\boldsymbol{j}$. First, the two

viscous shear modes decouple from the rest and thus the diffusion of $\delta \boldsymbol{j}_\perp$ can be considered separately. This leaves $\delta\varepsilon$, δn, and $\delta \boldsymbol{j}_\parallel$. The modes contributing to these are the two sound modes and the heat mode. Their relevancy depends on the frequency ω of the fluctuation [167]. At larger frequencies of order $\omega \sim v_s|\boldsymbol{p}| \gg D_p \boldsymbol{p}^2$ the fluctuations of the longitudinal component $\boldsymbol{j}_\parallel$ and the pressure p propagate through the system via sound waves at effectively constant entropy per baryon $\hat{s}$, since the latter is diffusive and thus much slower. On the other hand, at smaller frequencies of order $\omega \sim D_p \boldsymbol{p}^2 \ll v_s|\boldsymbol{p}|$ the sound modes are fast and thus can be integrated out, such that p and $\boldsymbol{j}_\parallel$ can be considered equilibrated, and one only has the diffusion of $\hat{s}$ at constant pressure.

As we have discussed above, due to critical slowing down near a second-order phase transition, the chiral order parameter potentially has to be included in the hydrodynamic description. However, as we have reviewed in Sec. 2.2.2, due to mixing the chiral order parameter simply follows the baryon density on sufficiently long timescales. With energy and momentum included here, we can employ a similar argument: After the chiral order parameter has adjusted to the local value of the baryon density on timescales of order $\sim 1/(\Gamma^\phi \tilde{m}^2)$, the baryon density itself adjusts to the local value of the specific entropy on timescales of order $\sim 1/(v_s|\boldsymbol{p}|)$, such that, on the longest (diffusive) timescales of order $\sim 1/(D_p \boldsymbol{p}^2)$ the specific entropy is the only remaining mode (besides $\boldsymbol{j}_\perp$). As such, in the small-frequency limit the only remaining modes are $\hat{s}$ and $\boldsymbol{j}_\perp$, since the latter is diffusive as well and thus its (non-critical) relaxation time of the same order of magnitude as the one of $\hat{s}$. These are the same modes as in Model H, which is in the same dynamic universality class as the liquid-gas critical point in a pure fluid [46, 168]. In Model H, the order parameter ϕ, most naturally represented by the entropy per baryon $\hat{s}$, has one component, is conserved, and couples reversibly to the transverse component $\boldsymbol{j}_\perp$ of the conserved momentum density of the fluid.

Having identified the slowest modes, it is instructive to inspect their (equilibrium) fluctuations, as given by their thermal variances (here in a finite volume V) [167],

$$V\langle(\delta\hat{s})^2\rangle = \frac{C_p}{n^2}\,, \qquad V\langle(\delta \boldsymbol{j}_\perp)^2\rangle = wT\,. \tag{2.121}$$

The first one diverges at the critical point since the specific heat C_p at constant pressure scales with the correlation length ξ according to $C_p \sim \xi^{2-\eta_\perp}$ with the anomalous dimension $\eta_\perp$ [166], as expected for order-parameter fluctuations, cf. the beginning of this section. On the other hand, the fluctuations of $\boldsymbol{j}_\perp$ stay finite at the critical point. As such, in the free energy (2.88) the momentum density appears simply in the form of a kinetic energy (where the enthalpy w would be replaced with the mass density ρ in the non-relativistic case [169]),

$$F = \int d^dx \left\{ \frac{1}{2}(\boldsymbol{\nabla}\phi)^2 + \frac{m^2}{2}\phi^2 + \frac{\lambda}{4!}\phi^4 + \frac{\boldsymbol{j}_\perp^2}{2w} \right\}. \tag{2.122}$$

Higher-order couplings between ϕ and $\boldsymbol{j}_\perp$ such as $\boldsymbol{j}_\perp^2\phi$, higher-order self-couplings of $\boldsymbol{j}_\perp$ such as $(\boldsymbol{j}_\perp^2)^2$, and terms involving gradients of $\boldsymbol{j}_\perp$, are RG irrelevant [111]. This can be seen by power-counting arguments, using the fact that the static fluctuations of the momentum density in (2.121) are non-critical.

By Noether's theorem, the components of the momentum density $\boldsymbol{j}$ are the generators of spa-

tial translations, so their Poisson-bracket algebra with the order parameter ϕ is given by[20] [140]

$$\{\phi(\boldsymbol{x}), j_l(\boldsymbol{x}')\} = \phi(\boldsymbol{x}')\frac{\partial}{\partial x'_l}\delta(\boldsymbol{x}-\boldsymbol{x}')\,, \tag{2.123}$$

$$\{j_l(\boldsymbol{x}), j_m(\boldsymbol{x}')\} = \left[j_l(\boldsymbol{x}')\frac{\partial}{\partial x'_m} - j_m(\boldsymbol{x})\frac{\partial}{\partial x_l}\right]\delta(\boldsymbol{x}-\boldsymbol{x}')\,. \tag{2.124}$$

With these Poisson brackets, we can express the equations of motion of Model H [46,168] as (in accordance with Eq. (2.83))

$$\frac{\partial\phi}{\partial t} = \sigma\boldsymbol{\nabla}^2\frac{\delta F}{\delta\phi} + g\{\phi, \boldsymbol{j}_\perp\}\cdot\frac{\delta F}{\delta \boldsymbol{j}_\perp} + \theta\,, \tag{2.125a}$$

$$\frac{\partial j_l^\perp}{\partial t} = \mathcal{T}_{lm}\left[\eta\boldsymbol{\nabla}^2\frac{\delta F}{\delta j_m^\perp} + g\{j_m^\perp, \phi\}\frac{\delta F}{\delta\phi} + g\{j_m^\perp, j_n^\perp\}\frac{\delta F}{\delta j_n^\perp}\right] + \xi_l\,, \tag{2.125b}$$

where $\mathcal{T}$ is a transverse projector, which in momentum space acts as $\mathcal{T}_{lm}(\boldsymbol{p}) = \delta_{lm} - p_l p_m/\boldsymbol{p}^2$. The kinetic coefficients start at order $\boldsymbol{\nabla}^2$ since both ϕ and $\boldsymbol{j}_\perp$ dissipate via diffusion, as discussed above, and the prefactors are the order-parameter mobility σ and the shear viscosity η. The Gaussian noise terms θ and $\boldsymbol{\xi}$ have vanishing expectation values and variances set by the FDR,

$$\begin{aligned}\langle\theta(t,\boldsymbol{x})\theta(t',\boldsymbol{x}')\rangle &= -2\sigma T\,\boldsymbol{\nabla}^2\delta(\boldsymbol{x}-\boldsymbol{x}')\delta(t-t')\,,\\ \langle\xi_l(t,\boldsymbol{x})\xi_m(t',\boldsymbol{x}')\rangle &= -2\eta T\,\mathcal{T}_{lm}\boldsymbol{\nabla}^2\delta(\boldsymbol{x}-\boldsymbol{x}')\delta(t-t')\,.\end{aligned} \tag{2.126}$$

By identifying the transverse component of the fluid velocity

$$\boldsymbol{v}_\perp \equiv \frac{\delta F}{\delta \boldsymbol{j}_\perp} = \frac{\boldsymbol{j}_\perp}{\rho}\,,$$

and evaluating the Poisson brackets explicitly according to (2.123) and (2.124), the terms in the equations of motion (2.125) can be individually interpreted as

$$\frac{\partial\phi}{\partial t} = \underbrace{\sigma\boldsymbol{\nabla}^2\frac{\delta F}{\delta\phi} + \theta}_{\text{thermal conduction+noise}} \underbrace{- g\boldsymbol{v}_\perp\cdot\boldsymbol{\nabla}\phi}_{\text{advection}}\,, \tag{2.127a}$$

$$\frac{\partial\boldsymbol{j}_\perp}{\partial t} = \mathcal{T}\Bigg[\underbrace{\eta\boldsymbol{\nabla}^2\boldsymbol{v}_\perp + \boldsymbol{\xi}}_{\text{viscosity+noise}} + \underbrace{g(\boldsymbol{\nabla}\phi)\frac{\delta F}{\delta\phi}}_{\text{reversibility}} - \underbrace{g(\boldsymbol{v}_\perp\cdot\boldsymbol{\nabla})\boldsymbol{j}_\perp}_{\text{convection}}\Bigg]\,, \tag{2.127b}$$

We go through the individual terms in order, from left to right, by comparing with non-relativistic hydrodynamics, starting with the equation of motion (2.127a) for the order parameter ϕ. The first term in (2.127a) is analogous to the general equation of heat transfer [169], since $\delta F/\delta\phi$, as the thermodynamically conjugate to $\phi \sim \delta\hat{s}$, is proportional to fluctuations δT of the system's local temperature. By Fourier's law of thermal conduction, a temperature gradient generally leads to a heat current $\delta\boldsymbol{q} = -\kappa\boldsymbol{\nabla}\delta T$ with the heat conductivity κ, and a divergence in $\delta\boldsymbol{q}$ in turn leads to a local change in entropy, $nT\partial_t\delta\hat{s} = -\boldsymbol{\nabla}\cdot\delta\boldsymbol{q} = \kappa\boldsymbol{\nabla}^2\delta T$. The first term on the right-hand side of (2.127a) is of this form, which allows us to relate the order-parameter mobility σ with the heat conductivity κ of the corresponding fluid. The noise θ is fixed by the FDR in local thermal equilibrium, see (2.126). Finally, the reversible term in (2.127a) which comes from

[20] For completeness, we note here that although the Poisson bracket (2.124) between different components of the momentum density $\boldsymbol{j}$ is non-vanishing, the Poisson brackets of the *total* momentum $\boldsymbol{J} \equiv \int d^dx\,\boldsymbol{j}(\boldsymbol{x})$ vanish, $\{J_l, J_m\} = 0$.

the Poisson bracket $\{\phi, j_l\}$ in (2.125a) describes advection of the order parameter by the fluid velocity.

The second equation (2.127b) is basically the transverse component of the general continuity equation for the momentum density,

$$\frac{\partial j_l}{\partial t} = -\frac{\partial T_{lk}}{\partial x_k}\,, \tag{2.128}$$

with the stress tensor T_{lk}, such that the individual terms on the right-hand side of (2.127b) can be traced back to corresponding terms in the constitutive equation of T_{lk}. We shall omit all terms from T_{lk} that are proportional either to $\boldsymbol{\nabla}\cdot\boldsymbol{v}$, or to δ_{lk}, since the former only involves the longitudinal part of the momentum density (which is assumed to be integrated out), and the latter would correspond to a total gradient in (2.128) which vanishes upon transversal projection. With this in mind, the terms on the right-hand side of (2.127b) correspond to the following terms in the stress tensor (in the same order) [51],

$$T_{lk} = -\eta\left(\frac{\partial v_l}{\partial x_k} + \frac{\partial v_k}{\partial x_l}\right) - s_{lk} + g(\partial_l\phi)\partial_k\phi + g\rho v_l v_k + \cdots \tag{2.129}$$

where s_{lk} is a Gaussian noise whose variance is fixed by the FDR,

$$\begin{aligned}\langle s_{lk}(t,\boldsymbol{x})\rangle &= 0\,,\\ \langle s_{lk}(t,\boldsymbol{x})s_{ij}(t,\boldsymbol{x}')\rangle &= 2\eta T(\delta_{li}\delta_{kj}+\delta_{lj}\delta_{ki})\delta(\boldsymbol{x}-\boldsymbol{x}')\delta(t-t')\,,\end{aligned}$$

and is related to the noise ξ_l in (2.127b) via $\xi_l = -\mathcal{T}\partial_k s_{lk}$. In particular, the reversible term stemming from the Poisson bracket $\{j_l, \phi\}$ in (2.127b) describes the back-reaction on $\boldsymbol{j}_\perp$ from the advection of ϕ, and is needed to ensure the exact conservation of F during ideal time evolution. It can be understood as a contribution from the canonical stress tensor of the scalar field ϕ in (2.129). By inserting the explicit form (2.122) of F, one can verify that this term evaluates to $-g(\boldsymbol{\nabla}\phi)\boldsymbol{\nabla}^2\phi$ in the equation of motion (2.127b). Being of third order in gradients, it goes beyond the standard Navier-Stokes equations [169]. Finally, the reversible self-interaction corresponding to the Poisson bracket $\{j_l, j_m\}$ in (2.127b) describes convection, and corresponds to the last term in (2.129).

Near the critical point the kinetic coefficients are expected to behave as $\sigma \sim \xi^{x_\sigma}$, $\eta \sim \xi^{x_\eta}$. In contrast to Model B, the order-parameter mobility σ itself diverges at the critical point and thus the dynamic critical exponent $z_\phi = 4 - \eta_\perp - x_\sigma$ of Model H is generally smaller than the dynamic critical exponent $z = 4 - \eta_\perp$ of Model B. In particular, x_σ and x_η are not independent since their sum is fixed by the following (hyper-)scaling relation [111],

$$x_\sigma + x_\eta = 4 - d - \eta_\perp\,. \tag{2.130}$$

This relation can be intuitively understood by the following heuristic argument based on mode-coupling theory [46]. First, without reversible mode couplings, i.e., for $g = 0$, the equation for ϕ in (2.125a) reduces to the one (2.101) of Model B, where σ does not diverge, $x_\sigma = 0$, leading to $z = 4 - \eta_\perp$. In Model H, on the other hand, $g \neq 0$ means that the order parameter is reversibly coupled to the fluctuating momentum density of the surrounding fluid. To see the difference to Model B in this case, first note that σ generally measures the linear response of the order-parameter current (2.99) to an inhomogeneous external source $H(\boldsymbol{x})$ applied in the free energy (2.88),

$$F \to F - \int d^d x\, H(\boldsymbol{x})\phi(\boldsymbol{x}) \tag{2.131}$$

causing

$$\boldsymbol{j}_\phi = \sigma \boldsymbol{\nabla} H \,. \tag{2.132}$$

Consider the contribution to σ in (2.132) from a region of the fluid whose volume is of order of a correlation volume $V \sim \xi^d$. Since correlations in the fluid are limited to regions of this size one can assume that the region moves approximately as a rigid body. Denote by $\bar{\phi}$ the order parameter averaged over this region. Due to the reversible mode coupling in (2.127b) there is an applied force $\boldsymbol{F}_{\text{appl}}$ on the region,

$$\boldsymbol{F}_{\text{appl}} \sim g\bar{\phi}\boldsymbol{E}\xi^d \,,$$

which causes the region to accelerate until the dissipative force due to viscous drag

$$\boldsymbol{F}_{\text{visc}} \sim -\eta \boldsymbol{v} \xi^{d-2}$$

balances the applied force, $\boldsymbol{F}_{\text{appl}} + \boldsymbol{F}_{\text{visc}} = 0$, leading to a terminal velocity of order $\boldsymbol{v} \sim (g\bar{\phi}\xi^2/\eta)\boldsymbol{E}$. Since the order parameter is advected by the moving fluid, cf. (2.127a), there is the resulting current

$$\boldsymbol{j}_\phi = g\bar{\phi}\boldsymbol{v} \sim \frac{g^2\bar{\phi}^2\xi^2}{\eta}\boldsymbol{E} \,. \tag{2.133}$$

By taking the thermal average over this expression, using the equipartition theorem $\langle\bar{\phi}^2\rangle = T\chi_\phi/\xi^d$, and comparing to (2.132), we find

$$\sigma \sim \frac{g^2 T \chi_\phi \xi^{2-d}}{\eta} \,.$$

Since the static order-parameter susceptibility χ_ϕ behaves as $\chi_\phi \sim \xi^{2-\eta_\perp}$ near the critical point, we thus get

$$\sigma\eta \sim \chi_\phi \xi^{2-d} \sim \xi^{4-d-\eta_\perp} \,,$$

which leads to (2.130).

Note that we have tacitly assumed that the mode coupling g stays finite at the critical point. As we shall see in Sec. 3.3.3 this is an essential feature of reversible mode couplings, where the non-renormalization of g is guaranteed by Ward identities of an extended temporal gauge symmetry. In Model H, with the Poisson brackets (2.123) and (2.124), this extended temporal gauge symmetry corresponds to the invariance of the equations of motion (2.125) under time-gauged Galilean boosts [108], as we discuss in Sec. 4.2.2 below.

2.2.5 Model G

Parts of this subsection have already been published in Ref. [2].

In its original formulation by Halperin and Hohenberg, Model G describes the dynamic universality class of an isotropic Heisenberg antiferromagnet [46]. The order parameter is a three-component vector and is interpreted as the staggered magnetization of the model which is not conserved. It couples dynamically to the conserved three-component magnetization through reversible mode couplings. This leads to the non-trivial value $z = d/2$ of the dynamic critical exponent (where d is the number of spatial dimensions). In this work, we consider a generalized formulation, where the order parameter is an N-component scalar field $\phi_a(x)$ which couples dynamically to an antisymmetric tensor of $N(N-1)/2$ charge densities $n_{ab}(x) = -n_{ba}(x)$.

This generalization of Model G is also known as the Sásvari-Schwabl-Szépfalusy (SSS) model [104,170]. The SSS model was previously inspected using field-theoretic methods in (e.g.) Refs. [104,110,171–173]. For $N = 2$ one recovers Model E, which describes the dynamic universality class of the critical point in the phase diagram of planar antiferromagnets. For $N = 3$ one obtains the standard formulation of Model G which describes the dynamic universality class of the Heisenberg antiferromagnet, see Ref. [174] for a recent study thereof. For $N = 4$ one obtains the anticipated extension of Model G which describes the dynamic universality class of the chiral phase transition in two-flavor QCD [62]. This is the relevant case for this work, although we will keep the number of field components N general in the derivation of the flow equations. Note that larger values of $N > 3$ do not correspond to any of the standard Halperin-Hohenberg dynamic universality classes [46]. However, previous analyses showed that $z = d/2$ as in the standard formulation of Model G still holds [62,66,104,110,163,170–173]. We thus use the term 'Model G' in the general sense also for $N \geq 3$, as frequently done especially in the literature on the SSS model.

In the context of QCD with two (nearly) massless quark flavors, the reasoning by Rajagopal and Wilczek [62,175] of the chiral phase transition being in the same dynamic universality class as Model G is as follows: First, the microscopic Lagrangian is (nearly) invariant under independent $U(2)_L$ and $U(2)_R$ transformations of the left and right-handed components $q_{R/L} = \frac{1}{2}(1 \pm \gamma^5)\, q$ of the quark Dirac spinors. This symmetry is spontaneously broken in the vacuum, signaled by a non-vanishing expectation value of the order parameter $M^i{}_j = \langle \bar{q}^i_L q_{Rj} \rangle$. Namely, under independent $(U_L, U_R) \in U(2)_L \times U(2)_R$ transformations of the left and right-handed quarks the order parameter transforms as

$$M \to U_L^\dagger M U_R \,. \tag{2.134}$$

Hence, a non-vanishing value for $M \propto \mathbf{1}$ indeed signals a (spontaneous) breaking of chiral symmetry, with symmetry-breaking pattern $U(2)_L \times U(2)_R \to U(2)_V$. However, this is not quite what we need, since the axial $U(1)_A$ symmetry, as described by the subgroup $U_L = e^{i\alpha}$ and $U_R = e^{-i\alpha}$ with real α, is anomalously broken in the vacuum, and we assume here that it stays sufficiently broken also at the chiral phase transition.[21] For a general number of flavors N_f, this problem is commonly solved by adding an 't Hooft determinant interaction to the effective Lagrangian [59]. Alternatively, one may remove $U(1)_A$ by restricting the general complex matrix M to be a special unitary matrix times a positive real number [175], since preserving this condition requires U_L and U_R to have equal phases, and thus effectively removes $U(1)_A$ from (2.134). The latter approach is especially well suited for the case of $N_f = 2$ flavors, since the condition of a 2×2 matrix M being a multiple of a unitary matrix is linear. This can be seen by parameterizing the special unitary part with the Pauli matrices $\boldsymbol{\tau} = (\tau^i) = (\tau_i)$, and using the relation

$$M = \bar{\sigma}\, e^{i\boldsymbol{\varphi}\cdot\boldsymbol{\tau}} = \bar{\sigma}\,(\cos(\varphi) + i \sin(\varphi)\, \hat{\boldsymbol{\varphi}} \cdot \boldsymbol{\tau}) \tag{2.135}$$

with $\hat{\boldsymbol{\varphi}} \equiv \boldsymbol{\varphi}/\varphi$, $\sigma = \bar{\sigma}\cos(\varphi)$, and $\boldsymbol{\pi} = \bar{\sigma}\sin(\varphi)\,\hat{\boldsymbol{\varphi}}$. Therefore, a matrix M in this restricted domain can be parameterized by four real numbers $\phi = (\sigma, \boldsymbol{\pi})$ as

$$M = \sigma + i\boldsymbol{\pi} \cdot \boldsymbol{\tau} \,. \tag{2.136}$$

[21] Otherwise, if $U(1)_A$ is effectively restored at the chiral phase transition, the symmetry breaking pattern would be $U(2)_L \times U(2)_R \to U(2)_V$. While no infrared stable fixed point was found at first-order in the ϵ-expansion [59], beyond this perturbative expansion around the upper-critical dimension of four, it is now widely accepted that such a fixed point in three dimensions exists [176,177]. So the fate of the axial $U_A(1)$ merely affects the universality class of the two-flavor chiral phase transition, but not its order.

In particular, the transformations (2.134) correspond to $O(4)$ transformations of ϕ. The order parameter M for the two-flavor chiral phase transition thus has the same symmetries as an $O(4)$ model, whose LGW free energy is given by (with $N = 4$)

$$F = \int_{\boldsymbol{x}} \left\{ \frac{1}{2}(\partial^i \phi_a)(\partial^i \phi_a) + \frac{m^2}{2}\phi_a\phi_a + \frac{\lambda}{4!N}(\phi_a\phi_a)^2 \right\} \tag{2.137}$$

where we have introduced the shorthand notation

$$\int_{\boldsymbol{x}} \equiv \int d^d x$$

for spatial integrals, with $m^2 < 0$ to spontaneously break the $O(4)$ symmetry at low temperatures, and $\lambda > 0$ for stability at large field values.

In Model G, the order parameter ϕ itself is not conserved but couples reversibly to the generators of the chiral transformations in (2.134), i.e., the $O(4)$ rotations of ϕ. In particular, Noether's theorem implies six conserved currents for the chiral $SU(2)_L \times SU(2)_R$ symmetry, namely

$$L^i_\mu \equiv \bar{q}_L \gamma_\mu \frac{\tau^i}{2} q_L \,, \qquad R^i_\mu \equiv \bar{q}_R \gamma_\mu \frac{\tau^i}{2} q_R \,. \tag{2.138}$$

These are equivalent to the iso-vector and iso-axial-vector currents

$$V^i_\mu \equiv L^i_\mu + R^i_\mu = \bar{q}\gamma_\mu \frac{\tau^i}{2} q \,, \tag{2.139a}$$

$$A^i_\mu \equiv L^i_\mu - R^i_\mu = \bar{q}\gamma_\mu \frac{\tau^i}{2}\gamma^5 q \,, \tag{2.139b}$$

which can be combined into one antisymmetric 4×4 matrix (n_{ab}) by setting $n_{0i} = A^0_i$ and $n_{ij} = \varepsilon_{ijk} V^0_k$. From the commutation relations of the currents (2.139) one can verify that the n_{ab}'s satisfy the $O(4)$ Lie algebra relations

$$[n_{ab}, n_{cd}] = i \left(\delta_{ac} n_{bd} + \delta_{bd} n_{ac} - \delta_{ad} n_{bc} - \delta_{bc} n_{ad}\right) . \tag{2.140}$$

By Noether's theorem again, the n_{ab}'s are the densities of the conserved charges that generate the $O(4)$ transformations. They thus represent the six charge densities needed for Model G with $N = 4$. In particular, one obtains the commutation relation

$$[\phi_a, n_{bc}] = i \left(\delta_{ac}\phi_b - \delta_{ab}\phi_c\right) \tag{2.141}$$

which describes how the order parameter ϕ (as an $O(4)$ vector) transforms under infinitesimal $O(4)$ transformations.

Importantly, the (static) iso-(axial-)vector charge susceptibility χ stays finite at the chiral phase transition [178], which means the static fluctuations of n_{ab} are Gaussian. As such, they enter the free energy (2.137) only quadratically, replacing

$$F \to F + \int_{\boldsymbol{x}} \frac{1}{4\chi} n_{ab} n_{ab} \,. \tag{2.142}$$

From this observation one can verify via power counting that higher-order couplings (or gradient terms) involving n_{ab} in (2.137) such as $n^2\phi^2$ or $(\boldsymbol{\nabla} n)^2$ are RG irrelevant [62]. In the corresponding $\lambda\phi^4$ theory, the charge densities n_{ab} would be given microscopically by Noether's theorem,

$$n_{ab} = \phi_a \frac{\partial}{\partial t}\phi_b - \phi_b \frac{\partial}{\partial t}\phi_a \,. \tag{2.143}$$

Using this definition of the Noether charge densities one readily derives the following explicit expressions for their Poisson brackets,

$$\{\phi_a, n_{bc}\} = \delta_{ac}\phi_b - \delta_{ab}\phi_c \tag{2.144}$$

and

$$\{n_{ab}, n_{cd}\} = \delta_{ac}n_{bd} + \delta_{bd}n_{ac} - \delta_{ad}n_{bc} - \delta_{bc}n_{ad}\,. \tag{2.145}$$

In particular, these correspond to the microscopic commutator expressions in Eqs. (2.140), (2.141) derived from the isovector and isoaxial-vector currents in QCD.[22] In the following, however, we consider the charge densities n_{ab} as separate degrees of freedom, independent the ϕ's. Rather, they can be considered as Hubbard fields to explicitly ensure the conservation of the corresponding Noether currents, with requiring the Poisson-bracket relations in Eqs. (2.144), (2.145).

Close to a second-order phase transition the dynamics is dominated by long-wavelength infrared modes. As it stands, however, the free energy (2.137) only encodes information on the static equilibrium distribution and hence only on the static universality class of the system. For the dynamic universality class we need the complete set of equations of motion, in addition. The equations of motion for the $O(4)$ Model G were written down by Rajagopal and Wilczek [62]. They are of the same form for any N, as described by the SSS Model with N non-conserved order-parameter components reversibly coupled to the conserved $O(N)$ generators [104, 170],

$$\frac{\partial\phi_a}{\partial t} = -\Gamma_0\frac{\delta F}{\delta\phi_a} + \frac{g}{2}\{\phi_a, n_{bc}\}\frac{\delta F}{\delta n_{bc}} + \theta_a\,, \tag{2.146a}$$

$$\frac{\partial n_{ab}}{\partial t} = \gamma\boldsymbol{\nabla}^2\frac{\delta F}{\delta n_{ab}} + g\{n_{ab}, \phi_c\}\frac{\delta F}{\delta\phi_c} + \frac{g}{2}\{n_{ab}, n_{cd}\}\frac{\delta F}{\delta n_{cd}} + \boldsymbol{\nabla}\cdot\boldsymbol{\zeta}_{ab}\,. \tag{2.146b}$$

Here, Γ_0 and $-\gamma\boldsymbol{\nabla}^2$ are the kinetic (Onsager) coefficients for the dynamics of the (non-conserved) order parameter and the (conserved) charge densities, respectively. The terms $\theta, \boldsymbol{\zeta}$ on the right-hand sides generate thermal fluctuations and are implemented as Gaussian white noises with vanishing expectation values,

$$\langle\theta_a(t,\boldsymbol{x})\rangle = 0\,, \qquad \langle\zeta^i_{ab}(t,\boldsymbol{x})\rangle = 0\,, \tag{2.147}$$

and variances

$$\langle\theta_a(t,\boldsymbol{x})\theta_b(t',\boldsymbol{x}')\rangle = 2\Gamma_0 T\delta_{ab}\delta(t-t')\delta(\boldsymbol{x}-\boldsymbol{x}')\,, \tag{2.148a}$$

$$\langle\zeta^i_{ab}(t,\boldsymbol{x})\zeta^j_{cd}(t',\boldsymbol{x}')\rangle = 2\gamma T(\delta_{ac}\delta_{bd} - \delta_{ad}\delta_{bc})\delta^{ij}\delta(t-t')\delta(\boldsymbol{x}-\boldsymbol{x}')\,, \tag{2.148b}$$

proportional to temperature T from Einstein relations to guarantee the classical FDR. On a structural level, the equations of motion (2.146) contain (i) irreversible dissipative or diffusive parts, as well as (ii) reversible conservative parts:

(i) The irreversible terms are the dissipative and diffusive terms with the kinetic coefficients Γ_0 and $-\gamma\boldsymbol{\nabla}^2$ but no Poisson brackets, and the thermal noises θ and ζ. The irreversible forces are diagonal here, i.e. only the gradient $\delta F/\delta\phi_a$ of the free energy with respect to ϕ_a enters the equation of motion (eom) of ϕ_a, and only $\delta F/\delta n_{ab}$ enters that of n_{ab}. The irreversible terms

[22] Poisson brackets and quantum-mechanical commutators are all defined at equal times and implicitly contain spatial δ-functions. They are related via the correspondence principle $\{\cdot,\cdot\} \to -i[\cdot,\cdot]$.

do not conserve the LGW free energy F and are responsible for driving the system towards the equilibrium (Boltzmann) distribution

$$P_{eq}[\phi, n] = \frac{1}{Z_{eq}} e^{-F[\phi,n]/T} \tag{2.149}$$

which also defines the associated equilibrium partition function[23]

$$Z_{eq} = \int \mathcal{D}\phi\, \mathcal{D}n\, e^{-F[\phi,n]/T} \,. \tag{2.150}$$

In the context of linearized hydrodynamics, the dissipative terms can be generally derived by expansion in conjugate variables (i.e. in gradients of the free energy) and requiring entropy production to be positive [61].

(*ii*) The reversible parts are all those that do contain a Poisson bracket. These are the conservative but off-diagonal forces and hence traditionally called 'reversible mode couplings'. They arise from the conservative dynamics with the underlying Lie algebra relations of charge densities and order parameter, cf. Eqs. (2.140) and (2.141) or (2.144) and (2.145). They conserve the free energy F exactly and are generally present whenever there are non-linear couplings between hydrodynamic modes. One can readily verify that they do not generate a current in the probability distribution, i.e. the 'streaming velocities' from (2.86) are here given by

$$V_a^\phi \equiv \frac{g}{2} \{\phi_a, n_{bc}\} \frac{\delta F}{\delta n_{bc}} \,, \qquad V_{ab}^n \equiv g \{n_{ab}, \phi_c\} \frac{\delta F}{\delta \phi_c} + \frac{g}{2} \{n_{ab}, n_{cd}\} \frac{\delta F}{\delta n_{cd}} \,, \tag{2.151}$$

and represent a vector field in the (ϕ, n) field space that is divergence-free with respect to the equilibrium Boltzmann distribution (2.149),

$$\int_{\boldsymbol{x}} \left[\frac{\delta}{\delta \phi_a} (V_a^\phi P_{eq}) + \frac{1}{2} \frac{\delta}{\delta n_{ab}} (V_{ab}^n P_{eq}) \right] = 0 \,, \tag{2.152}$$

as required in (2.84). Hence, the Boltzmann distribution remains unchanged in the presence of reversible mode couplings. This reflects the fact that knowing the equilibrium distribution (2.149), which encodes all *static* critical properties, is in general not enough to also know the *dynamic* universality class, because Eqs. (2.151) do not represent a unique solution to (2.152) but there are in general multiple others as well [137].

The physical interpretation of the reversible mode couplings (*ii*) in Model G is rather intuitive: the conserved Noether charges are the generators of $O(N)$ rotations. Therefore, a non-vanishing field value for some n induces a time-dependent $O(N)$ rotation of the ϕ's, as expressed by the Poisson-bracket term in (2.146a). Reversibility then requires the presence of a corresponding term in the equation of motion for the charge densities, as represented by the first Poisson bracket in (2.146b). The second Poisson-bracket term in (2.146b), which is present for $N > 2$, reflects the non-Abelian nature of the $O(N)$ symmetry group with non-vanishing Poisson brackets $\{n_{ab}, n_{cd}\} \neq 0$. It implies that a time-dependent rotation of the ϕ's caused by some n automatically comes along with a time-dependent rotation of other components of the conserved charges. These Poisson brackets lead to self-interactions among the conserved

[23] Path integrals over antisymmetric matrices n_{ab} are here defined to run only over the $N(N-1)/2$ independent components, i.e.

$$\int \mathcal{D}n \equiv \int \prod_{a<b} \mathcal{D}n_{ab}$$

together with identifying $n_{ab} \equiv -n_{ba}$ in the integrand for $a > b$.

charges when the underlying symmetry group that generates the reversible mode couplings is non-Abelian.[24]

In Chapter 3 we are primarily interested in the universal properties of the system defined by Eqs. (2.146) and (2.137) near a critical point, i.e., near a second-order phase transition. These are generally identified with fixed points of the (functional) RG flow. In general, there can be multiple fixed points, corresponding to the possible macroscopic (thermodynamic) phases the system can find itself in. They may be stable or unstable upon flowing towards the infrared. Linearizing the flow around a given fixed point reveals the set of associated critical exponents. The SSS model admits five different fixed points of the kinetic coefficients, see e.g. Ref. [110] and references therein. These are the usual Gaussian fixed point, the Model A fixed point (where the order parameter decouples from the conserved charges, which leads to purely dissipative dynamics), two 'weak-scaling' fixed points where the autocorrelation times of the order parameter and the conserved charges diverge with different (dynamic) critical exponents z_ϕ and z_n, respectively, and of course the 'strong-scaling' fixed point where the dynamic critical exponents of both sectors are locked, $z_\phi = z_n = d/2$, and thus the autocorrelation times for both the order parameter and the charge densities diverge at the same rate, $\xi_t \sim \xi^z$. A stability analysis to one-loop order reveals that of the latter three fixed points only the strong-scaling fixed point is stable [110], so, without additional fine-tuning, one expects to see strong-scaling behavior.

2.3 Functional renormalization group

Parts of this section have already been published in Refs. [1] and [2].

Instead of solving the path integral of a given theory for fluctuations at all scales at once, the general strategy of the FRG [72–74, 179, 180] is to implement the Wilsonian idea of successively 'integrating out' fluctuations momentum shell by momentum shell. In the pioneering formulation by Wetterich [72] this is achieved with adding an infrared (IR) cutoff to the theory, called the regulator R_k, which suppresses fluctuations of modes with momenta p smaller than the current 'FRG scale' k. At every given fixed scale k, fluctuations with $p \gtrsim k$, on the other hand, are assumed to have been integrated out. Then, instead of solving a functional integral such as (2.89) directly, one can equivalently follow the FRG flow down to $k \to 0$ in some truncation, where all relevant fluctuations are then fully taken into account. At the initial reference scale $k = \Lambda$ in the ultraviolet (UV) these fluctuations are assumed to be sufficiently suppressed so that the bare action (2.88) provides a suitable starting point for the FRG flow. In this way, the problem of solving a functional integral is converted into the problem of solving a functional differential equation. This works particularly well for the characteristic low-frequency long-wavelength fluctuations in the vicinity of a second-order phase transition, since the IR regulator suppresses all modes with momenta $p \lesssim k$, which means that contributions from critical fluctuations build up only gradually as the FRG scale k is lowered.

[24] For $N = 2$ there is only one independent conserved charge $n \equiv n_{12} = -n_{21}$ and hence no non-vanishing Poisson bracket. The underlying $O(2)$ symmetry is Abelian, and there are no self-interactions of charge density. In this case, the dynamic universality class is that of Model E according to Hohenberg and Halperin.

2.3.1 FRG flow for systems in thermal equilibrium

In this subsection, we shall first review the FRG in its standard (Euclidean) formulation for systems in thermal equilibrium, and then, in the following subsection, generalize the framework to the CTP. Before deriving the flow equation, we shall establish a few important functional relations. By promoting the LGW free energy[25] (2.88) to depend on external sources,

$$F \to F - \int_{\boldsymbol{x}} j(\boldsymbol{x})\phi(\boldsymbol{x})\,, \tag{2.153}$$

we can define the Schwinger functional

$$W[j] \equiv \frac{1}{\beta} \ln \int \mathcal{D}\phi\; e^{-\beta(F[\phi]-\int_{\boldsymbol{x}} j(\boldsymbol{x})\phi(\boldsymbol{x}))}\,, \tag{2.154}$$

which generates connected correlation functions of ϕ. In particular, the zeroth term in this expansion $-W[j=0]$ is the full thermodynamic free energy. A single functional derivative yields the expectation value of $\phi(\boldsymbol{x})$ in the presence of j,

$$\frac{\delta W[j]}{\delta j(\boldsymbol{x})} = \langle \phi(\boldsymbol{x}) \rangle_j\,, \tag{2.155}$$

and the second functional derivative the full propagator in the presence of j,

$$\frac{\delta^2 W[j]}{\delta j(\boldsymbol{x}) \delta j(\boldsymbol{y})} = \beta \left[\langle \phi(\boldsymbol{x})\phi(\boldsymbol{y}) \rangle_j - \langle \phi(\boldsymbol{x}) \rangle_j \langle \phi(\boldsymbol{y}) \rangle_j \right]\,. \tag{2.156}$$

The central object of the FRG in the formulation by Wetterich [72] is the effective action Γ, which is defined as the Legendre transform of the Schwinger functional (2.154),

$$\Gamma[\bar{\phi}] = \sup_j \left(\int_{\boldsymbol{x}} j(\boldsymbol{x})\bar{\phi}(\boldsymbol{x}) - W[j] \right) \tag{2.157}$$

Diagrammatically, Γ is the generator of one-particle irreducible (1PI) vertex functions [182]. Due to its definition as a Legendre transform, Γ is a convex functional of $\bar{\phi}(\boldsymbol{x})$. The supremum is assumed where the argument is stationary, i.e., for

$$0 = \frac{\delta}{\delta j(\boldsymbol{x})} \left(\int_{\boldsymbol{y}} j(\boldsymbol{y})\bar{\phi}(\boldsymbol{y}) - W[j] \right) \Big|_{j_{sup}} = \bar{\phi}(\boldsymbol{x}) - \frac{\delta W[j]}{\delta j(\boldsymbol{x})} \Big|_{j_{sup}} \implies \bar{\phi}(\boldsymbol{x}) = \frac{\delta W[j]}{\delta j(\boldsymbol{x})} \Big|_{j_{sup}} \tag{2.158}$$

which means that $\bar{\phi}(\boldsymbol{x}) = \langle \phi(\boldsymbol{x}) \rangle_{j_{sup}}$ is the order-parameter expectation value in the presence of the source $j = j_{sup}(\boldsymbol{x})$. In other words, one obtains the supremum $j_{sup}(\boldsymbol{x})$ for fixed field expectation value $\bar{\phi}(\boldsymbol{x})$ by inverting (2.158). Setting $j = j_{sup}$ to its value at the supremum in (2.157) and performing a functional derivative with respect to $\bar{\phi}(\boldsymbol{x})$ leads to

$$\frac{\delta \Gamma[\bar{\phi}]}{\delta \bar{\phi}(\boldsymbol{x})} = \frac{\delta}{\delta \bar{\phi}(\boldsymbol{x})} \left(\int_{\boldsymbol{y}} j_{sup}(\boldsymbol{y})\bar{\phi}(\boldsymbol{y}) - W[j_{sup}] \right) = j_{sup}(\boldsymbol{x}) \tag{2.159}$$

where we used the functional chain rule and (2.158) since j_{sup} implicitly depends on $\bar{\phi}$. Hence, if there is a value $\bar{\phi} = \bar{\phi}_{eq}$ for which j_{sup} vanishes, we obtain $\Gamma[\bar{\phi}_{eq}] = -W[j=0]$, i.e., the

[25] F is also commonly called the 'bare action' due to the formal similarity with Euclidean QFT. In particular, the d-dimensional free-energy functional (2.88) also arises in dimensional reduction near a thermal second-order phase transition of a ϕ^4 QFT in $d+1$ Euclidean spacetime dimensions [181].

thermodynamic free energy again. From (2.159) we see that at this point the effective action is stationary.

There is an exact relation between the propagator (2.156) and the Hessian $\Gamma^{(2)}$ of the effective action [180],

$$G(\boldsymbol{x},\boldsymbol{y}) = \left(\frac{\delta^2\Gamma[\phi]}{\delta\phi(\boldsymbol{x})\delta\phi(\boldsymbol{y})}\right)^{-1} \tag{2.160}$$

or in shorthand notation, $G = (\Gamma^{(2)})^{-1}$.

Here, the effective action has the direct physical interpretation of the thermodynamic free energy in the presence of a background expectation value $\bar{\phi}(\boldsymbol{x})$ of the order parameter. Its minima with respect to $\bar{\phi}$ correspond to the equilibrium states of the system. If fluctuations in ϕ are negligible or suppressed, as, e.g., sufficiently far away from the second-order phase transition such that a Ginzburg criterion is satisfied [135], and Λ is already sufficiently small such that the fluctuations from other microscopic degrees of freedom have already been integrated out, one approximately has $\Gamma[\bar{\phi}] \approx F[\bar{\phi}]$. This is the regime where mean-field (Landau) theory holds.

We have already stated that the difficult part of our particular problem lies in the large fluctuations of the long-wavelength modes of the order parameter close to the second-order phase transition. These fluctuations can be artificially suppressed by introducing an IR cutoff ΔF_k to the definition (2.154) of the Schwinger functional,

$$F \to F + \Delta F_k \tag{2.161}$$

which effectively gives momentum modes $\boldsymbol{p}$ with $|\boldsymbol{p}| \lesssim k$ a mass of order k. With the replacement (2.161), the Schwinger functional (2.154) becomes dependent on the FRG scale, $W \to W_k$. In the arguably simplest case, one chooses the regulator term ΔF_k to be a quadratic form of the fields, i.e., in Fourier space,

$$\Delta F_k = \frac{1}{2}\int_{\boldsymbol{p}} \phi(-\boldsymbol{p}) R_k(\boldsymbol{p}) \phi(\boldsymbol{p}) \tag{2.162}$$

which defines the regulator $R_k(\boldsymbol{p})$. We shall discuss its properties in more detail below. First, one defines the effective 'average' action Γ_k as a Legendre transform of W_k, but with an additional subtraction of the regulator term ΔF_k (commonly called a 'modified' Legendre transform),

$$\Gamma_k[\bar{\phi}] \equiv \sup_j \left(\int_{\boldsymbol{x}} j(\boldsymbol{x})\bar{\phi}(\boldsymbol{x}) - W_k[j]\right) - \Delta F_k[\bar{\phi}] \tag{2.163}$$

which can be interpreted as a 'coarse-grained' effective action where only the fluctuations from momentum modes $|\boldsymbol{p}| \gtrsim k$ have been taken into account. Since the regulator term ΔF_k is subtracted in the definition (2.163), Γ_k does not need to be convex. However, in the limit $k \to 0$, when the regulator is removed, the convexity of Γ_k is restored.

By successively lowering the value of k fluctuations of ϕ are gradually taken into account. The dependence of Γ_k on the FRG scale is described by an exact 'flow' equation which was first derived by Wetterich [72],

$$\partial_k \Gamma_k[\phi] = \frac{1}{2}\,\mathrm{tr}\left\{\partial_k R_k \circ \left(\Gamma_k^{(2)}[\phi] + R_k\right)^{-1}\right\} \tag{2.164}$$

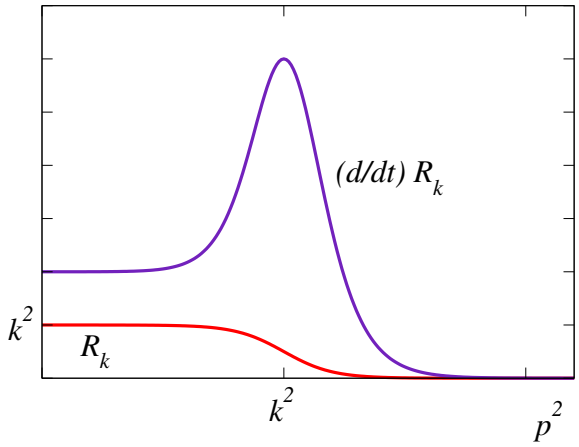

Figure 2.6: Typical shape of a regulator $R_k(\boldsymbol{p})$ (red), and its derivative $\partial_t R_k(\boldsymbol{p})$ with respect to FRG 'time' $t = \log(k/\Lambda)$ (purple). The derivative is peaked at $\boldsymbol{p}^2 \approx k^2$, and thus the flow (2.164) effectively implements the Wilsonian idea of integrating out fluctuations within momentum shells. Figure taken from Ref. [180].

where $\Gamma_k^{(2)}[\phi]$ denotes the Hessian matrix of $\Gamma_k[\phi]$. In particular, the term inside the trace involves the full field and FRG-scale dependent propagator,

$$G_k[\phi] = \left(\Gamma_k^{(2)}[\phi] + R_k\right)^{-1} , \tag{2.165}$$

which means that one can diagrammatically express the flow equation (2.164) in one-loop form,

$$\partial_k \Gamma_k = \frac{1}{2}$$ 

where the solid line denotes G_k and the cross denotes an insertion of the regulator derivative $\partial_k R_k$.

In order for the FRG flow to have a Wilsonian interpretation of integrating out fluctuations within momentum shells, the regulator $R_k(\boldsymbol{p})$ should satisfy the properties [180]

1. $R_k(\boldsymbol{p}) > 0$ for $\boldsymbol{p}^2 \ll k^2$,
2. $R_k(\boldsymbol{p}) \to 0$ for $k^2 \ll \boldsymbol{p}^2$,
3. $R_k(\boldsymbol{p}) \to \infty$ for $k \to \infty$.

These ensure that in the limit $k \to 0$ one obtains the full effective action, $\Gamma_k \xrightarrow{k\to 0} \Gamma$, and that at the UV cutoff $k = \Lambda$ one obtains the bare action, $\Gamma_{k=\Lambda} \approx F$. The latter can be seen by noting that at the UV cutoff $k = \Lambda$ a saddle-point approximation becomes exact [73]. A typical form of $R_k(\boldsymbol{p})$ satisfying these properties is shown in Fig. 2.6. One can see that the derivative $\partial_k R_k(\boldsymbol{p})$ is peaked around $|\boldsymbol{p}| \approx k$, and thus the flow equation (2.164) indeed realizes the Wilsonian idea of integrating out fluctuations within momentum shells.

In practice, applications of exact flow equations such as (2.164) to non-perturbative problems require truncation of the associated infinite tower of flow equations. For instance, in the context of critical phenomena, quantitative results for critical exponents and amplitude ratios of $O(N)$ universality classes have been obtained using the derivative expansion [77–80], which establishes the latter as a rapidly converging systematic truncation scheme in this context.

2.3.2 FRG on the closed-time path

The general idea of the FRG stays the same in the Keldysh formalism [105, 106]. The flow equation for the effective average (Keldysh) action Γ_k can be derived analogously by adding suitable external sources and regulator terms to a Keldysh action such as (2.51), to wit

$$S \to S + \int_x (j^c(x)\phi^q(x) + j^q(x)\phi^c(x)) + \Delta S_k \tag{2.166}$$

with

$$\Delta S_k = \frac{1}{2}\int_{xx'} (\phi^c(x), \phi^q(x)) \begin{pmatrix} R_k^{\widetilde{K}}(x,x') & R_k^A(x,x') \\ R_k^R(x,x') & R_k^K(x,x') \end{pmatrix} \begin{pmatrix} \phi^c(x') \\ \phi^q(x') \end{pmatrix} . \tag{2.167}$$

(Note the new variant of our shorthand notation $\int_x = \int_t \int_{\boldsymbol{x}} = \int dt\, d^dx$ here.) As such, compared to (2.162) the regulator R_k on the CTP is a 2×2 matrix in Keldysh (c, q) space. With the replacement (2.166), the partition function (2.48) becomes a scale (k) dependent generating functional for correlation functions of ϕ^c and ϕ^q,

$$Z_k[j^c, j^q] = \int \mathcal{D}\phi^c\, \mathcal{D}\phi^q \, \exp\left\{ iS + i\int_x (j^c(x)\phi^q(x) + j^q(x)\phi^c(x)) + i\Delta S_k \right\} \tag{2.168}$$

The k-dependent Schwinger functional is defined as

$$W_k[j^c, j^q] = -i \ln Z_k[j^c, j^q] \tag{2.169}$$

and the effective average (Keldysh) action again as a modified Legendre transform of W_k,

$$\Gamma_k[\bar{\phi}^c, \bar{\phi}^q] = W_k[j^c, j^q] - \int_x \left(j^c(x)\bar{\phi}^q(x) + j^q(x)\bar{\phi}^c(x) \right) - \Delta S_k \tag{2.170}$$

where $j^c(x)$ and $j^q(x)$ are given by inverting

$$\bar{\phi}^c(x) = \frac{\delta W[j^c, j^q]}{\delta j^q(x)} , \qquad \bar{\phi}^q(x) = \frac{\delta W[j^c, j^q]}{\delta j^c(x)} , \tag{2.171}$$

for fixed $\bar{\phi}^c(x)$ and $\bar{\phi}^q(x)$

Upon varying the FRG scale k, one obtains the flow equation [98, 106, 121]

$$\partial_k \Gamma_k[\phi^c, \phi^q] = \frac{i}{2} \operatorname{tr} \left\{ \partial_k R_k \circ \left(R_k + \Gamma_k^{(2)}[\phi^c, \phi^q] \right)^{-1} \right\} , \tag{2.172}$$

Compared to the Euclidean flow equation (2.164) one has an additional prefactor i, and the full field and FRG-scale dependent propagator

$$G_k[\phi^c, \phi^q] = W_k^{(2)}[j^c, j^q] = -\left(R_k + \Gamma_k^{(2)}[\phi^c, \phi^q] \right)^{-1} , \tag{2.173}$$

is a 2×2 matrix in Keldysh (c, q) space, with components

$$G_k(x,x') \equiv \begin{pmatrix} i\langle \phi^c(x)\phi^c(x') \rangle_{c,j} & i\langle \phi^c(x)\phi^q(x') \rangle_{c,j} \\ i\langle \phi^q(x)\phi^c(x') \rangle_{c,j} & i\langle \phi^q(x)\phi^q(x') \rangle_{c,j} \end{pmatrix} = \begin{pmatrix} G_k^K(x,x') & G_k^R(x,x') \\ G_k^A(x,x') & G_k^{\widetilde{K}}(x,x') \end{pmatrix} , \tag{2.174}$$

where the subscript in $_{c,j}$ indicates that the disconnected parts are subtracted $_j$, and that the correlation functions are understood in the presence of the sources $j^c(x)$ and $j^q(x)$. The

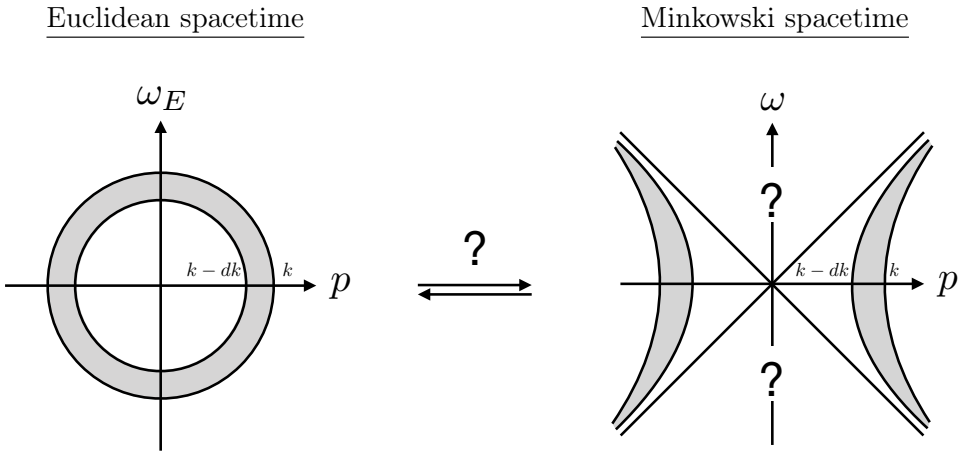

Figure 2.7: Illustration of a Wilsonian FRG flow which integrates out fluctuations within shells of constant invariant momentum in Euclidean spacetime (left), and in Minkowski spacetime (right). The question is in which sense one can realize a UV finite and Lorentz invariant FRG flow in Minkowski spacetime, since there one encounters the additional constraint of preserving the causality structure of the Keldysh action.

causality structure entails that the lower right 'anomalous' $G_k^{\tilde{K}} = i\langle\phi^q\phi^q\rangle_{c,j}$ correlation function must vanish for $j^q = 0$, in order to ensure that the effective average action stays zero for a vanishing expectation value $\phi^q = 0$ of the quantum field [118].

Despite the structural similarity of the real-time flow equation (2.172) and the Euclidean flow equation (2.164), a major conceptual difference between the two is the additional constraint of preserving the causality structure of the Keldysh action in the real-time case, which includes, e.g., the statement (2.36) that external perturbations can only affect the future (but not the past). The pressing issue here is that one typically finds that as soon as the regulator effectively cuts off frequencies, the causality structure is violated [90, 121, 183, 184].

In Euclidean FRG flows with only spacelike processes this issue is not immediately apparent, since the causality structure is in a certain sense 'hidden' in the generally ill-posed analytic continuation to the real-frequency axis, and thus not directly visible in, e.g., the Euclidean propagator. As such, a Euclidean FRG flow does not necessarily require the causality structure to be intact, unless of course one is interested in real-time quantities such as spectral functions during the FRG flow. Hence, there is no conceptual problem of realizing the Wilsonian idea of integrating out shells of invariant momenta, cf. the left panel of Fig. 2.7. However, this is not so in Minkowski spacetime with its additional causality structure, cf. the right panel of Fig. 2.7. In particular, a Lorentz invariant and UV finite regulator necessarily depends on frequency, and thus it is not at all clear under which conditions the causality structure is maintained, as we have discussed above.

In fact, the construction of frequency dependent and UV finite regulators that preserve the analytic structure of the theory is a known issue [84, 120, 121, 184, 185] which becomes especially demanding in any genuine real-time framework [90]. Rather recently, the issue was emphasized again in Ref. [184] since the approach developed there is based on the existence of the Källén-Lehmann spectral representation which goes hand in hand with the preservation of the causality structure [186].[26] In particular, it was pointed out in Ref. [184] that no regulator is known

[26]Note that the spectral function does not have to be positive in order for the causality structure to be intact.

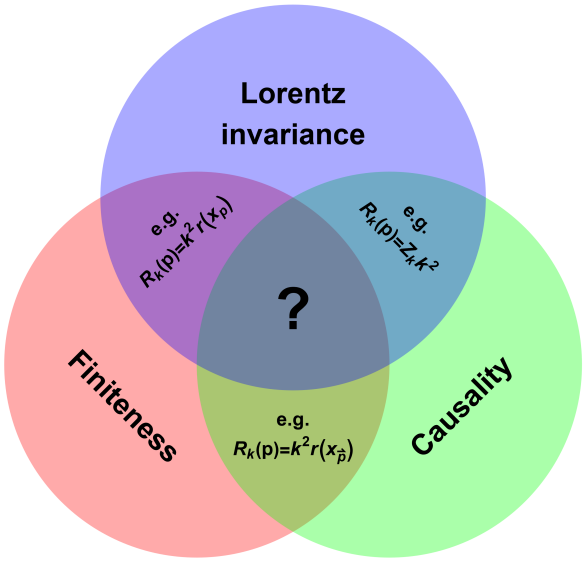

Figure 2.8: Illustration of the three desirable but competing properties of the regulator. See text for details. Figure taken from Ref. [184].

which is Lorentz invariant, UV-finite, and preserves the causality structure of the theory. Such a regulator would fall in the center of the Venn diagram in Fig. 2.8. On the other hand, by dropping one of the three requirements from Fig. 2.8, one can generally preserve the other two: First, Callan-Symanzik-type regulators satisfy the properties of Lorentz invariance and causality, but require additional processes such as 'flowing renormalization' since the FRG flow is no longer UV finite [184, 188–190] and thus no longer has the Wilsonian interpretation of integrating out fluctuations within momentum shells. Second, purely spatial (i.e., frequency independent) regulators guarantee the existence of a spectral representation and yield UV finite FRG flows [99, 120],[27] but are of course not Lorentz invariant. This is the option that is most suited for the study of critical phenomena near thermal second-order phase transitions, since these are intrinsically non-relativistic and thus not Lorentz invariant anyway. And third, regulators which are Lorentz invariant and UV finite (and thus necessarily frequency dependent) have been used in the past [121, 183] but have led to acausal regulator-induced poles which require careful treatment.

With these observations in mind, one might suspect that there is some 'no-go' theorem which prohibits the (naive) existence of regulators satisfying all three properties shown in Fig. 2.8 simultaneously. In the following, we analyze this issue from the perspective of the Keldysh formalism.

Assume adding some regulator part to the Keldysh action in the functional integral on the CTP that is bilinear in the fields $\Phi = (\phi^c, \phi^q)^T$ and spacetime translation invariant,

$$\Delta S_k[\Phi] = \frac{1}{2}\int_{xy} \Phi(x)^T R_k(x-y)\Phi(y)\,. \tag{2.175}$$

In order to maintain the causal structure of the Keldysh action, the regulator matrix R_k is

For instance, one can still have a local QFT with unphysical degrees of freedom that have an indefinite spectral function – a scenario that is possibly realized by the gluons of Landau gauge QCD [187].

[27] Assuming they vanish sufficiently quickly for $\boldsymbol{p} \to \infty$.

required to be of the form of a self-energy, i.e. (after Fourier transformation)

$$R_k(\omega,\boldsymbol{p}) = \begin{pmatrix} 0 & R_k^A(\omega,\boldsymbol{p}) \\ R_k^R(\omega,\boldsymbol{p}) & R_k^K(\omega,\boldsymbol{p}) \end{pmatrix} . \tag{2.176}$$

As any self-energy it can then always be represented, via Hubbard-Stratonovich linearization on the CTP, by a linear coupling of the fields Φ to a Gaussian ensemble of bosonic degrees of freedom. The modelling of such a causal self-energy regulator can therefore generally be shifted into the modelling of the FRG scale k dependent spectral distribution $J_k(\omega,\boldsymbol{p})$ of this ensemble to represent the regulator $R_k(\omega,\boldsymbol{p})$ via dispersion relations, as we will discuss explicitly below. Although one might thus intuitively think of an artificial scale-dependent heat bath to provide the damping of low frequency and momentum modes in a causal manner, there is more flexibility to choose such an artificial spectral distribution as it does not necessarily have to represent an ensemble of physical degrees of freedom, with a positive and normalizable spectral distribution.

In order to demonstrate this explicitly, we now assume that the regulator (2.176) on the CTP depends on frequency ω *without* violating causality, so that we can discuss the subsequent constraints that arise on its structure.[28] As a starting point for our discussion and as a general guiding principle, note the structural resemblance of the definition of the full propagator in the real-time FRG (here for a vanishing response-field expectation value $\phi^q(x) = 0$),

$$-\begin{pmatrix} G_k^K & G_k^R \\ G_k^A & 0 \end{pmatrix}^{-1} = \begin{pmatrix} 0 & \Gamma_k^{cq} \\ \Gamma_k^{qc} & \Gamma_k^{qq} \end{pmatrix} + \begin{pmatrix} 0 & R_k^A \\ R_k^R & R_k^K \end{pmatrix} , \tag{2.177}$$

with a Dyson equation. A quite non-trivial feature of the Keldysh technique is that the self-energy matrix, as defined by such a Dyson equation, generally inherits the causality structure of the Keldysh action [118]. It is thus a sufficient (if not even necessary) condition that the regulator also inherits this causal structure for causality to be conserved during the FRG flow. We can in fact turn this argument around, and interpret the statement that the regulator has the causal structure of a self-energy matrix, defined by a Dyson equation, as the technical definition of 'complying with causality'. Imposing the causal structure on the regulator tightly restricts its frequency dependence, as we shall see in the following.

First, this causal structure requires that retarded and advanced parts are connected by complex conjugation, i.e. $R_k^{R^*}(\omega,\boldsymbol{p}) = R_k^A(\omega,\boldsymbol{p})$. Moreover, in order to have real regulators for real scalar fields in the time domain, so that $\Delta S_k[\Phi]$ in (2.175) is real, we must also have $R_k^R(-\omega,\boldsymbol{p}) = R_k^{R^*}(\omega,\boldsymbol{p})$. This implies that the real/imaginary parts are even/odd in ω.

Since such a regulator thus has all the necessary analyticity properties of a retarded/advanced self-energy, we can therefore also write down a spectral representation. In order to include the class of frequency-independent regulators, we decompose the regulator in a frequency-dependent and a frequency-independent part. This can be done in various ways: If the regulator has a finite, non-vanishing and unique limit for ω towards complex infinity, this limit will necessarily be real and we can subtract it to define a standard spectral representation for the remainder which then vanishes for $\omega \to \pm\infty$. While this assumption might seem reasonable for regulators, self-energies in interacting theories typically do have singularities at infinity. Therefore, we alternatively assume here that the imaginary part of $R_k^{R/A}(\omega,\boldsymbol{p})$ vanishes for $\omega \to 0$, implying that

[28] Although we use the Keldysh formalism on the CTP here, with causality, any conclusion on the structure of the regulator (2.176) can be mapped one-to-one to a corresponding Euclidean regulator $R_k^E(\omega_E,\boldsymbol{p})$ with real Euclidean frequency ω_E by analytic continuation, via $R_k^E(\omega_E,\boldsymbol{p}) = -R_k^R(i|\omega_E|,\boldsymbol{p}) = -R_k^A(-i|\omega_E|,\boldsymbol{p})$.

the regulator does not introduce artificial massless excitations which could otherwise introduce infrared divergences. We call this the assumption of *infrared finiteness* which was one of the main original motivations for the Euclidean FRG [73].

IR finiteness: If the regulator is analytic at $\omega = 0$, we can define a real and momentum dependent *mass shift* via

$$\Delta M_k^2(\boldsymbol{p}) \equiv -R_k^{R/A}(0,\boldsymbol{p})\,. \tag{2.178}$$

This frequency-independent part is trivially causal and can be chosen as convenient, with the usual properties that any regulator should have [180]. In particular, it must necessarily be positive for all FRG scales k in order to properly regulate IR modes without introducing artificial acausal regulator singularities [90], i.e. $\Delta M_k^2(\boldsymbol{p}) > 0$. Because it does not vanish at infinity in the complex ω-plane, we then need to write down a subtracted spectral representation for $R_k^{R/A}(\omega,\boldsymbol{p})$, based on the analytic properties of $(R_k^{R/A}(\omega,\boldsymbol{p}) - R_k^{R/A}(0,\boldsymbol{p}))/\omega$ and assuming that $R_k^{R/A}(\omega,\boldsymbol{p})$ is analytic at $\omega = 0$, see Appendix A where the corresponding Kramers-Kronig relations are given as well. It amounts to writing

$$R^{R/A}(\omega,\boldsymbol{p}) \equiv -\Delta M_k^2(\boldsymbol{p}) + \Sigma_k^{R/A}(\omega,\boldsymbol{p})\,, \tag{2.179}$$

where the frequency-dependent part $\Sigma_k^{R/A}(\omega,\boldsymbol{p})$, which we will refer to as the 'spectral part' of the regulator in the following, is given by

$$\Sigma_k^{R/A}(\omega,\boldsymbol{p}) = -\int_0^\infty \frac{d\omega'}{2\pi}\,\frac{2\omega^2 J_k(\omega',\boldsymbol{p})}{\omega'((\omega\pm i\varepsilon)^2-\omega'^2)}\,. \tag{2.180}$$

It is expressed in terms of an FRG-scale k dependent spectral density $J_k(\omega,\boldsymbol{p})$ which is in turn given by the imaginary part of the regulator itself,

$$J_k(\omega,\boldsymbol{p}) = \pm 2\,\mathrm{Im}\,\Sigma_k^{R/A}(\omega,\boldsymbol{p}) = \pm 2\,\mathrm{Im}\,R_k^{R/A}(\omega,\boldsymbol{p})\,. \tag{2.181}$$

This spectral density must thus be an odd function of frequency as well, $J_k(-\omega,\boldsymbol{p}) = -J_k(\omega,\boldsymbol{p})$. Since we have assumed that the imaginary part of $R_k^{R/A}(\omega,\boldsymbol{p})$ vanishes for $\omega \to 0$, the integration limit of the spectral integral (2.180) in the infrared exists. One can furthermore see explicitly that the full spectral part of the regulator vanishes for $\omega \to 0$, i.e. $\Sigma_k^{R/A}(0,\boldsymbol{p}) = 0$, as it must by construction.

In order to include such a spectral part in a regulator for real-time FRG applications on the CTP one can therefore start with first devising a suitable imaginary part, i.e. a scale and frequency-dependent spectral density $J_k(\omega,\boldsymbol{p})$ which may be thought of as modelling an artificial external bath, and then compute the corresponding real part from the (subtracted) Kramers-Kronig relation.

For the physical interpretation of such a non-vanishing spectral density, we reiterate that such a self energy could have also been obtained by coupling our system to an external heat bath modelled as an ensemble of harmonic oscillators after Caldeira and Leggett [114] (cf. Sec. 2.1.2), or, equivalently, as a Gaussian ensemble of bosonic degrees of freedom, upon Gaussian integration of this ensemble. Therefore, a causal regulator with a non-vanishing spectral part (2.179), (2.180) can always be interpreted as arising from interactions with a fictitious external heat bath, specified by the scale dependent spectral density (2.181), which motivated the name 'heat-bath regulator' in earlier work [90].

If we translate our general expression (2.180) for the spectral part of a causal regulator to the Euclidean domain, we obtain the corresponding Euclidean regulator as

$$R_k^E(\omega_E, \boldsymbol{p}) = -R_k^R(i|\omega_E|, \boldsymbol{p}) = \Delta M_k^2(\boldsymbol{p}) + \int_0^\infty \frac{d\omega'}{\pi} \frac{\omega_E^2 \, J_k(\omega', \boldsymbol{p})}{\omega'(\omega_E^2 + \omega'^2)} \tag{2.182}$$

for real Euclidean frequencies ω_E. Notably, the spectral part, for a positive spectral density, always adds a positive contribution to the positive mass shift $\Delta M_k^2(\boldsymbol{p})$. In particular, for $\omega_E \to \infty$, this contradicts the UV finiteness of the Euclidean regulator in the frequency argument, as we discuss next.

UV finiteness: If the spectral density of the regulating bath vanishes for $\omega \to 0$ as we have assumed here, then we can also take the limit $\omega \to \infty$ in (2.180) to compute the ultraviolet limit of the regulator from

$$\lim_{\omega \to \pm\infty} R^{R/A}(\omega, \boldsymbol{p}) = -\Delta M_k^2(\boldsymbol{p}) - \int_0^\infty \frac{d\omega'}{\pi} \frac{J_k(\omega', \boldsymbol{p})}{\omega'} \,. \tag{2.183}$$

This shows that a semi-positive spectral density $J_k(\omega, \boldsymbol{p}) \geq 0$, corresponding to any kind of physically motivated external bath, together with a positive frequency-independent $\Delta M_k^2(\boldsymbol{p}) > 0$ is necessarily inconsistent with $R^{R/A}(\omega, \boldsymbol{p}) \to 0$ for $\omega \to \infty$. In other words, in such a physics motivated setup it is not possible to simultaneously cut off frequency integrals *and* respect the causal structure of the Keldysh action at all intermediate FRG scales k during the flow. Moreover, this result does not depend on our subtraction at $\omega = 0$ here. In fact the same conclusion is obtained with subtraction at complex infinity in Appendix A.

Lorentz invariance: Another issue frequently discussed in the literature [184] for real-time applications of the FRG in vacuum concerns Lorentz invariance of regulator and flow equations. Of course, a literal heat bath can at best be Lorentz covariant because it defines a preferred frame. In the context of our causal regulator (2.176) Lorentz invariance can be implemented assuming that the Gaussian ensemble of bosonic degrees of freedom is represented by local systems of Klein-Gordon fields in vacuum quantum field theory, which one can think of as a relativistic version of the Caldeira-Leggett model. This implies that the corresponding spectral density can be expressed as

$$J_k(\omega, \boldsymbol{p}) = 2\pi \, \mathrm{sgn}(\omega) \; \theta(p^2) \; \widetilde{J}_k(p^2) \tag{2.184}$$

in terms of the *invariant* spectral distribution $\widetilde{J}_k(p^2)$ which is a function of the squared invariant mass $s = p^2 = \omega^2 - \boldsymbol{p}^2$ alone. In this case, the spectral part (2.180) assumes the form of a standard (subtracted) Källén–Lehmann spectral representation,

$$\Sigma_k^{R/A}(\omega, \boldsymbol{p}) = -\int_0^\infty ds \, \frac{(\omega^2 - \boldsymbol{p}^2) \, \widetilde{J}_k(s)}{s \, ((\omega \pm i\varepsilon)^2 - \boldsymbol{p}^2 - s)} \,. \tag{2.185}$$

Moreover, the frequency independent $\Delta M_k(\boldsymbol{p}) \equiv \Delta M_k$ must then also be independent of the spatial momentum $\boldsymbol{p}$ in order to be consistent with Lorentz invariance. The $\omega = 0$ subtraction has become a light-cone subtraction which is allowed, as long as $\widetilde{J}_k(s)$ does not contain massless single-particle contributions (continuous contributions are allowed as long as $\widetilde{J}_k(s) \to 0$ for $s \to 0$).

As a practical example, consider the problem of respecting the $O(D)$ invariance of D-dimensional Euclidean spacetime in a causality-preserving way in the standard formulation of the FRG [121,183,185]. Assuming the causal structure of the corresponding Keldysh formulation in thermal equilibrium, a straightforward analytic continuation of (2.185) requires the Euclidean regulator to be of the form

$$R_k^E(\omega_E, \boldsymbol{p}) = \Delta M_k^2 + \int_0^\infty ds\, \frac{(\omega_E^2 + \boldsymbol{p}^2)\, \widetilde{J}_k(s)}{s\,(\omega_E^2 + \boldsymbol{p}^2 + s)} \tag{2.186}$$

with real Euclidean frequency ω_E, i.e. to consist of a Callan-Symanzik regulator plus some positive shift which depends on the Euclidean $O(D)$ invariant squared momentum variable $p_E^2 = \omega_E^2 + \boldsymbol{p}^2$. This form of the Euclidean regulator then guarantees the existence of a spectral representation of the propagator at all FRG scales k, which is not generally the case for an arbitrary regulator and requires extra attention [121, 183]. Moreover, note that the spectral integral in the momentum-dependent part of the regulator in (2.186) is ultraviolet finite only as long as $\widetilde{J}_k(s)/s \to 0$ for $s \to \infty$. While it is thus not intrinsically UV finite, for an arbitrary spectral density, this is not a severe restriction for a regulator, for which we intuitively expect that $\widetilde{J}_k(s) \to 0$ for $s \gg k^2$, anyway. On the other hand, and maybe more importantly however, without the Callan-Symanzik mass shift, i.e. for $\Delta M_k^2 = 0$, this expectation would in turn imply for $p_E^2 \gg s \sim k^2$ a *subtracted superconvergence relation* for the artificial regulator spectral density here,

$$\int_0^\infty ds\, \frac{\widetilde{J}_k(s)}{s} = 0\,, \tag{2.187}$$

in order to have

$$R_k^E(p_E^2) \to 0 \quad \text{for} \quad p_E^2 \gg k^2\,, \tag{2.188}$$

for our $O(D)$-invariant regulator with spectral representation. In particular, this also shows that it is not possible to maintain the positivity of the regulator spectral distribution $\widetilde{J}_k(s)$, *and* to have the Wilsonian realization of integrating out momentum shell by momentum shell in the FRG flow, at the same time. Instead, a flow generated by (2.186) with a positive spectral distribution $\widetilde{J}_k(s) \geq 0$ then necessarily has to be interpreted in the sense of Callan-Symanzik flows, shifting all squared masses uniformly by the square of the FRG scale k^2, and it thus represents a flow through 'theory space' [184].

Causality, Lorentz invariance, UV and IR finiteness: It is now straightforward to put together these individual requirements and discuss the consequences. Lorentz invariance entails that the regulator only depends on the invariant momentum, $R_k^{R/A} = R_k^{R/A}(p^2)$. Causality then requires it to be an analytic function in the cut-complex p^2 plane, with the only singularities at the discontinuity along the timelike real axis. The causally regulated theory corresponds to an open system where the self-energy regulator (2.175) has become the result of integrating a Gaussian ensemble of bosonic degrees of freedom which we may call the *environment* (with Lorentz invariance it is not a heat-bath, of course, but some local field system). Analytic continuation to the Euclidean domain and the existence of a spectral representation are then guaranteed. Ultraviolet finiteness of the Euclidean FRG flows demands that $R_k^{R/A}(p^2) = 0$ for $-p^2 \gg k^2$. For timelike $p^2 > 0$ the imaginary part is given by the invariant spectral distribution $\widetilde{J}_k(p^2)$ which describes the interactions of the system with states in the environment of total momentum p. The causal extension of the Wetterich equation leads to the conclusion that such artificial interactions in the regulated theory should not occur for $p^2 \gg k^2$, implying that

$\widetilde{J}_k(p^2) = 0$, for $p^2 \gg k^2$. The self-energy regulator therefore then vanishes in all directions at complex infinity of the p^2-plane, and no subtraction in its spectral representation is required in this case, in the first place. Instead of (2.179), (2.180) we can then simply write

$$R_k^{R/A}(p^2) = -\int_0^\infty ds\, \frac{\widetilde{J}_k(s)}{(\omega \pm i\varepsilon)^2 - \boldsymbol{p}^2 - s}\,, \tag{2.189}$$

see Appendix A. Without massless excitations introduced by the regulator, we can furthermore take the limit $p^2 \to 0$ here and obtain for the mass shift

$$\Delta M_k^2 = R_k^E(0) = -\int_0^\infty ds\, \frac{\widetilde{J}_k(s)}{s} \stackrel{!}{\geq} 0\,, \tag{2.190}$$

which must be positive to avoid tachyonic regulator singularities. This shows that causality, Lorentz invariance plus UV and IR finiteness together require that the spectral density of the artificial environment cannot be positive. The bosonic fields in the Gaussian ensemble of the environment thus necessarily violate positivity just as BRST quartets do in covariant gauge theory.[29] In fact, the Keldysh action does have a BRST invariance [82, 191–194], expressing the fact that the partition function for vanishing sources of the response fields, $j^q = 0$ with $Z[j^c, 0] = 1$, defines a topological quantum field theory. There are of course physical fields with positivity on the CTP, and hence with positive spectral distributions, but in presence of interactions the latter are usually ultraviolet divergent. In order to represent an FRG regulator contribution $\Delta S_k[\Phi]$ as in (2.175) in terms of local field systems, so that the regulated partition function and effective average action define a local quantum field theory at all FRG scales k during the flow, we can either have positivity or ultraviolet (and infrared) finiteness, but not both at the same time. (In other words, upon replacing 'Causality' with 'Positivity' in the lower-right corner of the diagram in Fig. 2.8, the form (2.189) of the regulator indeed excludes the threefold overlap region in the center.) In particular, we conclude that representing infrared and ultraviolet finite effective average actions in terms of polynomial algebras of local field systems, with spacelike (anti-)commutativity to maintain causality, necessarily requires a detour into indefinite metric spaces with BRST cohomology construction (of BRST closed modulo BRST exact states) of a physical state space during the flow.

We end this subsection with a brief mentioning of the implications that causal regulators with non-vanishing spectral parts (2.180) can have on the dynamics. Coupling any theory to an artificial environment, be it positive and hence physical or not, will evidently in general violate conservation laws. A causal heat-bath regulator, for example, induces artificial dissipation and therefore also possibly affects the conserved quantities. This can potentially lead to a change of the dynamic universality class in the Halperin-Hohenberg classification [46] during the flow, when the regulator is present. Most obviously, due to the auxiliary coupling to a regulating heat bath, energy is not conserved anymore, at least for excitations with frequencies in the support of $J_k(\omega, \boldsymbol{p})$. An Ohmic heat bath, with $J(\omega, \boldsymbol{p}) \sim \gamma\omega$, in the infrared, for example, yields the prototypical realization of Model A dynamics, for which heat-bath regulators are thus particularly well suited. Special attention is needed, on the other hand, when studying systems with conserved energy (e.g., certain microscopic theories that classify as Model C, but where the energy density is not explicitly coupled, such as in Ref. [88]). In fact, since imaginary and real parts of our causal regulators are always linked by Kramers-Kronig relations, and a non-vanishing

[29] The closed total system including the artificial environment can still represent a local field system with causality, but there is no spin-statistics theorem for which one needs positivity, in addition.

imaginary part always corresponds to a coupling to some external environment, we conclude that the arguably simplest way to maintain conservation laws is to assume that the regulator does not depend on ω, implying that the regulator spectral density vanishes, $J_k(\omega, \boldsymbol{p}) \equiv 0$, and the regulator is thus purely spatial, i.e.

$$R_k^{R/A}(\omega, \boldsymbol{p}) = -\Delta M_k^2(\boldsymbol{p})\,. \tag{2.191}$$

This seems particularly well justified when one is interested in the critical dynamics near thermal fixed points, where (a) Lorentz invariance is no issue in the first place, and (b) one is predominantly interested in an effective theory for the critical long-range infrared modes and ultraviolet finiteness is less of a concern.

Chapter 3

Critical dynamics near the chiral phase transition

Parts of this chapter have already been published in Ref. [2]. The numerical results presented in Sec. 3.4 were obtained in collaboration with Yunxin Ye.

As stated in the introduction, the chiral phase transition of QCD in the limit of two massless quark flavors is generally believed to be of second order and to fall into the $O(4)$ universality class [59]. Lattice QCD simulations performed close to the two-flavor chiral limit for lighter than physical pion masses indeed provide evidence of a second-order chiral phase transition [55, 56]. Although the universality class cannot be determined with confidence yet, the results from the HotQCD collaboration at least indicate that the quark-mass and temperature dependence of chiral condensate and susceptibility are consistent with $O(4)$ universality, as described by the corresponding universal scaling functions [55, 195]. While the discriminating power of available lattice results does not allow to nail the universality class, the window for a description in terms of universal scaling functions appears to extend up to the physical pion mass [70]. This window is not necessarily equal to the true scaling window, however. Results from functional methods for effective low-energy models and QCD have long suggested that the actual scaling region is restricted to much smaller pion masses [57, 196–198], with the most recent QCD estimate limiting the critical region for $O(4)$ scaling to pion masses below a few MeV, and to a similarly small range of temperatures around the transition [71].

On the other hand, the *dynamic* universality class of the two-flavor chiral phase transition is believed to be the one of a four-component Heisenberg antiferromagnet, i.e., an extension of the original Model G by Halperin and Hohenberg [46] to an $O(4)$ order parameter [62], as discussed in Sec. 2.2.5. This extension is frequently referred to also simply as 'Model G', although strictly speaking 'Model G' specifically referred to the antiferromagnetic $O(3)$ Heisenberg case in the original classification. The phenomenological consequences for heavy-ion collisions and the critical dynamics of Model G were previously studied in Refs. [61, 65–67]. In fact, it was suggested that an observed excess of soft pions in heavy-ion collisions [63] might be attributed to remnants of the second-order $O(4)$ transition [67]. With its critical dynamics thus being potentially relevant for the phenomenology of heavy-ion collisions, here we therefore further pursue the study of this model which has historically also been known as the SSS model [104,170] in the literature. Luckily, to observe the *strong dynamic scaling* of Model G, where the order parameter and the conserved charges are expected to relax with the same dynamic critical

exponent $z = d/2$ in d spatial dimensions, it is not a priori necessary to be strictly inside the potentially small static $O(4)$ scaling region.

In this chapter, we focus on studying Model G within the real-time FRG framework. This extends previous work in several ways: For example, a real-time FRG formulation of classical Langevin dynamics was used to calculate the dynamic critical exponent z of the purely dissipative Model A in [81, 82, 84] and of Model C in [83]. Quantum fluctuations can be incorporated by formulating the FRG on the Schwinger-Keldysh CTP. Such real-time formulations of the FRG on the CTP were used to study critical dynamics and spectral functions of the relativistic $O(4)$ model in Refs. [151, 199]. Without including the reversible mode couplings in presence of the conserved charges in these references this led to the dissipative dynamics of Model A, however, where the charges are not conserved. The truncation of Ref. [199] had thereby been adapted from Ref. [98] where it had been used to study spectral functions of the quartic-anharmonic oscillator in quantum mechanics. A combined vertex and loop expansion for the FRG on the CTP was formulated in [90] where the same quantum-mechanical system was studied with various different real-time methods for spectral functions. A field-theory extension of this real-time FRG formulation was developed in [1] and used to compute the critical spectral functions of the relaxational Models A, B, and C. In a recent update, a derivative expansion similar to the one used in Ref. [81] was employed to resolve the field dependence of the kinetic coefficient of Model A [154]. In this work, we take the real-time FRG from Sec. 2.3.2 to the next level by including the reversible mode couplings needed to study Model G dynamics in this framework. The subtleties associated with these reversible mode couplings will also be relevant for Model H, as we shall see in Chapter 4.

This chapter is organized as follows. In Sec. 3.1 we construct a generating functional for Model G using the MSR formalism. In the same section, we also discuss the symmetries of the MSR action of Model G, which will serve as a guiding principle for finding a suitable truncation of the FRG flow. In Sec. 3.2, we formulate the FRG for systems with reversible mode couplings and discuss how the regulator should be introduced so as to preserve all relevant symmetries. We show that the dynamics of the system does not affect the flow of the static LGW free energy. In Sec. 3.3 we formulate a truncation of the effective average action, derive corresponding flow equations for the LGW free energy and the kinetic coefficients, show that the mode-coupling constant g is protected from renormalization, and discuss our numerical methods used to solve the flow equations. In Sec. 3.4 we discuss the critical behavior of $O(4)$ Model G obtained from our real-time FRG study, including the critical exponents and a universal scaling function for the diffusion coefficient of the iso-vector and iso-axial-vector charge densities.

3.1 Martin-Siggia-Rose path-integral formulation

For the convenience of the reader, we copy the equations of motion (2.146) of Model G here,

$$\frac{\partial \phi_a}{\partial t} = -\Gamma_0 \frac{\delta F}{\delta \phi_a} + \frac{g}{2} \{\phi_a, n_{bc}\} \frac{\delta F}{\delta n_{bc}} + \theta_a \,, \tag{3.1a}$$

$$\frac{\partial n_{ab}}{\partial t} = \gamma \boldsymbol{\nabla}^2 \frac{\delta F}{\delta n_{ab}} + g \{n_{ab}, \phi_c\} \frac{\delta F}{\delta \phi_c} + \frac{g}{2} \{n_{ab}, n_{cd}\} \frac{\delta F}{\delta n_{cd}} + \boldsymbol{\nabla} \cdot \boldsymbol{\zeta}_{ab} \,, \tag{3.1b}$$

where the LGW free energy F is given by

$$F = \int_{\boldsymbol{x}} \left\{ \frac{1}{2} (\partial^i \phi_a)(\partial^i \phi_a) + \frac{m^2}{2} \phi_a \phi_a + \frac{\lambda}{4! N} (\phi_a \phi_a)^2 + \frac{1}{4\chi} n_{ab} n_{ab} \right\} . \tag{3.2}$$

By adding external sources to the LGW free energy,

$$F \to F - \int_{\boldsymbol{x}} \left(H_a \phi_a + \frac{1}{2} \mathcal{H}_{ab} n_{ab} \right) \tag{3.3}$$

we can promote the partition function (2.150) to a generating functional for static (equal-time) correlation functions in thermal equilibrium,

$$Z_{eq}[H, \mathcal{H}] = \int \mathcal{D}\phi \, \mathcal{D}n \, \exp\left\{ -\beta F[\phi, n] + \beta \int_{\boldsymbol{x}} \left(H_a(\boldsymbol{x}) \phi_a(\boldsymbol{x}) + \frac{1}{2} \mathcal{H}_{ab}(\boldsymbol{x}) n_{ab}(\boldsymbol{x}) \right) \right\} \tag{3.4}$$

From its behavior around the critical point all static universal properties like the critical exponents ν and η may be derived.

To study *dynamic* critical phenomena we need *unequal-time* correlation functions. A corresponding generating functional can be constructed with the MSR formalism [100–102] which we have already encountered in Sec. 2.1.4, but which we shall review here in more detail and from the perspective of starting with the stochastic equations of motion (3.1) of Model G. In the MSR approach, one reformulates a thermal expectation value $\langle O(\phi, n) \rangle$ of an operator $O(\phi, n)$ which may involve products of fields at different times as a real-time path integral. As in the Keldysh formalism, this is achieved by doubling the number of fields, cf. Sec. 2.1.1. In the MSR formalism one introduces auxiliary response fields $\tilde{\phi}$ and $\tilde{n}$, and constructs an MSR action

$$\begin{aligned} S = \int_x \Bigg[& - \tilde{\phi}_a \left(\frac{\partial \phi_a}{\partial t} + \Gamma_0 \frac{\delta F}{\delta \phi_a} - \frac{g}{2} \{ \phi_a, n_{bc} \} \frac{\delta F}{\delta n_{bc}} \right) \\ & - \frac{1}{2} \tilde{n}_{ab} \left(\frac{\partial n_{ab}}{\partial t} - \gamma \boldsymbol{\nabla}^2 \frac{\delta F}{\delta n_{ab}} - g \{ n_{ab}, \phi_c \} \frac{\delta F}{\delta \phi_c} - \frac{g}{2} \{ n_{ab}, n_{cd} \} \frac{\delta F}{\delta n_{cd}} \right) \\ & + i T \tilde{\phi}_a \Gamma_0 \tilde{\phi}_a - \frac{1}{2} i T \tilde{n}_{ab} \gamma \boldsymbol{\nabla}^2 \tilde{n}_{ab} \Bigg] , \end{aligned} \tag{3.5}$$

corresponding to the equations of motion (3.1) of Model G such that the expectation value of a multi-time observable $O(\phi, n)$ can be calculated from the corresponding path integral,

$$\langle O(\phi, n) \rangle = \int \mathcal{D}\phi \, \mathcal{D}\tilde{\phi} \, \mathcal{D}n \, \mathcal{D}\tilde{n} \, \mathcal{J}[\phi, n] \, \exp\{ i S \} \, O(\phi, n) \, . \tag{3.6}$$

In the MSR technique, one also needs to introduce a (generally) field-dependent Jacobian determinant $\mathcal{J}[\phi, n]$ to the path integral, which is the determinant of the Jacobian matrix of the map

$$E(\phi, n) \equiv \begin{pmatrix} E^{\phi}(\phi, n) & 0 \\ 0 & E^{n}(\phi, n) \end{pmatrix} \tag{3.7}$$

from the fields to the fluctuationless parts of the equations of motion, with components

$$E^{\phi}_a(\phi, n) \equiv \frac{\partial \phi_a}{\partial t} + \Gamma_0 \frac{\delta F}{\delta \phi_a} - \frac{g}{2} \{ \phi_a, n_{bc} \} \frac{\delta F}{\delta n_{bc}} \, , \tag{3.8a}$$

$$E^{n}_{ab}(\phi, n) \equiv \frac{\partial n_{ab}}{\partial t} - \gamma \boldsymbol{\nabla}^2 \frac{\delta F}{\delta n_{ab}} - g \{ n_{ab}, \phi_c \} \frac{\delta F}{\delta \phi_c} - \frac{g}{2} \{ n_{ab}, n_{cd} \} \frac{\delta F}{\delta n_{cd}} \, , \tag{3.8b}$$

i.e. the operators to which the response fields $\tilde{\phi}$ and $\tilde{n}$ couple linearly in the MSR action (3.5). With these the stochastic equations of motion (3.1) can then compactly be written as

$$E^{\phi}_a(\phi, n) = \theta_a \, , \qquad E^{n}_{ab}(\phi, n) = \boldsymbol{\nabla} \cdot \boldsymbol{\zeta}_{ab} \, . \tag{3.9}$$

Before we continue with the construction of the generating functional in the next subsection, in the following, for the convenience of the reader, we briefly review the structure of the MSR action (3.5) and the conceptual steps in its derivation.

Generally, a thermal expectation value $\langle O(\phi, n)\rangle$ of an operator $O(\phi, n)$ is given by an average of the observable over an ensemble of solutions $\phi_{\theta,\zeta}, n_{\theta,\zeta}$ to the equations of motion (3.1),

$$\langle O(\phi, n)\rangle = \int \mathcal{D}\theta\, \mathcal{D}\zeta\, P[\theta, \boldsymbol{\zeta}]\, O(\phi_{\theta,\zeta}, n_{\theta,\zeta}) \tag{3.10}$$

where the specific noise instances $\theta(t, \boldsymbol{x})$, $\boldsymbol{\zeta}(t, \boldsymbol{x})$ are randomly drawn from a Gaussian distribution with probability (density)

$$P[\theta, \boldsymbol{\zeta}] = \exp\left\{-\int_x \frac{\theta_a(x)\theta_a(x)}{4\Gamma_0 T}\right\} \exp\left\{-\int_x \frac{\zeta^i_{ab}(x)\zeta^i_{ab}(x)}{8\gamma T}\right\}, \tag{3.11}$$

which implements the white noise statistics (2.148), with variances set by the fluctuation-dissipation relation for thermal equilibrium at temperature T. One can now insert a trivial unity into (3.10), to introduce (path) integrals over $\phi_a(t, \boldsymbol{x})$ and $n_{ab}(t, \boldsymbol{x})$,

$$1 = \int \mathcal{D}\phi\, \mathcal{D}n\, \delta(\phi - \phi_{\theta,\zeta})\, \delta(n - n_{\theta,\zeta})\,. \tag{3.12}$$

The δ-functionals enforce the fields ϕ, n in the path integral to be solutions to the stochastic equations of motion (3.1). With the functional generalization of the identity $\delta(x - x_0) = |f'(x)|\, \delta(f(x))$, for a function $f(x)$ with a unique root at $x = x_0$, we can rewrite the δ-distributions in (3.12) to arrive at the somewhat more convenient form

$$\delta(\phi - \phi_{\theta,\zeta})\, \delta(n - n_{\theta,\zeta}) = \mathcal{J}[\phi, n]\, \delta(E^\phi - \theta)\, \delta(E^n - \boldsymbol{\nabla}\cdot\boldsymbol{\zeta})\,. \tag{3.13}$$

This expresses the fact that only the solutions to the equations of motion contribute to the path integral, i.e. those that satisfy $E^\phi_a(\phi, n) - \theta_a = 0$ and $E^n_{ab}(\phi, n) - \boldsymbol{\nabla}\cdot\boldsymbol{\zeta}_{ab} = 0$. This however necessitates the introduction of the functional Jacobian $\mathcal{J}[\phi, n]$ (which can be set to unity with a suitable time discretization, as discussed below). Next, one uses Fourier representations of the δ-functionals in (3.13), introducing the auxiliary 'response' fields $\tilde{\phi}_a$ and $\tilde{n}_{ab}$,

$$\delta(E^\phi_a - \theta_a)\, \delta(E^n_{ab} - \boldsymbol{\nabla}\cdot\boldsymbol{\zeta}_{ab}) = \int \mathcal{D}\tilde{\phi}\, \mathcal{D}\tilde{n}\, \exp\left\{-i\int_x \tilde{\phi}_a(E^\phi_a - \theta_a) - \frac{i}{2}\int_x \tilde{n}_{ab}(E^n_{ab} - \boldsymbol{\nabla}\cdot\boldsymbol{\zeta}_{ab})\right\}. \tag{3.14}$$

In total, one then arrives at

$$\begin{aligned}\langle O(\phi, n)\rangle = \int \mathcal{D}\theta\, \mathcal{D}\zeta\, \mathcal{D}\phi\, \mathcal{D}n\, \mathcal{D}\tilde{\phi}\, \mathcal{D}\tilde{n}\, \mathcal{J}[\phi, n]\, P[\theta, \boldsymbol{\zeta}] \times \\ \exp\left\{-i\int_x \tilde{\phi}_a(E^\phi_a - \theta_a) - \frac{i}{2}\int_x \tilde{n}_{ab}(E^n_{ab} - \boldsymbol{\nabla}\cdot\boldsymbol{\zeta}_{ab})\right\} O(\phi, n)\end{aligned} \tag{3.15}$$

for the thermal expectation value. The (path) integral over the stochastic noises is now Gaussian and can be performed analytically, yielding

$$\begin{aligned}\langle O(\phi, n)\rangle = \int \mathcal{D}\phi\, \mathcal{D}n\, \mathcal{D}\tilde{\phi}\, \mathcal{D}\tilde{n}\, \mathcal{J}[\phi, n] \times \\ \exp\left\{i\int_x \left[-\tilde{\phi}_a E^\phi_a - \frac{1}{2}\tilde{n}_{ab}E^n_{ab} + iT\tilde{\phi}_a\Gamma_0\tilde{\phi}_a - \frac{1}{2}iT\tilde{n}_{ab}\gamma\boldsymbol{\nabla}^2\tilde{n}_{ab}\right]\right\} O(\phi, n)\end{aligned} \tag{3.16}$$

which is precisely the anticipated expression (3.6) with the shorthand notation (3.8) for the fluctuationless parts in the equations of motion. The MSR path integral (3.6) is thus equivalent to (3.10), but more convenient for a field-theoretic treatment.

We close this subsection with a few comments on the Jacobian. On a fundamental level, the Jacobian ensures the normalization condition $\langle 1 \rangle = 1$ of the MSR path integral (3.6), which is expressed in the definition of a real-time partition function

$$Z \equiv \int \mathcal{D}\phi\, \mathcal{D}\tilde{\phi}\, \mathcal{D}n\, \mathcal{D}\tilde{n}\, \mathcal{J}[\phi, n]\, \exp\{iS\} = 1\,, \tag{3.17}$$

defined as the MSR path integral (3.6) when no observables are measured. Notably, this normalization condition is not just a choice of an overall (constant) normalization factor, but implies that for field-independent observables in (3.6) the path integral becomes 'topological'. We discuss this particular property of the MSR technique in Appendices B.1 and B.2, as it is related to the hidden BRST symmetry already mentioned in Sec. 2.1.1.

In the present case, we can achieve $\mathcal{J}[\phi, n] = 1$ by choosing a retarded (Ito) discretization of the stochastic equations of motion. There are other possible discretizations, however, in which $\mathcal{J}[\phi, n] \neq 1$, e.g. in the Stratonovich discretization. The fact that the choice of discretization is not unique becomes particularly important in systems with *multiplicative* noise, where the stochastic force terms in the equations of motion (3.1) are field dependent. Under such circumstances different discretizations can indeed lead to different continuum limits, which has historically also been known as the Ito–Stratonovich dilemma. In fact, already in the present case, without multiplicative noise here, one has to be slightly careful in obtaining the correct continuum limit of the Ito discretization [82]. We defer a discussion of this particular subtlety to Appendix B.1, and continue with the construction of a generating functional in the next subsection.

3.1.1 Generating functional for systems with reversible mode couplings

A generating functional for unequal-time correlation functions can be constructed by introducing external source terms in the general definition of an expectation value (3.6). First of all, *unphysical* sources $\tilde{H}_a$ and $\tilde{\mathcal{H}}_{ab}$ which are conjugate to the classical fields ϕ_a and n_{ab} are simply introduced as linear coupling terms on the level of the MSR action (3.5),

$$S \to S + \int_x \left(\tilde{H}_a \phi_a + \frac{1}{2} \tilde{\mathcal{H}}_{ab} n_{ab} \right) . \tag{3.18}$$

The partition function (3.17) then becomes a functional of $\tilde{H}$ and $\tilde{\mathcal{H}}$. Expectation values of classical fields can then be obtained as usual by functional differentiation of the partition function in presence of these sources, e.g.

$$\langle \phi_a(x) \rangle = -i \frac{\delta Z[\tilde{H}, \tilde{\mathcal{H}}]}{\delta \tilde{H}_a(x)}\bigg|_{\tilde{H}=\tilde{\mathcal{H}}=0}, \qquad \langle n_{ab}(x) \rangle = -i \frac{\delta Z[\tilde{H}, \tilde{\mathcal{H}}]}{\delta \tilde{\mathcal{H}}_{ab}(x)}\bigg|_{\tilde{H}=\tilde{\mathcal{H}}=0}, \tag{3.19}$$

where Z denotes the generating functional from here on, i.e. the partition function in the presence of external sources. One has to be more careful when one introduces *physical* source terms H and $\mathcal{H}$ conjugate to the response fields. They should be included in a way that the dynamic

response functions (i.e. the retarded propagators) of the system can be calculated via

$$G^R_{\phi_a\phi_b}(x,x')_{\text{unconn.}} = \left.\frac{\delta\langle\phi_a(x)\rangle_{H,\mathcal{H}}}{\delta H_b(x')}\right|_{H,\mathcal{H}=0}, \tag{3.20a}$$

$$G^R_{n_{ab}n_{cd}}(x,x')_{\text{unconn.}} = \left.\frac{\delta\langle n_{ab}(x)\rangle_{H,\mathcal{H}}}{\delta \mathcal{H}_{cd}(x')}\right|_{H,\mathcal{H}=0}, \tag{3.20b}$$

where the subscript 'unconn.' indicates that these denote *unconnected* correlation functions, i.e. the disconnected components are not subtracted here. As it turns out, the correct way of introducing such physical source terms is to add them one level earlier: Instead of adding the corresponding source terms directly to the MSR action, as done for the unphysical ones in (3.18), we add the physical sources to the free energy as in (3.3) for the static case, i.e. writing

$$F \to F - \int_{\boldsymbol{x}} \left(H_a\phi_a + \frac{1}{2}\mathcal{H}_{ab}n_{ab}\right), \tag{3.21}$$

which can now be time dependent, however, to be able to compute unequal-time correlations functions. This formal replacement is then used to obtain correspondingly modified deterministic force terms inside the MSR action in a second step. We will elaborate on the reasoning for this choice in more detail below. Crucially, when introduced in this way, the physical sources do not couple to the standard response fields $\tilde{\phi}_a$ and $\tilde{n}_{ab}$ directly, but to the following composite operators

$$\tilde{\Phi}_a \equiv \Gamma_0\tilde{\phi}_a - \frac{g}{2}\tilde{n}_{bc}\{n_{bc},\phi_a\}, \tag{3.22a}$$

$$\tilde{N}_{ab} \equiv -\gamma\boldsymbol{\nabla}^2\tilde{n}_{ab} - \frac{g}{2}\tilde{n}_{cd}\{n_{cd},n_{ab}\} - g\tilde{\phi}_c\{\phi_c,n_{ab}\}. \tag{3.22b}$$

This is because they then couple to all terms in the equations of motion (3.1) that contain (d-dimensional) functional derivatives of the free energy. In addition to the dissipative terms, this includes contributions from the reversible mode couplings, i.e. Poisson-bracket terms in the equations of motion. In fact, it has been argued that this is the natural way in which physical source terms *should* appear in effective field theories of dissipative hydrodynamics, see e.g. Ref. [200]. One can straightforwardly verify that by including (time-independent) source terms in this way, the stationary state of the system is still the Boltzmann distribution (but with the free energy (3.3) which then includes the static sources, of course). Correspondingly, the FDR in its usual form based on Kubo-Martin-Schwinger conditions [130,131] is maintained, even in the presence of static external sources. This is not entirely trivial in a system with reversible mode couplings. In fact, if one were to naively couple the sources directly to the elementary response fields $\tilde{\phi}_a$ and $\tilde{n}_{ab}$ in the MSR action (3.5), such a system would no longer approach the corresponding equilibrium Boltzmann distribution. This is shown in Appendix B.3.

Therefore, introducing the sources as described, we arrive at the generating functional

$$\begin{aligned} Z[H,\mathcal{H},\tilde{H},\tilde{\mathcal{H}}] = \int \mathcal{D}\phi\,\mathcal{D}\tilde{\phi}\,\mathcal{D}n\,\mathcal{D}\tilde{n}\,\exp\Big\{ iS[\phi,n,\tilde{\phi},\tilde{n}] + i\int_x \left(\tilde{H}_a\phi_a + \frac{1}{2}\tilde{\mathcal{H}}_{ab}n_{ab}\right) + \\ i\int_x \left(\Gamma_0\tilde{\phi}_a + \frac{g}{2}\{\phi_a,n_{bc}\}\tilde{n}_{bc}\right)H_a + \\ \frac{i}{2}\int_x \left(-\gamma\boldsymbol{\nabla}^2\tilde{n}_{ab} + g\{n_{ab},\phi_c\}\tilde{\phi}_c + \frac{g}{2}\{n_{ab},n_{cd}\}\tilde{n}_{cd}\right)\mathcal{H}_{ab}\Big\}, \end{aligned} \tag{3.23}$$

where we explicitly see that the sources H_a and $\mathcal{H}_{ab}$ couple to the composite fields (3.22). This formulation of the generating functional will form the basis of our treatment of Model G within the FRG in Sec. 3.2 below.

Note that the composite response fields (3.22) have the structure of a field-dependent linear transformation of the standard response fields,

$$\begin{pmatrix} \tilde{\Phi}_a \\ \tilde{N}_{bc} \end{pmatrix} = \begin{pmatrix} \delta_{ad}\Gamma_0 & \frac{g}{2}\{\phi_a, n_{ef}\} \\ g\{n_{bc}, \phi_d\} & -\frac{1}{2}\left(\delta_{be}\delta_{cf} - \delta_{bf}\delta_{ce}\right)\gamma\boldsymbol{\nabla}^2 + \frac{g}{2}\{n_{bc}, n_{ef}\} \end{pmatrix} \begin{pmatrix} \tilde{\phi}_d \\ \tilde{n}_{ef} \end{pmatrix} . \tag{3.24}$$

We emphasize that the matrix in (3.24) depends on the 'classical' fields ϕ and n, but *not* on the response fields $\tilde{\phi}$ and $\tilde{n}$. In particular, the reversible mode couplings with the Poisson brackets (2.144) and (2.145) only introduce classical fields $\{\phi, n\} \sim \phi$, $\{n, n\} \sim n$, but no response fields. Because this field-dependent matrix is used repeatedly throughout this work, we introduce the symbol $J(\psi)$ for it together with a compact 'superfield' notation $\psi \equiv (\phi, n)$, $\tilde{\Psi} \equiv (\tilde{\Phi}, \tilde{N})$ and $\tilde{\psi} \equiv (\tilde{\phi}, \tilde{n})$. We can then compactly write $\tilde{\Psi} = J(\psi)\tilde{\psi}$, and express the field-dependent matrix $J(\psi)$ as

$$\begin{aligned} J(x, x'; \psi) &= \frac{\delta\tilde{\Psi}(x)}{\delta\tilde{\psi}(x')} \\ &= \begin{pmatrix} \delta_{ad}\Gamma_0 & \frac{g}{2}\{\phi_a, n_{ef}\}(x) \\ g\{n_{bc}, \phi_d\}(x) & -\frac{1}{2}\left(\delta_{be}\delta_{cf} - \delta_{bf}\delta_{ce}\right)\gamma\boldsymbol{\nabla}_{\boldsymbol{x}}^2 + \frac{g}{2}\{n_{bc}, n_{ef}\}(x) \end{pmatrix} \delta(x - x') . \end{aligned} \tag{3.25}$$

Instead of formulating the path integral in terms of the standard response fields $\tilde{\phi}$ and $\tilde{n}$, we can also perform the change of variables (3.22) directly on the level of the path integral and formulate the action in terms of the composite response fields $\tilde{\Phi}$ and $\tilde{N}$. I.e., using the definition of the composite fields in (3.22) as a field transformation in the path integral (3.6) then yields

$$\begin{aligned} Z[H, \mathcal{H}, \tilde{H}, \tilde{\mathcal{H}}] = \int \mathcal{D}\phi\, \mathcal{D}\tilde{\Phi}\, \mathcal{D}n\, \mathcal{D}\tilde{N}\, \mathcal{J}'[\phi, n] \exp\Big\{ & iS'[\phi, n, \tilde{\Phi}, \tilde{N}] + \\ & i\int_x \big(\tilde{H}_a\phi_a + \frac{1}{2}\tilde{\mathcal{H}}_{ab}n_{ab} + \tilde{\Phi}_a H_a + \frac{1}{2}\tilde{N}_{ab}\mathcal{H}_{ab}\big)\Big\} \end{aligned} \tag{3.26}$$

with a formally different bare action S' that is obtained by substituting the response fields with the new composite fields,

$$S'[\phi, n, \tilde{\Phi}, \tilde{N}] = S[\phi, n, \tilde{\phi}, \tilde{n}] , \tag{3.27}$$

and with a field-dependent Jacobian $\mathcal{J}'[\phi, n]$ that arises due to the transformation of the measure. The transformed action S' is spatially non-local in the new fields since the inverse of the field transformation (3.22) is needed in its definition (3.27), which involves inverting the spatial Laplacian $\boldsymbol{\nabla}^2$. Moreover, because the field transformation is non-linear, the Jacobian determinant in (3.26),

$$\mathcal{J}'[\phi, n] = \left|\det \begin{pmatrix} \frac{\delta\tilde{\phi}}{\delta\tilde{\Phi}} & \frac{\delta\tilde{\phi}}{\delta\tilde{N}} \\ \frac{\delta\tilde{n}}{\delta\tilde{\Phi}} & \frac{\delta\tilde{n}}{\delta\tilde{N}} \end{pmatrix}\right| = \left|\det J^{-1}[\phi, n]\right| \tag{3.28}$$

depends on the fields ϕ and n, and thus needs special attention. Generally speaking, the sole purpose of such a Jacobian determinant in the MSR path integral is to ensure that the normalization condition $\langle 1 \rangle = 1$ is maintained. On a diagrammatic level, this requires the cancellation of all acausal diagrams[1] by corresponding 'ghost' diagrams, which arise from anti-commuting

[1] These are all diagrams which would otherwise vanish in the Keldysh/MSR formalism by standard causality arguments, for example those diagrams where two points x and x' are connected both by a retarded and an advanced propagator, $G^R(x, x')G^A(x, x') = 0$, or where a retarded/advanced propagator closes into a loop, $G^{R/A}(x, x) = 0$.

ghost degrees of freedom $\tilde{c}$ and c introduced to represent the Jacobian determinant as an integral over Grassmann variables,

$$\mathcal{J}'[\phi, n] = \int \mathcal{D}\tilde{c}\,\mathcal{D}c\, \exp\left\{ -\int_{xx'} \tilde{c}(x) \frac{\delta\tilde{\psi}(x)}{\delta\tilde{\Psi}(x')} c(x') \right\}, \tag{3.29}$$

here again expressed in our superfield notation. Knowing that this cancellation must occur, in practice, one may therefore simply dismiss the Jacobian together with all acausal diagrams [194]. For more technical details on the Jacobian, see Appendix B.2.

The unconnected physical response functions (i.e. the unconnected retarded propagators) are obtained as second functional derivatives of the generating functional

$$G^R_{\phi_a\phi_b}(x,x')_{\text{unconn.}} = -i \frac{\delta^2 Z[H,\mathcal{H},\tilde{H},\tilde{\mathcal{H}}]}{\delta\tilde{H}_a(x)\delta H_b(x')}\bigg|_{H,\mathcal{H}=0}, \tag{3.30}$$

$$G^R_{n_{ab}n_{cd}}(x,x')_{\text{unconn.}} = -i \frac{\delta^2 Z[H,\mathcal{H},\tilde{H},\tilde{\mathcal{H}}]}{\delta\tilde{\mathcal{H}}_{ab}(x)\delta\mathcal{H}_{cd}(x')}\bigg|_{H,\mathcal{H}=0}. \tag{3.31}$$

They describe the dynamic response at spacetime point $x = (t, \boldsymbol{x})$ of the system with respect to an external perturbation applied at $x' = (t', \boldsymbol{x}')$, cf. (3.20). *Connected* correlation functions are obtained from the corresponding Schwinger functional

$$W[H,\mathcal{H},\tilde{H},\tilde{\mathcal{H}}] = -i \log Z[H,\mathcal{H},\tilde{H},\tilde{\mathcal{H}}]\,. \tag{3.32}$$

For example, the connected propagators (here in the presence of arbitrary background sources $H(x)$, $\mathcal{H}(x)$) are given by

$$iF_{\phi_a\phi_b}(x,x') = \frac{\delta^2 W[H,\mathcal{H},\tilde{H},\tilde{\mathcal{H}}]}{\delta\tilde{H}_a(x)\delta\tilde{H}_b(x')} = i\langle\phi_a(x)\phi_b(x')\rangle - i\langle\phi_a(x)\rangle\langle\phi_b(x')\rangle\,, \tag{3.33a}$$

$$G^R_{\phi_a\phi_b}(x,x') = \frac{\delta^2 W[H,\mathcal{H},\tilde{H},\tilde{\mathcal{H}}]}{\delta\tilde{H}_a(x)\delta H_b(x')} = i\langle\phi_a(x)\tilde{\Phi}_b(x')\rangle - i\langle\phi_a(x)\rangle\langle\tilde{\Phi}_b(x')\rangle\,, \tag{3.33b}$$

$$G^A_{\phi_a\phi_b}(x,x') = \frac{\delta^2 W[H,\mathcal{H},\tilde{H},\tilde{\mathcal{H}}]}{\delta H_a(x)\delta\tilde{H}_b(x')} = i\langle\tilde{\Phi}_a(x)\phi_b(x')\rangle - i\langle\tilde{\Phi}_a(x)\rangle\langle\phi_b(x')\rangle\,, \tag{3.33c}$$

$$i\widetilde{F}_{\phi_a\phi_b}(x,x') = \frac{\delta^2 W[H,\mathcal{H},\tilde{H},\tilde{\mathcal{H}}]}{\delta H_a(x)\delta H_b(x')} = i\langle\tilde{\Phi}_a(x)\tilde{\Phi}_b(x')\rangle - i\langle\tilde{\Phi}_a(x)\rangle\langle\tilde{\Phi}_b(x')\rangle\,, \tag{3.33d}$$

and,

$$iF_{n_{ab}n_{cd}}(x,x') = \frac{\delta^2 W[H,\mathcal{H},\tilde{H},\tilde{\mathcal{H}}]}{\delta\tilde{\mathcal{H}}_{ab}(x)\delta\tilde{\mathcal{H}}_{cd}(x')} = i\langle n_{ab}(x)n_{cd}(x')\rangle - i\langle n_{ab}(x)\rangle\langle n_{cd}(x')\rangle\,, \tag{3.34a}$$

$$G^R_{n_{ab}n_{cd}}(x,x') = \frac{\delta^2 W[H,\mathcal{H},\tilde{H},\tilde{\mathcal{H}}]}{\delta\tilde{\mathcal{H}}_{ab}(x)\delta\mathcal{H}_{cd}(x')} = i\langle n_{ab}(x)\tilde{N}_{cd}(x')\rangle - i\langle n_{ab}(x)\rangle\langle\tilde{N}_{cd}(x')\rangle\,, \tag{3.34b}$$

$$G^A_{n_{ab}n_{cd}}(x,x') = \frac{\delta^2 W[H,\mathcal{H},\tilde{H},\tilde{\mathcal{H}}]}{\delta\mathcal{H}_{ab}(x)\delta\tilde{\mathcal{H}}_{cd}(x')} = i\langle\tilde{N}_{ab}(x)n_{cd}(x')\rangle - i\langle\tilde{N}_{ab}(x)\rangle\langle n_{cd}(x')\rangle\,, \tag{3.34c}$$

$$i\widetilde{F}_{n_{ab}n_{cd}}(x,x') = \frac{\delta^2 W[H,\mathcal{H},\tilde{H},\tilde{\mathcal{H}}]}{\delta\mathcal{H}_{ab}(x)\delta\mathcal{H}_{cd}(x')} = i\langle\tilde{N}_{ab}(x)\tilde{N}_{cd}(x')\rangle - i\langle\tilde{N}_{ab}(x)\rangle\langle\tilde{N}_{cd}(x')\rangle\,, \tag{3.34d}$$

The effective action, the generating functional of 1PI correlation functions, is obtained from a Legendre transformation of the Schwinger functional,

$$\Gamma[\bar{\phi},\bar{n},\bar{\tilde{\Phi}},\bar{\tilde{N}}] = W[H,\mathcal{H},\tilde{H},\tilde{\mathcal{H}}] - \int_x \Big(\tilde{H}_a\bar{\phi}_a + \frac{1}{2}\tilde{\mathcal{H}}_{ab}\bar{n}_{ab} + H_a\bar{\tilde{\Phi}}_a + \frac{1}{2}\mathcal{H}_{ab}\bar{\tilde{N}}_{ab} \Big) \tag{3.35}$$

with

$$\bar{\phi}_a(x) = \frac{\delta W[H,\mathcal{H},\tilde{H},\tilde{\mathcal{H}}]}{\delta \tilde{H}_a(x)}\,, \qquad \bar{\tilde{\Phi}}_a(x) = \frac{\delta W[H,\mathcal{H},\tilde{H},\tilde{\mathcal{H}}]}{\delta H_a(x)}\,, \tag{3.36}$$

$$\bar{n}_{ab}(x) = \frac{\delta W[H,\mathcal{H},\tilde{H},\tilde{\mathcal{H}}]}{\delta \tilde{\mathcal{H}}_{ab}(x)}\,, \qquad \bar{\tilde{N}}_{ab}(x) = \frac{\delta W[H,\mathcal{H},\tilde{H},\tilde{\mathcal{H}}]}{\delta \mathcal{H}_{ab}(x)}\,. \tag{3.37}$$

We have thereby indicated the field expectation values by bars. Since the classical sources actually couple to the composite operators (3.22), the effective action (3.35) is not a functional of the expectation values $\langle\tilde{\phi}_a(x)\rangle$ and $\langle\tilde{n}_{ab}(x)\rangle$ of the standard response fields, but instead a function of the expectation values of the composite operators (3.22), i.e., of

$$\bar{\tilde{\Phi}}_a(x) = \Gamma_0\langle\tilde{\phi}_a(x)\rangle - \frac{g}{2}\langle\tilde{n}_{bc}(x)\{n_{bc},\phi_a\}(x)\rangle\,, \tag{3.38a}$$

$$\bar{\tilde{N}}_{ab}(x) = -\gamma\boldsymbol{\nabla}^2\langle\tilde{n}_{ab}(x)\rangle - \frac{g}{2}\langle\tilde{n}_{cd}(x)\{n_{cd},n_{ab}\}(x)\rangle - g\langle\tilde{\phi}_c(x)\{\phi_c,n_{ab}\}(x)\rangle\,. \tag{3.38b}$$

In the following we will drop the bars from the field expectation values again since there will be generally no confusion with the fields appearing in the path integral (3.26). The various propagators (3.33) and (3.34) are then dependent on the background field expectation values instead of the external sources and can be expressed by

$$G[\psi,\tilde{\Psi}] = -(\Gamma^{(2)}[\psi,\tilde{\Psi}])^{-1} \tag{3.39}$$

where $\Gamma^{(2)}[\psi,\tilde{\Psi}]$ denotes the Hessian matrix of Γ in the superfield notation. In general, we indicate functional derivatives by superscripts, e.g.

$$\Gamma^{\tilde{\Psi}_i\psi_j}[\psi,\tilde{\Psi}](x,y) \equiv \frac{\delta^2\Gamma[\psi,\tilde{\Psi}]}{\delta\tilde{\Psi}_i(x)\delta\psi_j(y)} \tag{3.40}$$

where i,j here are indices in superfield space. When written in components, the compact relation (3.39) explicitly expands to [106]

$$G^R = -\left\{\Gamma^{\tilde{\Psi}\psi} - \Gamma^{\tilde{\Psi}\tilde{\Psi}}\circ(\Gamma^{\psi\tilde{\Psi}})^{-1}\circ\Gamma^{\psi\psi}\right\}^{-1}\,, \tag{3.41a}$$

$$G^A = -\left\{\Gamma^{\psi\tilde{\Psi}} - \Gamma^{\psi\psi}\circ(\Gamma^{\tilde{\Psi}\psi})^{-1}\circ\Gamma^{\tilde{\Psi}\tilde{\Psi}}\right\}^{-1}\,, \tag{3.41b}$$

$$iF = -\left\{\Gamma^{\psi\psi} - \Gamma^{\psi\tilde{\Psi}}\circ(\Gamma^{\tilde{\Psi}\tilde{\Psi}})^{-1}\circ\Gamma^{\tilde{\Psi}\psi}\right\}^{-1}\,, \tag{3.41c}$$

$$i\widetilde{F} = -\left\{\Gamma^{\tilde{\Psi}\tilde{\Psi}} - \Gamma^{\tilde{\Psi}\psi}\circ(\Gamma^{\psi\psi})^{-1}\circ\Gamma^{\psi\tilde{\Psi}}\right\}^{-1}\,, \tag{3.41d}$$

for the retarded, advanced, statistical, and anomalous propagators in superfield space. We have suppressed the two superfield indices and the two spacetime arguments on all two-point functions and propagators in (3.41), so that all objects are to be interpreted as matrices (and their inverses) in spacetime and in superfield space. Moreover, the symbol $\circ$ denotes matrix multiplication in superfield space as well as integration over adjacent spacetime coordinates, e.g.

$$(A\circ B)_{ij}(x,y) \equiv \int_z A_{il}(x,z)B_{lj}(z,y) \tag{3.42}$$

with superfield indices i,j,l, spacetime points x,y,z, and implicit summation over l.

To conclude this subsection, we furthermore note that our rule for functional derivatives with respect to the elements of antisymmetric $N\times N$ matrices such as $n_{ab} = -n_{ba}$, with only $N(N-1)/2$ independent components, is defined by the antisymmetric fundamental functional derivative as follows,

$$\frac{\delta n_{ab}(x)}{\delta n_{cd}(y)} = (\delta_{ac}\delta_{bd} - \delta_{ad}\delta_{bc})\,\delta(x-y)\,. \tag{3.43}$$

3.1.2 Symmetries of the MSR action

Symmetries generally provide powerful tools for practical calculations. For instance, they give rise to Ward identities of the effective action and hence to non-trivial relations between the n-point correlation functions. If the symmetry is continuous, Noether's theorem implies an associated conserved current, which means that continuous symmetries can be used as a guideline for the degrees of freedom that are part of an effective hydrodynamic description. Moreover, as a peculiarity of the real-time formalism, the question whether a system is in thermal equilibrium is also expressed as the presence (or absence) of a discrete symmetry, as discussed in [107]. In the context of the FRG, one can show that a given symmetry is exactly conserved by the FRG flow [180] (assuming that the regulator does not explicitly break the symmetry). This means that possible truncation schemes are restricted to those which conserve all symmetries that are already present at tree level. With this motivation in mind, our goal in this subsection is to discuss the various symmetries of the MSR action (3.5). We will use some of these symmetries in later sections to derive some important general results such as the FRG-scale independence of the reversible mode coupling g, or the independence of the 'static' FRG flow for the free energy of any real-time quantity, for example. They also allow one to restrict the possible operators that can occur within a given truncation of the FRG flow.

Thermal equilibrium. Thermal equilibrium is generally expressed as a symmetry of the MSR action [107]. The symmetry transformation can be most directly expressed as a transformation of the composite response fields (3.22), and is given by

$$\mathcal{T}_\beta \begin{pmatrix} \psi_i(\omega,\boldsymbol{p}) \\ \tilde{\Psi}_i(\omega,\boldsymbol{p}) \end{pmatrix} = \begin{pmatrix} 1 & 0 \\ -\beta\omega & 1 \end{pmatrix} \begin{pmatrix} \epsilon_i\psi_i(-\omega,\boldsymbol{p}) \\ \epsilon_i\tilde{\Psi}_i(-\omega,\boldsymbol{p}) \end{pmatrix} \tag{3.44}$$

(no summation over the superfield index i on the right-hand side) where $\epsilon_i = \pm 1$ are the time-reversal parities of the fields. (This symmetry of thermal equilibrium can of course also be expressed as a transformation of the standard response fields $\tilde{\phi}$ and $\tilde{n}$, in which case it is non-linear, however [201].) The occurrence of the time-reversal parity in this transformation is due to the fact that the symmetry expresses detailed balance when the system is in thermal equilibrium, which includes a time-reversal transformation [107]. Since the ϕ-field is the order parameter of the system and the order parameter is unchanged under time reversal, one assigns $\epsilon_\phi = +1$. The n-fields, on the other hand, represent the zero components of conserved currents, and their parity under time reversal thus is $\epsilon_n = -1$. We explicitly demonstrate in Appendix C that our bare action is indeed invariant under the symmetry transformation (3.44).

Temporal gauge and displacement symmetry. There is a symmetry that emerges due to the underlying Poisson-bracket structure of the reversible mode couplings. By construction, the free energy (3.2) and the equations of motion (3.1) are of course invariant under global $O(N)$ transformations. In fact, this global $O(N)$ symmetry can even be extended to cover *time-dependent* (but spatially constant) $O(N)$ transformations. This generalization is possible due to the Poisson-bracket structure of the conservative terms in the equations of motion (3.1). To see this, we first introduce some general notation. Recall that $O(N)$ transformations can generally be written as $O = \exp\{\frac{1}{2}\alpha_{ab}T_{ab}\} \in O(N)$, where the T_{ab}'s are the $N(N-1)/2$ generators of $O(N)$. The latter are elements of the Lie algebra $o(N)$. One possible representation that complies with the Poisson-bracket relations (2.144) and (2.145) is given by $(T_{ab})_{cd} = \delta_{ad}\delta_{bc} - \delta_{ac}\delta_{bd}$. The

generators satisfy the commutation relations

$$[T_{ab}, T_{cd}] = \delta_{ac}T_{bd} + \delta_{bd}T_{ac} - \delta_{ad}T_{bc} - \delta_{bc}T_{ad} \tag{3.45}$$

which defines the structure constants of the group. They are normalized according to

$$\mathrm{tr}(T_{ab}T_{cd}) = 2(\delta_{ad}\delta_{bc} - \delta_{ac}\delta_{bd})\,. \tag{3.46}$$

The Poisson-bracket relations reflect the transformation behavior of fields under infinitesimal $O(N)$ transformations, so we can express

$$\{\phi_a, n_{cd}\} = (T_{cd})_{ab}\phi_b\,, \qquad \{n_{ab}, n_{cd}\} = (T_{cd})_{ab,ef}n_{ef}\,, \tag{3.47}$$

in which $(T_{cd})_{ab,ef}$ denote the generators of the adjoint representation of $O(N)$. They are explicitly given by the structure constants of $O(N)$, which can be read off from the commutation relations (3.45). The order parameter ϕ, its associated response field $\tilde{\phi}$, and the corresponding noise term θ are all elements of the fundamental (defining) representation of $O(N)$ and thus transform as $\phi \to O\phi$, $\tilde{\phi} \to O\tilde{\phi}$, and $\theta \to O\theta$ under an action of O. The matrix of charge densities $n \equiv -\frac{1}{2}n_{ab}T_{ab}$, its associated response field $\tilde{n} \equiv -\frac{1}{2}\tilde{n}_{ab}T_{ab}$, and the corresponding noise $\zeta \equiv -\frac{1}{2}\zeta_{ab}T_{ab}$ are elements of the adjoint representation. They thus transform as $n \to OnO^T$, $\tilde{n} \to O\tilde{n}O^T$, $\zeta \to O\zeta O^T$. Similarly, the corresponding sources $H, \tilde{H}$ and $\mathcal{H}, \tilde{\mathcal{H}}$, for the order parameter and the conserved charges, are elements of the fundamental and the adjoint representation, respectively.

Now we let the transformation depend on time, $O \to O(t)$, i.e. we consider $\alpha_{ab} \to \alpha_{ab}(t)$. One can straightforwardly verify that the equations of motion (3.1) with the physical source terms included are invariant under the following time-dependent $O(N)$ transformations,

$$\begin{aligned}
\phi(t,\boldsymbol{x}) &\to O(t)\phi(t,\boldsymbol{x}) \\
\theta(t,\boldsymbol{x}) &\to O(t)\theta(t,\boldsymbol{x}) \\
n(t,\boldsymbol{x}) &\to O(t)n(t,\boldsymbol{x})O^T(t) \\
\zeta(t,\boldsymbol{x}) &\to O(t)\zeta(t,\boldsymbol{x})O^T(t) \\
\mathcal{H}(t,\boldsymbol{x}) &\to O(t)\mathcal{H}(t,\boldsymbol{x})O^T(t) + \frac{1}{g}O(t)\partial_t O^T(t)
\end{aligned} \tag{3.48}$$

which, importantly, requires an inhomogeneous transformation of the external (physical) source $\mathcal{H}$ of the charge densities by $\frac{1}{g}O(t)\partial_t O^T(t)$. This symmetry is therefore like a purely temporal (i.e. spatially constant) gauge symmetry in a non-Abelian gauge theory, e.g., with an incomplete Coulomb gauge fixing. The source $\mathcal{H}_{ab}$ plays the role of the zero-component $\mathcal{H}_{ab} = A^0_{ab}$ of an external non-Ablian gauge field A^μ_{ab}, and the gauge symmetry can be interpreted as the residual invariance under purely temporal gauge transformations that remains after choosing Coulomb gauge $\boldsymbol{\nabla}\cdot\boldsymbol{A}_{ab} = 0$. This is the non-Abelian generalization of the observation that sources A^μ for conserved $U(1)$ currents j^μ, due to the current conservation $\partial_\mu j^\mu = 0$, admit an Abelian gauge symmetry [192, 200].

In the special case of rigid rotations about a fixed axis, with $\alpha_{ab}(t) = \omega_{ab}\,t$ and constant angular velocity components ω_{ab} (i.e. in an Abelian subgroup of the gauge group), the purely temporal gauge transformations reduce to constant shifts or *displacements* of the external source $\mathcal{H}_{ab}$ by

$$\frac{1}{g}O(t)\partial_t O^T(t) = -\frac{1}{2}\omega_{ab}T_{ab}\,. \tag{3.49}$$

We will thus refer to this symmetry as the 'displacement symmetry' in the following. In QED, e.g. when completing the Coulomb gauge by requiring the zero component of the gauge field to be time independent, or in covariant gauges, an analogous displacement symmetry is left as part of the residual global gauge invariance after gauge fixing [202–204].[2]

Intuitively speaking, this symmetry states that the sole effect of a shift in the external source $\mathcal{H}$ is to induce a corresponding time-dependent rotation of all fields. In the language of the antiferromagnet, where the sole effect of a constant uniform magnetic field is to let all spins precess about the magnetic field with an angular frequency proportional to its strength, this phenomenon is known as Larmor precession.

Such a transformation behavior is usually called an 'extended' symmetry in the literature, as the corresponding change δS in the MSR action does not generally vanish, but is linear in the (composite) response fields and hence corresponds to a mere shift of the external sources [108, 109, 206, 207]. An extended symmetry poses just as strong constraints on the 1PI effective action as a normal symmetry does.

To formulate the time-dependent $O(N)$ transformations on the level of the MSR action (3.5), we need to transform the (composite) response fields instead of the noises,

$$\tilde{\phi}(t,\boldsymbol{x}) \to O(t)\tilde{\phi}(t,\boldsymbol{x})\,, \qquad \tilde{\Phi}(t,\boldsymbol{x}) \to O(t)\tilde{\Phi}(t,\boldsymbol{x})\,,$$
$$\tilde{n}(t,\boldsymbol{x}) \to O(t)\tilde{n}(t,\boldsymbol{x})O^T(t)\,, \qquad \tilde{N}(t,\boldsymbol{x}) \to O(t)\tilde{N}(t,\boldsymbol{x})O^T(t)\,.$$

Knowing that our extended symmetry acts on the external sources $\mathcal{H}_{ab}$ as a residual purely temporal $O(N)$ gauge symmetry, we may introduce corresponding covariant time derivatives for ϕ and n via

$$D_t\phi_a \equiv \partial_t\phi_a - \frac{g}{2}(T_{cd})_{ab}\mathcal{H}_{cd}\phi_b\,, \tag{3.50a}$$
$$D_t n_{ab} \equiv \partial_t n_{ab} - \frac{g}{2}(T_{cd})_{ab,ef}\mathcal{H}_{cd}n_{ef}\,. \tag{3.50b}$$

Including the coupling to the sources $\mathcal{H}$ into the definition of an extended MSR action,

$$S_{\mathcal{H}} \equiv S + \frac{1}{2}\int_x \mathcal{H}_{ab}\tilde{N}_{ab}\,,$$

we can then express $S_{\mathcal{H}}$ using these covariant derivatives (3.50) compactly as

$$S_{\mathcal{H}} = \int_x \Big[-\tilde{\phi}_a D_t\phi_a - \frac{1}{2}\tilde{n}_{ab}D_t n_{ab} - \tilde{\Phi}_a\frac{\delta F}{\delta\phi_a} - \frac{1}{2}\tilde{N}_{ab}\frac{\delta F}{\delta n_{ab}} + \tilde{\phi}_a iT\Gamma_0\tilde{\phi}_a - \frac{1}{2}\tilde{n}_{ab}iT\gamma\boldsymbol{\nabla}^2\tilde{n}_{ab}\Big]\,. \tag{3.51}$$

Here, the standard response fields $\tilde{\phi}_a$ and $\tilde{n}_{ab}$ are understood as functions of the composite response fields $\tilde{\Phi}_a$ and $\tilde{N}_{ab}$ (implicitly defined by the transformation (3.22)). Since the covariant derivatives transform covariantly under the purely temporal gauge transformations, the MSR action $S_{\mathcal{H}}$ (including the external source $\mathcal{H}$) is clearly seen to be invariant under these gauge transformations, and thus in particular also under the uniformly time-dependent $O(N)$ transformations with $\alpha_{ab}(t) = \omega_{ab}\,t$ of the displacement symmetry.

[2] In QED this global displacement symmetry is in fact always spontaneously broken, and the photon has been interpreted as the associated Goldstone boson to explain its masslessness [202, 205].

The transformation behavior of the MSR action S under such a residual gauge transformation can be compactly expressed as[3]

$$S[O\phi, O\tilde{\phi}, OnO^T, O\tilde{n}O^T] - \frac{1}{2}\int_x \mathrm{tr}\left(O\mathcal{H}O^T + \frac{1}{g}O\partial_t O^T\right) O\tilde{N}O^T = S[\phi, \tilde{\phi}, n, \tilde{n}] - \frac{1}{2}\int_x \mathrm{tr}\left(\mathcal{H}\tilde{N}\right) \tag{3.52}$$

with $O = O(t)$ here. For rigid rotations with infinitesimal angular frequencies (corresponding to infinitesimal shifts of the external source $\mathcal{H}$) we obtain the Ward identity

$$\begin{aligned}\int_x \Bigg[&\frac{1}{g}\tilde{N}_{ab}(x) + \frac{\delta\Gamma}{\delta\phi_{[a}(x)}\phi_{b]}(x)\, x^0 + \frac{\delta\Gamma}{\delta\tilde{\Phi}_{[a}(x)}\tilde{\Phi}_{b]}(x)\, x^0 + \\ &\frac{1}{2}\frac{\delta\Gamma}{\delta n_{cd}(x)}\left(\delta_{bc}n_{ad}(x) - \delta_{ac}n_{bd}(x) - \delta_{bd}n_{ac}(x) + \delta_{ad}n_{bc}(x)\right) x^0 + \\ &\frac{1}{2}\frac{\delta\Gamma}{\delta\tilde{N}_{cd}(x)}\left(\delta_{bc}\tilde{N}_{ad}(x) - \delta_{ac}\tilde{N}_{bd}(x) - \delta_{bd}\tilde{N}_{ac}(x) + \delta_{ad}\tilde{N}_{bc}(x)\right) x^0\Bigg] = 0\end{aligned} \tag{3.53}$$

for the effective action, which in the context of the FRG below will tightly constrain possible truncation schemes consistent with this displacement symmetry. Here we have already replaced the bare action S by the effective action Γ in the Ward identity, because, in absence of anomalies, the effective action admits the same symmetries as the bare action, e.g. see [180].

Charge conservation. For vanishing physical external sources $H = \mathcal{H} = 0$ the charges are conserved. This corresponds to a symmetry of the MSR action with respect to constant shifts in the standard response fields of the charges,

$$\tilde{n}_{ab}(x) \to \tilde{n}_{ab}(x) + \delta\tilde{n}_{ab} \tag{3.54}$$

with a constant but otherwise arbitrary $\delta\tilde{n}_{ab}$. Upon such a constant displacement the Lagrangian $\mathcal{L}$ in the MSR action (3.5) changes by a total time derivative

$$\delta\mathcal{L} = -\frac{1}{2}\delta\tilde{n}_{ab}\partial_t n_{ab}\,, \tag{3.55}$$

and hence the action is invariant. Using a formulation of Noether's theorem on the CTP [208], we then have $N(N-1)/2$ independent continuity equations (on average),

$$\langle\partial_\mu j^\mu_{ab}\rangle = 0 \tag{3.56}$$

corresponding to the conservation of the $N(N-1)/2$ charges

$$N_{ab} \equiv \int_{\boldsymbol{x}} n_{ab}(t, \boldsymbol{x})\,. \tag{3.57}$$

As a consequence of Noether's theorem, the conserved Lorentz vector current $j^\mu_{ab} = (j^0_{ab}, \boldsymbol{j}_{ab})$ can be derived using standard rules from the MSR action and the symmetry transformation (3.55) as e.g. illustrated in Sec. 2.4.3 of Ref. [208]. It is then given by

$$j^0_{ab} = n_{ab}\,, \tag{3.58}$$

$$\boldsymbol{j}_{ab} = -\frac{\gamma}{\chi}\boldsymbol{\nabla}n_{ab} + g(\phi_a\boldsymbol{\nabla}\phi_b - \phi_b\boldsymbol{\nabla}\phi_a) + i\gamma T\boldsymbol{\nabla}\tilde{n}_{ab}\,, \tag{3.59}$$

[3] Note that we can represent a contraction $A_{ab}B_{ab}$ as a trace, $A_{ab}B_{ab} = -\mathrm{tr}(AB)$ for two elements $A = \frac{1}{2}A_{ab}T_{ab}$, $B = \frac{1}{2}B_{ab}T_{ab}$ in the adjoint representation.

Since $\langle \tilde{n}_{ab} \rangle = 0$ due to causality, in fact, the last term in (3.59) does not contribute to the average in (3.56).

For non-vanishing external source fields H for the order parameter (which correspond to non-vanishing external magnetic fields in the language of the Heisenberg antiferromagnet, or to non-vanishing current quark masses in QCD with two light flavors), Eq. (3.56) is replaced by the familiar *partial* conservation of the currents,

$$\langle \partial_\mu j^\mu_{ab} \rangle = g \langle \phi_a H_b - \phi_b H_a \rangle \tag{3.60}$$

which is analogous to the PCAC relation in QCD.

BRST symmetry. The fundamental normalization condition $\langle 1 \rangle = 1$ of the MSR path integral implies

$$Z[J] \equiv Z[J, \tilde{J} = 0] = 1 \tag{3.61}$$

for arbitrary classical sources here collected in the (classical) superfield source $J = (H, \mathcal{H})$. I.e. for vanishing external response sources $\tilde{J} = (\tilde{H}, \tilde{\mathcal{H}})$ the generating functional is equal to unity, regardless of the values for the classical source terms, which means that the path integral becomes topological [209] in this limit. Such a condition is generally a consequence of the conservation of probability, i.e. the probability distribution of the field configurations ψ remains normalized under unitary time evolution of the corresponding probability amplitudes. Of course, this does *not* require the underlying evolution equations to be of conservative (Hamiltonian) form. This general property of the path integral on the CTP is enforced by a hidden BRST symmetry [192]: One can show that the total action that appears in the generating functional (3.26), when the Jacobian is expressed via anticommuting ghosts fields as in (3.29), is invariant under the following BRST transformation

$$\delta\psi_i = \epsilon c_i \,, \quad \delta c_i = 0 \,, \quad \delta\tilde{c}_i = -i\epsilon\tilde{\Psi}_i \,, \quad \delta\tilde{\Psi}_i = 0 \,, \quad \delta J_i = 0 \,, \tag{3.62}$$

where ϵ is an anti-commuting number in the Grassmann algebra of the ghosts, and i an index in superfield space. The normalization condition (3.61) is then a consequence of this BRST symmetry, see Appendix B.2. It is generated by the corresponding BRST charge

$$Q = c_i \frac{\delta}{\delta\psi_i} - i\tilde{\Psi}_i \frac{\delta}{\delta\tilde{c}_i} \,, \quad Q^2 = 0 \,. \tag{3.63}$$

In fact, the MSR action is BRST exact: In superfield notation, the total MSR action S_J including the classical sources J_i and the ghost action S_{gh} from (3.29)

$$S_J = S' + S_{gh} + J_i\tilde{\Psi}_i \tag{3.64}$$

can be expressed as a BRST variation,[4]

$$S_J = Q\left\{-i\tilde{c}_i\left(J^{-1^T}_{ij}(\psi)\partial_t\psi_j + \frac{\delta F}{\delta\psi_i} - J_i - iTJ^{-1^T}_{ij}(\psi)\tilde{\Psi}_j\right)\right\} . \tag{3.65}$$

We explain how (3.64) is obtained from (3.65) in Appendix B.2. In the form (3.65), the BRST invariance of the MSR action immediately follows from the nilpotency of the BRST charge Q. With vanishing response sources $\tilde{J} = (\tilde{H}, \tilde{\mathcal{H}})$, the MSR path integral computes the Witten index of a topological field theory and is hence independent of the classical sources $J = (H, \mathcal{H})$.

[4]Note, however, that the form of the BRST invariant action is not unique, and there are in general multiple BRST invariant actions that lead to the same MSR action (3.5), cf. Sec. 1.5 of [192].

3.2 FRG for dynamical systems with reversible mode couplings

A rather non-trivial task in devising a regulator suitable for systems with reversible mode couplings is to maintain all the symmetries of the MSR action we have discussed in Sec. 3.1.2 above. In particular, simply adding the regulator as a quadratic form in the fields directly to the MSR (or Keldysh) action, which works for systems without reversible mode couplings [1], here one immediately observes that some of the symmetries are then necessarily violated. For example, one can no-longer guarantee that the equilibrium distribution will be a Boltzmann distribution during the flow, and hence the usual formulation of the FDR no longer holds. Instead, as in the case of the physical sources in our construction of the generating functional in Sec. 3.1.1, we therefore add the regulator one step earlier to the LGW free energy,[5]

$$F \to F + \frac{1}{2}\int_{\boldsymbol{xy}} \left(\phi_a(\boldsymbol{x}) R_k^{\phi}(\boldsymbol{x},\boldsymbol{y}) \phi_a(\boldsymbol{y}) + \frac{1}{2} n_{ab}(\boldsymbol{x}) R_k^{n}(\boldsymbol{x},\boldsymbol{y}) n_{ab}(\boldsymbol{y}) \right) , \tag{3.66}$$

and obtain the MSR action with regulator terms from that. This guarantees that none of the symmetries from Sec. 3.1.2 are violated by the regulator terms.

Because of the Poisson brackets in the equations of motion (2.146), this gives rise to regulator terms in the MSR action that are no-longer quadratic in the original fields but couple to the *composite* response fields $\tilde{\Phi}_a$ and $\tilde{N}_{ab}$,

$$S \to S + \Delta S_k \,, \qquad \Delta S_k = -\int_{xy} \left(\tilde{\Phi}_a(x) R_k^{\phi}(x,y) \phi_a(y) + \frac{1}{2} \tilde{N}_{ab}(x) R_k^{n}(x,y) n_{ab}(y) \right) , \tag{3.67}$$

where

$$R_k^{\phi}(x,y) \equiv R_k^{\phi}(\boldsymbol{x},\boldsymbol{y})\, \delta(x^0 - y^0) \,, \text{ and } \; R_k^{n}(x,y) \equiv R_k^{n}(\boldsymbol{x},\boldsymbol{y})\, \delta(x^0 - y^0) \,. \tag{3.68}$$

The crucial generalization of the standard procedure here is that the regulators R_k^{ϕ} and R_k^{n} couple to the composite response fields $\tilde{\Phi}$ and $\tilde{N}$ in (3.67). On the other hand this then necessarily implies that the regulator term ΔS_k added to the MSR action, when expressed in terms of the standard response fields $\tilde{\phi}_a$ and $\tilde{n}_{ab}$, involves products of *three* fields.

As a side remark, also note that in (3.68) we have introduced equal-time regulators whose Fourier transforms are hence frequency independent. In this way, the causal structure of the MSR action [118] is maintained trivially by the regulators which is sufficient for our purposes here. If frequency dependent regulators are needed, on the other hand, a general construction scheme for causal regulators analogous to the one given in Sec. 2.3.2 can be used here as well.

The presence of the regulator term ΔS_k in addition to the bare MSR action lets the generating functional $Z \to Z_k$ and the Schwinger functional $W \to W_k$ depend on the FRG scale k. These can be viewed as their 'coarse-grained' counterparts where all fluctuations with momenta $p \lesssim k$ have been suppressed. In the FRG, the central object is the effective *average* action Γ_k, which can be similarly interpreted as a coarse-grained effective action. Γ_k is as usual defined by a modified Legendre transformation (as in (3.35) but with an additional subtraction of the regulator term) of the Schwinger functional W_k.

In line with the developments for systems with reversible mode couplings above, this modified Legendre transformation must be done here with respect to the physical sources inside the LGW

[5] We assume the regulator to be diagonal in field space to preserve the global $O(N)$ symmetry.

free energy, leading to the corresponding (expectation values of the) *composite* response fields in the effective average action,

$$\begin{aligned}\Gamma_k[\phi, n, \tilde{\Phi}, \tilde{N}] = W_k[H, \mathcal{H}, \tilde{H}, \tilde{\mathcal{H}}] - \Delta S_k[\phi, n, \tilde{\Phi}, \tilde{N}] \\ - \int_x \left(\tilde{H}_a \phi_a + \frac{1}{2} \tilde{\mathcal{H}}_{ab} n_{ab} + H_a \tilde{\Phi}_a + \frac{1}{2} \mathcal{H}_{ab} \tilde{N}_{ab} \right) .\end{aligned} \tag{3.69}$$

By expressing the regulator as a matrix in the two-dimensional $(\psi, \tilde{\Psi})$ MSR field space,

$$\hat{R}_k = \begin{pmatrix} 0 & R_k \\ R_k & 0 \end{pmatrix} , \tag{3.70}$$

the flow equation for the effective average action formulated in our compact superfield notation is given by

$$\partial_k \Gamma_k[\psi, \tilde{\Psi}] = \frac{i}{2} \operatorname{tr} \left\{ \partial_k \hat{R}_k \circ G_k[\psi, \tilde{\Psi}] \right\} \tag{3.71}$$

which is derived in Appendix D. The full FRG-scale and field-dependent propagators (3.33) and (3.34) appearing in the flow equation (3.71) are as usual related to the regulated two-point function via [106]

$$G_k[\psi, \tilde{\Psi}] = - \left(\Gamma_k^{(2)}[\psi, \tilde{\Psi}] - \hat{R}_k \right)^{-1} . \tag{3.72}$$

At the origin $\phi = n = 0$ and $\tilde{\Phi} = \tilde{N} = 0$ in field space the various propagators of the order parameter are diagonal and hence one can introduce scalar 'dressing' functions to write them as

$$G^R_{\phi_a \phi_b, k}(x, y) = G^R_{\phi, k}(x, y) \delta_{ab} , \tag{3.73a}$$
$$G^A_{\phi_a \phi_b, k}(x, y) = G^A_{\phi, k}(x, y) \delta_{ab} , \tag{3.73b}$$
$$iF_{\phi_a \phi_b, k}(x, y) = iF_{\phi, k}(x, y) \delta_{ab} , \tag{3.73c}$$

and similarly for the propagators of the charge densities,

$$G^R_{n_{ab} n_{cd}, k}(x, y) = G^R_{n, k}(x, y) \left(\delta_{ac} \delta_{bd} - \delta_{ad} \delta_{bc} \right) , \tag{3.74a}$$
$$G^A_{n_{ab} n_{cd}, k}(x, y) = G^A_{n, k}(x, y) \left(\delta_{ac} \delta_{bd} - \delta_{ad} \delta_{bc} \right) , \tag{3.74b}$$
$$iF_{n_{ab} n_{cd}, k}(x, y) = iF_{n, k}(x, y) \left(\delta_{ac} \delta_{bd} - \delta_{ad} \delta_{bc} \right) , \tag{3.74c}$$

where we have used the antisymmetric identity in the adjoint representation of $O(N)$ corresponding to the antisymmetric fundamental functional derivative (3.43). The corresponding scalar dressing functions in front δ_{ab} in (3.73) and in front of $(\delta_{ac}\delta_{bd} - \delta_{ad}\delta_{bc})$ in (3.74) can be derived from (3.72) and are explicitly given by

$$G^R_{\phi, k}(x, y) \delta_{ab} = - \left(\left. \frac{\delta^2 \Gamma_k}{\delta \tilde{\Phi}_a(x) \delta \phi_b(y)} \right|_0 - R^\phi_k(\boldsymbol{x}, \boldsymbol{y}) \delta_{ab} \right)^{-1} , \tag{3.75a}$$
$$G^A_{\phi, k}(x, y) \delta_{ab} = - \left(\left. \frac{\delta^2 \Gamma_k}{\delta \phi_a(x) \delta \tilde{\Phi}_b(y)} \right|_0 - R^\phi_k(\boldsymbol{x}, \boldsymbol{y}) \delta_{ab} \right)^{-1} , \tag{3.75b}$$
$$iF_{\phi, k}(x, y) \delta_{ab} = \int_{zw} G^R_{\phi, k}(x, z) \left. \frac{\delta^2 \Gamma_k}{\delta \tilde{\Phi}_a(z) \delta \tilde{\Phi}_b(w)} \right|_0 G^A_{\phi, k}(w, y) , \tag{3.75c}$$

in case of the order parameter, and by

$$G^R_{n,k}(x,y)\,(\delta_{ac}\delta_{bd}-\delta_{ad}\delta_{bc}) = -\left(\frac{\delta^2\Gamma_k}{\delta\tilde{N}_{ab}(x)\delta n_{cd}(y)}\bigg|_0 - R^n_k(\boldsymbol{x},\boldsymbol{y})\,(\delta_{ac}\delta_{bd}-\delta_{ad}\delta_{bc})\right)^{-1}, \tag{3.76a}$$

$$G^A_{n,k}(x,y)\,(\delta_{ac}\delta_{bd}-\delta_{ad}\delta_{bc}) = -\left(\frac{\delta^2\Gamma_k}{\delta n_{ab}(x)\delta\tilde{N}_{cd}(y)}\bigg|_0 - R^n_k(\boldsymbol{x},\boldsymbol{y})\,(\delta_{ac}\delta_{bd}-\delta_{ad}\delta_{bc})\right)^{-1}, \tag{3.76b}$$

$$iF_{n,k}(x,y)\,(\delta_{ac}\delta_{bd}-\delta_{ad}\delta_{bc}) = \int_{zw} G^R_{n,k}(x,z)\frac{\delta^2\Gamma_k}{\delta\tilde{N}_{ab}(z)\delta\tilde{N}_{cd}(w)}\bigg|_0 G^A_{n,k}(w,y)\,, \tag{3.76c}$$

in case of the charge densities. Note that the tensor structures δ_{ab} and $\delta_{ac}\delta_{bd}-\delta_{ad}\delta_{bc}$ match on both sides at the origin in field space, and hence the corresponding scalar dressing functions as $G^R_{\phi,k}(x,y)$ and $G^R_{n,k}(x,y)$ can be read off by a comparison of coefficients. For non-vanishing field expectation values (or finite external fields $H\neq 0$) the full expressions for the propagators in general involve various other $O(N)$ tensor structures besides the identities here, and hence become evidently rather cumbersome. For this reason we restrict ourselves to the origin in field space $\phi = n = 0$ for the scope of this work.

In thermal equilibrium, the symmetry of detailed balance (3.44) implies an FDR for the propagators in Fourier space[6] [192],

$$iF_{ij,k}(\omega,\boldsymbol{p}) = \frac{T}{\omega}\left(G^R_{ij,k}(\omega,\boldsymbol{p}) - G^A_{ij,k}(\omega,\boldsymbol{p})\right), \tag{3.77}$$

from which also follows (using (3.72))

$$\Gamma^{\tilde{\Psi}\tilde{\Psi}}_{ij,k}(\omega,\boldsymbol{p}) = \frac{T}{\omega}\left(\Gamma^{\tilde{\Psi}\psi}_{ij,k}(\omega,\boldsymbol{p}) - \Gamma^{\psi\tilde{\Psi}}_{ij,k}(\omega,\boldsymbol{p})\right), \tag{3.78}$$

where we have used the superfield notation $\psi = (\phi, n)$ and $\tilde{\Psi} = (\tilde{\Phi}, \tilde{N})$ again, to encompass the FDR for both types of fields concisely in one equation. Importantly, (3.77) would not hold in this particularly simple form if the non-composite standard response fields $\tilde{\phi}$ and $\tilde{n}$ were used to define the propagators. Besides two-point functions, one can use the invariance under the transformation (3.44) to derive generalized fluctuation-dissipation relations between higher-order n-point functions in the spirit of Ref. [210].

If the regulator couples to composite fields such as (3.22) one has to make sure that the effective average action still converges to the bare action in the limit $k\to\Lambda$, i.e., that the flow properly integrates out all fluctuations. For standard flows where the regulator term is a quadratic form in the elementary fields, this is usually shown using a saddle-point approximation. However, if the regulator couples to composite fields the situation is not as clear anymore. For a general discussion on this issue see, e.g., Sec. III C 4 of Ref. [179]. For the way the FRG flow is set up in the present work, we show in Appendix D that in the UV limit the effective average action converges to

$$\Gamma_k[\psi,\tilde{\Psi}] \xrightarrow{k\to\Lambda} S[\psi,\tilde{\psi}] - i\log|\det J^{-1}(\psi)| + \text{const.} \tag{3.79}$$

which, again, involves the Jacobian matrix (3.28). Roughly speaking, the additional Jacobian determinant in (3.79) compensates for the fact that the bare action depends on the elementary response fields $\tilde{\phi}$ and $\tilde{n}$, whereas the effective average action actually depends on the expectation

[6] For more details on the derivation of the FDR for dynamical systems with reversible mode couplings see Ref. [201].

values of our *composite* response fields $\tilde{\Phi}$ and $\tilde{N}$. As such, this is just another reflection of the Jacobian matrix (3.28) in our non-linear field transformation, since exponentiating (3.79) yields

$$e^{i\Gamma_k[\psi,\tilde{\Psi}]} \xrightarrow{k\to\Lambda} \left|\det J^{-1}(\psi)\right| \, e^{iS[\psi,\tilde{\psi}]} = \mathcal{J}'[\psi]\, e^{iS[\psi,\tilde{\psi}]} \tag{3.80}$$

(up to an irrelevant overall normalization factor). This thus coincides with the integrand in (3.26).

3.2.1 Static flow

Generally, one can assign a free energy $F_k = F_k[\phi, n]$ to the effective average MSR action $\Gamma_k = \Gamma_k[\phi, n, \tilde{\Phi}, \tilde{N}]$ by matching the functional derivative of F_k with respect to the classical fields ϕ, n to a functional derivative of Γ_k with respect to the composite response fields $\tilde{\Phi}, \tilde{N}$,

$$\frac{\delta F_k}{\delta \phi_a} \equiv -\frac{\delta \Gamma_k}{\delta \tilde{\Phi}_a}\bigg|_{\substack{\tilde{\Phi}=\tilde{N}=0\,,\\ \partial_t\phi=\partial_t n=0}}, \qquad \frac{\delta F_k}{\delta n_{ab}} \equiv -\frac{\delta \Gamma_k}{\delta \tilde{N}_{ab}}\bigg|_{\substack{\tilde{\Phi}=\tilde{N}=0\,,\\ \partial_t\phi=\partial_t n=0}}. \tag{3.81}$$

Using this matching procedure one can define an FRG-scale-dependent LGW functional $F_k[\phi, n]$ (up to an irrelevant additive constant), as motivated in more detail below.

We emphasize a central feature of our formulation here, namely that the such defined free energy F_k generally satisfies a closed flow equation on its own,

$$\partial_k F_k = \frac{T}{2}\,\mathrm{tr}\left\{\partial_k R_k \circ \left(F_k^{(2)} + R_k\right)^{-1}\right\}, \tag{3.82}$$

with the second functional derivative $F_k^{(2)}$, which is in superfield space $\psi = (\phi, n)$ given by

$$F^{(2)}_{ij,k}(\boldsymbol{x},\boldsymbol{y}) \equiv \frac{\delta^2 F}{\delta\psi_i(\boldsymbol{x})\delta\psi_j(\boldsymbol{y})},$$

where i and j are again superfield indices, and with the regulator $R_k = \mathrm{diag}(R_k^\phi, R_k^n)$ in superfield space. Remarkably, the right-hand side of (3.82) only depends on the free energy F_k again, but not on any genuine real-time quantity like the kinetic coefficients or the reversible mode coupling constant. We therefore say that the 'static' part of the flow given by the free energy (3.81), decouples from the 'dynamic' part of the flow, given by any remaining parts of the effective average MSR action which are not contained in (3.81) (as e.g. the kinetic coefficients Γ_0, $\gamma\boldsymbol{\nabla}^2$, or the reversible mode coupling g). Notably, Eq. (3.82) coincides with the standard flow equation (2.164) for equilibrium systems, which entails that the static critical behavior is not altered by changes in the dynamics, for instance whether the dynamics is relaxational, diffusive, or whether it includes reversible mode couplings or not, as long as the symmetry of detailed balance (3.44) holds. Moreover, this decoupling of F_k from the rest can be used as a powerful tool, since it means that one can derive flow equations for static quantities without having to invoke the entire complexity of the real-time formalism. For instance, one can employ well-developed methods from the standard formulation of the FRG in Euclidean space to find suitable truncation schemes for (3.82), for instance by expanding F_k in the number of derivatives [73]. There the lowest order would correspond to a local potential approximation (LPA) of the free energy.

To elaborate more on (3.81) and (3.82), we first discuss the reasoning for why the flow equation (3.82) of the free energy F_k should be closed (i.e. independent of the dynamics). Since

we add the regulators R_k^ϕ and R_k^n as well as the classical sources H and $\mathcal{H}$ directly to the free energy as in (3.66) and (3.3), we do not violate the symmetry of thermal equilibrium (3.44) throughout the flow, and hence the equilibrium distribution is given by a (regulated) Boltzmann distribution at all FRG scales.[7] As a non-trivial feature of our formulation, this implies that we have a physical theory (but with a regulated free energy (3.66)) at *all* FRG scales k. Hence, equal-time correlation functions can be obtained from the usual equilibrium generating functional (3.4) as averages over the Boltzmann distribution (2.149), but with the regulated free energy (3.66). More specifically, in the equilibrium formulation the FRG-scale-dependent free energy F_k is given by a (modified) Legendre transform of the equilibrium generating functional Z_k^{eq}, i.e.

$$F_k \equiv \sup_{H,\mathcal{H}} \left\{ \int_{\boldsymbol{x}} \left(H_a \phi_a + \frac{1}{2} \mathcal{H}_{ab} n_{ab} \right) - \Delta F_k - T \log Z_k^{eq} \right\} \tag{3.83}$$

where ΔF_k denotes the regulator term from (3.66). Following the standard derivation from [72], one can straightforwardly deduce that F_k satisfies the standard Euclidean flow equation (3.82).

Next, we motivate the definition (3.81) by relating F_k, as defined in (3.83), to the effective average MSR action Γ_k as defined in (3.69): For a purely classical and time-independent source configuration ($\tilde{H} = \tilde{\mathcal{H}} = 0$ and $\partial_t H = \partial_t \mathcal{H} = 0$) equal-time correlation functions can be computed in two equivalent ways: From functional derivatives of F_k in the equilibrium formalism, i.e. as an average over the Boltzmann distribution (2.149), or from functional derivatives of Γ_k in the real-time MSR formalism. In the equilibrium formalism, on the one hand, time-independent sources $H, \mathcal{H}$ are related to the first functional derivative of F_k via

$$H_a = \frac{\delta F_k}{\delta \phi_a} + R_k^\phi \phi_a \,, \qquad \mathcal{H}_{ab} = \frac{\delta F_k}{\delta n_{ab}} + R_k^n n_{ab} \,, \tag{3.84}$$

as can be straightforwardly derived from the modified Legendre transform (3.83). On the other hand, such a classical source configuration $H, \mathcal{H}$ is given as a special case of the real-time MSR formalism by setting $\tilde{H} = \tilde{\mathcal{H}} = 0$ and $\partial_t H = \partial_t \mathcal{H} = 0$ in the effective equations of motion (where the latter are given by the first functional derivative of the modified Legendre transform (3.69) with respect to $\tilde{H}_a$, and $\tilde{\mathcal{H}}_{ab}$, respectively)

$$H_a = -\frac{\delta \Gamma_k}{\delta \tilde{\Phi}_a}\bigg|_{\substack{\tilde{\Phi}=\tilde{N}=0\,,\\ \partial_t\phi=\partial_t n=0}} + R_k^\phi \phi_a \,, \qquad \mathcal{H}_{ab} = -\frac{\delta \Gamma_k}{\delta \tilde{N}_{ab}}\bigg|_{\substack{\tilde{\Phi}=\tilde{N}=0\,,\\ \partial_t\phi=\partial_t n=0}} + R_k^n n_{ab} \,. \tag{3.85}$$

Here we have used that the vanishing of response-field expectation values $\tilde{\Phi} = \tilde{N} = 0$ is a solution to the effective equations of motion for vanishing response sources $\tilde{H} = \tilde{\mathcal{H}} = 0$ which follows from the normalization condition $Z = 1$ of the MSR path integral, see e.g. [118], and that if the external classical source $\partial_t H = \partial_t \mathcal{H} = 0$ is time independent, so is the classical field expectation value $\partial_t \phi = \partial_t n = 0$ since our MSR action S does not carry any other explicit time dependence.

Since both the equilibrium (3.84) and the real-time MSR approach (3.85) have to yield the same static classical source H_a and $\mathcal{H}_{ab}$, we find the anticipated relation (3.81) between the free energy F_k and the effective average MSR action Γ_k by identifying (3.84) and (3.85). This relation allows us to generally extract the free energy F_k from a given Γ_k at all FRG scales. Then, by virtue of (3.82), we know that its flow equation is closed.

In addition to this general argument, an explicit derivation of (3.82) from (3.81) and the known flow equation (3.71) of Γ_k is provided in Appendix C.5 of Ref. [2].

[7] This can be shown via a Fokker-Planck equation to which the MSR path integral is equivalent, see e.g. [104] in the context of Model G.

3.2.2 Diagrammatics

Next, we want to derive the flow equations. In order to develop a straightforward way to derive the flow equations, it is much more convenient to carry out derivatives using Feynman rules. Here we want to give the diagrammatical representation of propagators, regulators, and vertices. The propagators are represented by

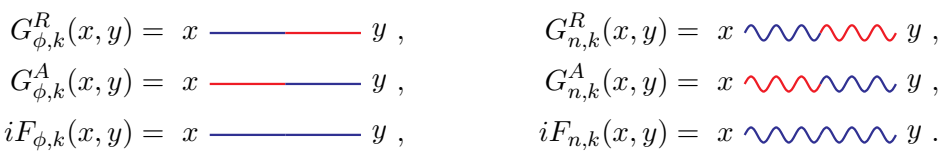

The regulators are diagrammatically represented by

Since regulators almost always appear in sums over all their possible combinations, we introduce a corresponding shorthand notation for a regulator inserted between two propagators (with the color of the external legs fixed) for the ϕ's,

$$B^F_{\phi,k} = -G^R_{\phi,k} \circ \partial_k R_{\phi,k} \circ iF_{\phi,k} - iF_{\phi,k} \circ \partial_k R_{\phi,k} \circ G^A_{\phi,k} \,, \tag{3.86a}$$
$$B^R_{\phi,k} = -G^R_{\phi,k} \circ \partial_k R_{\phi,k} \circ G^R_{\phi,k} \,, \tag{3.86b}$$
$$B^A_{\phi,k} = -G^A_{\phi,k} \circ \partial_k R_{\phi,k} \circ G^A_{\phi,k} \,, \tag{3.86c}$$

and the n's,

$$B^F_{n,k} = -G^R_{n,k} \circ \partial_k R_{n,k} \circ iF_{n,k} - iF_{n,k} \circ \partial_k R_{n,k} \circ G^A_{n,k} \,, \tag{3.87a}$$
$$B^R_{n,k} = -G^R_{n,k} \circ \partial_k R_{n,k} \circ G^R_{n,k} \,, \tag{3.87b}$$
$$B^A_{n,k} = -G^A_{n,k} \circ \partial_k R_{n,k} \circ G^A_{n,k} \,. \tag{3.87c}$$

Diagrammatically, we represent the B's via boxes,

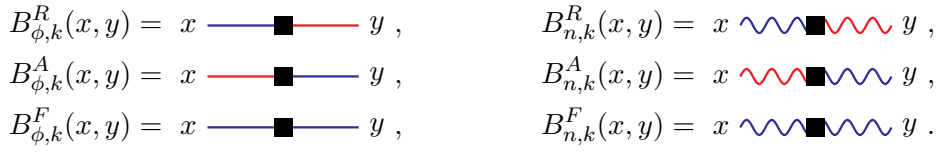

We employ the same shorthand notation as [98], i.e. that green lines denote a sum over all possible combinations of red and blue. With these, the flow equation of the scale dependent effective action can be compactly expressed as

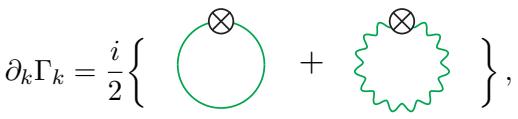

(3.88)

where in comparison to Refs. [1,90,98] the global minus sign is here absorbed into our definition of the regulator. Moreover, vertices are as usual represented by black dots, cf. Fig. 3.1 below.

3.3 Truncation and flow equations

As a starting point for practical applications within the FRG, one has to truncate the effective average action in a way that respects all relevant symmetries (here listed in Sec. 3.1.2). In the context of critical phenomena, a derivative expansion of the effective average action has proven to converge rather quickly towards quantitatively accurate results for critical exponents [78,211], universal amplitude ratios [79], and recently, the location of Yang-Lee edge singularities [212–214]. This suggests that a similar expansion in terms of derivatives is a sensible choice for a systematic truncation scheme also for Model G here. In the context of critical *dynamics*, a derivative expansion has been already employed in previous works in the purely relaxational Models A [82] and C [83], for example. However, in the presence of reversible mode couplings, it is rather difficult to set up a derivative expansion systematically since the temporal-gauge and its accompanying residual displacement symmetry from Sec. 3.1.2 prohibits a naive introduction of terms with ordinary time derivatives (rather, the covariant time derivative (3.50) that is manifestly invariant under the displacement symmetry must thus be used instead of the ordinary one in a systematic derivative expansion). For the calculation of spectral functions, the combined expansion scheme for the effective average action of Refs. [1, 90], first in terms of 1PI vertex functions and a second in the number of loops taken into account on the level of the flow equations (if possible self-consistently), has proven to be well suited to study their dynamic critical behavior in Models A, B and C [1], cf. Secs. 2.2.1, 2.2.2 and 2.2.3. For the scope of this chapter, we take the more pragmatic approach of *postulating* a suitable ansatz for the effective average action based on previous experience.

In particular, we construct our truncation by considering a generalized form of the bare MSR action (2.146) where all couplings are promoted to be running (i.e. to depend on the FRG scale k),

$$\begin{aligned}\Gamma_k = \int_x \Bigg[&- \tilde{\phi}_{a,k} \left(Z^{\omega}_{\phi,k} \frac{\partial \phi_a}{\partial t} + \gamma_{\phi,k}(\boldsymbol{\nabla}) \frac{\delta F_k}{\delta \phi_a} - \frac{g^{\phi n}_k}{2} \{\phi_a, n_{bc}\} \frac{\delta F_k}{\delta n_{bc}} \right) \\ &- \frac{1}{2} \tilde{n}_{ab,k} \left(Z^{\omega}_{n,k} \frac{\partial n_{ab}}{\partial t} + \gamma_{n,k}(\boldsymbol{\nabla}) \frac{\delta F_k}{\delta n_{ab}} - g^{n\phi}_k \{n_{ab}, \phi_c\} \frac{\delta F_k}{\delta \phi_c} - \frac{g^{nn}_k}{2} \{n_{ab}, n_{cd}\} \frac{\delta F_k}{\delta n_{cd}} \right) \\ &+ Z^{\omega}_{\phi,k} iT \tilde{\phi}_{a,k} \gamma_{\phi,k}(\boldsymbol{\nabla}) \tilde{\phi}_{a,k} + \frac{1}{2} Z^{\omega}_{n,k} iT \tilde{n}_{ab,k} \gamma_{n,k}(\boldsymbol{\nabla}) \tilde{n}_{ab,k} \Bigg] . \end{aligned} \tag{3.89}$$

We have included an arbitrary scale-dependent free-energy functional $F_k[\phi, n]$, temporal wave function renormalization factors $Z^{\omega}_{\phi,k}$ and $Z^{\omega}_{n,k}$, generalized kinetic coefficients $\gamma_{\phi,k}(\boldsymbol{\nabla})$ and $\gamma_{n,k}(\boldsymbol{\nabla})$ that involve arbitrary spatial gradients, and three different instances $g^{\phi n}_k$, $g^{n\phi}_k$ and g^{nn}_k of the reversible mode couplings corresponding to the three different Poisson brackets. To guarantee the conservation of the charges, the spatial Fourier transform of the kinetic coefficient $\gamma_{n,k}(\boldsymbol{p})$ must vanish in the limit $\boldsymbol{p} \to 0$, and thus its expansion in gradients must start at order $\boldsymbol{\nabla}^2$.

Moreover, note that the temporal wave function renormalization factors $Z^{\omega}_{\phi,k}$ and $Z^{\omega}_{n,k}$ are not independent of the other couplings, but can be eliminated via a redefinition of the response fields $\tilde{\phi}_k \to \tilde{\phi}_k / Z^{\omega}_{\phi,k}$, $\tilde{n}_k \to \tilde{n}_k / Z^{\omega}_{n,k}$ together with a corresponding rescaling of the kinetic coefficients $\gamma_{\phi,k}(\boldsymbol{p}) / Z^{\omega}_{\phi,k} \to \gamma_{\phi,k}(\boldsymbol{p})$, $\gamma_{n,k}(\boldsymbol{p}) / Z^{\omega}_{n,k} \to \gamma_{n,k}(\boldsymbol{p})$ and reversible mode couplings, $g^{\phi n}_k / Z^{\omega}_{\phi,k} \to g^{\phi n}_k$, $g^{n\phi}_k / Z^{\omega}_{n,k} \to g^{n\phi}_k$ and $g^{nn}_k / Z^{\omega}_{n,k} \to g^{nn}_k$. We can therefore safely set $Z^{\omega}_{\phi,k} = Z^{\omega}_{n,k} = 1$ from now on.

Finally, reversibility (i.e. requiring that the discrete transformation (3.44) of thermal equi-

librium remains a symmetry of the effective average action) implies that the matrix of reversible mode couplings is symmetric, i.e. that $g_k^{\phi n} = g_k^{n\phi}$, here.

The standard response fields $\tilde{\phi}$ and $\tilde{n}$ are related to the composite response fields $\tilde{\Phi}$ and $\tilde{N}$ by an FRG-scale-dependent generalization of (3.38),

$$\tilde{\Phi}_a \equiv \gamma_{\phi,k}(\boldsymbol{\nabla})\tilde{\phi}_{a,k} - \frac{g_k^{n\phi}}{2}\tilde{n}_{bc,k}\{n_{bc}, \phi_a\}\,, \tag{3.90a}$$

$$\tilde{N}_{ab} \equiv \gamma_{n,k}(\boldsymbol{\nabla})\tilde{n}_{ab,k} - \frac{g_k^{nn}}{2}\tilde{n}_{cd,k}\{n_{cd}, n_{ab}\} - g_k^{\phi n}\tilde{\phi}_{c,k}\{\phi_c, n_{ab}\}\,. \tag{3.90b}$$

In particular, this implies that in order to keep the composite response fields $\tilde{\Phi}$ and $\tilde{N}$ independent of the FRG scale k, the standard response fields $\tilde{\phi}_k$ and $\tilde{n}_k$ must necessarily depend on k. In the more compact superfield notation, this definition reads

$$\tilde{\Psi} = J_k(\psi)\tilde{\psi}_k \tag{3.91}$$

with the scale-dependent Jacobian $J_k(\psi)$ given by

$$J_k(\psi) = \begin{pmatrix} \delta_{ad}\,\gamma_{\phi,k}(\boldsymbol{\nabla}) & \frac{g_k^{n\phi}}{2}\{\phi_a, n_{ef}\} \\ g_k^{\phi n}\{n_{bc}, \phi_d\} & -\frac{1}{2}\left(\delta_{be}\delta_{cf} - \delta_{bf}\delta_{ce}\right)\gamma_{n,k}(\boldsymbol{\nabla}) + \frac{g_k^{nn}}{2}\{n_{bc}, n_{ef}\} \end{pmatrix}. \tag{3.92}$$

In our superfield notation the ansatz for the effective average action reads

$$\Gamma_k = -\tilde{\psi}_k^T\partial_t\psi + iT\tilde{\psi}_k^T\gamma_k\tilde{\psi}_k - \tilde{\psi}_k^T J_k^T(\psi)\frac{\delta F_k}{\delta\psi} \qquad \text{(old fields)} \tag{3.93}$$

$$= -\tilde{\Psi}^T {J_k^{-1}}^T(\psi)\partial_t\psi + iT\tilde{\Psi}^T J_k^{-1}(\psi)\tilde{\Psi} - \tilde{\Psi}^T\frac{\delta F_k}{\delta\psi} \qquad \text{(new fields)} \tag{3.94}$$

where also the Jacobian depends on the FRG scale k, and with the inverse kinetic coefficient γ_k in superfield space denoted by

$$\gamma_k(\boldsymbol{\nabla}) \equiv \begin{pmatrix} \gamma_{\phi,k}(\boldsymbol{\nabla}) & \\ & \gamma_{n,k}(\boldsymbol{\nabla}) \end{pmatrix}. \tag{3.95}$$

To extract vertices and propagators from (3.94), we introduce small but spacetime-dependent perturbations around (possibly) FRG-scale-dependent background fields, $\phi(x) = \phi_{0,k} + \delta\phi(x)$, $n(x) = n_{0,k} + \delta n(x)$,

$$J_k^{-1}(\psi) = J_k^{-1}(\psi_{0,k} + \delta\psi) \equiv \left(J_k(\psi_{0,k}) - \delta J_k(\delta\psi)\right)^{-1} \tag{3.96}$$

where the last equality defines the perturbation $\delta J(\delta\psi)$ of the Jacobian, which vanishes $\delta J(\delta\psi = 0) = 0$ for unperturbed background fields $\psi(x) = \psi_0$. Then we can expand the inverse Jacobian in a Neumann series in terms of powers of the field perturbations,

$$J_k^{-1}(\psi) = J_k^{-1}(\psi_{0,k}) + J_k^{-1}(\psi_{0,k}) \circ \delta J_k(\delta\psi) \circ J_k^{-1}(\psi_{0,k}) + \cdots\,, \tag{3.97}$$

where the circle $\circ$ denotes convolution again, i.e., summation over indices and integration over adjacent spacetime coordinates. The n-point vertices are given by taking the corresponding n^{th} functional derivative of the effective average action. In this chapter we expand around vanishing field expectation values, so we set the background fields to $\phi_0 = n_0 = 0$. At least in principle, one can generalize this scheme to (e.g.) an expansion around the scale-dependent minimum where the background field for the order parameter $\phi_0 = \phi_{0,k}$ becomes scale-dependent. However, the

corresponding Neumann series (3.97) and subsequent functional derivatives of Γ_k then become rather tedious, since a non-vanishing background expectation value of the order parameter ϕ_0 allows mixing of the pions with the iso-axial-vector charge densities. As it turns out, this mixing leads to numerous additional terms in the flow equations. As such, we restrict ourselves to the choice $\phi_0 = n_0 = 0$ for the scope of this work, i.e., to temperatures $T \geq T_c$ and vanishing external fields $H = 0$.

With this choice, the FRG-scale-dependent propagators (3.75) and (3.76) are given by (with $\chi_{\phi,k}(\boldsymbol{p})$ and $\chi_{n,k}(\boldsymbol{p})$ the corresponding FRG-scale-dependent static susceptibilities as extracted from the free energy, see Eq. (3.106) below)

$$G^R_{\phi,k}(\omega,\boldsymbol{p}) = -\frac{\gamma_{\phi,k}(\boldsymbol{p})}{i\omega - \gamma_{\phi,k}(\boldsymbol{p})\,\chi^{-1}_{\phi,k}(\boldsymbol{p})}\,, \tag{3.98a}$$

$$G^A_{\phi,k}(\omega,\boldsymbol{p}) = -\frac{\gamma_{\phi,k}(\boldsymbol{p})}{-i\omega - \gamma_{\phi,k}(\boldsymbol{p})\,\chi^{-1}_{\phi,k}(\boldsymbol{p})}\,, \tag{3.98b}$$

$$iF_{\phi,k}(\omega,\boldsymbol{p}) = \frac{2i\gamma_{\phi,k}(\boldsymbol{p})T}{\omega^2 + \left(\gamma_{\phi,k}(\boldsymbol{p})\,\chi^{-1}_{\phi,k}(\boldsymbol{p})\right)^2}\,, \quad \text{(fixed from the FDR)} \tag{3.98c}$$

for the order parameter, and by

$$G^R_{n,k}(\omega,\boldsymbol{p}) = -\frac{\gamma_{n,k}(\boldsymbol{p})}{i\omega - \gamma_{n,k}(\boldsymbol{p})\,\chi^{-1}_{n,k}(\boldsymbol{p})}\,, \tag{3.99a}$$

$$G^A_{n,k}(\omega,\boldsymbol{p}) = -\frac{\gamma_{n,k}(\boldsymbol{p})}{-i\omega - \gamma_{n,k}(\boldsymbol{p})\,\chi^{-1}_{n,k}(\boldsymbol{p})}\,, \tag{3.99b}$$

$$iF_{n,k}(\omega,\boldsymbol{p}) = \frac{2i\gamma_{n,k}(\boldsymbol{p})T}{\omega^2 + \left(\gamma_{n,k}(\boldsymbol{p})\,\chi^{-1}_{n,k}(\boldsymbol{p})\right)^2}\,, \quad \text{(fixed from the FDR)} \tag{3.99c}$$

for the charge densities. The static susceptibilities are defined as the equal-time correlation functions

$$\chi_{\phi_a\phi_b,k}(\boldsymbol{p}) = \int \frac{d^dx}{(2\pi)^d}\, e^{-i\boldsymbol{p}\cdot\boldsymbol{x}} \langle \phi_a(t,\boldsymbol{x})\phi_b(t,\boldsymbol{0})\rangle\,, \tag{3.100}$$

$$\chi_{n_{ab}n_{cd},k}(\boldsymbol{p}) = \int \frac{d^dx}{(2\pi)^d}\, e^{-i\boldsymbol{p}\cdot\boldsymbol{x}} \langle n_{ab}(t,\boldsymbol{x})n_{cd}(t,\boldsymbol{0})\rangle\,, \tag{3.101}$$

and are hence related to the statistical functions (3.98c) and (3.99c) via

$$\int \frac{d\omega}{2\pi}\, iF_{\phi,k}(\omega,\boldsymbol{p}) = T\chi_{\phi,k}(\boldsymbol{p})\,, \quad \text{and} \quad \int \frac{d\omega}{2\pi}\, iF_{n,k}(\omega,\boldsymbol{p}) = T\chi_{n,k}(\boldsymbol{p})\,. \tag{3.102}$$

For vanishing field expectation values, the static susceptibilities are diagonal in field space, i.e. we can parameterize them as

$$\chi_{\phi_a\phi_b,k}(\boldsymbol{p}) = \chi_{\phi,k}(\boldsymbol{p})\,\delta_{ab} \quad \text{and} \quad \chi_{n_{ab}n_{cd},k}(\boldsymbol{p}) = \chi_{n,k}(\boldsymbol{p})\,(\delta_{ac}\delta_{bd} - \delta_{ad}\delta_{bc})\,, \tag{3.103}$$

analogous to the propagators (3.73) and (3.74). They are related directly to the second functional derivatives of the FRG-scale-dependent free energy F_k via

$$\chi^{-1}_{\phi,k}(\boldsymbol{p})\,\delta_{ab} = \left.\frac{\delta^2 F_k}{\delta\phi_a(-\boldsymbol{p})\,\delta\phi_b(\boldsymbol{p})}\right|_{\phi=n=0} + R_{\phi,k}(\boldsymbol{p})\,\delta_{ab} \tag{3.104a}$$

$$\chi^{-1}_{n,k}(\boldsymbol{p})\,(\delta_{ac}\delta_{bd} - \delta_{ad}\delta_{bc}) = \left.\frac{\delta^2 F_k}{\delta n_{ab}(-\boldsymbol{p})\,\delta n_{cd}(\boldsymbol{p})}\right|_{\phi=n=0} + R_{n,k}(\boldsymbol{p})\,(\delta_{ac}\delta_{bd} - \delta_{ad}\delta_{bc}) \tag{3.104b}$$

The explicit expressions are given in Eq. (3.106) below, in the following subsection for the truncation of the free energy that we introduce next.

To conclude this subsection, we briefly comment on the physical argument concerning the convergence/applicability of the present truncation. For static critical phenomena it has been shown explicitly in (e.g.) Refs. [78, 79] that the standard derivative expansion rapidly converges towards the correct values for critical exponents and universal amplitude ratios. Hence, it is not unreasonable to expect that some variant of a derivative expansion is also a suitable truncation scheme for *dynamic* critical phenomena. One main difference is that, due to the lack of Lorentz invariance, space and time derivatives must be treated differently. For Model A, such systematic derivative expansions of the effective average MSR action have been employed e.g. in Refs. [81, 82, 84, 154], where it is mainly the thermal-equilibrium symmetry (3.44) that fixes all operators at any given truncation order in the number of time derivatives. However, for systems with reversible mode couplings such as Model G, there is also the extended temporal gauge symmetry (3.48) that has to be respected at any given truncation order in the number of time derivatives. Intuitively, one would expect that this means that time derivatives must always appear in the covariant form (3.50). However, the complication is that the covariant time-derivatives in (3.50) involve the *external* source $\mathcal{H}$ as the gauge field, which is in principle related again via $\mathcal{H} = \delta\Gamma/\delta\tilde{N}$ to the effective MSR action Γ. It is therefore not obvious at the moment which operators one has to include in Γ at any given order in the number of time derivatives such that (3.48) is still an extended symmetry. In the best case, one would also like to have an *exhaustive* list of operators (and presumably relations between their couplings) that can be included such that the time-gauged $O(N)$ transformation (3.48) is still an extended symmetry. This would make it possible to formulate a systematic derivative expansion also for Model G, or more generally, for systems with reversible mode couplings. Since this question is beyond the scope of the present work, we instead focus here on our more pragmatic ansatz (3.94).

3.3.1 Static couplings

We implement the (arguably simplest possible) truncation for the free energy by promoting the squared mass and the quartic coupling to depend on the FRG scale, i.e. we consider

$$F_k = \int_{\boldsymbol{x}} \left\{ \frac{1}{2}(\partial^i \phi_a)(\partial^i \phi_a) + \frac{m_k^2}{2}\phi_a\phi_a + \frac{\lambda_k}{4!N}(\phi_a\phi_a)^2 + \frac{1}{4\chi} n_{ab} n_{ab} \right\} . \tag{3.105}$$

The flow of the possibly scale-dependent static susceptibility $\chi_k \equiv \chi$ vanishes trivially since n only appears quadratically in the free energy and does not couple to ϕ therein. Recall that the flow of the free energy decouples from the rest of the flow, as we have discussed in Sec. 3.2.1 above. This allows us to study the flow of F_k in closed form, separately from the dynamics. In particular, the flow equations for the squared mass and the quartic coupling can be derived using well-established methods from the standard FRG for a ϕ^4-theory in $d = 3$ Euclidean spacetime dimensions. As a first step, one needs the propagators, which are here given by the static susceptibilities (3.104a) and (3.104b). For the truncation (3.105), they read

$$\chi_{\phi,k}(\boldsymbol{p}) = \frac{1}{m_k^2 + \boldsymbol{p}^2 + R_k^\phi(\boldsymbol{p})} \quad \text{and} \quad \chi_{n,k}(\boldsymbol{p}) = \frac{1}{\chi^{-1} + R_k^n(\boldsymbol{p})} . \tag{3.106}$$

for vanishing field expectation values $\phi_0 = n_0 = 0$. Moreover, one has the quartic interaction vertex

$$\frac{\delta^4 F_k}{\delta\phi_a(\boldsymbol{x})\delta\phi_b(\boldsymbol{y})\delta\phi_c(\boldsymbol{z})\delta\phi_d(\boldsymbol{w})} = \frac{\lambda_k}{3N}\,\left(\delta_{ab}\delta_{cd}+\delta_{ac}\delta_{bd}+\delta_{ad}\delta_{bc}\right)\,\delta(\boldsymbol{x}-\boldsymbol{y})\delta(\boldsymbol{y}-\boldsymbol{z})\delta(\boldsymbol{z}-\boldsymbol{w})\,. \tag{3.107}$$

Inserting the propagators and vertices into appropriate functional derivatives of the general flow equation (3.82) for the FRG-scale-dependent free energy F_k evaluated at vanishing field expectation values $\phi_0 = n_0 = 0$ results in the flow equations (here for an arbitrary momentum-dependent regulator $R_k^\phi(\boldsymbol{q})$)

$$\partial_k m_k^2 = -\frac{(N+2)\lambda_k T}{6N}\int\frac{d^dq}{(2\pi)^d}\frac{\partial_k R_k^\phi(\boldsymbol{q})}{\left(m_k^2+\boldsymbol{q}^2+R_k^\phi(\boldsymbol{q})\right)^2}\,, \tag{3.108}$$

$$\partial_k \lambda_k = \frac{(N+8)\lambda_k^2 T}{3N}\int\frac{d^dq}{(2\pi)^d}\frac{\partial_k R_k^\phi(\boldsymbol{q})}{\left(m_k^2+\boldsymbol{q}^2+R_k^\phi(\boldsymbol{q})\right)^3}\,. \tag{3.109}$$

By dimensional reduction at finite temperature, the flow equations (3.108) and (3.109) for m_k^2 and $\lambda_k T$ are the same as those for a corresponding d-dimensional $O(N)$ symmetric scalar quantum field theory in Euclidean spacetime at zero temperature, which are well known in the literature, see for instance [73]. The present truncation corresponds to the lowest order in a systematic expansion of the free energy in spatial gradients (usually called the local potential approximation, LPA) combined with a Taylor expansion of the effective potential up to the minimally necessary second order in the field invariant $\rho = \phi_a\phi_a$.

We emphasize here that the truncation used in this work can be straightforwardly improved by employing a more sophisticated truncation for the free energy F_k. Such sophisticated truncations are well-developed for the d-dimensional Euclidean $O(N)$ model. For the derivative expansion see e.g. [78, 79, 211].

3.3.2 Kinetic coefficients

Using the fluctuation-dissipation relation (3.78) between the two-point functions, one can extract the kinetic coefficients $\gamma_{\phi,k}(\boldsymbol{p})$ and $\gamma_{n,k}(\boldsymbol{p})$ generally from the low-frequency limit, $\omega \to 0$ of the two-point functions $\Gamma_k^{\tilde{\Phi}\tilde{\Phi}}(\omega,\boldsymbol{p})$ and $\Gamma_k^{\tilde{N}\tilde{N}}(\omega,\boldsymbol{p})$, respectively, taken at non-vanishing spatial momentum $\boldsymbol{p}\neq 0$,

$$\gamma_{\phi,k}(\boldsymbol{p}) = \lim_{\omega\to 0}\frac{2iT}{\Gamma_k^{\tilde{\Phi}\tilde{\Phi}}(\omega,\boldsymbol{p})}\,, \tag{3.110}$$

$$\gamma_{n,k}(\boldsymbol{p}) = \lim_{\omega\to 0}\frac{2iT}{\Gamma_k^{\tilde{N}\tilde{N}}(\omega,\boldsymbol{p})}\,. \tag{3.111}$$

Using the product rule, we find that their flow equations are hence given by

$$\partial_k\gamma_{\phi,k}(\boldsymbol{p}) = -\frac{\gamma_{\phi,k}^2(\boldsymbol{p})}{2iT}\lim_{\omega\to 0}\partial_k\Gamma_k^{\tilde{\Phi}\tilde{\Phi}}(\omega,\boldsymbol{p})\,, \tag{3.112}$$

$$\partial_k\gamma_{n,k}(\boldsymbol{p}) = -\frac{\gamma_{n,k}^2(\boldsymbol{p})}{2iT}\lim_{\omega\to 0}\partial_k\Gamma_k^{\tilde{N}\tilde{N}}(\omega,\boldsymbol{p})\,. \tag{3.113}$$

The diagrammatic representation of the flow of two-point functions is given in Fig. 3.1. We evaluate these flow equations at vanishing field expectation values $\phi = \tilde{\Phi} = n = \tilde{N} = 0$, which

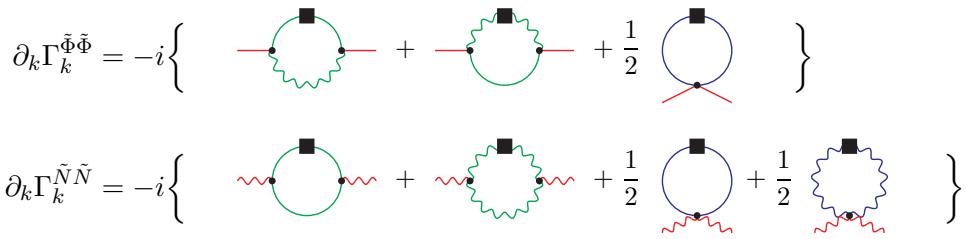

Figure 3.1: Flow of the 2-point functions $\Gamma_k^{\tilde{\Phi}\tilde{\Phi}}$ and $\Gamma_k^{\tilde{N}\tilde{N}}$ at the IR minimum $\phi = n = 0$, $\tilde{\Phi} = \tilde{N} = 0$ in the symmetry-restored phase $T \geq T_c$ without explicit symmetry breaking. Drawn using *JaxoDraw* [215].

is valid in the symmetry-restored phase, i.e. for $T \geq T_c$, and for vanishing explicit symmetry breaking $H = 0$, corresponding to vanishing current quark masses in QCD, in the chiral limit.

Using the truncation given in (3.94), and the method of expanding the Jacobian in powers of the fields, one can then compute the three and four-point vertices and find that the nonzero vertices are $\tilde{\Phi}\phi n$, $\tilde{N}\phi\phi$, $\tilde{N}nn$, $\tilde{\Phi}\tilde{\Phi}\phi\phi$, $\tilde{N}\tilde{N}\phi\phi$ and $\tilde{N}\tilde{N}nn$. Although the resulting expressions for the vertices are straightforward to derive (at least in principle), they are lengthy and not particularly illuminating, so instead of explicitly writing them here, we list them in Appendix E for completeness.

In principle, one could now use the flow equations (3.112) and (3.113) to flow the full momentum dependence of the kinetic coefficients $\gamma_{\phi,k}(\boldsymbol{p})$ and $\gamma_{n,k}(\boldsymbol{p})$. However, since this can be numerically expensive in general, we now discuss suitable approximation schemes. The standard argument which justifies a derivative expansion as a suitable truncation scheme for equilibrium critical phenomena is that the critical non-analyticity in correlation functions only builds up gradually in the limit of vanishing FRG scale k [73, 75, 78, 79, 211]. In particular, the momentum modes $|\boldsymbol{p}| \lesssim k$ that effectively contribute to loop diagrams receive finite masses (proportional to k^2) from the IR regulator. This argument still holds also in the dynamic case here, and implies that the momentum dependence of the kinetic coefficients for $|\boldsymbol{p}| \lesssim k$ is completely regular, justifying the usage of a Taylor expansion in $\boldsymbol{p}^2$. The leading orders in this expansion would be $\gamma_{\phi,k}(\boldsymbol{p}) \approx \Gamma_k^{\phi} + \mathcal{O}(\boldsymbol{p}^2)$ and $\gamma_{n,k}(\boldsymbol{p}) \approx \gamma_k \boldsymbol{p}^2 + \mathcal{O}(\boldsymbol{p}^4)$. Dynamic critical exponents can then be extracted from the power-law behavior of the leading coefficients $\Gamma_k^{\phi} \sim k^{-(2-\eta_\perp - z_\phi)}$ and $\gamma_k \sim k^{-(2-z_n)}$ in the FRG scale k, as we shall see in Chapter 4.

In contrast, if one is interested in the corresponding dynamic scaling function the full momentum dependence, including $|\boldsymbol{p}| \gtrsim k$, has to be resolved for $k \to 0$. In the present work, we exemplify this by calculating the universal scaling function $D_k^n(\boldsymbol{p})$ of the diffusion coefficient of the charge densities which can in principle be compared to results from classical-statistical simulations, in the future. Hence, we do not expand $\gamma_{n,k}(\boldsymbol{p})$ in powers of $\boldsymbol{p}$, but instead keep the full dependence of $\gamma_{n,k}(\boldsymbol{p}) \equiv \boldsymbol{p}^2 D_k^n(\boldsymbol{p})$. Based on the argument above, we maintain only the leading term in the order-parameter kinetic coefficient, $\gamma_{\phi,k}(\boldsymbol{p}) \approx \Gamma_k^{\phi}$, however.

The diagrams contributing to $\partial_k \Gamma_k^{\tilde{\Phi}\tilde{\Phi}}$ are given by:

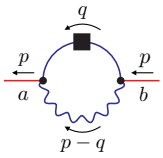

$$= (N-1)\delta_{ab} \int_q \left(\frac{g_k(p^0 - q^0)}{\Gamma_k^\phi \, \gamma_{n,k}(\boldsymbol{p}-\boldsymbol{q})} \right)^2 B^F_{\phi,k}(q) i F_{n,k}(p-q)\,, \tag{3.114}$$

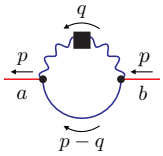

$$= (N-1)\delta_{ab} \int_q \left(\frac{g_k q^0}{\Gamma_k^\phi \, \gamma_{n,k}(\boldsymbol{q})} \right)^2 i F_{\phi,k}(p-q) B^F_{n,k}(q)\,, \tag{3.115}$$

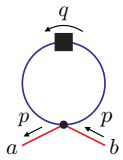

$$= (N-1)\delta_{ab} \left(-\frac{2g_k^2 iT}{(\Gamma_k^\phi)^2} \right) \int_q \left(\frac{1}{\gamma_{n,k}(\boldsymbol{q}-\boldsymbol{p})} + \frac{1}{\gamma_{n,k}(\boldsymbol{q}+\boldsymbol{p})} \right) B^F_{\phi,k}(q)\,. \tag{3.116}$$

The diagrams contributing to $\partial_k \Gamma_k^{\tilde{N}\tilde{N}}$ are given by:

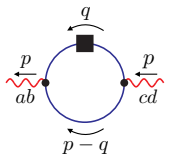

$$= 2(\delta_{ac}\delta_{bd} - \delta_{ad}\delta_{bc}) \int_q \left(\frac{g_k(p^0 - 2q^0)}{\Gamma_k^\phi \, \gamma_{n,k}(\boldsymbol{p})} \right)^2 B^F_{\phi,k}(q) i F_{\phi,k}(p-q)\,, \tag{3.117}$$

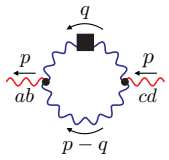

$$= 2(N-2)(\delta_{ac}\delta_{bd} - \delta_{ad}\delta_{bc}) \times \int_q \left[\frac{g_k}{\gamma_{n,k}(\boldsymbol{p})} \left(\frac{q^0}{\gamma_{n,k}(\boldsymbol{q})} + \frac{q^0 - p^0}{\gamma_{n,k}(\boldsymbol{q}-\boldsymbol{p})} \right) \right]^2 B^F_{n,k}(q) i F_{n,k}(p-q)\,, \tag{3.118}$$

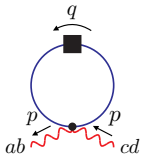

$$= -(\delta_{ac}\delta_{bd} - \delta_{ad}\delta_{bc}) \frac{8g_k^2 iT}{\Gamma_k^\phi \, \gamma_{n,k}^2(\boldsymbol{p})} \int_q B^F_{\phi,k}(q)\,, \tag{3.119}$$

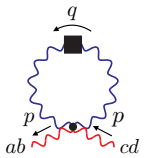

$$= -(N-2)(\delta_{ac}\delta_{bd} - \delta_{ad}\delta_{bc}) \frac{4g_k^2 iT}{\gamma_{n,k}^2(\boldsymbol{p})} \times \int_q \left(\frac{1}{\gamma_{n,k}(\boldsymbol{p}+\boldsymbol{q})} + \frac{1}{\gamma_{n,k}(\boldsymbol{p}-\boldsymbol{q})} \right) B^F_{n,k}(q) \tag{3.120}$$

3.3.3 Non-renormalization of reversible mode couplings

In this subsection we show that the reversible mode coupling coefficients are protected from renormalization, which means $g_k^{\phi n} = g_k^{n\phi} = g_k^{nn} = g$ at all FRG scales k. The starting point of our discussion is the temporal (non-Abelian) gauge symmetry of the MSR action of Model G, which is preserved by the FRG flow. Based on the discussion in Sec. 3.1.2, the change of the effective action under time-dependent (but spatially independent) rotations $O(t) \in O(N)$ of the

fields has to obey

$$\Gamma_k[O\phi, O\tilde{\phi}, OnO^T, O\tilde{n}O^T] - \Gamma_k[\phi, \tilde{\phi}, n, \tilde{n}] = \frac{1}{2}\int_x \mathrm{tr}\left[\left(\frac{1}{g}O\partial_t O^T\right) O\tilde{N}O^T\right] \tag{3.121}$$

Based on the explicit ansatz for the effective average action in Eq. (3.93), the change on the left-hand side in (3.121) can be expressed as

$$\begin{aligned}\Gamma_k[O\phi, O\tilde{\phi}, OnO^T, O\tilde{n}O^T] - \Gamma_k[\phi, \tilde{\phi}, n, \tilde{n}] = \\ \int_x \left[-\tilde{\phi}_a (O^T\partial_t O)_{ab}\phi_b - \tilde{n}_{ab}(O^T\partial_t O)_{ab,cd} n_{cd}\right]\end{aligned} \tag{3.122}$$

Considering an infinitesimal transformation $O \approx 1 + \frac{1}{2}\alpha_{ab}(t)T_{ab}$, with small $\alpha_{ab}(t)$,

$$O^T\partial_t O = \frac{1}{2}\dot{\alpha}_{ab}(t)T_{ab} + \mathcal{O}(\alpha^2)\,, \tag{3.123}$$

and the corresponding infinitesimal change of the effective action can then be evaluated as

$$\begin{aligned}\Gamma_k[O\phi, O\tilde{\phi}, OnO^T, O\tilde{n}O^T] - \Gamma_k[\phi, \tilde{\phi}, n, \tilde{n}] = \\ \int_x \left[-\frac{1}{2}\tilde{\phi}_a\dot{\alpha}_{cd}(t)(T_{cd})_{ab}\phi_b - \frac{1}{2}\tilde{n}_{ab}\dot{\alpha}_{ef}(t)(T_{ef})_{ab,cd}n_{cd}\right] + \mathcal{O}(\alpha^2)\,.\end{aligned} \tag{3.124}$$

Re-expressing the generators T_{ab} in terms of the Poisson-bracket relations of the fields ϕ and n in Eq. (3.47), one then obtains the following result for the left-hand side in (3.121)

$$\begin{aligned}\Gamma_k[O\phi, O\tilde{\phi}, OnO^T, O\tilde{n}O^T] - \Gamma_k[\phi, \tilde{\phi}, n, \tilde{n}] = \\ \int_x \left[-\frac{1}{2}\tilde{\phi}_a\dot{\alpha}_{cd}(t)\{\phi_a, n_{cd}\} - \frac{1}{2}\tilde{n}_{ab}\dot{\alpha}_{ef}(t)\{n_{ab}, n_{ef}\}\right] + \mathcal{O}(\alpha^2)\,.\end{aligned} \tag{3.125}$$

Next we consider the right-hand side in (3.121) which, for an infinitesimal $O(N)$ rotation (3.123), can be expressed as

$$\frac{1}{2}\int_x \mathrm{tr}\,\frac{1}{g}O\partial_t O^T O\tilde{N}O^T = \int_x \frac{1}{2g}\dot{\alpha}_{ab}(t)\tilde{N}_{ab} + \mathcal{O}(\alpha^2)\,.$$

Now, substituting the explicit expression in Eq. (3.90b) for the composite field $\tilde{N}_{ab}$ in terms of the standard response field $\tilde{\phi}$ and $\tilde{n}$, this can be written as[8]

$$\begin{aligned}\frac{1}{2}\int_x \mathrm{tr}\,\frac{1}{g}O\partial_t O^T O\tilde{N}O^T = \\ \int_x \left[-\frac{g_k^{\phi n}}{2g}\tilde{\phi}_a\dot{\alpha}_{cd}(t)\{\phi_a, n_{cd}\} - \frac{g_k^{nn}}{2g}\tilde{n}_{ab}\dot{\alpha}_{ef}(t)\{n_{ab}, n_{ef}\}\right] + \mathcal{O}(\alpha^2)\,,\end{aligned} \tag{3.126}$$

which is identical to the results in Eq. (3.125) except for the appearance of the factors $g_k^{\phi n}/g$ and g_k^{nn}/g. Since in order to comply with the displacement symmetry, the expressions in Eq. (3.125) and (3.126), which correspond to the left-hand side and right-hand side of Eq. (3.121), have to agree, one concludes that the reversible mode couplings do not get renormalized, i.e. one has

$$g_k^{\phi n} = g_k^{n\phi} = g_k^{nn} = g$$

at any FRG scale k.

[8] Note that we can drop a total derivative term proportional to $-\gamma_k\nabla^2\tilde{n}_{ab}$ here, since it vanishes upon performing the spatial integral.

To conclude this subsection, we remark that in the ϵ-expansion around $d = 4-\epsilon$ it is proven to all orders that g receives no loop corrections [104]. This was exploited in Ref. [62] to show that the dynamic critical exponent z of the $O(4)$ chiral transition is given by $z = d/2$ to all orders. Hence, although our proof of the non-renormalization of g relies on the specific form of our truncation in Eq. (3.93), one expects that this is a general statement that is actually independent of truncation as long as the time-gauged $O(N)$ transformation described in Sec. 3.1.2 is maintained as an (extended) symmetry of the effective average MSR action. In practice, this means that in our calculations we no longer need to compute the flow equation for the reversible mode coupling coefficient. Instead, one can simply set it to a constant value $g_k = g = \text{const.}$ during the flow.

3.3.4 Numerical implementation

For all our numerical calculations we choose the exponential regulator

$$R_{\phi,k}(\boldsymbol{p}) = \chi^{\frac{d+1}{d-1}} R_{n,k}(\boldsymbol{p}) = \frac{\boldsymbol{p}^2}{e^{\boldsymbol{p}^2/k^2} - 1}. \tag{3.127}$$

for both ϕ's and n's, where the factor $\chi^{\frac{d+1}{d-1}}$ is needed such that $R_{n,k}(\boldsymbol{p})$ has the same dimension as χ^{-1}, cf. Eq. (3.106). For the static couplings, we solve the flow equations of m_k^2 and λ_k, as in Eq. (3.108) and Eq. (3.109). For the dynamic couplings, we solve the flow equations given by Eq. (3.110) and Eq. (3.111). To resolve the momentum dependence of the kinetic coefficient $\gamma_{n,k}(\boldsymbol{p})$ for the charge densities, we discretize $\gamma_{n,k}(\boldsymbol{p})$ with a logarithmic grid spacing on a finite interval $[p_{\min}, p_{\max}]$. We need a small enough lower bound $p_{\min}$ to properly resolve the behavior of the flow in the IR. We choose the upper bound $p_{\max}$ of the grid large enough such that the flow of the diffusion coefficient $\gamma_{n,k}(\boldsymbol{p})/\boldsymbol{p}^2$ approximately goes to zero at $p \to p_{\max}$. In each step of the FRG flow, we evaluate m_k^2, λ_k, $\gamma_{\phi,k}$ (the latter being momentum independent in our truncation), and the function $\gamma_{n,k}(p)$ at each grid point, and then we interpolate $\log \gamma_{n,k}(p)$ as a function of $\log p$ with a GSL interpolator [216]. We use a simple forward Euler method to solve the flow equation with respect to the FRG flow time $t = \log k/\Lambda$.

The integrals involved in our loop diagrams are generally of the form

$$\int \frac{dq^0}{2\pi} \int \frac{d^d q}{(2\pi)^d} f(q^0, |\boldsymbol{q}|, p^0 - q^0, |\boldsymbol{p} - \boldsymbol{q}|)\,. \tag{3.128}$$

Frequency integrals are solved analytically using the residue theorem. To evaluate the momentum integral, we first exploit spatial isotropy to reduce the d-dimensional integration in (3.128) to two integrals over the momentum's magnitude $q \equiv |\boldsymbol{q}|$ and over the angle θ between $\boldsymbol{p}$ and $\boldsymbol{q}$, i.e.

$$\frac{S_{d-2}}{(2\pi)^d} \int_0^\infty dq\, q^{d-1} \int_0^\pi \sin^{d-2}\theta\, f\left(q^0, q, p^0 - q^0, \sqrt{p^2 + q^2 - 2pq\cos\theta}\right)\,, \tag{3.129}$$

where S_n is the surface area of the n-dimensional sphere S^n, with

$$S_{n-1} = \frac{2\pi^{n/2}}{\Gamma(n/2)} \tag{3.130}$$

(e.g. $S_1 = 2\pi$, $S_2 = 4\pi$, etc.) and $\Gamma(z)$ denotes the Γ-function. To solve these remaining two integrals, we employ two different methods, namely a Gauss quadrature method from the GSL [216] and the Cuhre function in the Cuba library [217].

$m_\Lambda^2/\lvert m_\Lambda^2\rvert$	$\lambda_\Lambda/\lvert m_\Lambda\rvert^{3-d}$	$\chi/\lvert m_\Lambda\rvert^{d-1}$	g	$\Gamma_\Lambda^\phi/\lvert m_\Lambda\rvert^{-1}$	$\gamma_\Lambda/\lvert m_\Lambda\rvert^{d-2}$	$T_c/\lvert m_\Lambda\rvert$
-1	1	1	1	1	1	17.371845

Table 3.1: Initial conditions used at the UV initial scale $k = \Lambda = 5.67|m_\Lambda|$. The resulting critical temperature T_c in $d = 3$ spatial dimensions is shown in the last column.

Using the GSL we solve the integral over the momentum magnitude using a Gauss-Legendre quadrature on a logarithmically spaced grid in q. By performing a variable substitution $u = \cos\theta$ to obtain the necessary weight function, we evaluate the angular integrals using a Gauss-Jacobi quadrature,

$$\int_0^\pi d\theta\, \sin^{d-2}\theta\, f(\cos\theta) = \int_0^\pi d\theta\, \left(1-\cos^2\theta\right)^{(d-2)/2} f(\cos\theta) = \int_{-1}^1 du\, (1-u^2)^{(d-3)/2} f(u)\,. \tag{3.131}$$

Gauss-Jacobi quadratures have a weight function of the form $(1-x)^\alpha(1+x)^\beta$ for $\alpha, \beta > -1$ and thus generalize the Gauss-Chebychev quadratures which use a weight function of $1/\sqrt{1-x^2}$. Our angular integral (3.131) is conveniently evaluated using the choice $\alpha = \beta = (d-3)/2$.

As a second numerical method, we use the Cuhre function from the Cuba library, since it is suited for the two-dimensional integration over q and θ in (3.128). (As in the Gauss-Jacobi quadrature in (3.131), we substitute $u \equiv \cos\theta$.) The integrand has singularities at $\boldsymbol{p} = \boldsymbol{q}$ and $\boldsymbol{p} = -\boldsymbol{q}$, but these are not problematic because they cancel each other. In practice, we remove a small sphere around $\boldsymbol{p} = \boldsymbol{q}$ and $\boldsymbol{p} = -\boldsymbol{q}$ and take the radius of the sphere to zero (resp. sufficiently small) afterwards.

We have explicitly verified that both numerical methods discussed in the present section lead to the same results within numerical precision.

For our numerical results in the next section, we generally employ the UV initial conditions listed in Table 3.1. Moreover, we will quote all dimensionful quantities implicitly in units of the mass parameter $|m_\Lambda|$ at the UV cutoff scale Λ, which is thereby chosen such that we obtain approximately the same critical temperature T_c in $d = 3$ spatial dimensions as in the classical-statistical lattice simulations of Ref. [87].

3.4 Results for dynamic critical behavior of $O(4)$ Model G

Based on the FRG flow equations for the static and dynamic couplings of the $O(N)$ Model G, we will now proceed to study the static and dynamic critical behavior. By numerically solving the FRG flow equations and analyzing the fixed point for the $N = 4$ case, we will first discuss the static critical behavior, which should match the $O(4)$ criticality, and then discuss the dynamic critical behavior of the $O(4)$ Model G.

3.4.1 Static critical behavior of the $O(4)$ model

We follow common procedure and extract the static critical behavior from a standard fixed point analysis. By introducing dimensionless couplings $\bar{m}_k^2 \equiv k^{-2} m_k^2$, $\bar{\lambda}_k \equiv k^{d-4} T \lambda_k$, and by rewriting the regulator $R_{\phi,k}(q) = q^2 r_\phi(q/k)$ using a dimensionless function $r_\phi(\bar{q})$ (with derivative $r'_\phi(\bar{q}) = dr_\phi(\bar{q})/d\bar{q}$), one can de-dimensionalize the static flow equations (3.108) and (3.109) and

obtain the corresponding β-functions for the dimensionless couplings $\bar{m}^2$ and $\bar{\lambda}$,

$$k\partial_k \bar{m}_k^2 = -2\bar{m}_k^2 + \frac{(N+2)\bar{\lambda}_k}{6N}\frac{S_{d-1}}{(2\pi)^d}\int_0^\infty \frac{d\bar{q}\,\bar{q}^{d+2}\,r'_\phi(\bar{q})}{\left(\bar{m}_k^2 + \bar{q}^2(1+r_\phi(\bar{q}))\right)^2} \equiv \beta_{\bar{m}^2}(\bar{m}_k^2, \bar{\lambda}_k) \tag{3.132}$$

$$k\partial_k \bar{\lambda}_k = (d-4)\bar{\lambda}_k - \frac{(N+8)\bar{\lambda}_k^2}{3N}\frac{S_{d-1}}{(2\pi)^d}\int_0^\infty \frac{d\bar{q}\,\bar{q}^{d+2}\,r'_\phi(\bar{q})}{\left(\bar{m}_k^2 + \bar{q}^2(1+r_\phi(\bar{q}))\right)^3} \equiv \beta_{\bar{\lambda}}(\bar{m}_k^2, \bar{\lambda}_k) \tag{3.133}$$

To determine the static critical exponent ν as usual in standard RG approaches, one first determines the Wilson-Fisher fixed point $(\bar{m}_k^2, \bar{\lambda}_k) = (\bar{m}_*^2, \bar{\lambda}_*)$ by setting the β-functions to zero $\beta_{\bar{m}^2}(\bar{m}_*^2, \bar{\lambda}_*) = \beta_{\bar{\lambda}}(\bar{m}_*^2, \bar{\lambda}_*) = 0$, solves the resulting system of equations for the fixed-point couplings $(\bar{m}_*^2, \bar{\lambda}_*)$, and then expands the right-hand side of Eqs. (3.132), (3.133) around the fixed point up to first order in $\delta\bar{m}_k^2 \equiv \bar{m}_k^2 - \bar{m}_*^2$ and $\delta\bar{\lambda}_k \equiv \bar{\lambda}_k - \bar{\lambda}_*$. Collecting the dimensionless β-functions in a vector, its Jacobian matrix (usually called the stability matrix)

$$(M_{ij}) = \begin{pmatrix} \partial\beta_{\bar{m}^2}/\partial\bar{m}^2 & \partial\beta_{\bar{m}^2}/\partial\bar{\lambda} \\ \partial\beta_{\bar{\lambda}}/\partial\bar{m}^2 & \partial\beta_{\bar{\lambda}}/\partial\bar{\lambda} \end{pmatrix}_{(\bar{m}^2,\bar{\lambda})=(\bar{m}_*^2,\bar{\lambda}_*)} \tag{3.134}$$

determines how the small perturbations $\delta\bar{m}_k$ and $\delta\bar{\lambda}_k$ behave at the fixed point. Since we are working within the local potential approximation, we have no spatial wave function renormalization factor, and hence our truncation yields a vanishing anomalous scaling dimension $\eta_\perp = 0$ of the order parameter. However, in our general analysis of the scaling relations below, we will keep $\eta_\perp$ arbitrary, and only set it to $\eta_\perp = 0$ in the end. By diagonalizing the stability matrix, the single negative eigenvalue ω_0 is then related to the critical exponent ν by $\nu = -1/\omega_0$. Specifically, for the $N = 4$ component theory in $d = 3$ spatial dimensions, and the exponential regulator (3.127), this procedure yields a value of $\nu = 0.553945$. This result lies between the mean-field value $\nu = 1/2$ and the value $\nu = 0.7377(41)$ which was determined very precisely from ab-initio simulations of the $O(4)$ spin model [218]. The deviation of our result from the ab-initio result gives us an estimate of the systematic error induced by our admittedly rather simple truncation. In the context of FRG, it is clear that one has to include more Taylor coefficients of the effective potential or even go to higher orders in the derivative expansion to improve the accuracy of the resulting critical exponents [78]. However, we emphasize again at this point that in the present work we are primarily interested in the conceptual question of how the dynamic critical behavior of systems with reversible mode couplings, such as Model G can *in principle* be studied using the FRG framework. Hence, we consider the more qualitative result for ν from above therefore as sufficient for the scope of the present work.

Beyond this fixed point analysis, it is also possible to approach the static critical behavior from a more physical perspective, where close to the critical temperature of a second-order phase transitions, the static critical exponent ν determines the divergence of the equilibrium correlation length (ξ) of order-parameter excitations as $\xi \sim \tau^{-\nu}$, where $\tau = (T - T_c)/T_c$ is the reduced temperature. By investigating the static limit of the iF propagator, one finds that the critical scaling of the infrared mass $m_{k=0}^2$ is in general given by $m_{k=0}^2 \sim \xi^{-2+\eta_\perp}$, and one can thus deduce that close to the critical temperature, it behaves as $m_{k=0}^2 \sim \tau^{(2-\eta_\perp)\nu}$. Similar arguments of dimensional analysis can also be applied to the quartic coupling which lead to $\lambda_{k=0} \sim \xi^{-(4-d-2\eta_\perp)}$, such that close to the critical temperature one finds $\lambda_{k=0} \sim \tau^{(4-d-2\eta_\perp)\nu}$. Specifically, for our setup in $d = 3$ dimensions, we thus expect to see $m_{k=0}^2 \sim \tau^{(2-\eta_\perp)\nu}$ and $\lambda_{k=0} \sim \tau^{(1-2\eta_\perp)\nu}$ in our numerical results below, with the value of ν extracted above from the eigenvalues of the stability matrix at the Wilson-Fisher fixed point, and with $\eta_\perp = 0$ in the

local potential approximation of the FRG flow equations. In Fig. 3.2 the static coupling in the infrared, $m^2_{k=0}$ and $\lambda_{k=0}$, are shown as a function of the reduced temperature τ on a logarithmic scale. The static critical exponent ν can be deduced from the slope of the FRG-simulated data. A line with the slope indicating the theoretical value of $\nu = 0.553945$ within our truncation is also shown in the plot for comparison. One can see that close to the critical temperature, the slope of the line obtained from FRG simulation indeed match the slope indicating the theoretical value of ν for our truncation.

Beyond the reduced temperature dependence of the static coefficients, it is also interesting to investigate the dependence on the FRG scale k. Since sufficiently close to the critical point the relevant infrared cutoff during the FRG flow is always set by the FRG scale $k \neq 0$, the correlation length is effectively determined as $\xi_k \sim 1/k$ and static and dynamic quantities exhibit scaling as a function of k. Based on the above discussion, one thus expects that the k dependence follows

$$m_k^2 \sim k^{2-\eta_\perp} \quad \text{and} \quad \lambda_k \sim k^{4-d-2\eta_\perp} \tag{3.135}$$

in the vicinity of the critical point. Within our truncation, where the anomalous dimension $\eta_\perp = 0$, this yields

$$m_k^2 \sim k^2 \quad \text{and} \quad \lambda_k \sim k^{4-d} \tag{3.136}$$

as can easily be deduced from the fact that in d spatial dimensions, the dimensionless couplings are given by $\bar{m}_k^2 \equiv k^{-2} m_k^2$, $\bar{\lambda}_k = k^{d-4} T \lambda_k$, along with the fact that $\partial_k \bar{m}_k^2 = 0$, $\partial_k \bar{\lambda}_k = 0$ at the Wilson-Fisher fixed point.

In Fig. 3.3, the scale dependent effective mass $m_k^2 + k^2$ and coupling λ_k are plotted with respect to the FRG scale k on a logarithmic scale for $d = 3$ spatial dimensions. In order to see the critical exponents more easily, we take one further derivative with respect to $\log k$, as depicted in the right panels, where $k\partial_k \log\left(m_k^2 + k^2\right)$ and $k\partial_k \log \lambda_k$ are shown. In these plots, the scaling region corresponds to a plateau and the corresponding critical exponents are indicated. From Fig. 3.3, one can see that in the scaling region the power laws $m_k^2 \sim k^2$ and $\lambda_k \sim k$, which correspond to Eq. (3.136) with $d = 3$, indeed hold. One can also see that by approaching the critical temperature, the scaling region gets larger. When generalising to different numbers d of spatial dimensions, one still has $m_k^2 \sim k^2$ in the scaling region, cf. Eq. (3.136), but $\lambda_k \sim k^{4-d}$ for the static four-point coupling. This is shown in Fig. 3.4, with the plateau in $k\partial_k \log \lambda_k$ with respect to $\log k$ forming around $k\partial_k \log \lambda_k = 0.5, 1.0$ and 1.5 correspondingly in $d = 3.5, 3$ and 2.5.

3.4.2 Dynamic critical behavior

Next we proceed with investigating the dynamic critical behavior of $O(4)$ Model G, which in addition to the static quantities is governed by the behavior of the kinetic coefficients Γ_k^ϕ and $\gamma_{n,k}(\boldsymbol{p})$ in the vicinity of the critical point. We first consider the divergence of the kinetic coefficient Γ_k^ϕ of the order parameter ϕ, which determines the relaxation rate of the order parameter $\omega_k^{\text{rel}} \sim \Gamma_k^\phi m_k^2$, as can be deduced from the pole of the retarded propagator in Eq. (3.98a). Since in the vicinity of the critical point the relaxation rate is expected to diverge as $\omega_{k=0}^{\text{rel}} \sim \xi^{-z_\phi} \sim \tau^{\nu z_\phi}$, one can extract the dynamic critical exponent z_ϕ of the order parameter field from the reduced temperature (τ) dependence of the kinetic coefficient $\Gamma_{k=0}^\phi$ evaluated in the infrared ($k = 0$). By using the relation $m_{k=0}^2 \sim \tau^{(2-\eta_\perp)\nu}$, the critical behavior of the kinetic coefficient $\Gamma_{k=0}^\phi$ is then

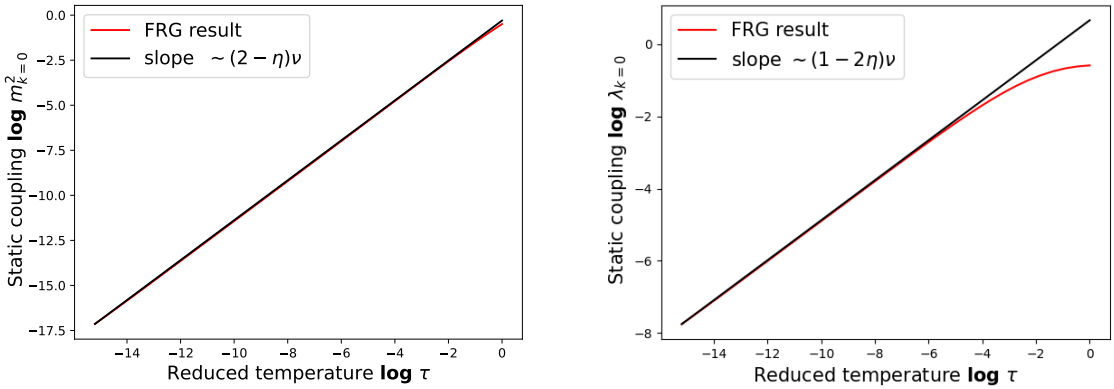

Figure 3.2: Static couplings m_k^2, λ_k in the IR ($k = 0$) versus reduced temperature $\tau = (T-T_c)/T_c$. The critical temperature here is given by $T_c = 17.371845$.

given by

$$\Gamma^{\phi}_{k=0}(\tau) = \Gamma^{\phi}_{+}\ \tau^{-\nu(2-\eta_\perp - z_\phi)}\,, \tag{3.137}$$

where Γ^{ϕ}_{+} is a non-universal amplitude. Similarly, one can also infer the critical behavior of the kinetic coefficient $\gamma_{n,k}(\boldsymbol{p})$ of the charge densities, by considering the long-wavelength limit of the charge diffusion coefficient

$$D^n_k(\boldsymbol{p},\tau) = \gamma_{n,k}(\boldsymbol{p},\tau)/\boldsymbol{p}^2\,, \tag{3.138}$$

where in the context of QCD in the chiral limit, this would be the diffusion coefficient of the isovector and isoaxial charge densities V_0^i and A_0^i. The diffusion coefficient $D^n_k(\boldsymbol{p})$ determines the relaxation rate of charge density perturbations as $\omega^{\mathrm{rel}}_k(\boldsymbol{p}) \sim D^n_k(\boldsymbol{p})\boldsymbol{p}^2$. Evaluated at the characteristic scale of the inverse correlation length $\boldsymbol{p} \sim 1/\xi \sim \tau^{\nu}$, the relaxation rate is again expected to behave as $\omega^{\mathrm{rel}}_k(\boldsymbol{p} \sim 1/\xi) \sim \xi^{-z_n} \sim \tau^{\nu z_n}$, which then gives rise to the following critical divergence,

$$D^n_{k=0}(\boldsymbol{p})|_{|\boldsymbol{p}|=1/\xi} = D^n_{+}\ \tau^{-\nu(2-z_n)}, \tag{3.139}$$

where in our truncation the correlation length is simply determined by $\xi = 1/m_{k=0}$.

Our numerical FRG results for $\log\Gamma^{\phi}_{k=0}$ and $\log(D^n_{k=0}(|\boldsymbol{p}| = 1/\xi))$ are presented in Fig. 3.5 as functions of (the logarithm of) the reduced temperature, $\log\tau$. Data obtained from our numerical FRG calculations is compared to the theoretical expectations in Eqs. (3.137) and (3.139), as indicated by the black lines with slopes $-\nu(2-\eta_\perp-z_\phi)$ (for $\Gamma^{\phi}_{k=0}$) and $-\nu(2-z_n)$ (for $D^n_{k=0}(|\boldsymbol{p}| = 1/\xi)$), where we employ the static critical exponents $\nu = 0.553945$ and $\eta_\perp = 0$ determined within our FRG truncation, and the dynamic critical exponent $z_\phi = z_n = d/2 = 1.5$, which is the theoretically expected value of the dynamic critical exponent from strong scaling in three spatial dimensions. From the results in Fig. 3.5, one can clearly observe that the slopes from our numerical FRG results approach their theoretically expected values as criticality is approached, $\tau \to 0$. As an alternative to the reduced-temperature dependence of the kinetic coefficients, we can also extract the dynamic critical exponents from their FRG scale k dependence sufficiently close to criticality. Similar to our discussion above, the scale dependent relaxation rate of the order parameter ω^{rel}_k is determined by the kinetic coefficient Γ^{ϕ}_k and the mass m^2_k as $\omega_k \sim \Gamma^{\phi}_k m^2_k$. Since close to the critical point one expects $m^2_k \sim k^{2-\eta_\perp}$ and $\omega^{\mathrm{rel}}_k \sim \xi_k^{z_\phi} \sim k^{z_\phi}$, one can deduce that the scaling of the kinetic coefficient of the order parameter with respect to the FRG scale

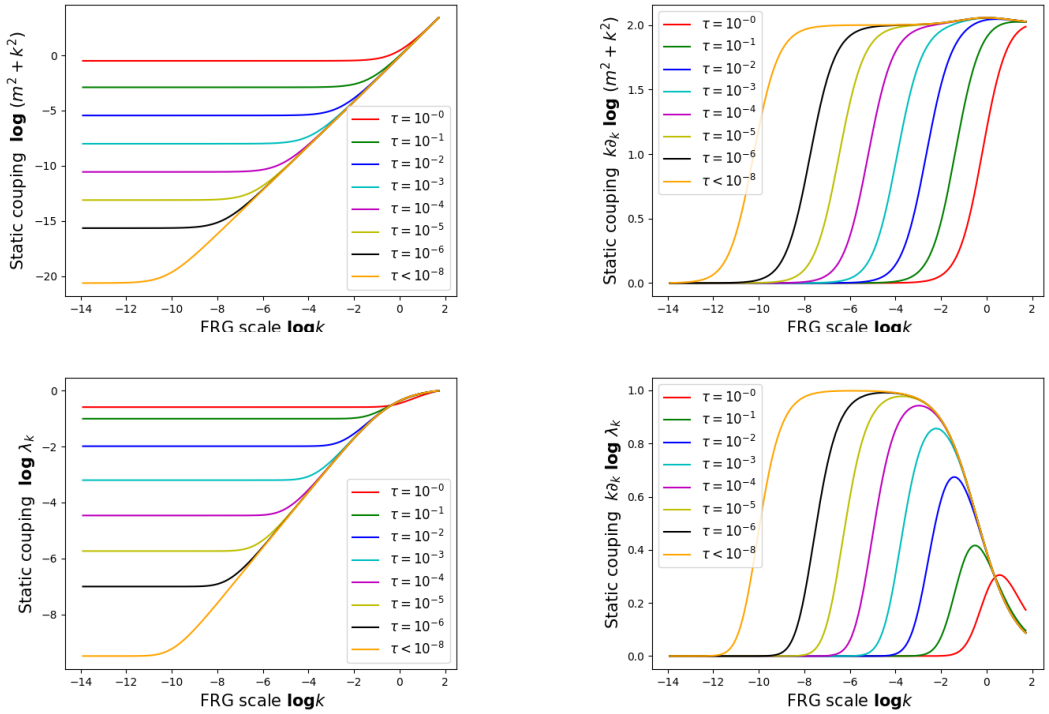

Figure 3.3: FRG scale k dependence of the static couplings $\log\left(m_k^2 + k^2\right)$, $\log \lambda_k$, as the temperature T is approaching the critical temperature T_c from above. The plots on the right show the respective derivatives of the couplings on the left, which coincide with the corresponding critical exponents in the scaling regime.

is given by $\Gamma_k^\phi \sim k^{-(2-\eta_\perp - z_\phi)}$. Similarly, one finds that the charge diffusion coefficient $D_k^n(k)$ exhibits the critical dependence $D_k^n(k) \sim k^{-(2-z_n)}$ on the FRG scale k, where z_n is the dynamic critical exponent for the charge diffusion constant, and one can thus extract z_ϕ and z_n from the FRG scale dependence of the kinetic coefficients Γ_k^ϕ and $D_k^n(k)$ close to criticality.

We present this analysis in Fig. 3.6, where the left panels show the dependence of the kinetic coefficients $\log \Gamma_k^\phi$ of the order parameter and the conserved charges $\log D_k^n(k)$ on the FRG scale $\log k$. Differently colored curves correspond to results obtained at different values of the reduced temperature in the symmetric phase of the $O(4)$ model, and one can clearly observe the build up of the critical divergence when lowering the reduced temperature.

Similar to our discussion of the static critical exponents, the dynamic critical exponents z_ϕ and z_n can be inferred from the right panel of Fig. 3.6, where we present the logarithmic derivatives $k\partial_k \log \Gamma_k^\phi$ and $k\partial_k \log D_k^n(k)$ of the kinetic coefficients. In the scaling region, which becomes broader and broader when approaching the critical temperature, the logarithmic derivative $k\partial_k \log \Gamma_k^\phi$ approaches a constant value which yields the exponent $-(2 - \eta_\perp - z_\phi)$. With $\eta_\perp = 0$, the value of -0.5 indicates that the dynamic critical exponent for the order parameter modes is around $z_\phi = 1.5$. Similarly, from the plot of $k\partial_k \log D_k^n(k)$ with respect to $\log k$, it can be seen that the dynamic critical exponent for the conserved charge density modes is also given by $z_n = 1.5$, since in the scaling region it also approaches $k\partial_k \log D_k^n(k) = -0.5$, as the temperature approaches T_c.

So far we have only considered the dynamic critical behavior in $d = 3$ spatial dimensions, where our results are consistent with the theoretical value of the dynamic critical exponent

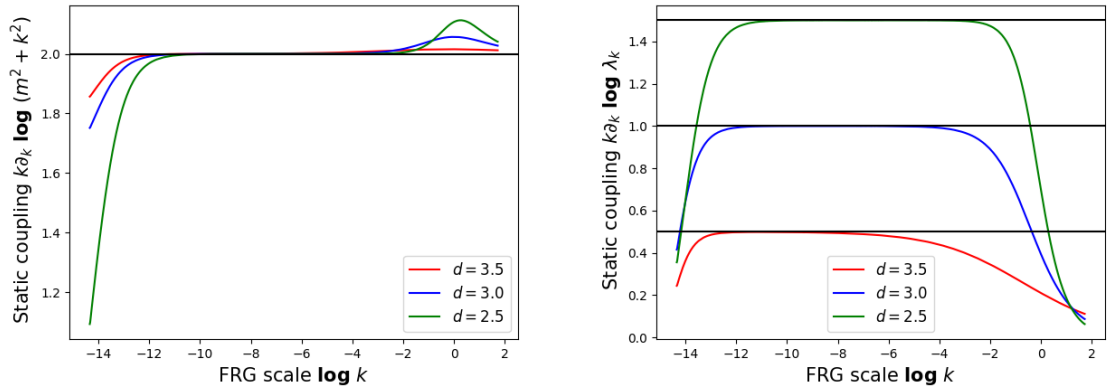

Figure 3.4: Static critical exponents in different dimensions. Here the reduced temperature is $\tau < 10^{-12}$.

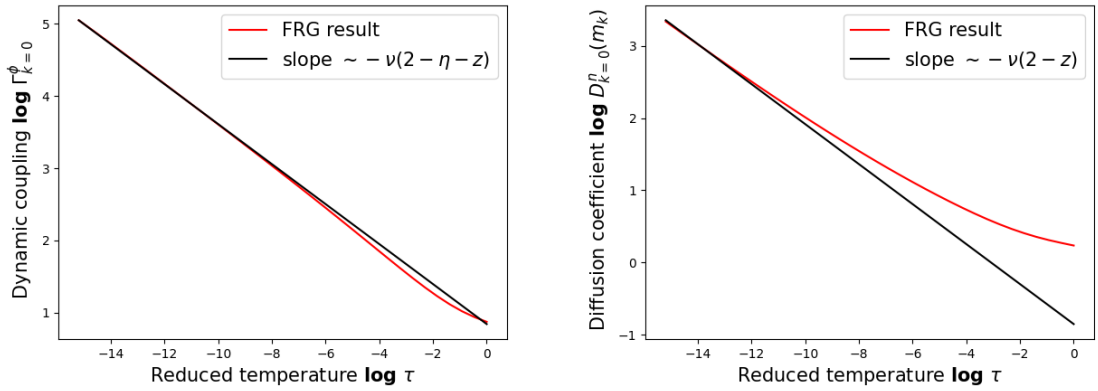

Figure 3.5: Double-logarithmic plots of the kinetic coefficient Γ^{ϕ}_{k} and the diffusion coefficient $D^{n}_{k}(m_k)$ in the IR ($k = 0$) over the reduced temperature τ.

$z_\phi = z_n = 3/2$, obtained from the strong-scaling prediction. To verify the expected dependence on the dimensionality of the system, we have also checked the flow of the kinetic coefficient Γ^{ϕ}_{k} of the order parameter field in $d = 2.5$ and $d = 3.5$ spatial dimensions, with the result shown in the left panel of Fig. 3.7. One can see from the plot of $k\partial_k \log \Gamma^{\phi}_{k}$ that for $d = 2.5$ the scaling region yields a plateau at the corresponding y-axis value of $-(2 - \eta_\perp - z_\phi) = -0.75$. When the spatial dimension is given by $d = 3.5$, the y-axis value corresponding to the plateau is given by -0.25. Similarly, from the right panel of Fig. 3.7, which shows the momentum p dependence of the diffusion coefficient $D^{n}_{k=0}(p)$, by considering $p\partial_p \log D^{n}_{k=0}(p)$ as a function of $\log p$ in various spatial dimensions, one can see that the kinetic coefficients both approach a power behavior with values of -0.75, -0.5 and -0.25 for the exponent $d/2 - 2$ in $d = 2.5$, $d = 3.0$ and $d = 3.5$, respectively.

Beyond comparing with the theoretical prediction for the dynamic critical exponents z_ϕ and z_n, we can also infer their values directly from our FRG calculations by determining the inflection point and respectively the minima of the logarithmic derivatives $k\partial_k \log \Gamma^{\phi}_{k}$, $k\partial_k \log D^{n}_{k}(k)$ and $p\partial_p \log D^{n}_{k=0}(p)$ in Figs. 3.6 and 3.9, for a range of reduced temperatures between $\tau = 10^{-8}$ and $\tau = 10^{-12}$, and subsequently extrapolating the results to the critical point at $\tau = 0$. Details of this procedure are provided in Appendix F. The results for the dynamic critical exponents z_ϕ

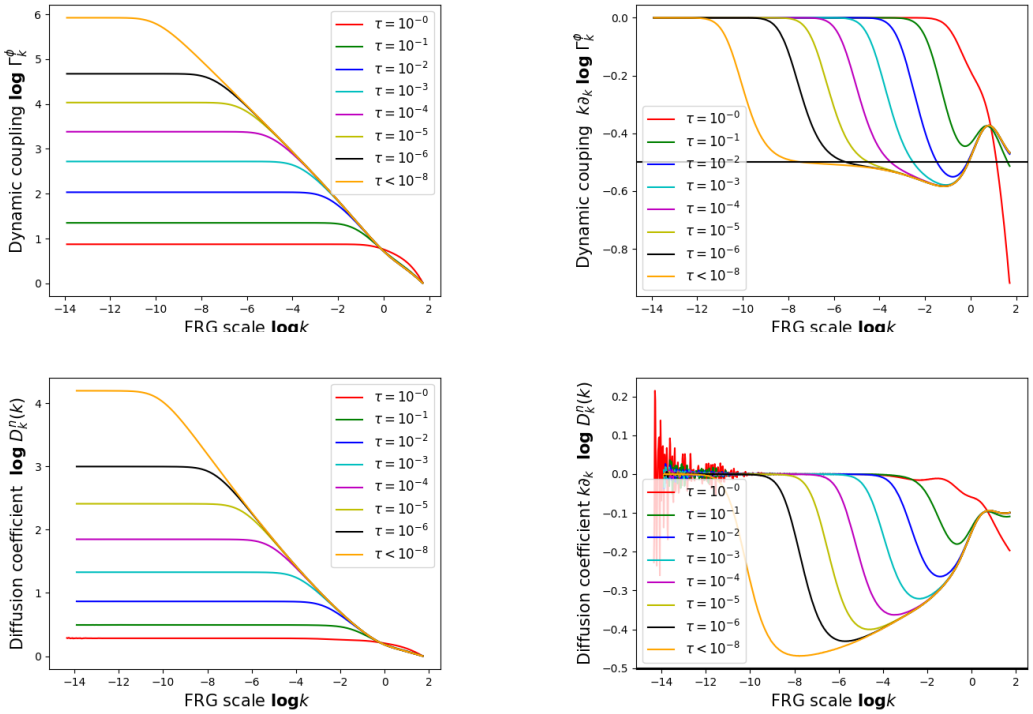

Figure 3.6: FRG scale dependence of the kinetic coefficient Γ_k^ϕ and the diffusion coefficient $D_k^n(k)$, as the temperature T is approaching the critical temperature T_c from above. The plots on the right show the respective derivatives of the couplings on the left, which coincide with the corresponding critical exponents in the scaling regime.

and z_n are compactly summarized in Fig. 3.8. This clearly indicates that our real-time FRG formalism does indeed produce the correct dynamic critical exponent $z_\phi = z_n = d/2$ expected for strong scaling in Model G.

3.4.3 Universal scaling of charge diffusion coefficients

In addition to the determination of the dynamic critical exponents z_ϕ and z_n, the real-time FRG framework also allows us to determine universal dynamic scaling functions, that describe the real-time dynamics in the vicinity of the critical point. In fact, the dynamic scaling hypothesis implies that sufficiently close to the critical point the resulting kinetic coefficient, e.g., of charge densities in the IR (at $k = 0$) is a homogeneous function of spatial momentum $\boldsymbol{p}$ and reduced temperature τ, i.e.,

$$\gamma_n(\boldsymbol{p}, \tau) = s^{-z_n} \gamma_n(s\boldsymbol{p}, s^{1/\nu}\tau)\,. \tag{3.140}$$

Based on an appropriate choice of the scaling variable s, this implies that the combined temperature and momentum dependence of γ_n can be described by a power law times a universal scaling function, which we can extract from our FRG calculations as described in the following. Using (3.140), we can infer the analogous scaling relation for the diffusion coefficient defined in Eq. (3.138), which evaluated at $k = 0$ assumes the form

$$D_n(\boldsymbol{p}, \tau) = s^{2-z_n} D_n(s\boldsymbol{p}, s^{1/\nu}\tau)\,. \tag{3.141}$$

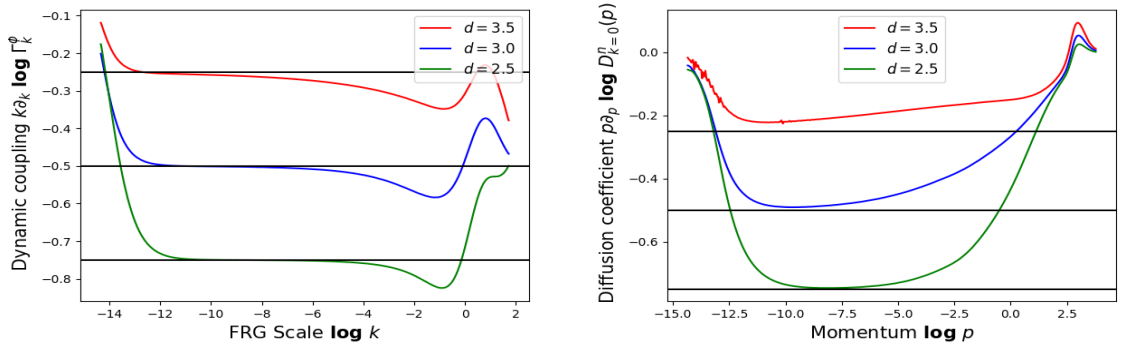

Figure 3.7: Dynamic critical exponents in spatial dimensions $d = 2.5, 3, 3.5$. Here the reduced temperature is $\tau < 10^{-12}$. See text for details.

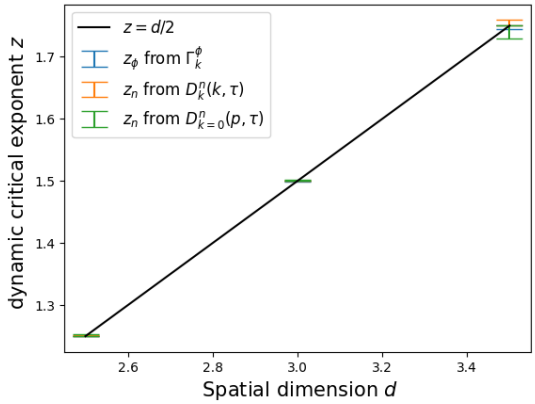

Figure 3.8: Extraction of the dynamic critical exponent z for spatial dimensions $d = 2.5, 3, 3.5$. The blue data points are extracted from extrapolating the inflection points of $k\partial_k \log \Gamma_k^\phi$ as a function of $\log k$ to $\tau = 0$, the orange data points from extrapolating the minima of $k\partial_k \log D_k^n(k)$ as a function of $\log k$, and the green data points from extrapolating the minima of $p\partial_p \log D^n_{k=0}(p)$ as a function of $\log p$.

Setting the scale parameter s so that $s^{1/\nu}\tau = 1$ in (3.141), the momentum and temperature dependence of the diffusion coefficient in Eq. (3.138) can equivalently be written as

$$D_n(\boldsymbol{p}, \tau) = \tau^{-\nu(2-z_n)} D_n(\tau^{-\nu}\boldsymbol{p}, 1)\,. \tag{3.142}$$

Expressing the dimensionless quantity $\tau^{-\nu}$ in terms of the correlation length

$$\xi(\tau) = f^+\tau^{-\nu} + \text{less singular}\,, \tag{3.143}$$

one then finds that the reduced temperature and momentum dependence of the diffusion constant can be expressed in terms of a universal scaling function $\mathcal{L}(x)$ as

$$D_n(\boldsymbol{p}, \tau) = D_n^+ \left(\frac{\xi(\tau)}{f^+}\right)^{2-z_n} \mathcal{L}\left(\xi(\tau)p\right)\,, \tag{3.144}$$

up to a non-universal amplitude D_n^+, which upon adopting the normalization condition $\mathcal{L}(1) = 1$, is determined from the critical divergence of the diffusion coefficient as

$$D_n^+ = \lim_{\tau\to 0^+} \tau^{\nu(2-z_n)} D_n(p = 1/\xi(\tau), \tau)\,. \tag{3.145}$$

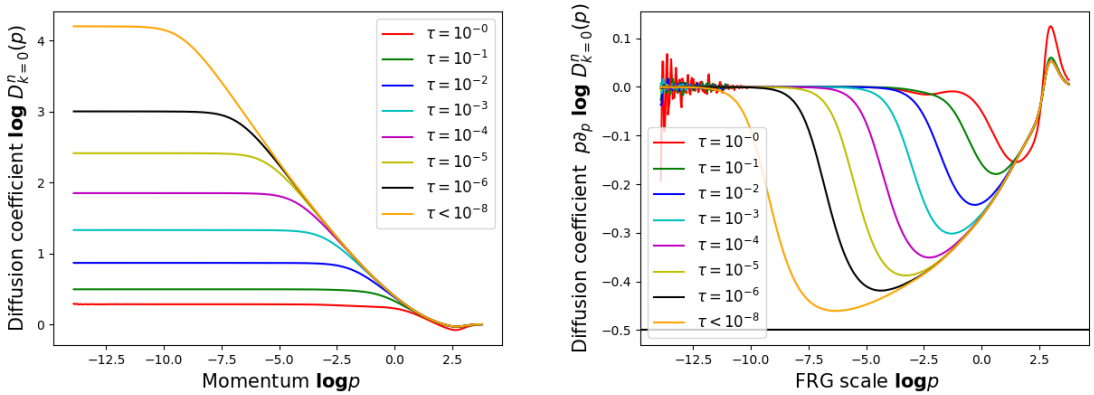

Figure 3.9: Diffusion coefficient $\log D^n_{k=0}(p)$ for the charge densities in the IR ($k = 0$) versus the logarithm of the external momentum scale $\log p$, as the temperature T is approaching the critical temperature T_c from above. The plot on the right shows the derivative of the plot on the left, i.e. the logarithmic derivative $p\partial_p \log D^n_{k=0}(p)$ of the diffusion coefficient with respect to spatial momentum, which coincides with the corresponding critical exponent in the scaling regime.

When considering $p \ll 1/\xi(\tau)$, the universal scaling function $\mathcal{L}(x \ll 1)$ approaches a constant such that one recovers the critical divergence of the diffusion coefficient,

$$D_n(\mathbf{0}, \tau) \sim \tau^{-\nu(2-z_n)} , \tag{3.146}$$

at zero spatial momentum. Conversely, for $p \gg 1/\xi(\tau)$ the universal scaling function $\mathcal{L}(x \gg 1)$ approaches a power law behavior $\mathcal{L}(x) \sim x^{-(2-z_n)}$, such that at the critical temperature one recovers the critical momentum dependence

$$D_n(\boldsymbol{p}, \tau = 0) \sim p^{-(2-z_n)} , \tag{3.147}$$

which then also implies the expected scaling of the relaxation rate of the charge density $\omega^n_{\text{rel}} \sim D_n(\boldsymbol{p})\boldsymbol{p}^2 \sim p^{z_n}$ at the critical point.

Now that we have established the theoretical basis, we proceed to take a look at the numerical results from our FRG calculation. We first note, that by combining the data of the temperature and momentum-dependent diffusion coefficient $D_n(p, \tau)$, as depicted in Fig. 3.9, one can extract the dynamic critical exponent z_n of the charge densities. By taking the logarithmic derivative with respect to p, one clearly observes the emergence of a scaling window as the reduced temperature is lowered, indicating the expected $D_n(p) \sim p^{-(2-z_n)}$ scaling at criticality.

We continue with the extraction of the scaling function $\mathcal{L}(x)$ from our FRG calculation, which by means of Eq. (3.144) can be achieved with plotting

$$\mathcal{L}\left(\xi(\tau)p\right) = \frac{(f^+)^{2-z_n}}{D_n^+} \xi^{-(2-z_n)}(\tau)\, D_n(\boldsymbol{p}, \tau) \tag{3.148}$$

against the scaling variable $x = \xi(\tau)p$. We determine the specific combination $(f^+)^{2-z_n}/D_n^+$ of non-universal amplitudes by choosing the normalization $\mathcal{L}(1) = 1$, which for our set of parameters results in the value given in Table 3.2.

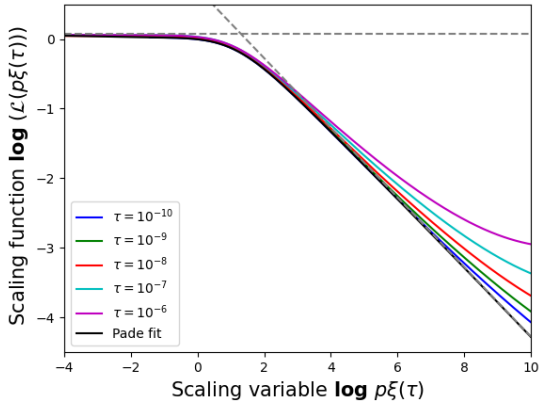

Figure 3.10: The universal scaling function $\mathcal{L}(x)$ from the scaled diffusion coefficient at different reduced temperatures. The universal scaling behavior is well fitted by $\mathcal{L}_{\rm fit}(x) = (a + bx^{0.5} + cx)/(1 + dx^{0.5} + ex + fx^{1.5})$, with $a = 1.073, b = -0.065, c = 0.444, d = 0.143, e = 0.099, f = 0.215$. The dotted gray lines indicate the asymptotic behavior with $\mathcal{L}_{\rm fit}(0) = a$ for $x \to 0$, and $\mathcal{L}_{\rm fit}(x) \to (c/f)\, x^{-0.5}$ for $x \to \infty$.

τ	$(f^+)^{2-z_n}/D_n^+$
10^{-10}	2.718
10^{-9}	2.718
10^{-8}	2.718
10^{-7}	2.718
10^{-6}	2.638

Table 3.2: Non-universal amplitudes $(f^+)^{2-z_n}/D_n^+$ at different reduced temperatures.

In the long-wavelength limit $\xi p \ll 1$, the universal scaling function approaches a constant $\mathcal{L}(x \ll 1) \to \mathcal{L}(0)$. In the short-wavelength limit $\xi p \gg 1$, the universal scaling function approaches $\mathcal{L}(x \gg 1) \sim x^{-(2-z_n)}$, which gives the correct power law $D_n(p,\tau) \sim p^{-(2-z_n)}$ for the momentum dependence of the diffusion coefficient at $\tau = 0$. In Fig. 3.10 we plot the quantity defined by the right-hand side of (3.148) for different reduced temperatures τ using the IR ($k = 0$) results from our FRG calculation. We see that the curves indeed beautifully converge towards a unique universal scaling function $\mathcal{L}(x)$ in the limit $\tau \to 0$. The quantitative shape of the resulting scaling function can rather accurately be determined by performing a fit to a Padé approximant of the order $[m/m+1]$ in the variable x^{2-z_n},

$$\mathcal{L}(x) = \frac{\sum_{j=0}^{m} a_j \left(x^{2-z_n}\right)^j}{1 + \sum_{k=1}^{m+1} b_k \left(x^{2-z_n}\right)^k}\,, \tag{3.149}$$

which yields $\mathcal{L}(0) = a_0$, and ensures the asymptotic behavior $\mathcal{L}(x) \to (a_m/b_{m+1})\, x^{-(2-z_n)}$ for large values of $x \gg 1$. For our results in Fig. 3.10 we find that already for $m = 2$ the method has converged to a sufficient accuracy. The resulting fit with its asymptotics are plotted in the same figure together with our numerical results. The corresponding values for the coefficients a_j, b_k are listed in the figure caption.

3.5 Discussion

We conclude this chapter by summarizing the main results and providing an outline for future applications of the developed formalism.

We have performed a real-time FRG study of Model G, which is conjectured to be the dynamic universality class of the chiral phase transition of two-flavor QCD in the (chiral) limit of vanishing current quark masses. We have constructed a corresponding path-integral formulation for Model G using the MSR technique by introducing auxiliary response fields. We discussed the various symmetries of the MSR action of Model G, which most prominently include a global $O(N)$ symmetry, an extended temporal gauge and displacement symmetry which reflects the underlying reversible mode coupling structure, the discrete symmetry of thermal equilibrium, and a hidden BRST-type symmetry which commonly appears in the MSR approach and expresses the fact that with non-vanishing physical sources, the real-time partition function $Z = 1$ is equal to unity. These symmetries restrict the possible form of the truncation of the effective action.

In the process of formulating a generating functional for Model G, it turned out that the 'traditional' way of introducing source terms as couplings to the elementary MSR response fields on the level of the MSR action is problematic, since for example it does not allow to recover the Boltzmann distribution as a stable equilibrium distribution, and correspondingly one does not recover the correct fluctuation-dissipation relations. Moreover, the underlying Poisson-bracket structure of the reversible mode couplings, which we expressed as an extended temporal gauge symmetry of the MSR action, is violated if the sources are coupled in this traditional way. We found that the correct way to couple physical source terms is to add them on the level of the LGW free energy, which indeed solves the above two problems, and leaves all relevant symmetries during the FRG flow intact. Because of the structure of the reversible mode couplings, in this approach the sources couple to *composite* response fields on the level of the MSR action. It turns out that the flow of the LGW free energy generally remains precisely the same as in the dimensionally reduced Euclidean theory which describes the static critical properties. This warrants that the presence of dynamics in Model G does not change the static critical behavior.

Practical applications of the FRG usually require a truncation of the infinite tower of flow equations, and it is no different in the present work. Here we have taken the pragmatic approach of postulating a truncation of the effective average MSR action by promoting all couplings in the bare MSR action to be running (i.e. to depend on the FRG scale) unless they are protected from renormalization. In addition, we have also included an arbitrarily momentum-dependent kinetic coefficient for the charge densities in order to extract the associated universal scaling function. Using a truncation where the effective average MSR action has the same form as the tree-level MSR action guarantees that all symmetries in Sec. 3.1.2 are exactly maintained during the FRG flow, which allows us to make exact statements about the latter. First, as we have discussed in Sec. 3.2.1 the symmetry of thermal equilibrium implies that the static LGW free energy decouples from the rest of the flow (including, in particular, the dynamic sector) and satisfies a closed d-dimensional Euclidean flow equation on its own. Second, as we have discussed in Sec. 3.3.3 the Ward identities of the (extended) temporal $O(N)$ gauge symmetry imply that the reversible mode coupling g is protected from renormalization.

Using our ansatz for the effective average MSR action, we have studied the flow of the static and dynamic couplings in $O(4)$ Model G. As a sanity check, we first focused on the

well-known static sector, which is purely described by an $O(4)$ symmetric LGW free energy. As one main feature of our approach, the corresponding flow equations are unaltered by the presence of dynamics. Using the arguably simplest truncation of promoting the couplings m^2 and λ to depend on the FRG scale, the static critical exponent ν is only slightly better than the mean-field value of $\nu = 1/2$. As in the results section above, we emphasize again that in the present work we are mainly interested in how a real-time FRG flow for systems with reversible mode couplings as Model G can be formulated *in principle*, and thus consider this result for ν as sufficient for our purposes. Moreover, because the free energy decouples from the dynamics within our approach, this result can be improved precisely in the same way as in the Euclidean case by including higher-order terms in the truncation of the free energy, see e.g. [78, 79], and thus poses no conceptual difficulty here.

In the dynamic sector, we have solved the flow equations for the kinetic coefficients of the order parameter and the conserved charge densities numerically, and we have verified that the dynamic critical exponents indeed come out as $z_\phi = z_n = d/2$, as predicted by Rajagopal and Wilczek [62]. From the numerical results of the FRG flow we have then systematically extracted a dimensionless dynamic scaling function $\mathcal{L}(x)$ describing the universal momentum and temperature dependence of the diffusion coefficient of the charge densities as a function of the dimensionless scaling variable $x = p\xi(\tau)$. In particular, the result is consistent with the analytical limits of large and small scaling variables $x \gg 1$ and $x \ll 1$.

One important task for the future would, e.g., be to extend the present truncation scheme to the full leading order in a systematic derivative expansion of the effective average MSR action. For the description of *static* critical phenomena in the $O(N)$ model it has been explicitly demonstrated in the literature [73, 75, 78, 79, 211] that a derivative expansion of the effective average action rapidly converges against high-precision results for critical exponents and universal amplitude ratios. Therefore, it is not unreasonable to expect that a similar expansion scheme is also applicable to *dynamic* critical phenomena, which would involve an additional expansion in the number of time derivatives. However, whereas an expansion of the static free energy in spatial derivatives poses no additional problems and works just as in the Euclidean case, the extended temporal gauge symmetry suggests that time derivatives must come in the form of covariant derivatives (see Eq. (3.50)), which makes the generalization to higher-order time derivatives more subtle.

With this chapter we have introduced the real-time FRG as a valuable tool complementary to ab-initio classical-statistical simulations [50, 66, 67] for the study of the critical dynamics of systems with reversible mode couplings. On the one hand, classical-statistical simulations are ab initio, but generically require a large numerical effort to measure universal quantities such as dynamic critical exponents and scaling functions. On the other hand, the infinite tower of FRG flow equations generally require truncation, but one can map out, e.g., dynamic scaling functions with comparably low numerical effort, as we have explicitly demonstrated in this chapter.

Chapter 4

Critical dynamics near the QCD critical point

Parts of this chapter have already been published in Ref. [3].

Relativistic heavy-ion collision experiments at various beam energies allow to probe the phase structure of QCD at finite temperature and baryon density. As stated in the introduction, one of the conjectured features of the QCD phase diagram thereby is the existence of a critical point at the end of a first-order transition line [219]. First-principle lattice-QCD simulations are limited to small baryon chemical potentials due to the notorious sign problem, and one has to resort to extrapolations, e.g., using Yang-Lee edge singularities [21, 22]. On the other hand, functional methods including the FRG and Dyson-Schwinger equations are not limited to small baryon chemical potentials and thus can estimate the location of the critical point [17–20], but it turns out to be a rather intricate task to estimate the systematic error in these approaches. Rather recently, a Bayesian analysis of models based on the gauge/gravity duality [23] has been performed to locate the critical point [24].

To identify a potential critical point experimentally, one searches for signatures of criticality in heavy-ion collisions, for example, in cumulants of conserved charges [35]. For instance, static Z_2 universality near the critical point can be used to predict a non-monotonic behavior of the kurtosis as the beam energy is varied [36]. However, the fireball created in a heavy-ion collision is a rapidly evolving system which experiences critical slowing down near the conjectured critical point, which means that the critical modes are guaranteed to fall out of equilibrium. Hence, one generally needs to understand the non-equilibrium time evolution of these critical fluctuations [42, 43]. As we have discussed in Sec. 2.2.4, the dynamic universality class relevant for the QCD critical point, from the Halperin-Hohenberg classification [46], is conjectured to be the one of Model H [47], which is also the one of the liquid-gas critical point in a pure fluid.

One practical application of Model H in the search for the QCD critical point is the Hydro+ framework [44, 45], which supplements the standard hydrodynamic description of heavy-ion collisions by additional slow modes whose momentum-dependent relaxation rates are described by universal scaling functions from Model H. However, at the moment these are only known approximately in $d = 3$ spatial dimensions, for example in the form proposed by Kawasaki [220]. Moreover, Model H was recently employed to derive a universal scaling function for the photon emission rate near the critical point [221] with an approximation similar to the one used by Kawasaki.

In this chapter, we adapt the real-time FRG formalism developed in Chapter 3 to Model H. We derive non-perturbative RG flow equations for the kinetic coefficients of Model H, i.e., for the heat conductivity σ and the shear viscosity η, study their fixed-point structure, and extract their dynamic critical exponents x_σ and x_η for spatial dimensions d in the range $2 < d < 4$. In parallel, we perform an analogous analysis for $O(N)$ Model G by studying the fixed-point structure of the FRG flow equations from Sec. 3.3 analytically within a simplified truncation. In particular, we emphasize the similarities and differences with Model H, and discuss the presence/absence of weak and strong dynamic scaling relations at the various fixed points of both models.

This chapter is organized as follows. In Sec. 4.1 we re-formulate the stochastic equations of Model H as an MSR path integral, and set up the FRG flow by coupling the sources and the regulator to composite response fields analogous to Chapter 3. In Sec. 4.2 we discuss our truncation of the FRG flow and derive analytical expressions for the associated flow equations for both Model H and G. In Sec. 4.3 we study the fixed points of the FRG flow in both models, corresponding scaling relations, and the dependence of the associated dynamic critical exponents on the spatial dimension d in the range $2 < d < 4$. We conclude this chapter in Sec. 4.4 by summarizing our main results and providing an outlook for possible future applications of the formalism.

4.1 MSR path-integral formulation of Model H

For the convenience of the reader, and to emphasize some changes in the notation compared to (2.125), we write the equations of motion of Model H here again,

$$\frac{\partial \phi}{\partial t} = \sigma \boldsymbol{\nabla}^2 \frac{\delta F}{\delta \phi} + g\{\phi, \boldsymbol{j}\} \cdot \frac{\delta F}{\delta \boldsymbol{j}} + \theta \,, \tag{4.1a}$$

$$\frac{\partial j_l}{\partial t} = \mathcal{T}_{lm} \left[\eta \boldsymbol{\nabla}^2 \frac{\delta F}{\delta j_m} + g\{j_m, \phi\} \frac{\delta F}{\delta \phi} + g\{j_m, j_n\} \frac{\delta F}{\delta j_n} \right] + \xi_l \,, \tag{4.1b}$$

where the Poisson brackets are given by (2.123) and (2.124), and the LGW free energy reads

$$F = \int d^d x \left\{ \frac{1}{2} (\boldsymbol{\nabla} \phi)^2 + \frac{m^2}{2} \phi^2 + \frac{\lambda}{4!} \phi^4 + \frac{\boldsymbol{j}^2}{2\rho} \right\} . \tag{4.2}$$

In particular, we have dropped the subscript $\perp$ from $\boldsymbol{j}_\perp$ for simplicity, and thus reserve the symbol $\boldsymbol{j}$ for the transverse part of the momentum density here. Note that this does not cause any confusion with the full momentum density, since the latter does not appear in this chapter. Moreover, we employ the notation of non-relativistic fluids, where the mass density ρ in the kinetic energy in (4.2) takes over the role of the enthalpy w from the relativistic case in (2.122).

Comparing the equations of motion (4.1) to the ones of Model G (3.1), one immediately notices that the two merely differ by: (a) the number of components of the order parameter field, (b) its kinetic coefficient reflecting whether it is conserved (Model H) or not (Model G), and (c) the detailed expressions for the reversible mode couplings. In Model G, the term in (3.1a) describes Larmor precession of the order parameter around the magnetic field generated by the fluctuating charge densities n_{ab}, while in Model H, the corresponding term in (4.1a) describes advection of the order parameter with the momentum density $\boldsymbol{j}$. Other than that, the structural similarities ensure that the real-time FRG methods developed in Chapter 3 can also be directly adapted to Model H. First, the stochastic equations of motion (4.1) are described by

the MSR partition function

$$Z = \int \mathcal{D}\phi\mathcal{D}\tilde{\phi}\mathcal{D}j\mathcal{D}\tilde{j}\, e^{iS} = 1\,, \tag{4.3}$$

with MSR action

$$\begin{aligned} S = \int_x \Big\{ &- \tilde{\phi}\left(\frac{\partial\phi}{\partial t} - \sigma\boldsymbol{\nabla}^2\frac{\delta F}{\delta\phi} - g\{\phi,\boldsymbol{j}\}\cdot\frac{\delta F}{\delta\boldsymbol{j}}\right) \\ &- \tilde{j}_l\left(\frac{\partial j_l}{\partial t} - \mathcal{T}_{lm}\left[\eta\boldsymbol{\nabla}^2\frac{\delta F}{\delta j_m} + g\{j_m,\phi\}\frac{\delta F}{\delta\phi} + g\{j_m,j_n\}\frac{\delta F}{\delta j_n}\right]\right) \\ &- iT\tilde{\phi}\sigma\boldsymbol{\nabla}^2\tilde{\phi} - iT\tilde{j}_l\eta\mathcal{T}_{lm}\boldsymbol{\nabla}^2\tilde{j}_m\Big\}\,. \end{aligned} \tag{4.4}$$

As explained in Sec. 3.1.1, by adding physical source terms to the free energy $F \to F - \int J\psi$ (instead of adding $S \to S + \int J\tilde{\psi}$ to the MSR action), and unphysical source terms to the MSR action $S \to S + \int \tilde{J}\psi$ as usual, the partition function (4.3) is promoted to a generating functional for multi-time correlation functions,

$$\begin{aligned} Z[H,\tilde{H},\boldsymbol{A},\tilde{\boldsymbol{A}}] = \int \mathcal{D}\phi\,\mathcal{D}\tilde{\phi}\,\mathcal{D}n\,\mathcal{D}\tilde{n}\,\exp\Big\{ iS + i\int_x \big(\tilde{H}\phi + \tilde{A}_l j_l\big) + \\ i\int_x H\big(-\sigma\boldsymbol{\nabla}^2\tilde{\phi} + g\{\phi,j_m\}\mathcal{T}_{mo}\tilde{j}_o\big) + \\ i\int_x A_l\big(-\eta\boldsymbol{\nabla}^2\mathcal{T}_{lo}\tilde{j}_o + g\mathcal{T}_{lm}\{j_m,\phi\}\tilde{\phi} + g\mathcal{T}_{lm}\{j_m,j_n\}\mathcal{T}_{no}\tilde{j}_o\big)\Big\}\,. \end{aligned} \tag{4.5}$$

We see from Eq. (4.5) that the physical sources H and $\boldsymbol{A}$ couple to the following composite operators:

$$\tilde{\Phi} \equiv -\sigma\boldsymbol{\nabla}^2\tilde{\phi} + g\{\phi,j_m\}\mathcal{T}_{mo}\tilde{j}_o\,, \tag{4.6a}$$

$$\tilde{J}_l \equiv -\eta\boldsymbol{\nabla}^2\mathcal{T}_{lo}\tilde{j}_o + g\mathcal{T}_{lm}\{j_m,\phi\}\tilde{\phi} + g\mathcal{T}_{lm}\{j_m,j_n\}\mathcal{T}_{no}\tilde{j}_o\,. \tag{4.6b}$$

Since these are proportional to the standard MSR response fields $\tilde{\phi}$ and $\tilde{\boldsymbol{j}}$, we refer to $\tilde{\Phi}$ and $\tilde{\boldsymbol{J}}$ as 'composite' response fields, cf. Eq. (3.22) in Chapter 3. The transverse projectors $\mathcal{T}$ in (4.6) ensure that only the transverse parts of the momentum densities contribute.

Recall that by coupling the classical external sources at the level of the free-energy, i.e. $F \to F - \int J\psi$, it is generally ensured that (i) the classical symmetry of thermal equilibrium [107] as well as (ii) the extended temporal gauge symmetry related to the reversible mode couplings, are maintained exactly in the presence of classical external sources. In Model H, the extended symmetry (ii) expresses an invariance under time-gauged Galilean boosts [222].

Next, to formulate the FRG flow equations [72], one furthermore adds an RG-scale k dependent (spatial) regulator term also on the level of the free energy, i.e. $F \to F + \frac{1}{2}\int \psi R_k \psi$, analogous to the way the (classical) external sources are introduced. The effective average action Γ_k is defined as the modified Legendre transform of the scale-dependent Schwinger functional $-i\log Z_k$, and here reads

$$\Gamma_k[\phi,\tilde{\Phi},\boldsymbol{j},\tilde{\boldsymbol{J}}] \equiv -i\log Z_k[H,\tilde{H},\boldsymbol{A},\tilde{A}] - \int_x \big(\tilde{H}\phi + H\tilde{\Phi} + \tilde{A}_l j_l + A_l\tilde{J}_l\big)\,. \tag{4.7}$$

Its FRG scale (k) dependence then satisfies the real-time flow equation (3.71) (here with the superfields $\psi = (\phi,\boldsymbol{j})$ and $\tilde{\Psi} = (\tilde{\Phi},\tilde{\boldsymbol{J}})$). Based on the above symmetries (i) and (ii), it was

shown in Sec. 3.3.3 and 3.2.1, respectively, that (a) the static FRG flow for the free energy (4.2) is independent of the dynamics and simply given by the standard d-dimensional Euclidean flow equation (3.82), and (b) the mode-coupling constant g is protected from renormalization. In practice, these two exact results can largely simplify the derivation of flow equations, as we have seen above.

Introducing the source and regulator terms on the level of the MSR action in the standard way (as if there were no reversible mode couplings), and as done in Ref. [223] also for Model H, the symmetries (i) and (ii) are generally not preserved. The violation of symmetries during the FRG flow, on the other hand, typically introduces RG relevant operators that would otherwise be excluded by symmetry. These operators then need to be carefully fine-tuned to vanish in the IR again in order to reach the correct fixed point. To avoid such an additional fine-tuning, and to guarantee the exact results that we discuss below, it is therefore necessary to set up an FRG flow that manifestly maintains all the relevant symmetries.

4.2 Truncation and flow equations

Analogous to Sec. 3.3, we truncate the effective average action Γ_k by promoting the kinetic coefficients σ, η, and the LGW free energy F in (4.4) to depend on the FRG scale k,

$$\begin{aligned}\Gamma_k = \int_x \Big\{ &- \tilde{\phi}\left(\frac{\partial\phi}{\partial t} - \sigma_k \boldsymbol{\nabla}^2 \frac{\delta F_k}{\delta\phi} - g\{\phi,\boldsymbol{j}\}\cdot\frac{\delta F_k}{\delta \boldsymbol{j}}\right)\\ &- \tilde{j}_l\left(\frac{\partial j_l}{\partial t} - \mathcal{T}_{lm}\left[\eta_k\boldsymbol{\nabla}^2\frac{\delta F_k}{\delta j_m} + g\{j_m,\phi\}\frac{\delta F_k}{\delta\phi} + g\{j_m,j_n\}\frac{\delta F_k}{\delta j_n}\right]\right)\\ &- iT\tilde{\phi}\sigma_k\boldsymbol{\nabla}^2\tilde{\phi} - iT\tilde{j}_l\eta_k\mathcal{T}_{lm}\boldsymbol{\nabla}^2\tilde{j}_m\Big\}, \end{aligned} \tag{4.8}$$

which ensures that the symmetries (i) and (ii) are preserved by the truncation. The standard response fields $\tilde{\phi}$ and $\tilde{\boldsymbol{j}}$ in (4.8) are understood as functions of the composite response fields $\tilde{\Phi}$ and $\tilde{\boldsymbol{J}}$, implicitly given by inverting

$$\tilde{\Phi} = -\sigma_k\boldsymbol{\nabla}^2\tilde{\phi} + g\{\phi,j_m\}\mathcal{T}_{mo}\tilde{j}_o\,, \tag{4.9a}$$

$$\tilde{J}_l = -\eta_k\boldsymbol{\nabla}^2\mathcal{T}_{lo}\tilde{j}_o + g\mathcal{T}_{lm}\{j_m,\phi\}\tilde{\phi} + g\mathcal{T}_{lm}\{j_m,j_n\}\mathcal{T}_{no}\tilde{j}_o\,. \tag{4.9b}$$

We employ the optimized regulator $R_k^\phi(\boldsymbol{p}) = (k^2-\boldsymbol{p}^2)\theta(k^2-\boldsymbol{p}^2)$ [224] for the order parameter ϕ and set the regulator for the momentum density $\boldsymbol{j}$ to zero, as its static fluctuations are anyway non-critical, and corresponding spatial regulator terms thus RG irrelevant, in general.

4.2.1 Static flow

Since the symmetry of thermal equilibrium (i) is preserved during the FRG flow, the flow of the LGW free energy (4.2) decouples from the rest [2] and satisfies the standard d-dimensional Euclidean flow equation [72]. Hence, the flow of the LGW free energy (4.2) can be investigated independently. Here we employ different truncations. First, the arguably simplest truncation of the effective free energy F_k consists of promoting the couplings m^2 and λ in (4.2) to depend on the FRG scale, $m^2 \to m_k^2$, $\lambda \to \lambda_k$, which amounts to a simple 'ϕ^4-truncation' of the static FRG flow. Combined with the flow of the kinetic coefficients this has the advantage to provide an entirely analytical description of the main qualitative features of dynamic scaling.

In that case, the flow equations for the static quantities m_k^2 and λ_k are given for arbitrary N in Eqs. (3.108) and (3.109). With the optimized regulator the flow of the dimensionless static couplings $\bar{m}_k^2 \equiv k^{-2} m_k^2$ and $\bar{\lambda}_k \equiv T k^{d-4} \lambda_k$ is given by (here for arbitrary N to cover also the case of $O(N)$ Model G)

$$k\partial_k \bar{m}_k^2 = -2\bar{m}_k^2 - \frac{\Omega_d}{(2\pi)^d} \frac{N+2}{3N} \frac{\bar{\lambda}_k}{(1+\bar{m}_k^2)^2} , \tag{4.10}$$

$$k\partial_k \bar{\lambda}_k = (d-4)\bar{\lambda}_k + \frac{\Omega_d}{(2\pi)^d} \frac{2(N+8)}{3N} \frac{\bar{\lambda}_k^2}{(1+\bar{m}_k^2)^3} , \tag{4.11}$$

with the volume $\Omega_d \equiv 2\pi^{d/2}/(\Gamma(d/2)\, d)$ of the d-dimensional unit ball (e.g. $\Omega_3 = 4\pi/3$), which is generally related via $\Omega_d = S_{d-1}/d$ to the surface area S_d of the d-dimensional sphere S^d given in (3.130). The case $N = 1$ corresponds the Z_2 symmetry of Model H.

Beyond this arguably simple ϕ^4-truncation of the static flow, we also consider the extended local-potential approximation (LPA') for the static free energy (4.2), using the ansatz

$$F_k = \int d^d x \left\{ \frac{Z_k^\perp}{2} (\partial^i \phi_a)(\partial^i \phi_a) + U_k(\rho) \right\} , \quad \rho = \phi_a \phi_a , \tag{4.12}$$

for the effective free energy, here generalized to an N-component order parameter. This truncation includes the full field dependence of the effective potential $U_k(\rho)$, and, in addition, a non-trivial wave function renormalization factor $Z_k^\perp$ evaluated at some (possibly k-dependent) field expansion point $\rho_{0,k}$,[1] which gives rise to a non-vanishing anomalous dimension $\eta_\perp = -k\partial_k \log Z_k^\perp$. We also introduce a factor of $Z_k^\perp$ in the optimized regulator, which becomes $R_k^\phi(\boldsymbol{p}) = Z_k^\perp (k^2 - \boldsymbol{p}^2)\theta(k^2 - \boldsymbol{p}^2)$. The flow equations for the effective potential $U_k(\rho)$ and the wave function renormalization factor $Z_k^\perp$ can be obtained using appropriate projections of the Wetterich equation [72]. For the dimensionless effective potential $\bar{U}_k(\bar{\rho})$, defined by $k^d T\, \bar{U}_k(\bar{\rho}) \equiv U_k(\rho)$ with $\rho \equiv k^{d-2} T \bar{\rho}/Z_k^\perp$, one obtains the well-known result [73]

$$\begin{aligned} k\partial_k \bar{U}_k(\bar{\rho}) = {} & -d\, \bar{U}_k(\bar{\rho}) + (d - 2 + \eta_k^\perp)\, \bar{\rho}\, \bar{U}_k'(\bar{\rho}) + \\ & + \frac{\Omega_d}{(2\pi)^d} \left(1 - \frac{\eta_k^\perp}{2+d}\right) \left(\frac{1}{1 + 2\bar{U}_k'(\bar{\rho}) + 4\bar{\rho}\, \bar{U}_k''(\bar{\rho})} + \frac{N-1}{1 + 2\bar{U}_k'(\bar{\rho})} \right) , \end{aligned} \tag{4.13}$$

where the k-derivative on the left-hand side is taken at fixed $\bar{\rho}$, and with the notation $\bar{U}_k'(\bar{\rho}) \equiv \partial \bar{U}_k / \partial \bar{\rho}$.

The flow of the wave function renormalization factor $Z_k^\perp$ at the scale-dependent minimum $\bar{\rho}_{0,k}$ of the effective potential, $\bar{U}_k'(\bar{\rho}_{0,k}) = 0$, is encoded in the anomalous dimension $\eta_k^\perp \equiv -k\partial_k \log Z_k^\perp$ of the order-parameter field. Projecting the Wetterich equation onto the pion (Goldstone) channel for values $N \geq 2$ yields [75]

$$\eta_k^\perp = \frac{32\, \Omega_d\, \bar{\rho}_0\, [\bar{U}_k''(\bar{\rho}_0)]^2}{(2\pi)^d\, (1 + 4\bar{\rho}_0\, \bar{U}_k''(\bar{\rho}_0))^2} , \tag{4.14}$$

By regarding this result as an analytic function of N one can extend its range of validity by analytic continuation to $N = 1$. It was found empirically that this procedure yields reasonable

[1] As we shall see below, an expansion around a non-vanishing (homogeneous) field expectation value $\phi \neq 0$ does not introduce additional tensor structures in the propagators and the 1PI vertex functions of Model H. This is unlike Model G, where a non-vanishing field expectation value $\phi \neq 0$ causes mixing between the pions and the iso-axial-vector charge densities, which leads to numerous additional terms in the flow equations, as discussed in Sec. 3.3. In Model H, such mixing is absent for homogeneous field expectation values ϕ since $\boldsymbol{j}$ couples to the gradient $\boldsymbol{\nabla}\phi$ of the order parameter.

values for the anomalous dimension [75] also in the Z_2 case, which is incentive enough for us to use the same procedure in the present work. In contrast, obtaining similarly accurate values for $\eta_\perp$ using a projection onto the longitudinal (sigma) channel requires the field dependence of $Z_k^\perp(\rho)$ [155], which we leave for future work.

In practice, we solve the LPA' system (4.13) and (4.14) for the potential $\bar{U}(\bar{\rho})$ and the anomalous dimension $\eta_\perp$ at the Wilson-Fisher fixed point $k\partial_k \bar{U}_k(\bar{\rho}) = 0$ numerically using a standard shooting method, as, e.g., discussed in Chapter 12.4 of Ref. [225]: First, requiring regularity at the origin demands the behavior

$$\bar{U}(\bar{\rho}) \sim \left(1 - \frac{\eta_\perp}{2+d}\right) \frac{\Omega_d}{(2\pi)^d\, d\,(1+2c_1)} + c_1 \bar{\rho} + \cdots \quad \text{for } \bar{\rho} \to 0\,.$$

Second, depending on the choices of c_1 and $\eta_\perp$, one generally encounters a singularity in the second derivative $\bar{U}''(\bar{\rho})$ already at a finite value of $\bar{\rho}$. The fixed-point solution is given for those values of c_1 and $\eta_\perp$ where the solution is regular for the entire domain $0 \leq \bar{\rho} < \infty$. Hence, we vary the parameters c_1 and $\eta_\perp$ so as to maximize the domain where the solution is regular until we reach the desired accuracy for c_1 and $\eta_\perp$.

In the following, we shall consider two versions of the LPA', where the flow equations for $Z_k^\perp$, σ_k and η_k are evaluated either at vanishing field expectation value, $\rho_{0,k} \equiv 0$,[2] or at the scale dependent minimum of the effective potential, $\rho_{0,k} = \rho_{\min,k}$, which satisfies $\bar{U}_k'(\bar{\rho}_{\min,k}) = 0$.

4.2.2 Reversible mode couplings

Since the temporal gauge symmetry (*ii*) is preserved, corresponding Ward identities of the effective average MSR action imply that the mode coupling g is protected from renormalization. This was shown explicitly for Model G in Sec. 3.3.3, and the proof directly translates to Model H as well. Nevertheless, it is worthwhile to look at the explicit form of the temporal gauge symmetry (*ii*) in the case of Model H. In analogy to Model G in (3.48), one can straightforwardly verify that the equations of motion (4.1) are invariant under (with $\boldsymbol{\alpha}(t)$ being an arbitrarily time-dependent displacement vector)

$$\phi(t,\boldsymbol{x}) \to \phi(t,\boldsymbol{x}-\boldsymbol{\alpha}(t))\,, \tag{4.15a}$$
$$\theta(t,\boldsymbol{x}) \to \theta(t,\boldsymbol{x}-\boldsymbol{\alpha}(t))\,, \tag{4.15b}$$
$$\boldsymbol{j}(t,\boldsymbol{x}) \to \boldsymbol{j}(t,\boldsymbol{x}-\boldsymbol{\alpha}(t))\,, \tag{4.15c}$$
$$\boldsymbol{\xi}(t,\boldsymbol{x}) \to \boldsymbol{\xi}(t,\boldsymbol{x}-\boldsymbol{\alpha}(t))\,, \tag{4.15d}$$
$$\boldsymbol{A}(t,\boldsymbol{x}) \to \boldsymbol{A}(t,\boldsymbol{x}-\boldsymbol{\alpha}(t)) - \frac{1}{g}\dot{\boldsymbol{\alpha}}(t)\,. \tag{4.15e}$$

On the level of the MSR action (4.4), one transforms the response fields $\tilde{\phi}$ and $\tilde{\boldsymbol{j}}$ instead of the noises θ and $\boldsymbol{\xi}$.

Some comments are in order concerning the interpretation of (4.15) as time-gauged Galilean boosts. Usually, one would expect an inhomogeneous term $\frac{\varrho}{g}\dot{\boldsymbol{\alpha}}(t)$ in (4.15c) when boosting the system by the instantenous velocity $\dot{\boldsymbol{\alpha}}(t)$ [108]. However, one should keep in mind that the proper interpretation of $\boldsymbol{j}$ is the *canonical* momentum density of the fluid [140]. The *physical*

[2] Note that with $\rho_{0,k} \equiv 0$ one recovers standard LPA again, since the flow $k\partial_k Z_k^\perp = 0$ vanishes in this case.

fluid velocity, on the other hand, is given by

$$\boldsymbol{v} = \frac{\delta F}{\delta \boldsymbol{j}}\,, \tag{4.16}$$

which indeed transforms under (4.15) as

$$\boldsymbol{v}(t,\boldsymbol{x}) \to \boldsymbol{v}(t,\boldsymbol{x}-\boldsymbol{\alpha}(t)) + \frac{1}{g}\dot{\boldsymbol{\alpha}}(t)\,, \tag{4.17}$$

including the inhomogeneous term $\frac{1}{g}\dot{\boldsymbol{\alpha}}(t)$ from the transformation (4.15e) of the source field $\boldsymbol{A}$, which gives rise to the anticipated fictitious-force term $\frac{1}{g}\ddot{\boldsymbol{\alpha}}(t)$ in the equation of motion for $\boldsymbol{v}$ after the transformation (4.15).

4.2.3 Kinetic coefficients

We use the FDR to project the flow onto the kinetic coefficients, as discussed for the order-parameter damping rate Γ_k^ϕ and charge mobility γ_k of Model G in Sec. 3.3.2. For Model H, the scale-dependent order-parameter mobility σ_k and shear viscosity η_k can be similarly obtained from second functional derivatives of the effective average MSR action Γ_k with respect to composite response fields $\tilde{\Phi}$ and $\tilde{\boldsymbol{J}}$,

$$\frac{1}{\sigma_k} = \frac{1}{2iT}\lim_{\boldsymbol{p}\to 0}\boldsymbol{p}^2 \lim_{\omega\to 0}\frac{\delta^2\Gamma_k}{\delta\tilde{\Phi}(-\omega,-\boldsymbol{p})\delta\tilde{\Phi}(\omega,\boldsymbol{p})}\bigg|_{\rho_{0,k}}\,, \tag{4.18}$$

$$\frac{1}{\eta_k} = \frac{1}{2iT}\lim_{\boldsymbol{p}\to 0}\boldsymbol{p}^2 \lim_{\omega\to 0}\frac{\mathcal{T}_{lm}(\boldsymbol{p})}{d-1}\frac{\delta^2\Gamma_k}{\delta\tilde{J}_l(-\omega,-\boldsymbol{p})\delta\tilde{J}_m(\omega,\boldsymbol{p})}\bigg|_{\rho_{0,k}}\,, \tag{4.19}$$

evaluated at constant classical field expectation value of the order parameter $\rho_{0,k} = \phi_{0,k}^2$ and vanishing expectation values of all other fields, $\tilde{\Phi} = 0$, $\boldsymbol{j} = \tilde{\boldsymbol{J}} = 0$, as indicated by $(\cdots)|_{\rho_{0,k}}$.

We project the real-time FRG flow onto the kinetic coefficients σ_k and η_k by differentiating Eqs. (4.18) and (4.19) with respect to the FRG scale k, which results in

$$\partial_k\sigma_k = -\frac{\sigma_k^2}{2iT}\lim_{\boldsymbol{p}\to 0}\boldsymbol{p}^2 \lim_{\omega\to 0}\frac{\delta^2\partial_k\Gamma_k}{\delta\tilde{\Phi}(-\omega,-\boldsymbol{p})\delta\tilde{\Phi}(\omega,\boldsymbol{p})}\bigg|_{\rho_{0,k}}\,, \tag{4.20}$$

$$\partial_k\eta_k = -\frac{\eta_k^2}{2iT}\lim_{\boldsymbol{p}\to 0}\boldsymbol{p}^2 \lim_{\omega\to 0}\frac{\mathcal{T}_{lm}(\boldsymbol{p})}{d-1}\frac{\delta^2\partial_k\Gamma_k}{\delta\tilde{J}_l(-\omega,-\boldsymbol{p})\delta\tilde{J}_m(\omega,\boldsymbol{p})}\bigg|_{\rho_{0,k}}\,. \tag{4.21}$$

The corresponding second functional derivatives in (4.20) and (4.21) of the tree-level flow equation (3.71) can be expressed as a sum over Feynman diagrams,

$$\partial_k\Gamma_k^{\tilde{\Phi}\tilde{\Phi}}(p) = \quad -i$$

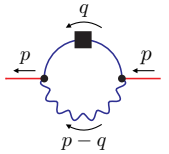

$$- \frac{i}{2}$$

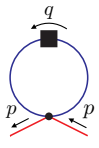

$$, \tag{4.22}$$

$$\partial_k\Gamma_k^{\tilde{J}_l\tilde{J}_m}(p) = \quad -i$$

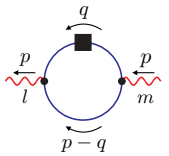

$$- \frac{i}{2}$$

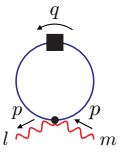

$$, \tag{4.23}$$

with four vectors $p \equiv (\omega, \boldsymbol{p})^T$ and q, and notation analogous to Sec. 3.2.2, i.e., solid lines denote the order parameter ϕ, wiggly lines the momentum density j_l, and the color coding distinguishes the classical fields ϕ, j_l (blue) from the corresponding response fields $\tilde{\Phi}$, $\tilde{J}_l$ (red).

To evaluate these, we need expressions for the propagators and 1PI vertex functions. From our ansatz (4.8) for the effective average MSR action we obtain the following expressions for the two-point functions of the order parameter ϕ,

$$\Gamma_k^{\tilde{\Phi}\phi}(\omega, \boldsymbol{p}) = +\frac{i\omega}{\sigma_k \boldsymbol{p}^2} - m_k^2 - \boldsymbol{p}^2 \,, \tag{4.24a}$$

$$\Gamma_k^{\phi\tilde{\Phi}}(\omega, \boldsymbol{p}) = -\frac{i\omega}{\sigma_k \boldsymbol{p}^2} - m_k^2 - \boldsymbol{p}^2 \,, \tag{4.24b}$$

$$\Gamma_k^{\tilde{\Phi}\tilde{\Phi}}(\omega, \boldsymbol{p}) = \frac{2iT}{\sigma_k \boldsymbol{p}^2} \,, \tag{4.24c}$$

where m_k^2 can be generally related to the curvature of the effective potential $U_k(\rho)$ from (4.12) via $m_k^2 = 2U_k'(\rho_{0,k}) + 4\rho_{0,k} U_k''(\rho_{0,k})$.

On the other hand, the two-point functions of the momentum density $\boldsymbol{j}$ are given by

$$\Gamma_k^{\tilde{J}_l j_m}(\omega, \boldsymbol{p}) = \left(+\frac{i\omega}{\eta_k \boldsymbol{p}^2} - \frac{1}{\rho} \right) \mathcal{T}_{lm}(\boldsymbol{p}) \,, \tag{4.25a}$$

$$\Gamma_k^{j_l \tilde{J}_m}(\omega, \boldsymbol{p}) = \left(-\frac{i\omega}{\eta_k \boldsymbol{p}^2} - \frac{1}{\rho} \right) \mathcal{T}_{lm}(\boldsymbol{p}) \,, \tag{4.25b}$$

$$\Gamma_k^{\tilde{J}_l \tilde{J}_m}(\omega, \boldsymbol{p}) = \frac{2iT \mathcal{T}_{lm}(\boldsymbol{p})}{\eta_k \boldsymbol{p}^2} \,. \tag{4.25c}$$

The full propagator G_k is related to the inverse of the regulated 2-point function, $G_k = -(\Gamma_k^{(2)} - R_k)^{-1}$, where $\Gamma_k^{(2)}$ denotes the second functional derivative of Γ_k. Written in components, this amounts to

$$G^R_{\phi\phi,k}(x,y) = -\left(\frac{\delta^2 \Gamma_k}{\delta\tilde{\Phi}(x)\delta\phi(y)}\bigg|_{\rho_{0,k}} - R_k^\phi(\boldsymbol{x},\boldsymbol{y}) \right)^{-1} , \tag{4.26a}$$

$$G^A_{\phi\phi,k}(x,y) = -\left(\frac{\delta^2 \Gamma_k}{\delta\phi(x)\delta\tilde{\Phi}(y)}\bigg|_{\rho_{0,k}} - R_k^\phi(\boldsymbol{x},\boldsymbol{y}) \right)^{-1} , \tag{4.26b}$$

$$iF_{\phi\phi,k}(x,y) = \int_{zw} G^R_{\phi,k}(x,z) \frac{\delta^2 \Gamma_k}{\delta\tilde{\Phi}(z)\delta\tilde{\Phi}(w)}\bigg|_{\rho_{0,k}} G^A_{\phi,k}(w,y) \,, \tag{4.26c}$$

which results in (after Fourier transform)

$$G^{R/A}_{\phi\phi,k}(\omega, \boldsymbol{p}) = -\frac{\sigma_k \boldsymbol{p}^2}{\pm i\omega - \sigma_k \boldsymbol{p}^2 (m_k^2 + \boldsymbol{p}^2 + R_k^\phi(\boldsymbol{p}))} \,, \tag{4.27a}$$

$$iF_{\phi\phi,k}(\omega, \boldsymbol{p}) = \frac{2i\sigma_k \boldsymbol{p}^2 T}{\omega^2 + (\sigma_k \boldsymbol{p}^2)^2 \, (m_k^2 + \boldsymbol{p}^2 + R_k^\phi(\boldsymbol{p}))^2} \,. \tag{4.27b}$$

On the other hand, the various propagators of the momentum density $\boldsymbol{j}$ are given by (with the

corresponding regulator set to zero)

$$G^R_{j_l j_m,k}(x,y) = -\left(\frac{\delta^2\Gamma_k}{\delta\tilde{J}_l(x)\delta j_m(y)}\bigg|_{\rho_{0,k}}\right)^{-1}, \tag{4.28a}$$

$$G^A_{j_l j_m,k}(x,y) = -\left(\frac{\delta^2\Gamma_k}{\delta j_l(x)\delta\tilde{J}_m(y)}\bigg|_{\rho_{0,k}}\right)^{-1}, \tag{4.28b}$$

$$iF_{j_l j_m,k}(x,y) = \int_{zw} G^R_{j_l j_n,k}(x,z)\frac{\delta^2\Gamma_k}{\delta\tilde{J}_n(z)\delta\tilde{J}_o(w)}\bigg|_{\rho_{0,k}} G^A_{j_o j_m,k}(w,y)\,, \tag{4.28c}$$

which results in

$$G^{R/A}_{j_l j_m,k}(\omega,\boldsymbol{p}) = -\frac{\eta_k \boldsymbol{p}^2 \mathcal{T}_{lm}(\boldsymbol{p})}{\pm i\omega - \eta_k \boldsymbol{p}^2/\rho}\,, \qquad iF_{j_l j_m,k}(\omega,\boldsymbol{p}) = \frac{2i\eta_k \boldsymbol{p}^2 T \mathcal{T}_{lm}(\boldsymbol{p})}{\omega^2 + (\eta_k \boldsymbol{p}^2/\rho)^2}\,. \tag{4.29}$$

Since the symmetry of thermal equilibrium is preserved during the FRG flow, the statistical functions are set by the classical FDR in both cases,

$$iF_{\phi\phi,k}(\omega,\boldsymbol{p}) = \frac{T}{\omega}\left(G^R_{\phi\phi,k}(\omega,\boldsymbol{p}) - G^A_{\phi\phi,k}(\omega,\boldsymbol{p})\right)\,,$$
$$iF_{j_l j_m,k}(\omega,\boldsymbol{p}) = \frac{T}{\omega}\left(G^R_{j_l j_m,k}(\omega,\boldsymbol{p}) - G^A_{j_l j_m,k}(\omega,\boldsymbol{p})\right)\,.$$

The 1PI vertex functions of Model H can be derived via functional derivatives of the effective average MSR action. To perform these derivatives efficiently, we employ the *DoFun* package [226] for Mathematica. The 1PI vertex functions which appear in (4.22) and (4.23) are

$$\Gamma_k^{\tilde{\Phi}\phi j_l}(p,q,r) = -g\,\frac{r^0\,(\mathcal{T}_{\boldsymbol{r}}\boldsymbol{p})_l}{\eta_k \boldsymbol{r}^2\,\sigma_k \boldsymbol{p}^2}\,, \tag{4.30a}$$

$$\Gamma_k^{\tilde{J}_l\phi\phi}(p,q,r) = g\,\frac{q^0\,(\mathcal{T}_{\boldsymbol{p}}\boldsymbol{q})_l}{\eta_k \boldsymbol{p}^2\,\sigma_k \boldsymbol{q}^2} + g\,\frac{r^0\,(\mathcal{T}_{\boldsymbol{p}}\boldsymbol{r})_l}{\eta_k \boldsymbol{p}^2\,\sigma_k \boldsymbol{r}^2}\,, \tag{4.30b}$$

$$\Gamma_k^{\tilde{\Phi}\tilde{\Phi}\phi\phi}(p,q,r,s) = \frac{2ig^2T}{\sigma_k \boldsymbol{p}^2\,\sigma_k \boldsymbol{q}^2}\left(\frac{\mathcal{T}_{lm}(\boldsymbol{p}+\boldsymbol{r})}{\eta_k(\boldsymbol{p}+\boldsymbol{r})^2} + \frac{\mathcal{T}_{lm}(\boldsymbol{q}+\boldsymbol{r})}{\eta_k(\boldsymbol{q}+\boldsymbol{r})^2}\right) r_l s_m\,, \tag{4.30c}$$

$$\Gamma_k^{\tilde{J}_l\tilde{J}_m\phi\phi}(p,q,r,s) = 2ig^2T\,\frac{(\mathcal{T}_{\boldsymbol{p}}(\boldsymbol{p}+\boldsymbol{r}))_l\,(\mathcal{T}_{\boldsymbol{q}}(\boldsymbol{q}+\boldsymbol{s}))_m}{\eta_k \boldsymbol{p}^2\,\eta_k \boldsymbol{q}^2\,\sigma_k(\boldsymbol{p}+\boldsymbol{r})^2} + 2ig^2T\,\frac{(\mathcal{T}_{\boldsymbol{p}}(\boldsymbol{p}+\boldsymbol{s}))_l\,(\mathcal{T}_{\boldsymbol{q}}(\boldsymbol{q}+\boldsymbol{r}))_m}{\eta_k \boldsymbol{p}^2\,\eta_k \boldsymbol{q}^2\,\sigma_k(\boldsymbol{q}+\boldsymbol{r})^2}\,, \tag{4.30d}$$

with the notation $(\mathcal{T}_{\boldsymbol{p}}\boldsymbol{q})_l \equiv \mathcal{T}_{lm}(\boldsymbol{p})q_m$, i.e., $\mathcal{T}_{\boldsymbol{p}}\boldsymbol{q}$ denotes the component of $\boldsymbol{q}$ transverse to $\boldsymbol{p}$.

Inserting the propagators (4.27), (4.29), and the 1PI vertex functions (4.30) into (4.22) and (4.23), evaluating the frequency integrals via the residue theorem and the momentum integrals analytically (which is possible due to the choice of the optimized regulator), we obtain

$$\partial_k\sigma_k = \frac{2g^2\Omega_d Z_k^\perp k^{d-1}T}{(2\pi)^d}\,\frac{(d-1)(d-\eta_\perp)}{d(d-2)}\,\frac{1}{\eta_k}\left(\frac{\sigma_k^2}{(\eta_k/\rho + \sigma_k(Z_k^\perp k^2 + m_k^2))^2} - \frac{1}{(Z_k^\perp k^2 + m_k^2)^2}\right)\,, \tag{4.31}$$

$$\partial_k\eta_k = -\frac{g^2\Omega_d (Z_k^\perp)^2 k^{d+1}T}{(2\pi)^d\,(2+d)\sigma_k(Z_k^\perp k^2 + m_k^2)^3}\,. \tag{4.32}$$

As it turns out, the physically relevant information is conveniently encoded in the following dimensionless combinations of the kinetic coefficients [104],

$$w_H \equiv \rho\,\frac{\sigma_k Z_k^\perp k^2}{\eta_k}\,, \qquad f_H \equiv \frac{d\,\Omega_d\,g^2T}{(2\pi)^d}\,\frac{k^{d-4}}{Z_k^\perp \sigma_k \eta_k}\,. \tag{4.33}$$

Here, w_H is proportional to the ratio of the relaxation rates of the order parameter and the momentum density at criticality, while f_H conveniently represent the pre-factors of the loop diagrams in the flow of the kinetic coefficients.

By applying a k-derivative to the definitions in (4.33), inserting the flow equations for the kinetic coefficients (4.31) and (4.32), and using the usual dimensionless mass parameter $\bar{m}^2 \equiv (Z_k^\perp)^{-1}k^{-2}m^2$ (which is related to the dimensionless effective potential $\bar{U}(\bar{\rho})$ via $\bar{m}^2 = 2\bar{U}'(\bar{\rho}_0) + 4\bar{\rho}_0\bar{U}''(\bar{\rho}_0)$), we can derive the dimensionless flow equations for f_H and w_H,

$$k\partial_k f_H = (d-4+\eta_\perp)f_H + f_H^2\left[\frac{1}{d(d+2)}\frac{1}{(1+\bar{m}^2)^3} - \frac{2(d-1)(d-\eta_\perp)}{d^2\,(d-2)}\left(\frac{1}{(1/w_H+(1+\bar{m}^2))^2} - \frac{1}{(1+\bar{m}^2)^2}\right)\right], \tag{4.34}$$

$$k\partial_k w_H = (2-\eta_\perp)w_H + w_H f_H\left[\frac{1}{d(d+2)}\frac{1}{(1+\bar{m}^2)^3} + \frac{2(d-1)(d-\eta_\perp)}{d^2\,(d-2)}\left(\frac{1}{(1/w_H+(1+\bar{m}^2))^2} - \frac{1}{(1+\bar{m}^2)^2}\right)\right]. \tag{4.35}$$

Importantly, these no-longer depend on the non-universal parameters ρ, g, and T, which stresses the universal character of these non-perturbative flow equations.

Similar analytical expressions for the flow equations of the kinetic coefficients Γ_k^ϕ and γ_k in $O(N)$ Model G can be obtained from the results of Sec. 3.3.2 by neglecting the non-trivial momentum dependence of $\gamma_{n,k}(\boldsymbol{p}) \approx \gamma_k \boldsymbol{p}^2$ considered therein. We again use the optimized regulator $R_k^\phi(\boldsymbol{p})$ for the order parameter, and set the regulator $R_k^n(\boldsymbol{p}) = 0$ for the charge densities n_{ab} to zero. With these choices, the momentum integrals in (3.114)–(3.120) can be solved analytically (in addition to the frequency integrals which are solved analytically anyway using the residue theorem), and the result for the flow equations of the kinetic coefficients is

$$\partial_k \Gamma_k^\phi = \frac{g^2\,(N-1)\,d\,\Omega_d k^{d-1} T}{(2\pi)^d\,\left(k^2+m_k^2\right)\,\gamma_k}\left\{\frac{\Gamma_k^\phi}{k^2\gamma_k/\chi + \Gamma_k^\phi(k^2+m_k^2)} - \frac{2+(d-4)\;{}_2F_1\left(1, \frac{d-2}{2}; \frac{d}{2}; -\frac{k^2\gamma_k/\chi}{\Gamma_k^\phi(k^2+m_k^2)}\right)}{(d-2)\,\left(k^2+m_k^2\right)}\right\}, \tag{4.36}$$

$$\partial_k \gamma_k = -\frac{2g^2\Omega_d k^{d+1} T}{(2\pi)^d\,\Gamma_k^\phi\,\left(k^2+m_k^2\right)^3}, \tag{4.37}$$

with the hypergeometric function ${}_2F_1$ in (4.36).

Analogous to Model H, the physically relevant information is encoded in the dimensionless combinations of the kinetic coefficients, now in Model G,

$$w_G \equiv \chi\,\frac{\Gamma_k^\phi}{\gamma_k}, \qquad f_G \equiv \frac{d\,\Omega_d\,g^2 T}{(2\pi)^d}\,\frac{k^{d-4}}{\Gamma_k^\phi\gamma_k}. \tag{4.38}$$

Inserting the usual dimensionless mass parameter $\bar{m}^2 \equiv k^{-2}m^2$ into the flow equations for the kinetic coefficients (4.36) and (4.37) one obtains the dimensionless flow equations for f_G and w_G in Model G,

$$k\partial_k f_G = f_G(d-4) + f_G^2\left(\frac{2}{d(1+\bar{m}_k^2)^3} - (N-1)I_d(\bar{m}^2, w_G)\right), \tag{4.39}$$

$$k\partial_k w_G = w_G f_G\left[\frac{2}{d(1+\bar{m}_k^2)^3} + (N-1)I_d(\bar{m}^2, w_G)\right],$$

with the shorthand notation

$$I_d(\bar{m}^2, w_G) \equiv -\frac{1}{(1+\bar{m}^2)^2}\left\{\frac{1}{1+(1+\bar{m}^2)w_G} + \frac{4-d}{d-2}\left[1 - {}_2F_1\left(1, \frac{d-2}{2}; \frac{d}{2}; -\frac{1}{(1+\bar{m}^2)w_G}\right)\right]\right\}.$$

4.3 Dynamic critical behavior of Model H and G

Close to a critical point, the dynamic critical exponent z describes the divergence of the correlation time $\xi_t \sim \xi^z$ relative to the correlation length ξ. Sufficiently close to the critical point, on the other hand, the relevant infrared cutoff during the FRG flow is set by the FRG scale $k > 0$, and the correlation length effectively behaves as $\xi \sim 1/k$, while the correlation time ξ_t can be inferred from the position ω_p of the lowest lying pole of the dynamic response function, as $\xi_t \sim 1/\mathrm{Im}(\omega_p)$. Since for both, Model G and H, the kinetic coefficients themselves show critical power-law divergences with the FRG scale k, which can be quantified in terms of logarithmic k-derivatives of the kinetic coefficients in the scaling regime, i.e., $x_{\Gamma^\phi} = -k\partial_k \log \Gamma^\phi_k$ and $x_\gamma = -k\partial_k \log \gamma_k$ for Model G, or $x_\sigma = -k\partial_k \log \sigma_k$ and $x_\eta = -k\partial_k \log \eta_k$ for Model H, these divergences also contribute to the dynamic critical exponents.

We first focus on the critical dynamics of the order parameter field ϕ. In Model G the order parameter is not conserved, and an explicit calculation of its (retarded) propagator in our FRG truncation simply yields $\omega_\phi = -i\Gamma^\phi_k m_k^2 \sim k^{2-x_{\Gamma^\phi}}$, we therefore have $z_\phi = 2 - x_{\Gamma^\phi}$. In contrast, in Model H the order parameter, defined from the entropy per particle, is conserved, and one obtains the dispersion relation $\omega_\phi = -i\sigma_k \boldsymbol{p}^2(m_k^2 + \boldsymbol{p}^2)$. Setting the external momentum to $|\boldsymbol{p}| \sim k$, one thus obtains an additional factor k^2 in the dispersion relation, yielding $\omega_\phi \sim \sigma_k k^4 \sim k^{4-x_\sigma}$, so that $z_\phi = 4 - x_\sigma$ in Model H. Note that we have omitted the anomalous dimension $\eta_\perp$ of the order-parameter field here, which vanishes in our ϕ^4-truncation of the spatial flow. For $\eta_\perp \neq 0$, these dynamic critical exponents generalize to $z_\phi = 2 - \eta_\perp - x_{\Gamma^\phi}$ in Model G, and $z_\phi = 4 - \eta_\perp - x_\sigma$ in Model H, respectively.

Moreover, in either case, the conserved charge densities n_{ab} and $\boldsymbol{j}$ of Model G and H, both also experience critical slowing down due to the reversible couplings to the order parameter. Setting the external momentum to $|\boldsymbol{p}| \sim k$ again, their dispersion relations, $\omega_n = -i\gamma_k \boldsymbol{p}^2/\chi$ and $\omega_j = -i\eta_k \boldsymbol{p}^2/\rho$, both exhibit power laws, $\omega_n \sim k^{2-x_\gamma}$ and $\omega_j \sim k^{2-x_\eta}$, as well, from which one can deduce the dynamic critical exponents $z_n = 2 - x_\gamma$ for the charge densities n_{ab} in Model G and $z_j = 2 - x_\eta$ for the transverse momentum density $\boldsymbol{j}$ in Model H.

Since the critical point corresponds to a fixed point of the FRG flow, it is instructive to investigate the flow diagrams for Model G and H, which are shown in Figs. 4.1 and 4.2, respectively, where the FRG flow lines are plotted in the compactified $(w_{G/H}, f_{G/H})$ plane.[3] As already anticipated in Sec. 2.2.5, in Model G there are two unstable fixed points at $w^*_G = 0$ and $w^*_G = \infty$, and a stable fixed point at finite $0 < w^*_G < \infty$. In contrast, in the flow diagram of Model H, there is only one stable fixed point at $w^*_H = 0$. With this information we can then look for the stable fixed points in the dimensionless flow equations of $f_{G/H}$ analytically:

For Model G, with $w^*_G \neq 0$ and $f^*_G \neq 0$ in Eqs. (4.39), the stable fixed point (in our

[3] The dimensionless static coupling $\bar{m}^2$ is set to its value at the Wilson-Fisher fixed point within our truncation of the static free energy, which we obtain by solving the static sector of our flow equations. This poses no problem because the static flows are independent of the dynamics, as we have discussed in Sec. 3.2.1.

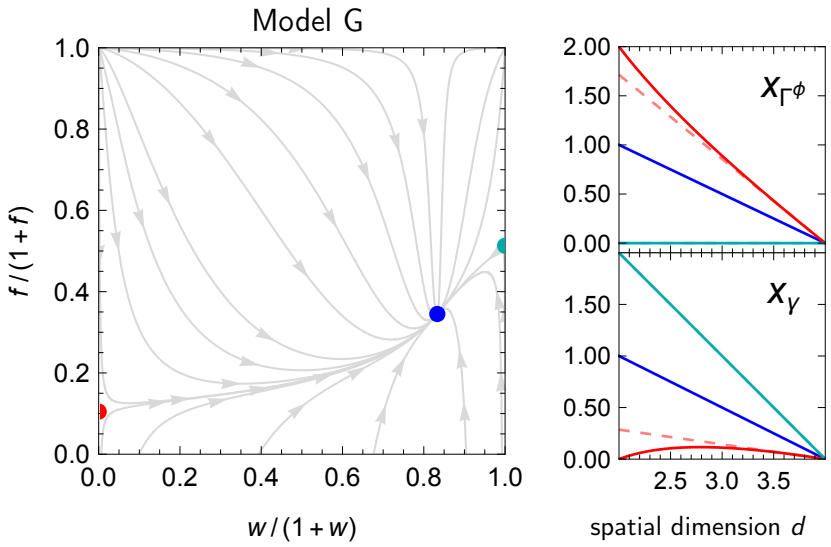

Figure 4.1: Left: flow diagram of $3d$ Model G with one purely attractive stable strong-scaling fixed point (blue) at $(f_G^*, w_G^*) \approx (0.527, 4.998)$ in our ϕ^4-truncation, and two unstable weak-scaling fixed points at $w_G^* \in \{0, \infty\}$ (red and green) [104]. Right: the critical exponents $x_{\Gamma\phi}$ and x_γ of order-parameter damping rate and charge mobility at the various fixed points (solid lines in matching colors), compared to the results from the 1st-order ϵ-expansion in Ref. [110] (dashed lines).

truncation) is located at

$$f_G^* = \frac{(4-d)d(1+\bar{m}^2)^3}{4}\,. \tag{4.40}$$

For Model H, $w_H^* = 0$ implies that the term with $1/w_H$ in the denominator in (4.35) will tend to zero at the stable fixed point and thus can be safely neglected, yielding

$$f_H^* = \frac{(d-2)(4-d-\eta_\perp)(1+\bar{m}^2)^3}{\frac{2(d-1)(d-\eta_\perp)}{d^2}(1+\bar{m}^2) + \frac{d-2}{d(d+2)}}\,. \tag{4.41}$$

Now, using $k\partial_k f_G = (d-4+\eta_\perp+x_{\Gamma\phi}+x_\gamma)f_G$ for Model G and $k\partial_k f_H = (d-4+\eta_\perp+x_\sigma+x_\eta)f_H$ for Model H, which follow directly from the definitions in Eqs. (4.38) and (4.33) (here including field renormalization), we can deduce that as long as the fixed-point value f^* is finite (i.e. $0 < f^* < \infty$), the following *weak-scaling* relations [104, 110] hold at the fixed point in either case,

$$x_{\Gamma\phi} + x_\gamma = x_\sigma + x_\eta = 4 - d - \eta_\perp\,. \tag{4.42}$$

If w^* assumes a finite fixed-point value (i.e. $0 < w^* < \infty$) as well, as in the case of the stable fixed point in Model G, then, from $k\partial_k w_G = w_G(x_\gamma - x_{\Gamma\phi} - \eta_\perp)$, we also have the *strong-scaling* relation,

$$x_{\Gamma\phi} = x_\gamma - \eta_\perp\,. \tag{4.43}$$

With both w_G^* and f_G^* non-vanishing and finite at the stable strong-scaling fixed point of Model G (cf. Fig. 4.1), Eqs. (4.42) and (4.43) are sufficient to uniquely fix the scaling exponents of both kinetic coefficients to

$$x_{\Gamma\phi} + \eta_\perp = x_\gamma = 2 - \frac{d}{2}\,, \tag{4.44}$$

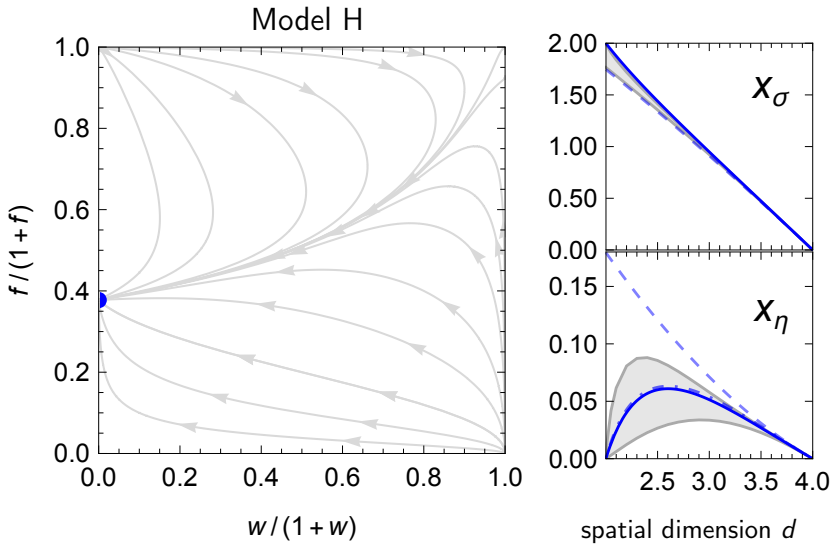

Figure 4.2: Left: flow diagram of $3d$ Model H with only a single stable weak-scaling fixed point at $w_H^* = 0$. Right: the associated critical exponents x_σ and x_η of order-parameter mobility and shear viscosity in our ϕ^4-truncation (solid blue lines) compared to the 2^{nd}-order ϵ-expansion for Model H in Refs. [111,112] (dashed blue), and the result for x_η (bottom) by Ohta and Kawasaki [227] from mode-coupling theory (dashed-dotted blue). Gray bands between corresponding real-time FRG results from full LPA' truncations of the free energy in (4.12), based on the fixed expansion point $\rho_{0,k} = 0$ (upper gray line) and on using the scale-dependent minimum $\rho_{0,k} = \rho_{\min,k}$ (lower gray line), are included to assess the quantitative uncertainty of the ϕ^4-truncation.

as represented by the solid blue lines for x_{Γ^ϕ} and x_γ in the right panel of Fig. 4.1. Moreover, with $z_\phi = 2 - \eta_\perp - x_{\Gamma^\phi}$ and $z_n = 2 - x_\gamma$ from above, these dynamic scaling relations imply that one exactly recovers the dynamic critical exponents $z_\phi = z_n = d/2$ at this strong-scaling fixed point in Model G. This is the fixed point we have observed numerically in Sec. 3.4.

With $w_H^* = 0$ but $f_H^* \neq 0$ and finite at the Model H fixed point (cf. the left panel of Fig. 4.2), on the other hand, there is no such strong-scaling relation as in (4.43). Instead, inserting Eq. (4.41) into the FRG flow equations (4.31) and (4.32) for σ_k and η_k, we then obtain the following analytical expressions for Model H,

$$x_\sigma = \frac{2(d-1)(d-\eta_\perp) f_H^*}{d^2\,(d-2)(1+\bar{m}^2)^2}\,, \qquad x_\eta = \frac{f_H^*}{d\,(d+2)(1+\bar{m}^2)^3}\,, \tag{4.45}$$

with f_H^* given by (4.41). In the ϕ^4-truncation of the static flow, cf. Sec. 4.2.1, the Wilson-Fisher fixed point is located at

$$\bar{m}^{2*} = -\frac{4-d}{16-d}\,, \qquad \bar{\lambda}^* = \frac{(2\pi)^d}{\Omega_d}\frac{(4-d)(1+\bar{m}^{2*})^3}{6}\,, \tag{4.46}$$

and has $\eta_\perp = 0$. Plugging the fixed-point value $\bar{m}^{2*}$ into (4.45), one can explicitly verify that an expansion of (4.45) in $\epsilon = 4 - d$ around $\epsilon = 0$ reproduces the standard result from 1^{st}-order ϵ-expansion [111] exactly, but deviates at higher orders.[4] Our FRG results (4.45) are

[4] We emphasize that our results are not restricted to the presumably small regime around $d = 4$ in which 1^{st}-order ϵ-expansion is valid. On the contrary, the power of non-perturbative/self-consistent approaches is that they

plotted as the solid blue lines in the right panel of Fig. 4.2 along with results from 2^{nd}-order ϵ-expansion [111, 112],

$$x_\sigma = \frac{18}{19}\epsilon(1 - 0.039\epsilon + \mathcal{O}(\epsilon^2))\,, \qquad x_\eta = \frac{1}{19}\epsilon(1 + 0.353\epsilon + \mathcal{O}(\epsilon^2))\,, \tag{4.47a}$$

which currently is the highest order available in this case. While the critical exponent of the mobility x_σ deviates from the latter only on a quantitative level, that of the shear viscosity shows an entirely different qualitative behavior. In fact, our FRG result for x_η in the ϕ^4-truncation closely resembles that of a self-consistent mode-coupling calculation with $\eta_\perp = 0$ by Ohta and Kawasaki [227]. For completeness, we note that a similar non-monotonic behavior of x_η was observed in Ref. [223]. Specifically, with $z_\phi = d + x_\eta$, in $d = 3$ spatial dimensions, we obtain the dynamic critical exponent $z_\phi \approx 3.051$ while the result from [227] corresponds to $z_\phi \approx 3.054$; for comparison, the 2^{nd}-order ϵ-expansion yields $z_\phi \approx 3.071$ [112]. In the numerical simulation of Model H recently performed in Refs. [50, 51] the value $z_\phi = 3.013 \pm 0.058$ was obtained, which is consistent with the analytical results listed above.

In order to verify the robustness of our analytical results for Model H from this simple ϕ^4-truncation, we also consider the LPA' truncation of the static FRG flow, as discussed in Sec. 4.2.1 above. Our numerical results from the LPA' are shown as solid gray lines in the right panel of Fig. 4.2. For both diagrams (x_σ and x_η) the upper gray curves correspond to $\rho_{0,k} \equiv 0$, and the lower gray curves to using the comoving $\rho_{0,k} = \rho_{\min,k}$, which includes a non-vanishing anomalous dimension $\eta_\perp \neq 0$. One can see that the qualitative behavior of the ϕ^4-truncation remains unchanged, in particular with $x_\eta \to 0$ for $d \to 2$. The corresponding numerical values for the dynamic critical exponent in $d = 3$ are $z_\phi \approx 3.058$ for fixed $\rho_{0,k} = 0$ with $\eta_\perp = 0$, and $z_\phi \approx 3.034$ for the comoving $\rho_{0,k} = \rho_{\min,k}$ with $\eta_\perp \approx 0.0443$.[5] Since an exact solution of the FRG flow would be independent of the expansion point $\rho_{0,k}$, these residual differences can serve to estimate the systematic uncertainties in the truncation.

4.4 Discussion

We close this chapter by summarizing our results and outlining possible future applications of the present formalism.

We have used our novel real-time FRG approach to dynamical systems with reversible mode couplings developed in Chapter 3 to study the critical dynamics of Model H, which is conjectured to be in the same dynamic universality class as the QCD critical point. This was possible due to the structural similarities with Model G. In parallel, we have used our formalism to study the fixed-point structure of the FRG flow in Model G, which supplements the numerical findings of Sec. 3.4 by analytical results.

Within our framework we have derived one-loop exact non-perturbative FRG flow equations for the kinetic coefficients of Model G and H. The associated fixed-point structure is qualitatively in line with 1^{st}-order ϵ-expansion [104], comprising one stable strong-scaling and two unstable weak-scaling fixed points in Model G, as compared to only a single weak-scaling fixed point in

are capable of describing the correct qualitative behavior of certain observables for large values of the expansion parameter ($\epsilon \sim 1 - 2$ here), even if they deviate from exact perturbative results for small values of the expansion parameter ($\epsilon \ll 1$ here).

[5] For comparison, the result from the corresponding comoving LPA (with $\eta_\perp = 0$) is practically indistinguishable, yielding $z_\phi \approx 3.033$ in $d = 3$, which shows that the effect of field renormalization is negligible here.

Model H. We have obtained the corresponding strong and weak dynamic relations and computed the dynamic critical exponents x_i of the kinetic coefficients in $2 < d < 4$ spatial dimensions. For the $O(4)$ chiral transition in QCD these determine the singular behavior of chiral order-parameter and Goldstone pion damping rate $\Gamma_k^\phi \sim k^{-x_{\Gamma\phi}}$, and the iso-(axial-)vector charge mobilities $\gamma_k \sim k^{-x_\gamma}$ of Model G. The mobility $\sigma_k \sim k^{-x_\sigma}$ of the conserved order parameter of Model H determines the singular behavior of the entropy per baryon at the QCD critical point and that of transverse momentum densities the shear viscosity $\eta_k \sim k^{-x_\eta}$, as discussed in Sec. 2.2.4. For the dynamic critical exponents z_i the strong-scaling relations of Model G imply the exact result $z_\phi = z_n = d/2$. In Model H, we obtain numerically in $d = 3$ spatial dimensions $x_\sigma \approx 0.949$ and $x_\eta \approx 0.051$ in quite close agreement with the mode-coupling calculations by Ohta and Kawasaki [227], implying $z_\phi \approx 3.051$ for the critical fluctuations of the entropy per baryon.

Evidently, the true power of this formalism is that it can be extended to include more sophisticated truncations of the effective action, e.g., improving the static truncation for the effective LGW free energy, including derivative couplings and anomalous dimensions, for improved precision. For instance, including self-consistent momentum dependencies of the kinetic coefficients $\sigma_k(\boldsymbol{p})$ and $\eta_k(\boldsymbol{p})$, as for the iso-(axial-)vector charge diffusion coefficient in Chapter 3, the framework can be used to compute universal dynamic scaling functions [2, 88, 89] that go beyond the common Kawasaki approximation [44, 45, 220]. In particular, without the technical limitation of our truncation to the symmetric phase (in contrast to Model G, cf. Sec. 3.3), a natural next step would be to map out dynamic scaling functions in Model H which describe the temperature, external field, and momentum dependence of σ and η.

Chapter 5

Real-time dynamics of the quark-meson model

Parts of this chapter have already been made available as a preprint in [4].

Functional methods allow for practical calculations at finite baryon chemical potential, and thus have offered various predictions on the features of the QCD phase diagram, including the location of the conjectured critical point, the existence of inhomogeneous phases or variants thereof, the equation of the state at large baryon densities, etc. (see for instance Refs. [17, 19, 228–230]). However, most of these calculations are based on Euclidean field theory. In order to connect these predictions more directly to the phenomenology of heavy-ion collisions, one also needs to understand their impact on the *dynamics* of the rapidly evolving system created in these collisions.

One promising approach to obtain access to the real-time dynamics and spectral properties of strongly interacting systems also from Euclidean field theory is an analytic continuation on the level of the functional equations themselves. This approach avoids the generally ill-posed inverse problem of spectral reconstruction from discrete numerical Euclidean data. Particularly relevant for the present chapter are Refs. [15, 99, 231–234], where the phase diagram and spectral functions of low-energy effective theories for QCD (including the quark-meson and the parity-doublet model) were computed using the analytically continued functional renormalization group (aFRG). The flow equation of the effective potential was solved in a Euclidean setup, and the phase diagram was computed in the (μ, T)-plane. The spectral functions were computed using analytic continuation, exploiting the 1-loop structure of the flow equations for the two-point functions. For similar approaches based on analytic continuations and/or spectral representations, see e.g. Refs. [183, 184, 189, 235–239]. Despite the merits of such approaches, it is still unclear to which extent one can describe arbitrary real-time dynamics in Euclidean setups. On the other hand, the real-time FRG provides the possibility of including arbitrary dynamics of the system from the beginning. One of our goals in the present chapter is to incorporate fermions into the real-time FRG, and use the framework to study the dynamics of the quark-meson model directly from a real-time perspective. A related functional approach is the 2PI formalism, which has been used in Refs. [240, 241] to study non-equilibrium dynamics in the quark-meson model.

One main difference between the Keldysh formalism and the imaginary-time formalism is that the former allows the system to be out of equilibrium. As discussed in Sec. 2.1.3 above, the special case of the system being in thermal equilibrium instead corresponds to a symmetry

of the Keldysh action [107, 113], which leads to FDR's between real-time correlation functions. Keeping this symmetry intact during the FRG flow constrains the form of the effective average action and therefore simplifies the task of finding suitable truncation schemes. Hence, in the present chapter, we will generalize the symmetry of thermal equilibrium [107, 113] to relativistic Dirac fermions, and use it to constrain the fermionic sector of the effective average (Keldysh) action.

Studying the real-time dynamics of the quark-meson model is also worthwhile from the point of view of the universal critical dynamics around second-order phase transitions in the QCD phase diagram discussed in Chapters 3 and 4. While Model G and H describe at least the universal part of the dynamics of the chiral phase transition in the two-flavor chiral limit, and near the QCD critical point, respectively, it is important to also quantify non-universal corrections to the universal scaling behavior. From the point of view of universal dynamics, fermionic excitations are irrelevant, since they always have a Matsubara mass of πT and hence never become long-wavelength modes. However, at a large enough 'distance' to a second-order phase transition it is important to also include quark dynamics into the effective model picture, in order to more accurately describe the dynamics of QCD.

Having a real-time formulation of the standard quark-meson model at hand, one can start to model the real-time dynamics of the system more accurately. For example, it is known that the chiral order parameter, here described by the $O(4)$ vector ϕ, is not conserved. To incorporate this into the standard quark-meson model, one can introduce dissipation for ϕ in the spirit of the Caldeira-Leggett model [114] by coupling the system to an ensemble of harmonic oscillators and integrating out the latter. This procedure turns the quark-meson model into an open quantum system. Although this procedure can be performed analogously also in Euclidean spacetime, one encounters the problem that the extraction of real-time quantities such as the associated damping coefficients from the Euclidean effective action, nevertheless requires an analytic continuation again.[1] In contrast, genuine real-time methods such as the one used in the present work provide direct access to real-time quantities such as the kinetic coefficients and thus are the natural tool for describing dissipative quantum systems.

We have already discussed in Sec. 3.2.1 that in classical-statistical systems such as Model G the static sector, described by the free energy, is independent of the dynamic sector, which allows for a clear distinction between 'static' and 'dynamic' properties in the first place. As we will see below, the underlying reason is that in a classical-statistical system the only contribution to the static sector comes from the zeroth Matsubara mode, which does not contain any dynamic information of the system. However, for a quantum system such as quark-meson model, this is no-longer the case. In this chapter, we therefore use the quark-meson model as a simple example where all Matsubara modes contribute to the flow of the effective average action, to demonstrate that the non-zero Matsubara modes generally contain dynamic information of the system. This will then in general also have an effect on the 'static sector' described by the effective potential. However, this influence of the dynamics on the static sector is quantitatively small, as we will show comparing the phase diagram and screening masses with zero damping, finite damping and infinite damping.

This chapter is organized as follows. In Sec. 5.1 we introduce the formalism of the real-time quark-meson model using the Schwinger-Keldysh path integral. In particular, the symmetry of

[1] For the damping coefficient one would need the frequency derivative of the retarded self-energy at vanishing external frequency.

thermal equilibrium in a combined system containing both, bosons and fermions is discussed. We then formulate damping terms for sigma and pions which preserve $O(4)$ symmetry, in the spirit of the Caldeira-Leggett model where dissipation is introduced by a coupling to a Gaussian ensemble of bosonic degrees of freedom [114]. In Sec. 5.2, we derive the real-time FRG flow equation for a system with both fermionic and bosonic fields, and the flow equation for the effective potential of the quark-meson model. The fact that the dynamic information of the system has an influence on the static sector is also discussed. In Sec. 5.3, we present our numerical results on the phase diagram of the quark-meson model as well as the temperature and chemical potential dependence of static observables such as screening masses and dynamic observables such as pole masses without damping, with physically motivated finite damping, and in the limit of infinitely strong over-damping. We show that despite the dynamic information having an influence on the static sector, in general, this influence is quantitatively rather small. In particular, all qualitative features of the phase diagram remain unchanged. In Sec. 5.4, we summarize our findings, discuss the conclusions from this chapter and give an outlook on further studies.

5.1 The quark-meson model on the closed-time path

5.1.1 Schwinger-Keldysh formalism

As a low-energy effective model of QCD, the Lagrangian of the quark-meson model with $N_f = 2$ flavors of quarks and $N_c = 3$ color degrees of freedom is given by

$$\mathcal{L} = \bar{\Psi}(i\gamma^\mu\partial_\mu - g(\sigma + i\gamma_5\boldsymbol{\tau}\cdot\boldsymbol{\pi}))\Psi + \frac{1}{2}((\partial_\mu\sigma)(\partial^\mu\sigma) + (\partial_\mu\boldsymbol{\pi})\cdot(\partial^\mu\boldsymbol{\pi})) - U_\Lambda(\rho) + c\sigma \tag{5.1}$$

where the bare potential $U_\Lambda(\rho)$ is defined at the UV scale Λ and depends on the $O(4)$ field invariant $\rho = \sigma^2 + \boldsymbol{\pi}^2$. The explicit symmetry breaking term $-c\sigma$ gives rise to finite (current) quark masses. As usual, we combine σ and $\boldsymbol{\pi}$ into an $O(4)$ vector $\phi = (\sigma, \boldsymbol{\pi})$.

To study the real-time dynamics of the quark-meson model we use the Schwinger-Keldysh formalism. The starting point is the Keldysh action, which in continuum notation is given by

$$S = \int_x \left(\mathcal{L}(\bar{\Psi}^+, \Psi^+, \phi^+) - \mathcal{L}(\bar{\Psi}^-, \Psi^-, \phi^-)\right) , \tag{5.2}$$

where the '+' and '−' fields live on the forward and backward branches of the CTP, respectively. The associated partition function Z is given by [118]

$$Z = \int \mathcal{D}\bar{\Psi}^+\mathcal{D}\Psi^+\mathcal{D}\phi^+\mathcal{D}\bar{\Psi}^-\mathcal{D}\Psi^-\mathcal{D}\phi^- \, e^{iS} = 1 . \tag{5.3}$$

For the bosonic fields ϕ one can define classical and quantum components with a rotation in Keldysh space,

$$\phi^c = \frac{1}{\sqrt{2}}(\phi^+ + \phi^-) , \qquad \phi^q = \frac{1}{\sqrt{2}}(\phi^+ - \phi^-) .$$

For the fermionic fields Ψ, it is customary to perform the Keldysh rotation according to[2]

$$\Psi_1 = \frac{1}{\sqrt{2}}(\Psi^+ + \Psi^-) , \qquad \Psi_2 = \frac{1}{\sqrt{2}}(\Psi^+ - \Psi^-) .$$

[2]Note that we do not use the labels 'classical' and 'quantum' here, but instead simply '1' and '2'. This is because in the Keldysh formalism, fermions (unlike bosons) never have a 'classical' meaning in the sense of satisfying a classical equation of motion in the limit $\hbar \to 0$ [118].

In the Larkin-Ovchinnikov convention [118] it is agreed that the conjugate fields $\bar{\Psi}$ transform in the opposite way,[3] namely

$$\bar{\Psi}_1 = \frac{1}{\sqrt{2}}(\bar{\Psi}^+ - \bar{\Psi}^-)\,, \qquad \bar{\Psi}_2 = \frac{1}{\sqrt{2}}(\bar{\Psi}^+ + \bar{\Psi}^-)\,,$$

which has the benefit that the causal structure of the propagator (i.e. the placement of retarded, advanced, and Keldysh components in the 2×2 matrix, see Eqs. (5.11) and (5.12) below) is exactly the same as for its inverse, unlike the bosonic case.

Substituting the Keldysh rotation into (5.2) and massaging the terms, the Keldysh action can be written as

$$\begin{aligned} S = \int_x \Bigg[&(\bar{\Psi}_1, \bar{\Psi}_2) \begin{pmatrix} i\gamma^\mu\partial_\mu - \frac{g}{\sqrt{2}}(\sigma^c + i\gamma_5\boldsymbol{\tau}\cdot\boldsymbol{\pi}^c) & -\frac{g}{\sqrt{2}}(\sigma^q + i\gamma_5\boldsymbol{\tau}\cdot\boldsymbol{\pi}^q) \\ -\frac{g}{\sqrt{2}}(\sigma^q + i\gamma_5\boldsymbol{\tau}\cdot\boldsymbol{\pi}^q) & i\gamma^\mu\partial_\mu - \frac{g}{\sqrt{2}}(\sigma^c + i\gamma_5\boldsymbol{\tau}\cdot\boldsymbol{\pi}^c) \end{pmatrix} \begin{pmatrix} \Psi_1 \\ \Psi_2 \end{pmatrix} \\ &+ \frac{1}{2}(\sigma^c, \sigma^q) \begin{pmatrix} 0 & -\partial^2 \\ -\partial^2 & 0 \end{pmatrix} \begin{pmatrix} \sigma^c \\ \sigma^q \end{pmatrix} + \frac{1}{2}(\boldsymbol{\pi}^c, \boldsymbol{\pi}^q) \begin{pmatrix} 0 & -\partial^2 \\ -\partial^2 & 0 \end{pmatrix} \begin{pmatrix} \boldsymbol{\pi}^c \\ \boldsymbol{\pi}^q \end{pmatrix} - U_\Lambda(\rho^+) + U_\Lambda(\rho^-) + \sqrt{2}\, c\sigma^c \Bigg]\,, \end{aligned} \tag{5.4}$$

with $\rho^\pm \equiv \phi_a^\pm \phi_a^\pm$ and $\partial^2 \equiv \partial_\mu\partial^\mu$. We first discuss the bosonic part of the action. According to the rules of Gaussian integration, the matrix in the quadratic part at some (purely classical, i.e. $\phi^q = 0$) field expectation value $\phi^c = \sqrt{2}\,\phi$ can be identified with the inverse of the free propagator,

$$G^{-1} = \begin{pmatrix} 0 & (G^A)^{-1} \\ (G^R)^{-1} & (G^K)^{-1} \end{pmatrix} = \begin{pmatrix} 0 & \partial^2 + M^2 \\ \partial^2 + M^2 & 0 \end{pmatrix} \tag{5.5}$$

where we have added a (conventional) additional global minus sign on the right-hand side, and with the mass matrix

$$M^2_{ab} = 2U'_\Lambda(\rho)\delta_{ab} + 4\phi_a\phi_b U''_\Lambda(\rho)\,. \tag{5.6}$$

By inverting (5.5) one can then (in principle) find the free propagator,

$$G = \begin{pmatrix} G^K & G^R \\ G^A & 0 \end{pmatrix}\,. \tag{5.7}$$

However, as it stands, (5.5) has no unique inverse. To make its inverse unique, we have to add infinitesimal ϵ-terms which implement the correct causal (retarded and advanced) boundary conditions. As discussed in Sec. 2.1, one chooses these infinitesimal ϵ-terms to reproduce the known free retarded/advanced Green functions (see e.g. [119])

$$G^{R/A}(\omega, \boldsymbol{p}) = -\frac{1}{(\omega \pm i\epsilon)^2 - \boldsymbol{p}^2 - M^2}\,, \tag{5.8}$$

(where the inverse is taken in 4×4 field space). Moreover, in thermal equilibrium, the Keldysh propagator is generally set by the FDR

$$G^K(\omega, \boldsymbol{p}) = \coth\left(\frac{\omega}{2T}\right)\left(G^R(\omega, \boldsymbol{p}) - G^A(\omega, \boldsymbol{p})\right)\,. \tag{5.9}$$

[3] The conjugate fields $\bar{\Psi}$ are as (Grassmann) variables independent from Ψ, so (unlike in the bosonic case) one can choose a different transformation behavior than for Ψ under the Keldysh rotation.

Eqs. (5.8) and (5.9) tell us which infinitesimal ϵ-terms we have to add to the action in order for them to be reproduced by the rules of Gaussian integration, namely

$$S_b = \int_x \Bigg[\frac{1}{2}(\sigma^c, \sigma^q) \begin{pmatrix} 0 & -\partial^2 + \epsilon u^\mu \partial_\mu \\ -\partial^2 - \epsilon u^\mu \partial_\mu & -2\epsilon u^\mu \partial_\mu \coth \frac{i u^\mu \partial_\mu}{2T} \end{pmatrix} \begin{pmatrix} \sigma^c \\ \sigma^q \end{pmatrix} + \frac{1}{2}(\boldsymbol{\pi}^c, \boldsymbol{\pi}^q) \begin{pmatrix} 0 & -\partial^2 + \epsilon u^\mu \partial_\mu \\ -\partial^2 - \epsilon u^\mu \partial_\mu & -2\epsilon u^\mu \partial_\mu \coth \frac{i u^\mu \partial_\mu}{2T} \end{pmatrix} \begin{pmatrix} \boldsymbol{\pi}^c \\ \boldsymbol{\pi}^q \end{pmatrix} \Bigg] \tag{5.10}$$

where we have introduced a 4-vector $(u^\mu) = (1, 0, 0, 0)$ to make the action Lorentz covariant. These infinitesimal ϵ-terms ensure that the free bosonic Green functions (5.8) and (5.9) are reproduced by the rules of Gaussian integration.

For the fermionic part of the Schwinger-Keldysh action, because of the different convention of the Keldysh rotation for the conjugate fields $\bar{\Psi}$, the fermionic Green function has a different layout in Keldysh space than the bosonic Green function. The inverse fermionic propagator has the structure (again at constant classical (bosonic) field expectation value $\phi^c = (\sigma^c, \boldsymbol{\pi}^c)$, but vanishing quantum field $\phi^q = 0$)

$$\mathcal{G}^{-1} = \begin{pmatrix} (\mathcal{G}^R)^{-1} & (\mathcal{G}^K)^{-1} \\ 0 & (\mathcal{G}^A)^{-1} \end{pmatrix} = \begin{pmatrix} -i\gamma^\mu \partial_\mu + \mathcal{M} & 0 \\ 0 & -i\gamma^\mu \partial_\mu + \mathcal{M} \end{pmatrix}, \tag{5.11}$$

with $\mathcal{M} = \frac{g}{\sqrt{2}}(\sigma^c + i\gamma_5 \boldsymbol{\tau} \cdot \boldsymbol{\pi}^c)$. The inverse of (5.11) (i.e., the free propagator) is given by

$$\mathcal{G} = \begin{pmatrix} \mathcal{G}^R & \mathcal{G}^K \\ 0 & \mathcal{G}^A \end{pmatrix}. \tag{5.12}$$

Notice that the retarded, advanced, and Keldysh components have the same places as in (5.11) due to the the Larkin-Ovchinnikov convention for the Keldysh rotation. It is known that the free fermionic retarded and advanced Green functions should be given by (see e.g. [119])

$$\mathcal{G}^{R/A}(\omega, \boldsymbol{p}) = -\left(\gamma^0(\omega \pm i\epsilon) - \boldsymbol{\gamma} \cdot \boldsymbol{p} - \mathcal{M}\right)^{-1}. \tag{5.13}$$

Moreover, in thermal equilibrium at temperature T and chemical potential μ, the fermionic Keldysh propagator is also generally set by the (fermionic) FDR,

$$\mathcal{G}^K(\omega, \boldsymbol{p}) = \tanh\left(\frac{\omega - \mu}{2T}\right)\left(\mathcal{G}^R(\omega, \boldsymbol{p}) - \mathcal{G}^A(\omega, \boldsymbol{p})\right). \tag{5.14}$$

Eqs. (5.13) and (5.14) tell us the ϵ-terms which we have to add to action in order for these Green functions to be reproduced by Gaussian integration.

Putting all together, the Keldysh action for the quark-meson model in thermal equilibrium

at temperature T and quark chemical potential μ is given by

$$\begin{aligned} S = \int_x \Bigg[& (\bar{\Psi}_1, \bar{\Psi}_2) \begin{pmatrix} i\gamma^\mu\partial_\mu + i\epsilon u_\mu\gamma^\mu & 2i\epsilon u_\mu\gamma^\mu \tanh\frac{iu^\mu\partial_\mu-\mu}{2T} \\ 0 & i\gamma^\mu\partial_\mu - i\epsilon u_\mu\gamma^\mu \end{pmatrix} \begin{pmatrix} \Psi_1 \\ \Psi_2 \end{pmatrix} \\ & -\frac{g}{\sqrt{2}}(\bar{\Psi}_1, \bar{\Psi}_2) \begin{pmatrix} \sigma^c + i\gamma_5\boldsymbol{\tau}\cdot\boldsymbol{\pi}^c & \sigma^q + i\gamma_5\boldsymbol{\tau}\cdot\boldsymbol{\pi}^q \\ \sigma^q + i\gamma_5\boldsymbol{\tau}\cdot\boldsymbol{\pi}^q & \sigma^c + i\gamma_5\boldsymbol{\tau}\cdot\boldsymbol{\pi}^c \end{pmatrix} \begin{pmatrix} \Psi_1 \\ \Psi_2 \end{pmatrix} \\ & +\frac{1}{2}(\sigma^c, \sigma^q) \begin{pmatrix} 0 & -\partial^2 + \epsilon u^\mu\partial_\mu \\ -\partial^2 - \epsilon u^\mu\partial_\mu & -2\epsilon u^\mu\partial_\mu \coth\frac{iu^\mu\partial_\mu}{2T} \end{pmatrix} \begin{pmatrix} \sigma^c \\ \sigma^q \end{pmatrix} \\ & +\frac{1}{2}(\boldsymbol{\pi}^c, \boldsymbol{\pi}^q) \begin{pmatrix} 0 & -\partial^2 + \epsilon u^\mu\partial_\mu \\ -\partial^2 - \epsilon u^\mu\partial_\mu & -2\epsilon u^\mu\partial_\mu \coth\frac{iu^\mu\partial_\mu}{2T} \end{pmatrix} \begin{pmatrix} \boldsymbol{\pi}^c \\ \boldsymbol{\pi}^q \end{pmatrix} \\ & -U_\Lambda(\rho^+) + U_\Lambda(\rho^-) + \sqrt{2}\, c\sigma^c \Bigg] . \end{aligned} \tag{5.15}$$

5.1.2 The symmetry of thermal equilibrium

Before writing down a truncation for the effective average action it is instructive to first look at the symmetries of the bare action. Those symmetries of the bare action that are not violated by source terms or FRG regulators are also symmetries of the effective average action [180] and can therefore restrict the form of possible truncation schemes.

In the Keldysh formalism systems do not need to be in thermal equilibrium, but if they are, this is reflected in a symmetry of the Keldysh action [107, 113]. In general, thermal equilibrium implies that expectation values of various numbers of operators, evaluated at arbitrary space-time points, satisfy FDRs. These FDRs can be shown to be equivalent to the invariance of the Keldysh action under a combination of quantum-mechanical time-reversal (which guarantees the micro-reversibility of the Hamiltonian) and the KMS conditions (which guarantee that the density operator describes a grand-canonical ensemble) [107, 113].

Before going into the fermionic thermal-equilibrium symmetry, let us first review the argument behind the bosonic thermal-equilibrium symmetry in a way that can be straightforwardly adapted to fermions [107]. For a real bosonic wave function φ,[4] which could represent either σ or $\boldsymbol{\pi}$, the time-reversal transformation is given by

$$T\varphi(t, \boldsymbol{x}) = \eta_\varphi\, \varphi(-t, \boldsymbol{x}) , \tag{5.16}$$

where $\eta_\varphi = \pm 1$ denotes the time parity of the field φ, i.e. $\eta_\varphi = +1$ for the scalar sigma and $\eta_\varphi = -1$ for the pseudoscalar pions. On the CTP, the '+' and '−' parts of the contour are switched upon time reversal, and thus the time-reversal transformation for bosons on the CTP is given by

$$T\varphi_\pm(t, \boldsymbol{x}) = \eta_\varphi\, \varphi_\mp(-t, \boldsymbol{x}) . \tag{5.17}$$

To formulate the KMS condition on the CTP, one defines a transformation $\mathcal{K}$ according to [107]

$$\mathcal{K}\varphi_\pm(t, \boldsymbol{x}) = \varphi_\mp(t \mp i\beta/2, \boldsymbol{x}) . \tag{5.18}$$

[4] Note that the transformations in this subsection are formulated for the (either real or Grassmann valued) fields from the coherent-state path integral, *not* for the field *operators*. This difference will become more apparent in the fermionic case below.

However, the transformation in the KMS condition also causes an operator reordering relative to the thermal density operator in correlation functions, cf. Sec. 2.1.3. To effectively 'undo' this relative reordering of operators, one applies another time-reversal transformation. Thermal equilibrium is then expressed as an invariance of the Keldysh action under such a combination $\mathcal{T} = T\mathcal{K}$ of the time-reversal transformation T and the KMS transformation $\mathcal{K}$, i.e. under

$$\mathcal{T}\varphi_\pm(t,\boldsymbol{x}) = \eta_\varphi\,\varphi_\pm(-t \pm i\beta/2,\boldsymbol{x})\,. \tag{5.19}$$

One can perform the Keldysh rotation and Fourier transformation to frequency/momentum space, and obtain the symmetry of thermal equilibrium which, for our real bosonic fields $\phi = (\sigma,\boldsymbol{\pi})$, is then given by

$$\mathcal{T}\begin{pmatrix}\phi^c(\omega,\boldsymbol{p})\\ \phi^q(\omega,\boldsymbol{p})\end{pmatrix} = \eta_\varphi\begin{pmatrix}\cosh\left(\frac{\omega}{2T}\right) & -\sinh\left(\frac{\omega}{2T}\right)\\ -\sinh\left(\frac{\omega}{2T}\right) & \cosh\left(\frac{\omega}{2T}\right)\end{pmatrix}\begin{pmatrix}\phi^c(-\omega,\boldsymbol{p})\\ \phi^q(-\omega,\boldsymbol{p})\end{pmatrix}. \tag{5.20}$$

We now turn to the task of generalizing this symmetry to Dirac fermions. First, we need the time-reversal transformation T. Time reversal for a Dirac-fermion wave function is given by[5] [242]

$$T\Psi(t,\boldsymbol{x}) = K\bar{\Psi}^T(-t,\boldsymbol{x})\,, \tag{5.21}$$

where the matrix K acts in Dirac space and satisfies

$$K^{-1}\gamma^0 K = \gamma^{0T}\,, \qquad K^{-1}\gamma^i K = -\gamma^{iT}\,. \tag{5.22}$$

In the Dirac representation, one e.g. has $K = \gamma^1\gamma^3\gamma^0$. On the CTP, time reversal exchanges the '+' path and '−' parts of the contour. For fermionic degrees of freedom one needs to be more careful here, since switching the '+' and '−' parts on the contour introduces a reverse ordering of Grassmann variables [113]. Taking this into account, the time-reversal transformation for fermions on the CTP is given by

$$T\Psi_\pm(t,\boldsymbol{x}) = \pm K\bar{\Psi}^T_\mp(-t,\boldsymbol{x})\,. \tag{5.23}$$

The time-reversal transformation for the bar field $\bar{\Psi}$ follows from $T^2 = -1$ and reads

$$T\bar{\Psi}_\pm(t,\boldsymbol{x}) = \mp\Psi^T_\mp(-t,\boldsymbol{x})K^{-1}\,. \tag{5.24}$$

Next, we need the transformation $\mathcal{K}$ used in the KMS condition. At zero chemical potential $\mu = 0$ the transformation $\mathcal{K}$ is given just as in the bosonic case,

$$\mathcal{K}\Psi_\pm(t,\boldsymbol{x}) = \Psi_\mp(t \mp i\beta/2,\boldsymbol{x})\,, \tag{5.25a}$$
$$\mathcal{K}\bar{\Psi}_\pm(t,\boldsymbol{x}) = \bar{\Psi}_\mp(t \mp i\beta/2,\boldsymbol{x})\,. \tag{5.25b}$$

At non-vanishing chemical potential $\mu \neq 0$, the transformation $\mathcal{K}$ is generalized to

$$\mathcal{K}\Psi_\pm(t,\boldsymbol{x}) = e^{\pm\beta\mu/2}\Psi_\mp(t \mp i\beta/2,\boldsymbol{x})\,, \tag{5.26a}$$
$$\mathcal{K}\bar{\Psi}_\pm(t,\boldsymbol{x}) = e^{\mp\beta\mu/2}\Psi_\mp(t \mp i\beta/2,\boldsymbol{x})\,. \tag{5.26b}$$

[5] Note again that the transformations here are formulated for the Grassmann-valued fields Ψ in the coherent-state path integral, not for the field operators. Hence, complex conjugation does not imply charge conjugation here. See Chapter 15.13 and especially Eq. (15.144) in the textbook by Bjorken and Drell [186] for a discussion about this difference between field operators and wave functions.

Just as in the bosonic case, the symmetry of thermal equilibrium is again equivalent to the invariance under the combination $\mathcal{T} = T\mathcal{K}$ of time reversal and KMS transformation [113], and is explicitly given by

$$\mathcal{T}\Psi_{\pm}(t,\boldsymbol{x}) = \pm e^{\pm\beta\mu/2}\, K\bar{\Psi}^T_{\pm}\left(-t \pm i/(2T),\boldsymbol{x}\right) , \tag{5.27a}$$

$$\mathcal{T}\bar{\Psi}_{\pm}(t,\boldsymbol{x}) = \mp e^{\mp\beta\mu/2}\, \Psi^T_{\pm}(-t \pm i/(2T),\boldsymbol{x})K^{-1} . \tag{5.27b}$$

Finally, one can perform the Keldysh rotation and a Fourier transformation to frequency and momentum space to obtain

$$\mathcal{T}\begin{pmatrix}\Psi_1(\omega,\boldsymbol{p})\\ \Psi_2(\omega,\boldsymbol{p})\end{pmatrix} = \begin{pmatrix}\cosh\left(\frac{\omega-\mu}{2T}\right) & -\sinh\left(\frac{\omega-\mu}{2T}\right)\\ -\sinh\left(\frac{\omega-\mu}{2T}\right) & \cosh\left(\frac{\omega-\mu}{2T}\right)\end{pmatrix}\begin{pmatrix}K\bar{\Psi}^T_1(-\omega,\boldsymbol{p})\\ K\bar{\Psi}^T_2(-\omega,\boldsymbol{p})\end{pmatrix} , \tag{5.28}$$

$$\mathcal{T}\begin{pmatrix}\bar{\Psi}_1(\omega,\boldsymbol{p})\\ \bar{\Psi}_2(\omega,\boldsymbol{p})\end{pmatrix} = \begin{pmatrix}-\cosh\left(\frac{\omega+\mu}{2T}\right) & \sinh\left(\frac{\omega+\mu}{2T}\right)\\ \sinh\left(\frac{\omega+\mu}{2T}\right) & -\cosh\left(\frac{\omega+\mu}{2T}\right)\end{pmatrix}\begin{pmatrix}\Psi^T_1(-\omega,\boldsymbol{p})K^{-1}\\ \Psi^T_2(-\omega,\boldsymbol{p})K^{-1}\end{pmatrix} . \tag{5.29}$$

One can explicitly verify that the Keldysh action (5.4) for the quark-meson model indeed satisfies the combined thermal-equilibrium symmetry of bosons and fermions, which means that it is invariant under the combined transformation $\mathcal{T}$. It can also be shown that the invariance under $\mathcal{T}$ leads to the well-known FDR

$$G^K(\omega,\boldsymbol{p}) = \coth\left(\frac{\omega}{2T}\right)\left(G^R(\omega,\boldsymbol{p}) - G^A(\omega,\boldsymbol{p})\right) \tag{5.30}$$

for the bosonic propagator, and

$$\mathcal{G}^K(\omega,\boldsymbol{p}) = \tanh\left(\frac{\omega-\mu}{2T}\right)\left(\mathcal{G}^R(\omega,\boldsymbol{p}) - \mathcal{G}^A(\omega,\boldsymbol{p})\right) \tag{5.31}$$

for the fermionic propagator.

5.1.3 Bosonic heat bath

To study the dissipative dynamics of the chiral order parameter, we consider the $O(4)$ vector ϕ to be coupled to an external heat bath. A coupling of the mesons to a heat bath will introduce finite decay widths in their respective spectral functions. In the vacuum, it is well known that the decay width of the sigma is much bigger than that of the pion. Our goal in this subsection is therefore to model the heat bath in a way that allows different decay widths for σ and $\boldsymbol{\pi}$ in the symmetry-broken phase, while simultaneously keeping the $O(4)$ symmetry of the effective average action intact. As a further requirement, the additional terms added to the Keldysh action should satisfy the symmetry of thermal equilibrium from Sec. 5.1.2 above. In order to meet these requirements, we consider a physical picture where the mesonic part of the action is coupled to an ensemble of harmonic oscillators in the spirit of the Caldeira-Leggett model [114].

As a starting point, we consider additional interaction terms in the Lagrangian (5.1) which describe the coupling between the mesons and two new sets of heat-bath oscillators $\{\varphi_s\}$ and $\{\chi_{s,a}\}$ (enumerated by s), where the former are $O(4)$ scalars and the latter $O(4)$ vectors. On the level of the Lagrangian (5.1) they couple to the system via

$$\mathcal{L}_{int} = \sum_s \frac{g_s}{2}\varphi_s\phi_a\phi_a + \sum_s h_s\chi_{s,a}\phi_a , \tag{5.32}$$

with two sets of coupling constants $\{g_s\}$ and $\{h_s\}$. This extra piece of the interacting Lagrangian will introduce extra terms in the Keldysh action in the following way (after Keldysh rotation),

$$S_{int} = \int_x \left[\sum_s \frac{g_s}{\sqrt{2}} \big(\varphi_s^c \phi_a^c \phi_a^q + \frac{1}{2}\varphi_s^q \phi_a^c \phi_a^c + \frac{1}{2}\varphi_s^q \phi_a^q \phi_a^q\big) + \sum_s h_s \big(\chi_{s,a}^c \phi_a^q + \chi_{s,a}^q \phi_a^c\big) \right]. \tag{5.33}$$

For later convenience, in addition to the standard field invariant $\rho = \frac{1}{2}\phi_a^c \phi_a^c$, we introduce the shorthand notation $\rho^q \equiv \phi_a^c \phi_a^q$ and $\rho^{qq} \equiv \frac{1}{2}\phi_a^q \phi_a^q$ for the other $O(4)$ field invariants. At the leading order in fluctuations $\delta\phi$ around the field expectation value $\phi_0^c = (\sqrt{2}\sigma_0, 0)$ these reduce to $\rho = \sigma_0^2 + \sqrt{2}\sigma_0\, \delta\sigma^c + \mathcal{O}(\delta\phi^2)$ and $\rho^q = \sqrt{2}\sigma_0\, \delta\sigma^q + \mathcal{O}(\delta\phi^2)$, whereas $\rho^{qq} \sim \mathcal{O}(\delta\phi^2)$ yields true quantum corrections which are absent from the classical MSR action.

Then there is also the non-interacting (kinetic) part of the Lagrangian for the heat-bath oscillators, which specifies their real-time Green functions,

$$\begin{aligned} S_{bath} = -\frac{1}{2}\int_{\omega \boldsymbol{p}} \Bigg[& \sum_s (\varphi_s^c, \varphi_s^q)_{-\omega,-\boldsymbol{p}} \begin{pmatrix} 0 & [D_{\varphi,s}^{-1}]^R(\omega,\boldsymbol{p}) \\ [D_{\varphi,s}^{-1}]^A(\omega,\boldsymbol{p}) & [D_{\varphi,s}^{-1}]^K(\omega,\boldsymbol{p}) \end{pmatrix} \begin{pmatrix} \varphi_s^c \\ \varphi_s^q \end{pmatrix}_{\omega,\boldsymbol{p}} \\ & \sum_s \big(\chi_{s,a}^c, \chi_{s,a}^q\big)_{-\omega,-\boldsymbol{p}} \begin{pmatrix} 0 & [D_{\chi,s}^{-1}]^R(\omega,\boldsymbol{p}) \\ [D_{\chi,s}^{-1}]^A(\omega,\boldsymbol{p}) & [D_{\chi,s}^{-1}]^K(\omega,\boldsymbol{p}) \end{pmatrix} \begin{pmatrix} \chi_{s,a}^c \\ \chi_{s,a}^q \end{pmatrix}_{\omega,\boldsymbol{p}} \Bigg]. \end{aligned} \tag{5.34}$$

We require the heat bath to be in thermal equilibrium, which mean that the real-time Green functions of the heat-bath oscillators are related by the FDR

$$D_{\varphi,s}^K(\omega,\boldsymbol{p}) = \coth\left(\frac{\omega}{2T}\right)\big(D_{\varphi,s}^R(\omega,\boldsymbol{p}) - D_{\varphi,s}^A(\omega,\boldsymbol{p})\big)\,, \tag{5.35a}$$

$$D_{\chi,s}^K(\omega,\boldsymbol{p}) = \coth\left(\frac{\omega}{2T}\right)\big(D_{\chi,s}^R(\omega,\boldsymbol{p}) - D_{\chi,s}^A(\omega,\boldsymbol{p})\big)\,. \tag{5.35b}$$

Since the heat-bath oscillators φ_s and $\chi_{s,a}$ are quadratic in the Keldysh action, one can integrate them out and obtain the terms

$$\begin{aligned} S \to S + \int_{\omega\boldsymbol{p}} \Bigg\{ & \sum_s \frac{h_s^2}{2} (\phi_a^c, \phi_a^q)_{-\omega,-\boldsymbol{p}} \begin{pmatrix} 0 & D_{\chi,s}^A(\omega,\boldsymbol{p}) \\ D_{\chi,s}^R(\omega,\boldsymbol{p}) & D_{\chi,s}^K(\omega,\boldsymbol{p}) \end{pmatrix} \begin{pmatrix} \phi_a^c \\ \phi_a^q \end{pmatrix}_{\omega,\boldsymbol{p}} \\ & + \sum_s \frac{g_s^2}{4} \Big[\rho^q(-\omega,-\boldsymbol{p})\, D_{\varphi,s}^R(\omega,\boldsymbol{p})\, \big(\rho(\omega,\boldsymbol{p}) + \rho^{qq}(\omega,\boldsymbol{p})\big) \\ & + \big(\rho(-\omega,-\boldsymbol{p}) + \rho^{qq}(-\omega,-\boldsymbol{p})\big)\, D_{\varphi,s}^A(\omega,\boldsymbol{p})\, \rho^q(\omega,\boldsymbol{p}) + \rho^q(-\omega,-\boldsymbol{p})\, D_{\varphi,s}^K(\omega,\boldsymbol{p})\, \rho^q(\omega,\boldsymbol{p}) \Big] \Bigg\}, \end{aligned} \tag{5.36}$$

where we have reorganized the terms in the first line (coming from the χ-oscillators) into a quadratic form in ϕ^c and ϕ^q to emphasize the structure of the self energy which the system particle acquires due to mixing with the χ-oscillators. One can introduce spectral densities $J_\varphi(\omega,\boldsymbol{p})$ and $J_\chi(\omega,\boldsymbol{p})$ to rewrite the retarded and the advanced heat-bath propagators as

$$\sum_s g_s^2 D_{\varphi,s}^{R/A}(\omega,\boldsymbol{p}) = -\int_0^\infty \frac{d\omega'}{2\pi} \frac{2\omega' J_\varphi(\omega',\boldsymbol{p})}{(\omega \pm i\epsilon)^2 - \omega'^2}\,, \tag{5.37a}$$

$$\sum_s h_s^2 D_{\chi,s}^{R/A}(\omega,\boldsymbol{p}) = -\int_0^\infty \frac{d\omega'}{2\pi} \frac{2\omega' J_\chi(\omega',\boldsymbol{p})}{(\omega \pm i\epsilon)^2 - \omega'^2}\,. \tag{5.37b}$$

Using the FDR, the Keldysh components of the heat-bath propagators are given by

$$\sum_s g_s^2 D_s^K(\omega,\boldsymbol{p}) = \sum_s g_s^2 \coth\left(\frac{\omega}{2T}\right) 2i\ \mathrm{Im}\, D_s^R(\omega,\boldsymbol{p}) = \coth\left(\frac{\omega}{2T}\right) i J_\varphi(\omega,\boldsymbol{p})\,, \tag{5.38}$$

$$\sum_s h_s^2 D_s^K(\omega,\boldsymbol{p}) = \sum_s h_s^2 \coth\left(\frac{\omega}{2T}\right) 2i\, \mathrm{Im}\, D_s^R(\omega,\boldsymbol{p}) = \coth\left(\frac{\omega}{2T}\right) i J_\chi(\omega,\boldsymbol{p})\,, \tag{5.39}$$

Here we consider Ohmic spectral densities for both ensembles of heat-bath oscillators,

$$J_\chi(\omega,\boldsymbol{p}) = 2\gamma\omega \quad \text{and} \quad J_\varphi(\omega,\boldsymbol{p}) = 2Y\omega\,, \tag{5.40}$$

with two different damping coefficients γ and Y. With this ansatz, after absorbing an infinite constant at $\omega = 0$, $\boldsymbol{p} = \boldsymbol{0}$ into renormalized squared mass and quartic coupling, one obtains

$$\begin{aligned} S \to S + \int_{\omega\boldsymbol{p}} \Bigg\{ & \frac{1}{2}\left(\phi_a^c, \phi_a^q\right)_{-\omega,-\boldsymbol{p}} \begin{pmatrix} 0 & -i\gamma\omega \\ i\gamma\omega & 2i\gamma\omega\coth\left(\frac{\omega}{2T}\right) \end{pmatrix} \begin{pmatrix} \phi_a^c \\ \phi_a^q \end{pmatrix}_{\omega,\boldsymbol{p}} \\ & + \frac{1}{2}\rho^q(-\omega,-\boldsymbol{p})\; iY\omega\left(\rho(\omega,\boldsymbol{p}) + \rho^{qq}(\omega,\boldsymbol{p})\right) + \frac{1}{2}\rho^q(-\omega,-\boldsymbol{p})\; iY\omega\coth\left(\frac{\omega}{2T}\right)\; \rho^q(\omega,\boldsymbol{p}) \Bigg\}\,, \end{aligned} \tag{5.41}$$

for the additional terms in the Keldysh action. Undoing the Fourier transformation, we can therefore write

$$\begin{aligned} S \to S + \int_x \Bigg\{ & \frac{1}{2}\left(\phi_a^c(x), \phi_a^q(x)\right) \begin{pmatrix} 0 & \gamma u^\mu\partial_\mu \\ -\gamma u^\mu\partial_\mu & -2\gamma u^\mu\partial_\mu\coth\left(\frac{iu^\mu\partial_\mu}{2T}\right) \end{pmatrix} \begin{pmatrix} \phi_a^c(x) \\ \phi_a^q(x) \end{pmatrix} \\ & - \frac{1}{2}\rho^q(x)\, Y u^\mu\partial_\mu\left(\rho(x) + \rho^{qq}(x)\right) - \frac{1}{2}\rho^q(x)\, Y u^\mu\partial_\mu\coth\left(\frac{iu^\mu\partial_\mu}{2T}\right)\; \rho^q(x) \Bigg\}\,, \end{aligned} \tag{5.42}$$

where we have again introduced the 4-velocity u^μ of the heat bath, given by $(u^\mu) = (1,0,0,0)$ in the local rest frame, to make the action Lorentz covariant. Eq. (5.42) constitutes our model of an Ohmic heat bath that produces different damping constants for the longitudinal and transverse components in field space while keeping the action $O(4)$ invariant. Specifying $\phi_0^c = (\sqrt{2}\sigma_0, 0)$ for symmetry breaking in the direction of the sigma meson, from the imaginary parts of the inverses of the retarded propagators of pions and sigma meson at tree level, with

$$\begin{aligned} & \rho^q Y u^\mu\partial_\mu(\rho + \rho^{qq}) = \delta\sigma^q 2\sigma_0^2\, Y u^\mu\partial_\mu\delta\sigma^c + \mathcal{O}(\delta\phi^3)\,, \quad \text{and} \\ & \rho^q Y u^\mu\partial_\mu\coth\left(\frac{iu^\mu\partial_\mu}{2T}\right)\; \rho^q = \delta\sigma^q 2\sigma_0^2\, Y u^\mu\partial_\mu\coth\left(\frac{iu^\mu\partial_\mu}{2T}\right)\; \delta\sigma^q + \mathcal{O}(\delta\phi^3)\,, \end{aligned}$$

we can identify their respective damping constants as

$$\gamma_\pi = \gamma \quad \text{and} \quad \gamma_\sigma = \gamma + \sigma_0^2\, Y\,. \tag{5.43}$$

Thus our model (5.42) indeed leads to different damping constants for sigma meson and pions, with the difference $\gamma_\sigma - \gamma_\pi \sim \sigma_0^2$ being proportional to the squared symmetry-breaking field expectation value.

5.2 Real-time FRG with fermions

The standard (Euclidean) formulation of the FRG has been applied rather successfully in the past to study the phase structure of the quark-meson model and variants thereof, e.g., see Refs. [14, 15, 99, 231–234, 243–249]. However, genuine real-time formulations of the FRG on the Schwinger-Keldysh contour have been applied mostly to quantum systems with only bosonic degrees of freedom in the past, e.g., in Refs. [1, 90, 98, 106, 151, 199]. The purpose of the present section is twofold: we extend the real-time FRG to include fermionic degrees of freedom, and establish some general notation used in this chapter.

To formulate the FRG flow equation we follow the standard procedure of adding an infrared regulator ΔS_k to the bare Keldysh action (5.2),

$$S \to S + \Delta S_k \,. \tag{5.44}$$

The regulator term ΔS_k has the purpose of suppressing the fluctuations of modes with momentum smaller than the FRG scale k. In the simplest case the regulator term ΔS_k can be taken to be a quadratic form of the fields, i.e.

$$\begin{aligned}\Delta S_k = \frac{1}{2}\int_{xx'} (\phi_a^c(x), \phi_a^q(x)) \begin{pmatrix} R^{\tilde{K}}_{ab,k}(x,x') & R^A_{ab,k}(x,x') \\ R^R_{ab,k}(x,x') & R^K_{ab,k}(x,x') \end{pmatrix} \begin{pmatrix} \phi_b^c(x') \\ \phi_b^q(x') \end{pmatrix} \\ + \int_{xx'} (\bar{\psi}_1(x), \bar{\psi}_2(x)) \begin{pmatrix} \mathcal{R}_k^R(x,x') & \mathcal{R}_k^K(x,x') \\ \mathcal{R}_k^{\tilde{K}}(x,x') & \mathcal{R}_k^A(x,x') \end{pmatrix} \begin{pmatrix} \psi_1(x') \\ \psi_2(x') \end{pmatrix} .\end{aligned} \tag{5.45}$$

To simplify the notation, one can introduce Keldysh indices i, j (with $i, j = 1, 2$ for fermions and $i, j = c, q$ for bosons) to write the regulator term as

$$\Delta S_k = \int_{xx'} \left[\frac{1}{2} \phi_a^i(x) R^{ij}_{ab,k}(x,x') \phi_b^j(x') + \bar{\psi}_i(x) \mathcal{R}_{ij,k}(x,x') \psi_j(x') \right] . \tag{5.46}$$

Adding the regulator term (5.44) to the bare action means that the generating functional (G.1) and the Schwinger functional (G.2), both explicitly given in Appendix G.1 to introduce our notations and conventions, become dependent on the FRG scale k: $Z \to Z_k$, $W \to W_k$. One then defines the effective *average* action Γ_k as a 'modified' Legendre transform of the now scale-dependent Schwinger functional W_k, via

$$\Gamma_k = W_k - \Delta S_k - \int_x \left[j_a^q \phi_a^c + j_a^c \phi_a^q + \bar{\eta}_1 \psi_2 + \bar{\psi}_2 \eta_1 + \bar{\eta}_2 \psi_1 + \bar{\psi}_1 \eta_2 \right] . \tag{5.47}$$

The effective average action Γ_k can be interpreted as the effective action (G.4) but with modes of momenta larger than the FRG scale k integrated out. The flow of Γ_k can then be derived following the standard procedure by Wetterich [72]. The result here reads

$$\partial_k \Gamma_k = i \,\mathrm{Tr}\left\{ \partial_k \mathcal{R}_k \circ \mathcal{G}_k \right\} - \frac{i}{2} \,\mathrm{Tr}\left\{ \partial_k R_k \circ G_k \right\} . \tag{5.48}$$

The full field-dependent fermionic propagator $\mathcal{G}_k$ is related to the inverse two-point function $\Gamma_k^{(2)}$ via

$$\mathcal{G}_{ij,k}(x,x') = -\left[\frac{\overrightarrow{\delta}}{\delta \bar{\psi}_i(x)} \Gamma_k \frac{\overleftarrow{\delta}}{\delta \psi_j(x')} + \mathcal{R}_{ij,k}(x,x') \right]^{-1} , \tag{5.49}$$

where $i, j = 1, 2$ are the indices in Keldysh space with Larkin-Ovchinnikov conventions again. Similarly, the full field-dependent bosonic propagator G_k is given by the inverse

$$G^{ij}_{ab,k}(x,x') = -\left[\frac{\delta^2 \Gamma_k}{\delta \phi_a^i(x) \delta \phi_b^j(x')} + R^{ij}_{ab,k}(x,x') \right]^{-1} , \tag{5.50}$$

with $i, j = c, q$ here denoting the classical/quantum components in Keldysh space, and $a, b = 1, \ldots, 4$ the $O(4)$ indices of the corresponding field components.

For the rest of this chapter, we assume that both the bosonic and fermionic regulator terms in (5.46) are chosen to comply with the causal structure of the Keldysh action [118]. As discussed in Sec. 2.3.2, this implies that the retarded/advanced components of the regulators admit

spectral representations, and that their anomalous components $R_k^{\tilde{K}} = 0$ and $\mathcal{R}_k^{\tilde{K}} = 0$ vanish. Moreover, we assume that the regulators themselves satisfy the symmetries of thermal equilibrium from Sec. 5.1.2. This means that they must be spacetime-translation invariant, and that their respective Keldysh components are set by the FDR, i.e. after Fourier transformation,

$$R^K_{ab,k}(\omega,\boldsymbol{p}) = \coth\left(\frac{\omega}{2T}\right)\left(R^R_{ab,k}(\omega,\boldsymbol{p}) - R^A_{ab,k}(\omega,\boldsymbol{p})\right) \tag{5.51}$$

and

$$\mathcal{R}^K_k(\omega,\boldsymbol{p}) = \tanh\left(\frac{\omega-\mu}{2T}\right)\left(\mathcal{R}^R_k(\omega,\boldsymbol{p}) - \mathcal{R}^A_k(\omega,\boldsymbol{p})\right)\,. \tag{5.52}$$

For later use we also define,

$$B^R_{ab,k}(x,x') \equiv \int_{yy'} G^R_{ac,k}(x,y)\,\partial_k R^R_{cd,k}(y,y')\,G^R_{db,k}(y',x')\,, \tag{5.53a}$$

$$B^A_{ab,k}(x,x') \equiv \int_{yy'} G^A_{ac,k}(x,y)\,\partial_k R^A_{cd,k}(y,y')\,G^A_{db,k}(y',x')\,, \tag{5.53b}$$

$$\begin{aligned} B^K_{ab,k}(x,x') \equiv \int_{yy'} \Big[&G^R_{ac,k}(x,y)\,\partial_k R^R_{cd,k}(y,y')\,G^K_{db,k}(y',x') + \\ &+ G^K_{ac,k}(x,y)\,\partial_k R^A_{cd,k}(y,y')\,G^A_{db,k}(y',x') + G^R_{ac,k}(x,y)\,\partial_k R^K_{cd,k}(y,y')\,G^A_{db,k}(y',x')\Big]\,, \end{aligned} \tag{5.53c}$$

and, analogously,

$$\mathcal{B}^R_k(x,x') \equiv \int_{yy'} \mathcal{G}^R_k(x,y)\,\partial_k \mathcal{R}^R_k(y,y')\,\mathcal{G}^R_k(y',x')\,, \tag{5.54a}$$

$$B^A_k(x,x') \equiv \int_{yy'} \mathcal{G}^A_k(x,y)\,\partial_k \mathcal{R}^A_k(y,y')\,\mathcal{G}^A_k(y',x')\,, \tag{5.54b}$$

$$\begin{aligned} \mathcal{B}^K_k(x,x') \equiv \int_{yy'} \Big[&\mathcal{G}^R_k(x,y)\,\partial_k \mathcal{R}^R_k(y,y')\,\mathcal{G}^K_k(y',x') \\ &+ \mathcal{G}^K_k(x,y)\,\partial_k \mathcal{R}^A_k(y,y')\,\mathcal{G}^A_k(y',x') + \mathcal{G}^R_k(x,y)\,\partial_k \mathcal{R}^K_k(y,y')\,\mathcal{G}^A_k(y',x')\Big]\,. \end{aligned} \tag{5.54c}$$

In thermal equilibrium, the respective Keldysh components are also fixed by the FDR,

$$B^K_{ab,k}(\omega,\boldsymbol{p}) = \coth\left(\frac{\omega}{2T}\right)\left(B^R_{ab,k}(\omega,\boldsymbol{p}) - B^A_{ab,k}(\omega,\boldsymbol{p})\right) \tag{5.55}$$

and

$$\mathcal{B}^K_k(\omega,\boldsymbol{p}) = \tanh\left(\frac{\omega-\mu}{2T}\right)\left(\mathcal{B}^R_k(\omega,\boldsymbol{p}) - \mathcal{B}^A_k(\omega,\boldsymbol{p})\right)\,. \tag{5.56}$$

With the flow equation (5.48) one can proceed to study the flow of the scale dependent effective potential which will allow one to compute the phase diagram.

5.2.1 Flow equation of the effective potential

One can generally extract the effective potential $V_k(\phi)$ (with $\phi \equiv \phi^c/\sqrt{2}$) from the effective average Keldysh action Γ_k via[6]

$$-\frac{\partial V_k}{\partial \phi_a} \equiv \frac{1}{\sqrt{2}}\frac{\delta \Gamma_k}{\delta \phi^q_a(x)}\bigg|_{\substack{\phi^c_a(x)\equiv\sqrt{2}\,\phi_a\,,\,\phi^q_a(x)\equiv 0\,,\\ \bar{\Psi}(x)\equiv 0\,,\,\Psi(x)\equiv 0}}\,. \tag{5.57}$$

[6]To obtain the effective potential $V(\phi)$ from the effective (Keldysh) action Γ one has to perform at least one functional derivative with respect to the quantum field ϕ^q, since otherwise the partition function would be $Z = 1$ and the effective action hence identically equal to zero, $\Gamma = 0$.

One can then use the flow equation Eq. (5.48) to compute the flow of the effective potential. Using (5.57), upon Fourier transformation, the flow equation of $\partial V_k/\partial\phi_a$ can be written as

$$
\begin{aligned}
-\sqrt{2}\,\partial_k\left(\frac{\partial V_k}{\partial\phi_a}\right) = \\
i\int_{pq}\Big[\Gamma_k^{\bar\Psi_2\phi_a^q\Psi_1}(p,q,-p)\,\mathcal{B}_k^K(p)+\Gamma_k^{\bar\Psi_1\phi_a^q\Psi_1}(p,q,-p)\,\mathcal{B}_k^R(p)+\Gamma_k^{\bar\Psi_2\phi_a^q\Psi_2}(p,q,-p)\,\mathcal{B}_k^A(p)\Big] \\
-\frac{i}{2}\int_{pq}\Big[\Gamma_k^{\phi_b^c\phi_a^q\phi_c^c}(p,q,-p)\,B_{cb,k}^F(p)+\Gamma_k^{\phi_b^q\phi_a^q\phi_c^c}(p,q,-p)\,B_{cb,k}^R(p)+\Gamma_k^{\phi_b^c\phi_a^q\phi_c^q}(p,q,-p)\,B_{cb,k}^A(p)\Big]\,,
\end{aligned}
\tag{5.58}
$$

where all quantities are understood in front of a constant and purely classical bosonic field expectation value $\phi_a^c(x)\equiv\sqrt{2}\,\phi_a$. Let us first look at the bosonic contribution in (5.58). Along the lines of Ref. [2] it can be shown that the bosonic contribution in (5.58) can be formally integrated with respect to ϕ and that the result can be written as

$$
\partial_k V_k(\phi)=\frac{i}{4}\int_{\omega\boldsymbol{p}}\coth\left(\frac{\omega}{2T}\right)\left(G_{ab,k}^R(\omega,\boldsymbol{p})\,\partial_k R_{ba,k}^R(\omega,\boldsymbol{p})-G_{ab,k}^A(\omega,\boldsymbol{p})\,\partial_k R_{ba,k}^A(\omega,\boldsymbol{p})\right)\,. \tag{5.59}
$$

One can evaluate the frequency integral via the residue theorem. There one effectively picks up the poles corresponding to the bosonic Matsubara frequencies: For the part with the retarded propagator, one closes the contour in the upper half-plane so as to pick up the positive Matsubara modes. For the advanced propagator, one closes the contour in the lower half-plane to pick up the negative Matsubara frequencies. When the contour crosses the pole at $\omega=0$, the residue contributes half of its value to the integral (this happens twice, however, for the retarded and for the advanced propagator). Then one can evaluate the frequency integral to obtain

$$
\begin{aligned}
\partial_k V_k(\phi)=-\frac{T}{2}\int_{\boldsymbol{p}}\Bigg[&\frac{1}{2}\left(G_{ab,k}^R(0,\boldsymbol{p})\,\partial_k R_{ba,k}^R(0,\boldsymbol{p})+G_{ab,k}^A(0,\boldsymbol{p})\,\partial_k R_{ba,k}^A(0,\boldsymbol{p})\right)+ \\
&\sum_{n=1}^{\infty}G_{ab,k}^R(i\omega_n,\boldsymbol{p})\,\partial_k R_{ba,k}^R(i\omega_n,\boldsymbol{p})+\sum_{n=-\infty}^{-1}G_{ab,k}^A(i\omega_n,\boldsymbol{p})\,\partial_k R_{ba,k}^A(i\omega_n,\boldsymbol{p})\Bigg]\,,
\end{aligned}
\tag{5.60}
$$

with the bosonic Matsubara frequencies $\omega_n=2\pi nT$. We now connect Eq. (5.60) to its Euclidean counterpart. The Euclidean propagator G_k^E is connected to the retarded/advanced propagators $G_k^{R/A}$ from the Keldysh formalism through analytic continuation. For the retarded propagator, one has (where we have suppressed the $O(4)$ indices a and b)

$$
G_k^R(\omega,\boldsymbol{p})=\lim_{\epsilon\to0}G_k^E(\omega_E=-i(\omega+i\epsilon),\boldsymbol{p})\,. \tag{5.61a}
$$

which is valid for all complex ω from the upper half-plane, i.e. for any ω with $\operatorname{Im}\omega\geq0$. Similarly, for the advanced propagator one has

$$
G_k^A(\omega,\boldsymbol{p})=\lim_{\epsilon\to0}G_k^E(\omega_E=-i(\omega-i\epsilon),\boldsymbol{p})\,. \tag{5.61b}
$$

which is valid for all complex ω from the *lower* half-plane, $\operatorname{Im}\omega\leq0$. Plugging the n^{th} Matsubara frequency $\omega_E=\omega_n$ into (5.61), we find

$$
G_k^E(\omega_n,\boldsymbol{p})=\begin{cases}G_k^R(i\omega_n,\boldsymbol{p}) & \text{for } n\geq0\\ G_k^A(i\omega_n,\boldsymbol{p}) & \text{for } n\leq0\end{cases} \tag{5.62}
$$

Assuming that the real-time regulator is chosen to comply with the causal structure of the Keldysh action (see Sec. 2.3.2), the Euclidean regulator can be similarly related,

$$R_k^E(\omega_n, \boldsymbol{p}) = -\begin{cases} R_k^R(i\omega_n, \boldsymbol{p}) & \text{for } n \geq 0 \\ R_k^A(i\omega_n, \boldsymbol{p}) & \text{for } n \leq 0 \end{cases} \tag{5.63}$$

With this, (5.60) becomes

$$\partial_k V_k(\phi) = \frac{T}{2} \sum_{n=-\infty}^{\infty} \int_{\boldsymbol{p}} G_{ab,k}^E(\omega_n, \boldsymbol{p})\, \partial_k R_{ba,k}^E(\omega_n, \boldsymbol{p})\,, \tag{5.64}$$

which concludes the bosonic contribution to the flow of the effective potential.

At high temperatures $T \gg \omega$ (or small frequencies) one can expand $\coth(\omega/2T)$ in a Taylor series and take the leading order, such that $\coth(\omega/2T) \approx 2T/\omega$ in the Rayleigh-Jeans limit. Note that in this case only the zeroth Matsubara mode contributes to the frequency integral, such that one is left with

$$\partial_k V_k(\phi) = \frac{T}{2} \int_{\boldsymbol{p}} G_{ab,k}^E(0, \boldsymbol{p}) \partial_k R_{ba,k}^E(0, \boldsymbol{p})\,. \tag{5.65}$$

In this limit one can observe two things: First, at high temperatures T all quantum fluctuations are effectively suppressed, such that the flow of the effective potential is purely generated by thermal fluctuations. Second, one can see that in this limit only the propagator at $\omega = 0$ enters. Hence, any information about the time dependence of fluctuations drop out from the right-hand side of the flow equation. This is generally the case and simply means that dynamic properties of the system do not influence the static flow in the classical limit (here explicitly verified for the flow of the effective potential), which we have already discussed in Sec. 3.2.1 for the flow of the coarse-grained free energy in classical-statistical systems with reversible mode couplings. As such, in this limit the flow (5.64) of the effective potential becomes independent of the damping coefficients in (5.43), since those only appear in the bosonic propagators for non-zero frequencies $\omega \neq 0$.

However, if we look at moderate to small temperatures, then all Matsubara modes contribute to the flow of the effective potential. In this case, quantum fluctuations also contribute via the non-zero Matsubara frequencies. Although this may sound trivial, it can have important consequences: In the present work, for example, these contributions imply that the damping/kinetic coefficients (5.43) in the advanced/retarded propagators at non-vanishing frequency generally also enter to the flow of the effective potential. Because of this, the dynamic properties of the system can be expected to have an effect on the thermodynamic grand potential as well. Then one can naturally ask the questions: will different dynamic properties (here for example the presence or absence of the bosonic damping in (5.43), or more generally dissipative versus diffusive dynamics with potential conservation laws and reversible mode couplings according to the different dynamic models) have an influence on the phase diagram of the theory, and if so, how large is this effect? For the quark-meson model with or without dissipation by meson damping, these questions will be addressed in Sec. 5.3.

Now we turn to the fermionic contribution in the flow (5.58) of the effective potential. We consider a truncation in which the vertices $\Gamma_k^{\bar{\Psi}_1 \phi_a^q \Psi_1} = \Gamma_k^{\bar{\Psi}_2 \phi_a^q \Psi_2} = g_k$ are given by an FRG scale k dependent but field and momentum independent Yukawa coupling g_k. In this case, the anomalous vertices $\Gamma_k^{\bar{\Psi}_1 \phi_a^q \Psi_2} = \Gamma_k^{\bar{\Psi}_2 \phi_a^q \Psi_1} = 0$ vanish, and the only fermionic contribution to the

flow of the effective potential is given by

$$-\sqrt{2}\,\partial_k\left(\frac{\partial V_k}{\partial\phi_a}\right) = i\,g_k\,\mathrm{Tr}\Big[\int_p \mathcal{B}_k^K(p)\Big]\,, \tag{5.66}$$

where Tr here stands for the trace over Dirac and color indices. One can use the fermionic FDR (5.56) to write Eq. (5.66) as

$$-\sqrt{2}\,\partial_k\left(\frac{\partial V_k}{\partial\phi_a}\right) = i\,g_k\,\mathrm{Tr}\Big[\int_p \tanh\left(\frac{\omega-\mu}{2T}\right)\left(\mathcal{B}_k^R(p)-\mathcal{B}_k^A(p)\right)\Big]\,. \tag{5.67}$$

The integral over frequency can be evaluated analytically using the residue theorem. To evaluate the integral over p^0 for the $\mathcal{B}_k^R(p)$ term, we close the contour in the upper half-plane. To evaluate the p^0 integral for the $\mathcal{B}_k^A(p)$ term, we close the integration contour in the lower half-plane. The result is

$$-\sqrt{2}\,\partial_k\left(\frac{\partial V_k}{\partial\phi_a}\right) = -ig_k\mathrm{Tr}\Big[\int_{\boldsymbol{p}}\big(2T\sum_{n=0}^{\infty}\mathcal{B}_k^R(i\tilde{\omega}_n,\boldsymbol{p})+2T\sum_{n=-\infty}^{-1}\mathcal{B}_k^A(i\tilde{\omega}_n,\boldsymbol{p})\big)\Big]\,, \tag{5.68}$$

in which the frequencies in the retarded and advanced propagators are substituted by the fermionic Matsubara frequencies $i\tilde{\omega}_n = (2n+1)\pi T i + \mu$ with the chemical potential μ. Using the relations

$$\frac{\delta\mathcal{G}_k^R}{\delta\phi_a} = \sqrt{2}\,\mathcal{G}_k^R g_k\mathcal{G}_k^R\,, \qquad \frac{\delta\mathcal{G}_k^A}{\delta\phi_a} = \sqrt{2}\,\mathcal{G}_k^A g_k\mathcal{G}_k^A\,, \tag{5.69a}$$

Eq. (5.68) can be integrated with respect to ϕ,

$$\partial_k V_k(\phi) = T\int_{\boldsymbol{p}}\mathrm{Tr}\left[\sum_{n=0}^{\infty}\mathcal{G}_k^R(i\tilde{\omega}_n,\boldsymbol{p})\partial_k\mathcal{R}_k^R(i\tilde{\omega}_n,\boldsymbol{p})+\sum_{n=-\infty}^{-1}\mathcal{G}_k^A(i\tilde{\omega}_n,\boldsymbol{p})\partial_k\mathcal{R}_k^A(i\tilde{\omega}_n,\boldsymbol{p})\right]. \tag{5.70}$$

Using the (fermionic) analytic continuation of the propagator,

$$\mathcal{G}_k^E(\tilde{\omega}_n,\boldsymbol{p}) = \begin{cases}\mathcal{G}_k^R(i\tilde{\omega}_n,\boldsymbol{p}) & \text{for } n\geq 0\\ \mathcal{G}_k^A(i\tilde{\omega}_n,\boldsymbol{p}) & \text{for } n<0\end{cases} \tag{5.71}$$

and of the regulator (again assuming that it complies with the causal structure of the Keldysh action [118]),

$$\mathcal{R}_k^E(\tilde{\omega}_n,\boldsymbol{p}) = -\begin{cases}\mathcal{R}_k^R(i\tilde{\omega}_n,\boldsymbol{p}) & \text{for } n\geq 0\\ \mathcal{R}_k^A(i\tilde{\omega}_n,\boldsymbol{p}) & \text{for } n<0\end{cases}\,, \tag{5.72}$$

we obtain

$$\partial_k V_k(\phi) = -T\sum_{n=-\infty}^{\infty}\int_{\boldsymbol{p}}\mathrm{Tr}\left[\mathcal{G}_k^E(\tilde{\omega}_n,\boldsymbol{p})\partial_k\mathcal{R}_k^E(\tilde{\omega}_n,\boldsymbol{p})\right] \tag{5.73}$$

for the fermionic contribution to the flow.

For fermions, there is no zeroth Matsubara mode and hence all fermionic fluctuations are quantum. The leading fermionic contribution to the flow of the effective potential at asymptotically high temperatures T vanishes.

Combining fermionic and bosonic contribution, the flow of the effective potential is given by

$$\partial_k V_k(\phi) = \frac{T}{2}\sum_{n=-\infty}^{\infty}\int_{\boldsymbol{p}} G_{ab,k}^E(\omega_n,\boldsymbol{p})\,\partial_k R_{ba,k}^E(\omega_n,\boldsymbol{p}) - T\sum_{n=-\infty}^{\infty}\int_{\boldsymbol{p}}\mathrm{Tr}\left[\mathcal{G}_k^E(\tilde{\omega}_n,\boldsymbol{p})\partial_k\mathcal{R}_k^E(\tilde{\omega}_n,\boldsymbol{p})\right], \tag{5.74}$$

which precisely agrees with the standard Euclidean flow equation for the effective potential.

5.2.2 Truncation

In order to carry out the remaining momentum integration and Matsubara sums, we need to specify our truncation and the regulators. In local potential approximation (LPA) only the mesonic effective potential $U_k(\rho)$ is assumed to depend on the FRG scale k, such that the truncated effective average action is given by

$$\begin{aligned}\Gamma_k = \int_x \Bigg[& (\bar{\Psi}_1, \bar{\Psi}_2) \begin{pmatrix} i\gamma^\mu \partial_\mu + i\epsilon u_\mu \gamma^\mu & 2i\epsilon u_\mu \gamma^\mu \tanh \frac{iu^\mu \partial_\mu - \mu}{2T} \\ 0 & i\gamma^\mu \partial_\mu - i\epsilon u_\mu \gamma^\mu \end{pmatrix} \begin{pmatrix} \Psi_1 \\ \Psi_2 \end{pmatrix} \\ & - \frac{g}{\sqrt{2}} (\bar{\Psi}_1, \bar{\Psi}_2) \begin{pmatrix} \sigma^c + i\gamma_5 \boldsymbol{\tau} \cdot \boldsymbol{\pi}^c & \sigma^q + i\gamma_5 \boldsymbol{\tau} \cdot \boldsymbol{\pi}^q \\ \sigma^q + i\gamma_5 \boldsymbol{\tau} \cdot \boldsymbol{\pi}^q & \sigma^c + i\gamma_5 \boldsymbol{\tau} \cdot \boldsymbol{\pi}^c \end{pmatrix} \begin{pmatrix} \Psi_1 \\ \Psi_2 \end{pmatrix} \\ & + \frac{1}{2} (\phi_a^c, \phi_a^q) \begin{pmatrix} 0 & -\partial^2 + \gamma u^\mu \partial_\mu \\ -\partial^2 - \gamma u^\mu \partial_\mu & -2\gamma u^\mu \partial_\mu \coth \frac{iu^\mu \partial_\mu}{2T} \end{pmatrix} \begin{pmatrix} \phi_a^c \\ \phi_a^q \end{pmatrix} \\ & - \frac{1}{2} \rho^q(x)\, 2Y u^\mu \partial_\mu \coth \left(\frac{iu^\mu \partial_\mu}{2T} \right) \rho^q(x) - \frac{1}{2} \rho^q(x)\, Y u^\mu \partial_\mu \left(\rho(x) + \rho^{qq}(x) \right) \\ & - U_k(\rho + \rho^q + \rho^{qq}) + U_k(\rho - \rho^q + \rho^{qq}) + \sqrt{2}\, c\sigma^c \Bigg] . \end{aligned} \tag{5.75}$$

In this truncation, the fermionic sector is kept to be the same as the bare action, but we couple the bosonic part to an external heat bath with (FRG-scale-independent) damping coefficients γ and Y as described in Sec. 5.1.3. The coefficient ϵ in the fermionic Green function is infinitesimal, $\epsilon \to 0^+$. A non-vanishing chemical potential for fermions is included. Such a chemical potential enters through the Keldysh propagator as $\tanh((\omega - \mu)/2T)$, which ensures that the symmetry of thermal equilibrium is maintained at finite temperature and chemical potential.

In this chapter, we choose the optimized regulator [224]

$$R^R_{ab,k}(\omega, \boldsymbol{p}) = -(k^2 - \boldsymbol{p}^2)\, \theta(k^2 - \boldsymbol{p}^2)\, \delta_{ab} , \tag{5.76a}$$
$$R^A_{ab,k}(\omega, \boldsymbol{p}) = -(k^2 - \boldsymbol{p}^2)\, \theta(k^2 - \boldsymbol{p}^2)\, \delta_{ab} , \tag{5.76b}$$
$$R^K_{ab,k}(\omega, \boldsymbol{p}) = 0 \tag{5.76c}$$

for the bosons, and its fermionic extension

$$\mathcal{R}^R_k(\omega, \boldsymbol{p}) = -\boldsymbol{\gamma} \cdot \boldsymbol{p} \left(\sqrt{\frac{k^2}{\boldsymbol{p}^2}} - 1 \right) \theta(k^2 - \boldsymbol{p}^2) , \tag{5.77a}$$

$$\mathcal{R}^A_k(\omega, \boldsymbol{p}) = -\boldsymbol{\gamma} \cdot \boldsymbol{p} \left(\sqrt{\frac{k^2}{\boldsymbol{p}^2}} - 1 \right) \theta(k^2 - \boldsymbol{p}^2) , \tag{5.77b}$$

$$\mathcal{R}^K_k(\omega, \boldsymbol{p}) = 0 \tag{5.77c}$$

for the quarks. As such, we restrict ourselves to a frequency-independent regulator here. If one needs to use a frequency-dependent regulator for some reason, one can follow the general construction scheme introduced in Sec. 2.3.2, where one imagines the regulator to represent a coupling to an FRG-scale-dependent fictitious heat bath. We expect that a similar construction scheme is also possible in the fermionic case. In the spirit of Ref. [248], it would be interesting to try different frequency-dependent regulators and assess the changes this induces in phase diagram from the perspective of the real-time formalism.

From the effective average action (5.75) one can extract the longitudinal (sigma) and transverse (pion) propagators. At constant classical field expectation value $\phi^c \neq 0$ and $\phi^q = 0$

(with $\rho = \frac{1}{2}\phi_a^c\phi_a^c$), one can decompose the bosonic propagator into longitudinal and transverse components (in field space) via

$$G^X_{ab,k}(\omega,\boldsymbol{p}) = G^X_{\sigma,k}(\omega,\boldsymbol{p})\frac{\phi_a^c\phi_b^c}{2\rho} + G^X_{\pi,k}(\omega,\boldsymbol{p})\left(\delta_{ab} - \frac{\phi_a^c\phi_b^c}{2\rho}\right), \tag{5.78}$$

with $X = R, A, K$. From (5.75), we then obtain

$$G^R_{\sigma,k}(\omega,\boldsymbol{p}) = \frac{-1}{\omega^2 + i(\gamma + Y\rho)\omega - \boldsymbol{p}^2 - m_\sigma^2 + R_k^R(\omega,\boldsymbol{p})}, \tag{5.79a}$$

$$G^A_{\sigma,k}(\omega,\boldsymbol{p}) = \frac{-1}{\omega^2 - i(\gamma + Y\rho)\omega - \boldsymbol{p}^2 - m_\sigma^2 + R_k^A(\omega,\boldsymbol{p})}, \tag{5.79b}$$

$$G^K_{\sigma,k}(\omega,\boldsymbol{p}) = \coth\left(\frac{\omega}{2T}\right)\left(G^R_{\sigma,k}(\omega,\boldsymbol{p}) - G^A_{\sigma,k}(\omega,\boldsymbol{p})\right) \tag{5.79c}$$

for the longitudinal (sigma) propagators with (scale dependent) Euclidean mass parameter $m_\sigma^2 \equiv 2U_k'(\rho) + 4\rho U_k''(\rho)$, and

$$G^R_{\pi,k}(\omega,\boldsymbol{p}) = \frac{-1}{\omega^2 + i\gamma\omega - \boldsymbol{p}^2 - m_\pi^2 + R_k^R(\omega,\boldsymbol{p})}, \tag{5.80a}$$

$$G^A_{\pi,k}(\omega,\boldsymbol{p}) = \frac{-1}{\omega^2 - i\gamma\omega - \boldsymbol{p}^2 - m_\pi^2 + R_k^A(\omega,\boldsymbol{p})}, \tag{5.80b}$$

$$G^K_{\pi,k}(\omega,\boldsymbol{p}) = \coth\left(\frac{\omega}{2T}\right)\left(G^R_{\pi,k}(\omega,\boldsymbol{p}) - G^A_{\pi,k}(\omega,\boldsymbol{p})\right) \tag{5.80c}$$

for the transverse (pion) propagators with $m_\pi^2 \equiv 2U_k'(\rho)$. The fermionic propagators are given by

$$\mathcal{G}_k^R(\omega,\boldsymbol{p}) = -\left((\omega + i\epsilon)\gamma^0 - \boldsymbol{\gamma}\cdot\boldsymbol{p} - \mathcal{M} + \mathcal{R}_k^R(\omega,\boldsymbol{p})\right)^{-1}, \tag{5.81a}$$

$$\mathcal{G}_k^A(\omega,\boldsymbol{p}) = -\left((\omega - i\epsilon)\gamma^0 - \boldsymbol{\gamma}\cdot\boldsymbol{p} - \mathcal{M} + \mathcal{R}_k^A(\omega,\boldsymbol{p})\right)^{-1}, \tag{5.81b}$$

$$\mathcal{G}_k^K(\omega,\boldsymbol{p}) = \tanh\left(\frac{\omega-\mu}{2T}\right)\left(\mathcal{G}_k^R(\omega,\boldsymbol{p}) - \mathcal{G}_k^A(\omega,\boldsymbol{p})\right), \tag{5.81c}$$

with $\mathcal{M} = \frac{g}{\sqrt{2}}(\sigma^c + i\gamma_5\boldsymbol{\tau}\cdot\boldsymbol{\pi}^c)$.

With a frequency independent regulator one can carry out the Matsubara sums in (5.74) analytically and, with the convenient form of the optimized regulator (5.76) and its fermionic extension (5.77), also analytically perform the momentum integration, to obtain explicitly the LPA flow of the effective potential in the form

$$\partial_k U_k(\rho) = \frac{1}{2}I_\sigma + \frac{3}{2}I_\pi - 2N_c I_\psi, \tag{5.82}$$

with

$$I_\sigma = \frac{k^4}{3\pi^2}\left\{-\frac{T}{k^2+m_\sigma^2} + \frac{i}{2\pi E_\sigma}\left[\psi\left(\frac{\frac{i}{2}(\gamma+Y\rho)+E_\sigma}{2\pi i T}\right) - \psi\left(\frac{\frac{i}{2}(\gamma+Y\rho)-E_\sigma}{2\pi i T}\right)\right]\right\}, \tag{5.83a}$$

$$I_\pi = \frac{k^4}{3\pi^2}\left\{-\frac{T}{k^2+m_\pi^2} + \frac{i}{2\pi E_\pi}\left[\psi\left(\frac{\frac{i}{2}\gamma+E_\pi}{2\pi i T}\right) - \psi\left(\frac{\frac{i}{2}\gamma-E_\pi}{2\pi i T}\right)\right]\right\}, \tag{5.83b}$$

$$I_\psi = \frac{k^4}{6\pi^2}\frac{\tanh\left(\frac{E_\psi-\mu}{2T}\right) + \tanh\left(\frac{E_\psi+\mu}{2T}\right)}{E_\psi}, \tag{5.83c}$$

where $\psi(x)$ is the digamma function, and the scale-dependent single-particle energies are given by

$$E_\sigma = \sqrt{k^2 + m_\sigma^2 - \tfrac{1}{4}(\gamma + Y\rho)^2}\,, \tag{5.84a}$$

$$E_\pi = \sqrt{k^2 + m_\pi^2 - \tfrac{1}{4}\gamma^2}\,, \tag{5.84b}$$

$$E_\psi = \sqrt{k^2 + m_\psi^2}\,, \tag{5.84c}$$

with the (scale-dependent) quark mass $m_\psi^2 \equiv g^2\rho$. For sufficiently small values of the damping constants, i.e. for $\gamma_\sigma = \gamma + Y\rho < 2m_\sigma$ and/or $\gamma_\pi = \gamma < 2m_\pi$, the sigma and/or pion fluctuations are represented by weakly-damped quasiparticle excitations. Otherwise, the corresponding single-particle energies in Eqs. (5.84) become pure imaginary at $k^2 = (\gamma + Y\rho)^2/4 - m_\sigma^2$ and/or $k^2 = \gamma^2/4 - m_\pi^2$, respectively, during the FRG flow, which corresponds to the sigma and/or pion excitations turning purely relaxational in the overdamped case.

In the limit $\gamma \to 0$ and $Y \to 0$ the flow equation (5.82) reduces to the standard flow [14] of the effective potential in the quark-meson model, which can be shown using the identity of the digamma function,

$$\psi(-z) - \psi(z) = 1/z + \pi\cot(\pi z)\,. \tag{5.85}$$

In particular, with this, we obtain

$$I_\sigma = \frac{k^4}{6\pi^2}\frac{\coth\left(\frac{E_\sigma}{2T}\right)}{E_\sigma}\,, \qquad I_\pi = \frac{k^4}{6\pi^2}\frac{\coth\left(\frac{E_\pi}{2T}\right)}{E_\pi}\,, \tag{5.86a}$$

and the single-particle energies in (5.84) reduce to

$$E_\sigma = \sqrt{k^2 + m_\sigma^2}\,, \qquad E_\pi = \sqrt{k^2 + m_\pi^2}\,. \tag{5.87}$$

Another interesting limit is sending the pion and/or sigma damping to infinity. On the one hand, if we send only $Y \to \infty$ to infinity, the (infinite) overdamping only affects the sigma, and the corresponding loop function I_σ becomes (see Appendix G.2 for a derivation)

$$I_\sigma \to \frac{k^4}{3\pi^2}\frac{T}{k^2 + m_\sigma^2}\,. \tag{5.88}$$

On the other hand, if we send $\gamma \to \infty$ to infinity, both sigma and pions will be (infinitely) overdamped, and in addition to (5.88) we then also have

$$I_\pi \to \frac{k^4}{3\pi^2}\frac{T}{k^2 + m_\pi^2}\,. \tag{5.89}$$

Hence, the infinite-damping limit corresponds to taking into account contributions only from the zeroth Matsubara mode in (5.64). This is precisely the classical limit, where all quantum fluctuations are suppressed and only thermal fluctuations survive, the latter being determined by the Rayleigh-Jeans distribution. And just as in classical-statistical systems (cf. Sec. 3.2.1), the bosonic flow becomes independent of the dynamics, in this limit.

Nevertheless, in the general case of non-vanishing and finite bosonic damping coefficients, we find that even though damping/dissipation is a dynamic property of the system, the damping coefficients indeed potentially affect the flow equation of the effective potential through the non-zero Matsubara modes. The question now is how large the effect is, quantitatively, and we now turn to address this in the next section.

γ	Y/MeV^{-1}	Λ/MeV	b_1/MeV^2	b_2	c/MeV^3	g
0	0	1000	$3.15 \cdot 10^5$	0.50	$1.75 \cdot 10^6$	3.2
Eq. (5.91)	0.064	1000	$2.90 \cdot 10^5$	0.86	$1.75 \cdot 10^6$	3.2
Eq. (5.92)	0.064	1000	$2.90 \cdot 10^5$	0.86	$1.75 \cdot 10^6$	3.2

Table 5.1: UV initial conditions for vanishing (first row) and physically motivated (second and third rows) pion and sigma damping constants, with $\gamma_\pi = \gamma$ and $\gamma_\sigma = \gamma + Y\rho$, cf. Eq. (5.43). The UV parameters are tuned such that the resulting vacuum observables are practically the same in the IR, for all cases.

5.3 Results for phase diagram with dissipation

With the flow equation of the effective potential, one computes the sigma condensate as the minimum of the effective potential at $k = 0$, which is the order parameter of the system, for different temperatures and chemical potentials to obtain the phase diagram. In the numerical solution, we reformulate the flow equation (5.82) as an advection-diffusion equation for the derivative $U_k'(\rho)$ [250], and discretize the resulting continuity equation on a grid in field space using the upwind scheme described in [251].

5.3.1 Finite bosonic damping

In LPA only the mesonic effective potential $U_k(\rho)$ is scale dependent, whereas especially the coefficients γ and Y that characterize the bosonic damping are fixed. One may also employ temperature and chemical-potential dependent values here, $\gamma = \gamma(\mu, T)$, $Y = Y(\mu, T)$. At the UV scale $k = \Lambda$, we start the flow with the parameterization

$$U_\Lambda(\rho) = b_1\rho + b_2\rho^2 \tag{5.90}$$

of the effective potential, with the values from Table 5.1. We stop the flow in the IR at a sufficiently small scale of $k_{\mathrm{IR}} = 40\,\mathrm{MeV}$, where we obtain the approximate values $\sigma_0 \approx 94$ MeV for the chiral order parameter (identified with the pion decay constant f_π here), $m_\psi \approx 300$ MeV for the constituent quark mass, and $m_\sigma \approx 503$ MeV and $m_\pi \approx 136$ MeV for the Euclidean mass parameters of sigma meson and pions, respectively. We employ three different choices for the damping coefficients γ and Y, and compare the resulting phase diagrams. The parameter set for the zero-damping case $\gamma = 0$ and $Y = 0$ corresponds to the one used in Ref. [99], and the resulting phase diagram can be seen in Fig. 5.1 (a). As a main feature, it has a first order phase transition at large chemical potentials and small temperatures, which terminates in a critical point at around $\mu_c \approx 293\,\mathrm{MeV}$ and $T_c \approx 10\,\mathrm{MeV}$.

To see what back-reaction a finite bosonic damping has on the phase diagram, we first turn on a non-zero value of $Y = 0.064\,\mathrm{MeV}^{-1}$, which results in a sigma damping of $\gamma_\sigma = 556\,\mathrm{MeV}$ in the vacuum.[7] With the width of the sigma given by $\gamma_\sigma/2$, this value yields the imaginary part of a sigma pole at approximately $(425 - i278)\,\mathrm{MeV}$ which is reasonably close to the corresponding physical two-pion resonance pole, e.g., see Ref. [115].

[7] Note that at any fixed field expectation value ρ the pair (γ, Y) can be used interchangeably with $(\gamma_\pi, \gamma_\sigma)$, as the two pairs are related by $\gamma_\pi = \gamma$ and $\gamma_\sigma = \gamma + Y\rho$. If nothing else is specified, by γ_σ we mean the sigma damping at the IR minimum $\rho = \sigma_0^2$.

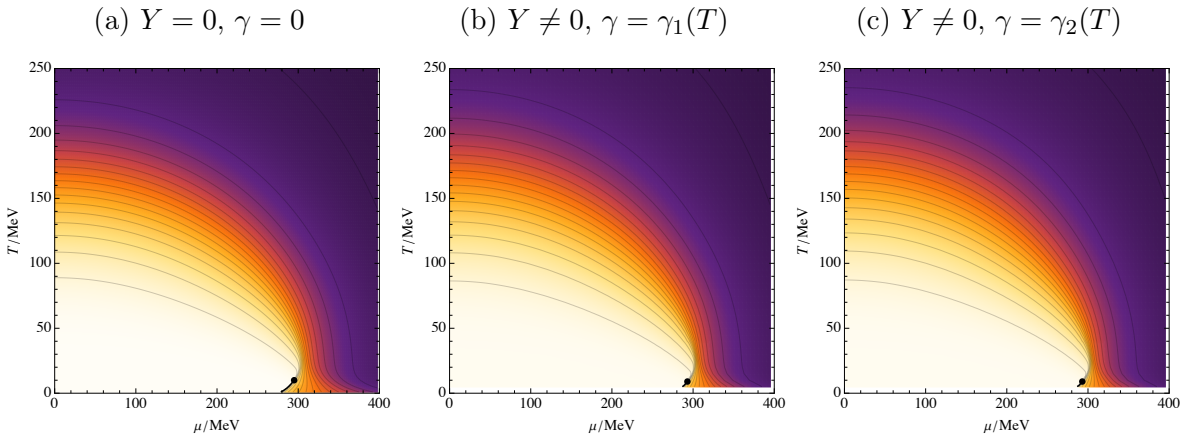

Figure 5.1: Quark-meson model phase diagram (a) for zero damping, (b) for constant Y adjusted so that the sigma pole reproduces that of the broad two-pion resonance in the vacuum combined with the $O(4)$-symmetric damping $\gamma = \gamma_1(T)$ from Eq. (5.91), and (c) for Y chosen as in (b) but with $\gamma = \gamma_2(T)$ from Eq. (5.92).

At finite temperature, the spectral function of the pion is known to be broadened by decay and capture processes from the medium [99]. To include these effects, we have to rely on external (phenomenological) input for the pion damping, since we do not solve for the damping self-consistently. At low temperatures, the behavior of the pion damping is known from chiral perturbation theory where, at leading order, one has $\gamma(T) = T^5/(12 f_\pi^4)$ with $f_\pi = 93$ MeV [116,252]. To model the high-temperature behavior of the pion damping, we follow two different approaches: The results of Ref. [117] suggest a linear behavior $\gamma(T) \sim T$ at high temperatures. Using the arguably simplest functional form that interpolates between the two behaviors at some matching temperature T_*, we parametrize

$$\gamma_1(T) = \frac{T^5}{12 f_\pi^4} \cdot \frac{1}{1 + (T/T_*)^4} \tag{5.91}$$

for the pion damping as a function of temperature. For the matching point T_* we choose the pseudocritical temperature $T_* = T_{pc} \approx 175$ MeV. This constitutes our first model $\gamma_1(T)$ for the pion damping. (For the scope of this work, we neglect any dependence on chemical potential.) The proportionality constant for the linear behavior $\gamma(T) \sim T$ at high $T \gg T_*$ is fixed to $T_*^4/(12 f_\pi^4) \approx 1.04$ and yields, e.g., at $T = 220$ MeV to a pion damping of $\gamma \approx 164$ MeV. Because the data of Ref. [117] suggests that the pion damping should be much larger at this temperature already, however, with a value of the order ~ 636 MeV, we also employ a second model for the pion damping, which reads

$$\gamma_2(T) = \frac{T^5}{12 f_\pi^4}\big(1 - F(T/T_{**})\big) + \alpha T\, F(T/T_{**})\,, \tag{5.92}$$

where $F(x)$ represents an interpolating function with $F(x) \to 1$ for $x \gg 1$, and $F(x) \to 0$ for $x \to 0$ faster than x^4 (so that the chiral perturbation theory result is not changed at low temperatures). T_{**} again denotes a matching point between the two asymptotic behaviors, and α the proportionality constant at high temperatures. We use the arguably simplest interpolation function $F(x) = x^5/(1+x^5)$ that is consistent with these requirements, and choose the remaining constants α and T_{**} by roughly matching the model (5.92) to the results from [117], which leads to $\alpha \approx 5.5$ and $T_{**} \approx 200$ MeV. This in total then constitutes our second model $\gamma_2(T)$ explored

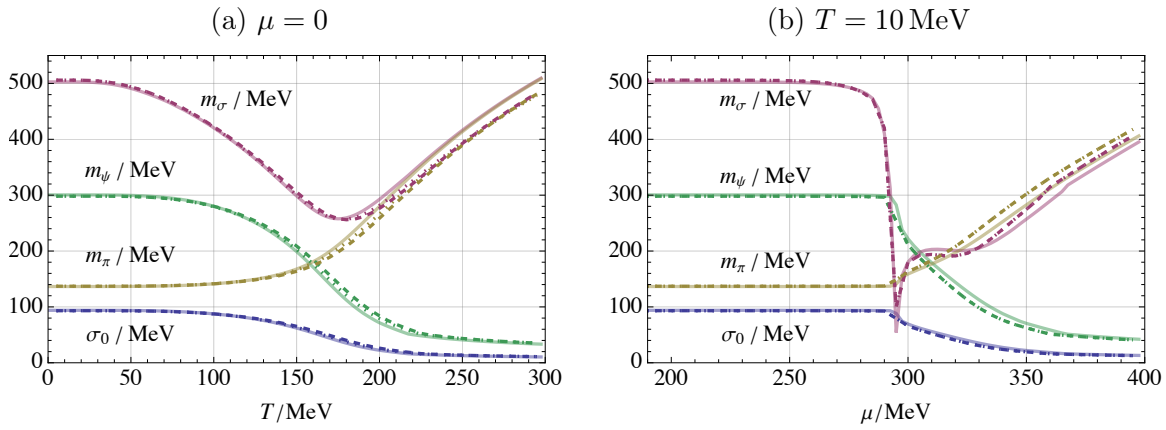

Figure 5.2: Static IR observables that correspond to the three phase diagrams in Fig. 5.1, for zero damping (solid lines), for the first model $\gamma = \gamma_1(T)$ defined in (5.91) (dotted), and for the second model $\gamma = \gamma_2(T)$ defined in (5.92) (dashed). As discussed in the main text, in both cases with $O(4)$-symmetric damping $\gamma \neq 0$ we use the same constant Y in the sigma damping to reproduce the broad two-pion resonance pole in the vacuum.

for the pion damping here. For more details and some caveats in this matching procedure, see App. H.

The phase diagrams for the two models $\gamma_1(T)$ and $\gamma_2(T)$ are shown in Fig. 5.1 (b) and (c). One can see that there are only very minor quantitative changes in the phase diagram, when compared to the zero-damping case in (a). In Fig. 5.2, we plot the Euclidean (curvature) mass parameters in the IR, which are identical with the static screening masses in our present truncation, both as a function of temperature at $\mu = 0$ and as a function of chemical potential at roughly the critical temperature, $T = 10\,\mathrm{MeV}$. The solid lines are the results for vanishing damping $\gamma = 0$ and $Y = 0$, and coincide with Fig. 4 of Ref. [99]. The dotted lines correspond to $Y \neq 0$ and $\gamma = \gamma_1(T)$ modeled according to Eq. (5.91). The dashed lines correspond to $Y \neq 0$ and $\gamma = \gamma_2(T)$ modeled according to Eq. (5.92). For $\mu = 0$ in Fig. 5.2 (a), one observes that the finite damping starts having an influence on the static observables essentially only at temperatures $T \gtrsim 150\,\mathrm{MeV}$, whereas at lower temperatures, for $T \lesssim 150\,\mathrm{MeV}$ where the pion damping becomes small anyway, the presence of the finite sigma damping has hardly any effect either.

Qualitatively, the finite damping causes the static observables (e.g. the condensate σ_0) to lag behind their corresponding zero-damping values when the temperature is increased. In particular, the non-zero damping shifts the pseudocritical temperature (here defined as the minimum of m_σ) to slightly larger values. This concurs with physical intuition, because a non-zero damping implies that bosonic fluctuations decay into the heat bath and, consequently, one needs higher temperatures for the same amount of fluctuations as compared to the case without damping, where all fluctuations are stable.

Similarly small effects on the static screening masses are observed at $T = 10$ MeV in their chemical potential dependence in Fig. 5.2 (b), where modifications due to damping, if any, become noticeable also essentially only in the chirally restored regime, here for $\mu \gtrsim \mu_c$. In summary, although there is indeed some dependence of the phase diagram on the dynamics, consistent with our discussion in Sec. 5.2.1, the quantitative effects on static observables are all rather minor for these physically motivated (realistic) values of the sigma and pion damping.

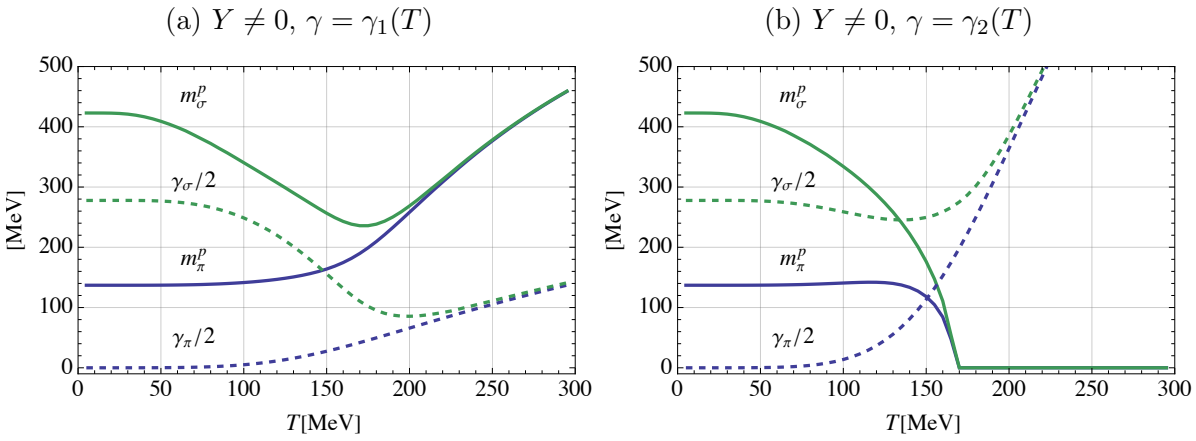

Figure 5.3: Temperature dependence of real and imaginary parts of the sigma and pion poles at $\mu = 0$, where (a) on the left and (b) on the right correspond to the two different models of pion damping $\gamma = \gamma_1(T)$ and $\gamma_2(T)$ as defined in Eqs. (5.91) and (5.92), respectively.

In contrast, the effects of the two different models in Eqs. (5.91) and (5.92) for the meson damping on dynamic quantities such as pole masses are much more pronounced. This can be seen in Fig. 5.3, where we plot both, the real and imaginary parts of the complex sigma and pion poles at $\omega_{\sigma,\pi} = m^p_{\sigma,\pi} - i\gamma_{\sigma,\pi}/2$ (in the IR) as functions of temperature T at $\mu = 0$, for $Y \neq 0$, corresponding to a sigma damping that is always larger than that of the pion which vanishes in the vacuum. At finite temperature, the latter is given by the $O(4)$-symmetric damping γ, for which we compare the two physically motivated models: (a) with $\gamma = \gamma_1(T)$ according to Eq. (5.91) in the left panel of Fig. 5.3, and (b) with $\gamma = \gamma_2(T)$ from Eq. (5.92) in the right panel of Fig. 5.3. With $Y \neq 0$ in either case, we have $\gamma_\sigma - \gamma_\pi = Y\rho_0$, and the difference thus tends to zero as chiral symmetry gets restored, here at finite temperature (for $\mu = 0$) in the crossover around the (static) pseudocritical temperature $T_{pc} \approx 175$ MeV.

Above this crossover, the finite but still relatively small $O(4)$-symmetric pion and sigma damping γ from Eq. (5.91), relative to the real parts of their pole masses in Fig. 5.3 (a), merely leads to a small correction of the latter as compared to the static high-temperature screening masses of pion and sigma in Fig. 5.2 (a).

This picture changes considerably, however, if a high-temperature pion damping is chosen of the order of magnitude as in the recent spectral reconstructions from lattice-QCD data [117]. This is demonstrated in Fig. 5.3 (b) where we use our second model from Eq. (5.92) for the temperature dependence of the pion damping in the chirally restored phase. The relatively large damping at high temperatures in this case causes the sigma and pion poles to become pure imaginary at temperatures above $T \gtrsim 170\,\text{MeV}$. This implies that the sigma and pion excitations are no-longer propagating, but become purely relaxational at these high temperatures and dissolve on time scales of the order of $1/\gamma_{\sigma,\pi}$ into the heat bath. It is interesting to note that the temperature of $T \approx 170$ MeV where this happens roughly matches the (static) pseudo-critical temperature $T_{pc} \approx 175$ MeV. In this spirit, our second model (5.92) can be seen to describe a 'deconfined' phase in which pions (and the sigma meson) no-longer exist as propagating quasi-particle excitations in the thermal medium. Nevertheless, even with a such qualitatively very different dynamic behavior as in the cases (a) and (b), especially at high temperatures, the effects on phase diagram and static observables such as the screening masses remain relatively minor, cf. Figs. 5.1 and 5.2. This is an example of the difficulty distinguishing different dynamics, such

γ	Y	Λ/MeV	b_1/MeV^2	b_2	c/MeV^3	g
0	0	647.3	$0.56 \cdot 10^5$	2.2	$1.75 \cdot 10^6$	3.2
0	∞	647.3	$0.72 \cdot 10^5$	1.77	$1.75 \cdot 10^6$	3.2
∞	0	647.3	$1.12 \cdot 10^5$	0.5	$1.75 \cdot 10^6$	3.2

Table 5.2: UV initial conditions for infinite damping. The parameters are tuned such that the resulting vacuum observables in the IR are the same in all cases. In the third case ($\gamma_\sigma = \gamma_\pi \to \infty$) we had to lower the UV cutoff from $\Lambda = 1000\,\text{MeV}$ to $\Lambda = 647.3\,\text{MeV}$ in order to reproduce the value for $m_\sigma \approx 503$ MeV of Sec. 5.3.1 (with $\Lambda = 1000\,\text{MeV}$). For a better comparison (especially at temperatures of order $2\pi T \sim \Lambda$) we have adjusted the UV cutoff to this lower value also in the other two cases here.

as the qualitatively different behavior of the excitations in Figs. 5.3 (a) and (b), by just looking at static observables such as those in Fig. 5.2 alone.

5.3.2 Infinite damping

To study the maximum effect of dissipation on the phase diagram that the couplings to the bosonic heat baths can have, we now investigate two different extreme cases of strong bosonic damping. First, we consider a strong but purely $O(4)$-invariant heat-bath coupling, corresponding to the $Y \to \infty$ limit at $\gamma = 0$, which results in an infinite damping for the sigma, via $\gamma_\sigma \to \infty$, but vanishing damping for the pions, $\gamma_\pi = 0$. In the second example, we consider only the $O(4)$-vector coupling to the heat bath, sending $\gamma \to \infty$ at $Y = 0$, which then corresponds to an infinite damping for both, sigma and pions, in an $O(4)$-symmetric way, with $\gamma_\sigma = \gamma_\pi \to \infty$. We compare both of these limits again to the zero-damping $\gamma_\sigma = \gamma_\pi = 0$ phase diagram. In all cases we tune to the initial UV parameters such that we obtain the same vacuum observables in the IR as in Sec. 5.3.1. Note that in the case of infinite damping for both the sigma and the pions, we had to lower the UV cutoff Λ from $\Lambda = 1000$ MeV to $\Lambda = 647.3$ MeV in order to be able to obtain the same value for the Euclidean sigma mass parameter $m_\sigma \approx 503$ MeV as in Sec. 5.3.1. For a most direct comparison with the other two cases here, we then generally use this lower UV cutoff for all results in this subsection. The corresponding values for the UV initial conditions are given in Table 5.2.

The resulting phase diagrams for the three cases are shown in Fig. 5.4. First, the zero-damping case, plotted in Fig. 5.4 (a), yields essentially the same phase diagram as in Fig. 5.1 (a), here with the smaller UV cutoff $\Lambda = 647.3$ MeV, however. It is therefore expectable that some quantitative differences can occur for temperature of the order of $T \sim \Lambda/(2\pi) \sim 103$ MeV. These quantitative differences are visible when comparing the solid lines from Fig. 5.2 (a) and Fig. 5.5 (a) for temperatures $T \gg 103$ MeV. While not our main focus here, such a residual dependence on the UV cutoff can in principle be addressed by requiring RG consistency of the resulting IR effective action [253].

Continuing with the second case in Fig. 5.4 (b), where only the sigma damping is infinite, $\gamma_\sigma \to \infty$, but the pion damping vanishes, $\gamma_\pi = 0$, we can conclude that the phase diagram remains qualitatively unchanged with some quantitative changes which are nevertheless comparatively rather small. Still qualitatively unchanged but with somewhat more pronounced quantitative changes the phase diagram for the third case, in which both damping constants are infinite, with $\gamma_\sigma = \gamma_\pi \to \infty$, is shown in Fig. 5.4 (c).

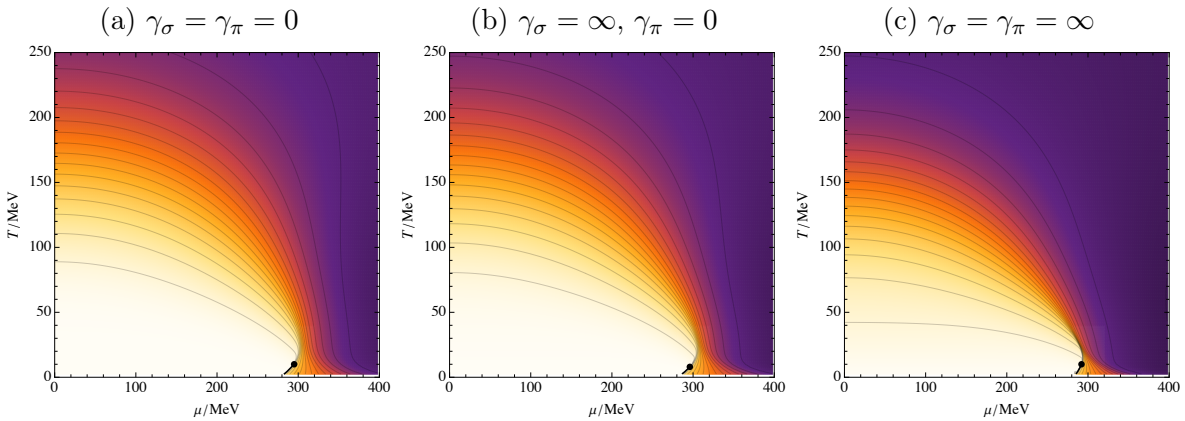

Figure 5.4: Phase diagrams for (a) zero damping, (b) infinite damping for the sigma, but zero damping for the pion, and (c) infinite damping for both sigma and pions. Here the UV cutoff is reduced to $\Lambda = 647.3$ MeV, which quantitatively changes also the zero-damping phase diagram in (a) compared to the one in Fig. 5.1 (a) at high temperatures $T \sim \Lambda/(2\pi) \sim 103$ MeV.

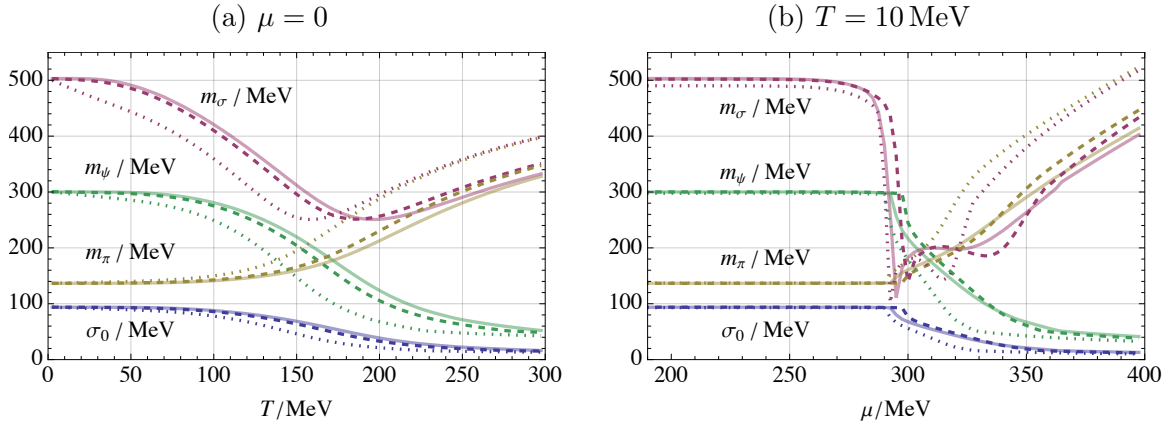

Figure 5.5: Static IR observables for $\gamma_\sigma = \gamma_\pi = 0$ (solid), $\gamma_\sigma = \infty$, $\gamma_\pi = 0$ (dashed) and $\gamma_\sigma = \gamma_\pi = \infty$ (dotted). Here the UV cutoff is $\Lambda = 647.3\,\mathrm{MeV}$.

In order to assess these modifications in some more detail, either from maximally strong overdamping of sigma alone or of pion and sigma excitations together, in Fig. 5.5 we plot the same static IR observables as in Fig. 5.2, again both, as a function of temperature at $\mu = 0$, and as a function of chemical potential at $T = 10$ MeV. We see once more that even quantitatively the changes compared to the zero-damping case (solid lines) are still rather small in the strong sigma-damping limit (dashed) and somewhat more pronounced for strong $O(4)$-symmetric damping of sigma and pions (dotted). One remarkable feature, which is also more prominent in the $\gamma_\sigma = \gamma_\pi \to \infty$ case, is the shift of the pseudocritical temperature to smaller values. Physically, this can be understood by recalling that in the infinite-damping limit, the bosonic contributions to the flow equation in Eqs. (5.88) and (5.89) become classical. Hence, the strength of thermal fluctuations of frequency ω is given by the Rayleigh-Jeans distribution T/ω instead of the Bose-Einstein distribution $1/(e^{\omega/T} - 1)$. The former is always bigger than the latter, since quantum-mechanically, degrees of freedom can 'freeze out' if their frequency is much higher than the temperature. Classically, however, the equipartition theorem gives all degrees of freedom an average kinetic energy of $\frac{3}{2}T$ (with $k_B = 1$), independent of frequency. Hence, in the classical limit, it takes a smaller temperature for sufficiently strong bosonic fluctuations to

restore chiral symmetry, as compared to the quantum mechanical case.

Note the non-monotonous behavior of the finite temperature transitions here: In the physically motivated damping models of the previous subsection the effect of dissipation of fluctuations dominated to delay chiral symmetry restoration, while in both strong-overdamping limits discussed here, in Fig. 5.5 (a), the enhanced fluctuations of the classical Rayleigh-Jeans limit apparently overcompensate this general trend of dissipation to cause the opposite overall effect.

While the chiral order parameter σ_0 melts more quickly with temperature in both overdamped cases, in line with the physical argument above, the behavior of its low-temperature dependence on the chemical potential in Fig. 5.5 (b) is more complicated. While the critical chemical potential $\mu_c \sim 280$ MeV of the first-order transition for $T \to 0$ still roughly matches the zero-damping case in both strong-overdamping limits, the shape of the first-order line with increasing temperatures $0 < T < T_c$ and the location of the critical point at $T = T_c$ change. For $\gamma_\sigma \to \infty$, $\gamma_\pi = 0$, the temperature of $T = 10$ MeV Fig. 5.5 (b) is just in the crossover region above T_c already, but due to the backbending of the contour lines of Fig. 5.4 (b) in this region the corresponding chiral transition (dashed lines) in Fig. 5.5 (b) is shifted to larger chemical potentials. With the $O(4)$-symmetric overdamping of sigma and pions, $\gamma_\sigma = \gamma_\pi \to \infty$, on the other hand, this backbending in Fig. 5.4 (c) is reduced, and the corresponding chiral transition (dotted lines) in Fig. 5.5 (b) occurs at a somewhat smaller chemical potential already. To a similar effect, at a fixed finite temperature $T > 0$, it takes smaller chemical potentials to reach the same amount of chiral-symmetry restoration, as compared to the zero damping, in this case as well. This is evident from Figs. 5.4 (a) and (c), and can also be seen by comparing the solid ($\gamma_\sigma = \gamma_\pi = 0$) and the dotted ($\gamma_\sigma = \gamma_\pi \to \infty$) lines for chemical potentials $\mu \gtrsim 300$ MeV in Fig. 5.5 (b).

5.4 Discussion

We conclude this chapter by summarizing the main developments and by outlining possible future extensions of the present formalism.

In this chapter, we have studied the real-time dynamics of the quark-meson model. In a first step, in Sec. 5.1 we have presented the general real-time formalism of the quark-meson model on the Schwinger-Keldysh CTP. In particular, in Sec. 5.1.1 we have constructed the Keldysh action for relativistic Dirac fermions by using the Larkin-Ovchinnikov convention [118] in the fermionic Keldysh rotation. Based on the discrete symmetry of thermal equilibrium previously known for bosons [107] and for non-relativistic fermions [113], we have formulated a symmetry of thermal equilibrium for relativistic Dirac fermions in Sec. 5.1.2. This symmetry expresses the invariance of the Keldysh action (and hence of correlation functions) under a combination of a Kubo-Martin-Schwinger transformation with time reversal, and leads to fermionic fluctuation-dissipation relations between real-time correlation functions.

With our real-time formulation of the quark-meson model at hand, we have then continued in Sec. 5.2.2 with incorporating bosonic dissipation (damping) by coupling the system to an external heat bath with Ohmic spectral distribution. To distinguish between pion and sigma damping in an $O(4)$ invariant way, we have introduced two independent sets of Gaussian degrees of freedom in the bath, where one set consists of an ensemble of $O(4)$ vectors $\chi_{s,a}$ and couples linearly via $\chi_{s,a}\phi_a$ to the system vector $\phi = (\sigma, \boldsymbol{\pi})$ of sigma meson and pions, and the other one

represents an ensemble of $O(4)$ scalars φ_s which couple to the $O(4)$ field invariant $\rho = \phi_a\phi_a$ via $\varphi_s\rho$. Integrating out both of these oscillator sets and choosing Ohmic spectral distributions as in Eqs. (5.40) then gives rise to distinct pion and sigma damping terms. In particular, in this approach the difference between the two is related to the field expectation value, $\gamma_\sigma - \gamma_\pi \sim \rho$, and hence to the realization of chiral symmetry.

In Sec. 5.2 we have re-derived the fermionic part of the FRG flow equation within the real-time formalism. Since we start from the real-time theory, analytic continuation to the Euclidean domain is well defined and unique. We have shown explicitly, that via such an analytic continuation the standard Euclidean flow equation [14] for the effective potential is recovered in the real-time approach. In particular, we have demonstrated that the flow equation of the effective potential can in principle depend on the 'dynamic' properties through the contributions from non-zero Matsubara modes. The latter generally contain indirect information on the time-dependence of the excitations in the system, and hence about the dynamics. This implies that, in principle, static properties (e.g. the phase diagram and static screening masses) can depend on the dynamic properties. This is unlike classical systems, where only the zeroth Matsubara modes contribute to static observables, which can be used to prove that the static properties are independent of the dynamics [2].

In Sec. 5.3 we have considered two different QCD-inspired models for the temperature dependence of the pion and sigma damping, to exemplify this effect and to investigate its quantitative extent. Both models are based on the leading-order result from chiral perturbation theory [116, 252] at low temperatures, with $\gamma_\pi \sim T^5$, which is combined by interpolation with linear temperature dependencies at asymptotically high temperatures, where $\gamma_\sigma = \gamma_\pi \sim T$, of different strengths. With these physically motivated choices for the mesonic dampings, we have found the quantitative effects on the phase diagram to be rather minor. In contrast, however, our two distinct models have served to demonstrate how dynamic properties such as the pole masses can be drastically different for these choices at the same time. In particular, we have found that in our second model, as motivated from reconstructions of pion spectral functions at high temperatures from lattice-QCD data performed in Ref. [117], the poles in the retarded sigma and pion propagators become pure imaginary describing purely relaxational meson excitations at temperatures roughly right above the pseudocritical temperature.

To estimate the largest possible effect of bosonic damping we have also considered two limits of maximally strong overdamping, where either only the (longitudinal) sigma damping or the $O(4)$-symmetric damping for sigma and pion are sent to infinity. Even in these extreme cases, the quantitative effects on the phase diagram, although more pronounced than for finite damping, still remain comparatively small. Interestingly, however, in the case of maximally strong overdamping of sigma and pions, with $\gamma_\sigma = \gamma_\pi \to \infty$, the bosonic flow becomes purely classical, corresponding to the Rayleigh-Jeans limit of the Bose-Einstein distribution. In particular, this also implies that at strictly zero temperature all bosonic fluctuations (both thermal and quantum) are suppressed, such that the corresponding purely fermionic flow of a so-called extended mean-field approximation becomes exact in this limit.

In the future, the present work can be extended in various directions. First, for a somewhat more fundamental description of the environment, one might promote the non-relativistic Ohmic dampings in Eqs. (5.40) by a relativistic formulation in terms of Gaussian ensembles of Klein-Gordon fields with spectral distributions in terms of the invariant $s = \omega^2 - \boldsymbol{p}^2$. In such a formulation, the distinction between space and time arises only from the thermal density matrix,

i.e. from the bosonic and fermionic distribution functions in the Keldysh component of the self energies, cf. Eq. (5.10), whereas the retarded and advanced components of the self-energy would be fully Lorentz-invariant (at least at tree level).

Another direction one could follow would be to introduce dissipation also for the fermions, and to investigate the corresponding effects on the phase diagram. Here one has to be more careful, since in order for the chemical potential to remain well defined, the dissipation must not violate the conservation of the Noether current associated with the $U(1)_B$ symmetry. Because of this, dissipation in the fermionic sector should rather be described in terms of baryon-charge diffusion. This would require coupling conserved baryon-number current $j^\mu = \bar{\psi}\gamma^\mu\psi$ to an ensemble of equally conserved vector Hubbard fields. At finite density and quark masses, density fluctuations are well known to mix with those of the chiral condensate, as discussed in Sec. 2.2.2. In presence of this mixing the critical mode becomes a linear combination of both [47], so that a proper inclusion of the diffusion of baryon charge would allow to incorporate at least Model-B dynamics in the quark-meson model. One could then go beyond the universal properties of Model B, and also estimate non-universal corrections (which are present at any finite 'distance' to the critical point) within an effective description of the different realizations of chiral symmetry in dense QCD matter and the transitions between them, as a first step towards assessing to which extend critical dynamics can be observed near the QCD critical point.

Chapter 6

Conclusion & Outlook

Our central motivation for this work was to investigate the near-equilibrium dynamic critical behavior of hot and dense QCD matter near the two-flavor chiral phase transition, and the conjectured critical point at finite baryon chemical potential, respectively. In parallel, we have developed a novel real-time formulation of the FRG specifically tailored to dynamical systems with reversible mode couplings, as needed for Models G and H.

In Chapter 2 we have reviewed some theoretical basics as a foundation for the subsequent developments in the following chapters, including the Schwinger-Keldysh CTP formalism of real-time QFT, the MSR formalism of classical-statistical systems, dynamic critical phenomena with special emphasis on the dynamic universality classes represented by Models A, B, C, G & H from the Halperin-Hohenberg classification and their relation to QCD, and the FRG in its formulation on the CTP. In particular, we have reviewed some of our previous results [1] on the critical spectral functions of Models A, B & C, and the limitations that arise for suitable regulators in real-time QFT computations due to the causal structure of the Keldysh action.

In Chapter 3 we have considered $O(N)$ Model G, which for $N = 4$ is conjectured to be in the same dynamic universality class as the two-flavor chiral phase transition. As a starting point for the FRG, we have constructed a generating functional for unequal-time correlation functions using the MSR formalism. We have discussed that the MSR action of Model G possesses the discrete symmetry of thermal equilibrium [107], and an (extended [109]) temporal gauge symmetry which expresses the fact that a time-dependent $O(N)$ transformation of the fields can be removed by a corresponding time-dependent shift of the external magnetic field. To preserve these symmetries exactly during the FRG flow, we have added the regulator not on the level of the MSR action, but instead (one step earlier) on the level of the Landau-Ginzburg-Wilson (LGW) free energy. As a consequence, we found that the regulator couples to composite (response) fields on the level of the MSR action. With this technique, we were able to prove exact statements about the resulting FRG flow, including the non-renormalization of the mode-coupling constant g and the independence of the flow of the LGW free energy from the dynamics. Using an ansatz for the effective average action we have shown that our formalism reproduces the non-trivial value $z = d/2$ for the dynamic critical exponent at the strong-scaling fixed point of Model G. By including a momentum-dependent kinetic coefficient for the charge densities in our truncation, we have computed a novel scaling function which describes the universal momentum and temperature dependence of the iso-(axial-)vector charge diffusion coefficient.

In Chapter 4 we have adapted our real-time FRG formalism to Model H, which is in the

same dynamic universality class as the conjectured Z_2 critical point at finite baryon chemical potential in the QCD phase diagram. Within a ϕ^4-truncation of the static sector we were able to derive analytical expressions for the dynamic critical exponents x_σ and x_η of the heat conductivity and the shear viscosity, respectively. While our FRG results for x_σ were in good agreement with 2^{nd}-order ϵ-expansion [111, 112], we found that x_η exhibits a maximum at some spatial dimension $2 < d < 4$, and approaches zero again for $d = 2$, which is not seen in 2^{nd}-order ϵ-expansion. We have discussed that this result is in quantitative agreement with the self-consistent 'mode-coupling' calculation by Ohta and Kawasaki [227]. In order to verify the robustness of our results, we have implemented the more sophisticated LPA' truncation of the LGW free energy, which gave us an estimate for the systematic error of our results. In parallel, we have derived similar analytical expressions for the FRG flow of the kinetic coefficients in $O(N)$ Model G based on the flow equations of Chapter 3, which have revealed the rather rich fixed-point structure in the dynamic sector known from ϵ-expansion [104]. Moreover, we have discussed how weak and strong scaling relations are related to the finiteness of the fixed-point values for certain dimensionless combinations of the kinetic coefficients, denoted by f and w. In particular, the absence of strong scaling was related to a vanishing fixed-point value of w, as was the case at the single fixed point of Model H as well as at the two weak-scaling fixed points of Model G.

In Chapter 5 we have formulated the quark-meson model on the CTP and derived the corresponding Keldysh action. One central result of Chapter 3 was that the FRG flow of the LGW free energy is independent of the equations of motion as long as the classical symmetry of thermal equilibrium holds. This has raised the question to which extent similar statements apply to quantum systems. To address this question, we have first generalized the known symmetry of thermal equilibrium [107, 113] to a Keldysh action which describes relativistic Dirac fermions. We have included dissipation in a chirally symmetric manner by coupling two sets of heat-bath oscillators in the spirit of the Caldeira-Leggett model, which has allowed us to include different damping constants for σ and $\boldsymbol{\pi}$ while preserving chiral symmetry. After setting up a real-time FRG flow for fermions, we have shown that the dissipative dynamics indeed potentially affects the FRG flow of the effective potential via the contributions from non-zero Matsubara modes. (This is unlike classical-statistical systems, where only the zeroth Matsubara mode effectively contributes, enabling a clear distinction between static and dynamic properties.) We have considered two phenomenlogical models for the pion damping constant, motivated from chiral perturbation theory at small temperatures T [116] and results from spectral reconstruction of lattice-QCD data at high T [117]. We found that, although there is an influence on the phase diagram and screening masses, the influence is quantitatively small. However, while these 'static' observables where evidently rather insensitive to the dissipative dynamics, we also found that the effect on 'dynamic' properties such as pole masses can be dramatic: For instance, when the damping became large enough, we found a transition from underdamped to overdamped dynamics, where the physical picture of weakly-damped quasi particles changes to purely relaxational excitations. To estimate the maximal possible effect of bosonic dissipation on the phase diagram, we considered limits where the damping constants approach infinity. In these extreme limits the quantitative effects on the 'static' observables were more noticable, but still remained comparatively small. In particular, the qualitative features of the phase diagram with its critical point and the first-order transition line remained unchanged.

In the future, the results of this work may be extended in several directions. For instance, the developments presented in Chapter 3 and 4 provide the basis for applications of this real-

time FRG approach to various other systems with reversible mode couplings. One example is fluctuating hydrodynamics, where the non-linear self-coupling of the momentum density $\boldsymbol{j}$ (cf. Eq. (2.125b)) leads to a non-trival renormalization of the shear viscosity [254]. By using the present techniques, this effect could be computed non-perturbatively and compared to the one-loop result of Ref. [254].

While Model G would describe the critical dynamics of hot QCD matter in the chiral crossover region [61,68,69], there has to be a transition to Model-H dynamics when approaching the Z_2 critical point from the pseudo-critical chiral transition line. A related observation [47] is that the maximal achievable correlation length in a heavy-ion collision, estimated at $\xi \approx 2-3$ fm, is not much larger than the correlation length in the pion channel, which is of order $m_\pi^{-1} \approx 1.4$ fm. This raises the question whether the full order-parameter multiplet (including the pions) should be included in a realistic hydrodynamic description near the critical point. From a theoretical perspective, the two scaling behaviors ($O(4)$ Model G and Z_2 Model H) should be connected, in principle, via the conjectured tricritical point [9]. It is reasonable to ask whether the tricritical point itself has an observable impact on the dynamics of QCD matter at the physical point. To study tricritical scaling with the FRG, one could use models similar to those of Refs. [163,255]. In particular, in Ref. [163] the conserved baryon density and energy-momentum tensor were added to the equations of motion of Model G, and it was shown that the energy density is indeed irrelevant due to the negative specific heat exponent in the static $O(4)$ universality class, as expected. However, at the tricritical point, the specific heat exponent $\alpha = 1/2$ is positive [62], and thus the energy density might become relevant. Hence, it is not a priori clear which kind of dynamic critical behavior is realized at the tricritical point. This question could be naturally addressed with the real-time FRG by identifying a stable fixed point in the dynamic sector of a model similar to the one of Ref. [163] but tuned to the tricritical point, and computing the corresponding dynamic critical exponents.[1]

An important open question concerns the size of the dynamic scaling region around the two-flavor chiral phase transition of QCD in the chiral limit, and whether or not it includes the physical point. Based on the results of Chapters 3 and 5, a computation of the dynamic scaling region in a low-energy effective theory such as the quark-meson model could be realized in several steps of a dedicated effort: Since the setup of Chapter 3 was practically limited to vanishing external fields $H = 0$, which translate to vanishing current quark masses (i.e., the chiral limit) in QCD, a first step would be to include explicit symmetry breaking. However, this involves an expansion around a non-vanishing order-parameter expectation value, which suffers from the technical difficulties outlined in Sec. 3.3, with numerous additional terms appearing in the flow equations. The idea would be to set up a computer algebra system such as Mathematica or FORM to perform, e.g., functional derivatives and index contractions automatically. In a second step, the task would be to embed Model G into the real-time FRG flow for the quark-meson model from Chapter 5. In particular, in order to ensure Model-G dynamics in the infrared, one could explicitly couple the conserved iso-vector and iso-axial-vector Noether currents $\boldsymbol{\rho}^\mu$ and $\boldsymbol{a}_1^\mu$ associated with $SU(2)_L \times SU(2)_R$ chiral symmetry to the quarks [256]. By choosing suitable UV parameters to reproduce IR observables in vacuum, the external fields can be related to vacuum pion masses. Finally, a scaling analysis in the spirit of Ref. [71] can be performed to estimate the impact of universal critical dynamics on the near-equilibrium time evolution of QCD matter at the physical point.

[1] In particular, such an analysis should investigate whether or not the strong-scaling fixed point of Model G is unstable against the coupling to the divergent energy fluctuations.

Acknowledgements

First of all, I would like to thank my supervisor Lorenz von Smekal for giving me the opportunity to work on this fascinating topic, for his constant support and encouragement along the way, and for the countless illuminating discussions. It has been a great pleasure for me to work with him, and a privilege to benefit from his enormous knowledge.

Second, I thank Christian Fischer for readily agreeing to be the second referee of this thesis.

I would like to thank Sören Schlichting and Yunxin Ye for the great collaboration during the last years, the numerous fruitful discussions during our weekly meetings, and for my productive stay at Bielefeld University. In particular, I want to express my gratitude to Yunxin for her valuable involvement, and gratefully acknowledge her contributions to this work.

Special thanks are dedicated towards my present and former colleagues Robin Kehr, Leon Sieke, Jonathan Yigzaw, Ugo Mire, Patrick Niekamp, Mattia Recchi, Milad Ghanbarpour, Dominik Schweitzer, Fabian Rennecke, and Arno Tripolt for all scientific and non-scientific discussions during coffee breaks, CRC meetings, workshops, and conferences. In particular, I am indebted to both Robin and Leon for proofreading parts of this thesis, and to Leon for many fruitful discussions, especially during the time of our Bachelor theses. Moreover, I would like to thank Markus Huber for his competent guidance in setting up and using DoFun.

I gratefully acknowledge instructive conversations with Adrien Florio, Eduardo Grossi, Peter Lowdon, Jan Pawlowski, and Derek Teaney during conferences and workshops, from which I have greatly benefited.

On a personal level, I would like to thank my friends and family for all their support, especially Jannis Hamp, Cedric Schacht, and my parents Ulrike and Manfred Roth. I also want to thank my uncle Gerhard Roth, who showed continued interest in this work, but sadly did not live to see its completion.

Finally, I would like to express my deepest gratitude towards my wife Laura Becker for her unconditional support and love, for her enduring patience during all my highs and lows, and for always believing in me.

Appendix A

Causality and Kramers-Kronig relations

In Sec. 2.3.2, we started with assuming that the regulator $R_k^{R/A}(\omega, \boldsymbol{p})$ is analytic at $\omega = 0$ for infrared finiteness. One can then write down subtracted Kramers-Kronig relations based on the analytic properties of $(R_k^{R/A}(\omega, \boldsymbol{p}) - R_k^{R/A}(0, \boldsymbol{p}))/\omega$,

$$\mathrm{Re}\, R^{R/A}(\omega, \boldsymbol{p}) = \mathrm{Re}\, R^{R/A}(0, \boldsymbol{p}) \pm P \int_{-\infty}^{\infty} \frac{d\omega'}{2\pi} \frac{2\omega^2\, \mathrm{Im}\, R^{R/A}(\omega', \boldsymbol{p})}{\omega'(\omega'^2 - \omega^2)}\,, \tag{A.1a}$$

$$\mathrm{Im}\, R^{R/A}(\omega, \boldsymbol{p}) = \mp P \int_{-\infty}^{\infty} \frac{d\omega'}{2\pi} \frac{2\omega\ \mathrm{Re}\, R^{R/A}(\omega', \boldsymbol{p})}{\omega'^2 - \omega^2}\,, \tag{A.1b}$$

where P denotes the Cauchy principal value of the integral. Here, we have furthermore used that $\mathrm{Im}\, R^{R/A}(0, \boldsymbol{p}) = 0$ for an analytic function with odd imaginary part, so that Eq. (A.1b) stays formally the same as in the unsubtracted case in Eq. (A.6b) below. The subtracted Kramers-Kronig relations (A.1a) and (A.1b) are combined in the subtracted spectral representation,

$$R^{R/A}(\omega, \boldsymbol{p}) = R^{R/A}(0, \boldsymbol{p}) - \int_0^{\infty} \frac{d\omega'}{2\pi} \frac{2\omega^2 J(\omega', \boldsymbol{p})}{\omega'((\omega \pm i\epsilon)^2 - \omega'^2)}\,, \tag{A.2}$$

corresponding to Eqs. (2.179), (2.180) of Sec. 2.3.2.

Alternatively to first assuming analyticity of the regulator at $\omega = 0$, as described in Sec. 2.3.2, we might as well start with assuming that the regulator is analytic at complex infinity, and perform the subtraction of the frequency-independent mass shift there. Then, for any finite value of k the limit

$$\Delta M^2_{\infty,k}(\boldsymbol{p}) \equiv -\lim_{\omega\to\infty} R_k^{R/A}(\omega, \boldsymbol{p}) \tag{A.3}$$

exists, is real, and unique in the sense that it can be taken in any direction and there is no singularity at infinity in the complex ω-plane. We can then formally separate this part from the regulator and use this as an alternative definition of the spectral part of the self-energy regulator,

$$\Sigma_k^{R/A}(\omega, \boldsymbol{p}) \equiv R_k^{R/A}(\omega, \boldsymbol{p}) + \Delta M^2_{\infty,k}(\boldsymbol{p})\,, \tag{A.4}$$

replacing (2.179) by the one subtracted at infinity. Then, by definition we have in this case,

$$\Sigma_k^{R/A}(\omega, \boldsymbol{p}) \to 0 \ \text{ for } \omega \to \infty\,. \tag{A.5}$$

Because it vanishes at infinity, its real and imaginary parts are now related by unsubtracted Kramers-Kronig relations, for the retarded/advanced components $\Sigma^{R/A}(\omega,\boldsymbol{p})$ of the spectral part of the regulator,

$$\mathrm{Re}\,\Sigma^{R/A}(\omega,\boldsymbol{p}) = \pm P\int_{-\infty}^{\infty}\frac{d\omega'}{2\pi}\frac{2\omega'\ \mathrm{Im}\,\Sigma^{R/A}(\omega',\boldsymbol{p})}{\omega'^2-\omega^2}\,, \tag{A.6a}$$

$$\mathrm{Im}\,\Sigma^{R/A}(\omega,\boldsymbol{p}) = \mp P\int_{-\infty}^{\infty}\frac{d\omega'}{2\pi}\frac{2\omega\ \mathrm{Re}\,\Sigma^{R/A}(\omega',\boldsymbol{p})}{\omega'^2-\omega^2}\,, \tag{A.6b}$$

Together, these imply the unsubtracted (standard) spectral representation replacing (2.180),

$$\Sigma_k^{R/A}(\omega,\boldsymbol{p}) = -\int_0^{\infty}\frac{d\omega'}{2\pi}\frac{2\omega' J_k(\omega',\boldsymbol{p})}{(\omega\pm i\varepsilon)^2-\omega'^2}\,, \tag{A.7}$$

where the FRG-scale dependent spectral density $J_k(\omega,\boldsymbol{p})$ is again given by the imaginary part of the regulator,

$$J_k(\omega,\boldsymbol{p}) = \pm 2\,\mathrm{Im}\,\Sigma_k^{R/A}(\omega,\boldsymbol{p}) = \pm 2\,\mathrm{Im}\,R_k^{R/A}(\omega,\boldsymbol{p})\,. \tag{A.8}$$

Eqs. (A.6a) and (A.6b) use the analyticity of $\Sigma^{R(A)}(\omega,\boldsymbol{p})$ in the upper (lower) half plane. They are thus valid for any retarded (advanced) function $f(\omega)$ in the complex plane, as long as it falls off at complex infinity, $f(\omega)\to 0$ for $\omega\to\infty$. In particular, analyticity at complex infinity implies that

$$\Sigma_k^R(\omega,\boldsymbol{p}) \to \frac{iC_k(\boldsymbol{p})}{\omega} \ \text{ or faster for } \omega\to\pm\infty\,, \tag{A.9}$$

with possibly non-vanishing but real $C_k(\boldsymbol{p})$. Contour integration then yields

$$\int_{-\infty}^{\infty}\frac{d\omega}{2\pi}\left(\Sigma_k^R(\omega,\boldsymbol{p})+\Sigma_k^A(\omega,\boldsymbol{p})\right) = C_k(\boldsymbol{p})\,. \tag{A.10}$$

This shows explicitly that, when the spectral part $\Sigma_k^{R/A}(\omega,\boldsymbol{p})$ tends to zero faster than $1/\omega$ for $\omega\to\infty$, i.e. for $C_k(\boldsymbol{p})\equiv 0$, we obtain the typical causality sum rule

$$0 = \int_{-\infty}^{\infty}\frac{d\omega}{2\pi}\left(\Sigma_k^R(\omega,\boldsymbol{p})+\Sigma_k^A(\omega,\boldsymbol{p})\right) = \int_0^{\infty}\frac{d\omega}{2\pi}\,4\,\mathrm{Re}\,\Sigma_k^R(\omega,\boldsymbol{p})\,. \tag{A.11}$$

The real part $\mathrm{Re}\,\Sigma_k^{R/A}(\omega,\boldsymbol{p})$ of our causal regulator then necessarily has a zero crossing along the frequency axis. As a manifestation of this zero crossing we furthermore observe that a positive spectral density $J_k(\omega,\boldsymbol{p})$, which also vanishes when $\omega\to 0$ for IR finiteness, then necessarily leads to a *negative* shift in the squared mass caused by the spectral part (A.7) of the regulator,

$$\Delta m_k^2(\boldsymbol{p}) \equiv -\Sigma_k^{R/A}(0,\boldsymbol{p}) = -\int_0^{\infty}\frac{d\omega'}{\pi}\frac{J_k(\omega',\boldsymbol{p})}{\omega'}\,. \tag{A.12}$$

Assuming that the regulator is IR and UV finite with respect to frequencies, i.e. that the large-frequency limit (A.3) vanishes as well, and hence $\Delta M_{\infty,k}^2(\boldsymbol{p})\equiv 0$, we obtain the same result as in Sec. 2.3.2 again,

$$0 \overset{!}{\leq} \Delta m_k^2(\boldsymbol{p}) = R_k^E(0,\boldsymbol{p}) = -\int_0^{\infty}\frac{d\omega'}{\pi}\frac{J_k(\omega',\boldsymbol{p})}{\omega'}\,, \tag{A.13}$$

to avoid acausal regulator singularities. And this contradicts the positivity of the regulator spectral density $J_k(\omega,\boldsymbol{p})$ in exactly the same way as in Sec. 2.3.2, when infrared and ultraviolet finiteness are required for the regulator at the same time.

Appendix B

Details on the MSR path-integral formulation of Model G

In this appendix, we discuss some subtleties of the MSR path-integral formulation of Model G which we did not fully cover in the main text: In Sec. B.1 we discuss how the Ito discretization can be properly formulated in the continuum (which corresponds, as we shall see, to a regularization of expressions as $\theta(0)$, i.e. the value of the Heaviside step function at zero). In Sec. B.2 we show that the presence of the Jacobian determinant in our generating functional (3.26) after the non-linear field transformation can be understood as the determinant that is always (but usually implicitly) present in the MSR path integral, and that it can be represented on a diagrammatical level as additional interactions with Grassmann-valued ghost fields that ensure the normalization condition $Z = 1$. Finally, we show in Sec. B.3 that if the physical sources would be coupled in the 'traditional' way to the elementary response fields $\tilde{\psi}$ and $\tilde{n}$ instead of the composite response fields $\tilde{\Phi}$ and $\tilde{N}$, the Boltzmann distribution would no longer be the stationary state of the system.

B.1 Continuum formulation of the Ito discretization

In perturbation theory, there can be acausal diagrams where a retarded or advanced propagator closes into a loop. Such diagrams should naively vanish due to causality. This is true in the Ito discretization since there the response fields appear always at greater times in the interaction terms than the classical fields (a quartic interaction term in a $\lambda\phi^4$ theory, for instance, would be of the form $\tilde{\Phi}_{i+1}\phi_i\phi_i\phi_i$, with the indices i, $i-1$ labeling time slices in this subsection). As such, the acausal loop will be proportional to expressions as $\langle\tilde{\Phi}_{i+1}\phi_i\rangle$. These expressions generally vanish due to causality, since $\langle\tilde{\Phi}_i\phi_j\rangle \sim G^A_{ij}$ is *advanced* (i.e. it vanishes for $i > j$), and i is always *before* $i+1$. However, in a naive continuum limit the difference between $i+1$ and i disappears. Instead, in the continuum limit the retarded/advanced propagators are proportional to the Heaviside step function, $G^R(t,t') = G^A(t',t) \sim \theta(t-t')$. Hence, the ambiguity can be pushed into a specification of $\theta(0)$ in the propagators (since it closes in a loop at the vertex). Indeed, a possible continuum formulation of the Ito discretization can be obtained by requiring the value $G^R_0(t,t) = G^A_0(t,t) \sim \theta(0) \equiv 0$ of the bare retarded/advanced propagators at equal times. With this regularization, acausal diagrams which involve closed loops of retarded/advanced propagators vanish. However, this regularization becomes slightly subtle to achieve in frequency

space since there we would naively have (after Fourier transform),

$$G_0^{R/A}(t,t) = \int_{-\infty}^{\infty} \frac{d\omega}{2\pi}\, G_0^{R/A}(\omega) = -\int_{-\infty}^{\infty} \frac{d\omega}{2\pi}\, \frac{\Gamma_0}{\pm i\omega - \Gamma_0 m^2} = \frac{\Gamma_0}{2} \tag{B.1}$$

(here for simplicity in $d = 0$ spatial dimensions). This is because the integrand does not fall fast enough for $\omega \to \infty$ when applying the residue theorem. Obtaining a proper continuum limit of the Ito discretization can be achieved by shifting the time argument of the response fields in the definition of the propagators by an infinitesimal amount ε into the future [82],

$$G_\varepsilon^R(t,t') = i\langle \phi(t)\tilde{\Phi}(t'+\varepsilon)\rangle \sim \theta(t-(t'+\varepsilon)) \tag{B.2a}$$

$$G_\varepsilon^A(t,t') = i\langle \tilde{\Phi}(t+\varepsilon)\phi(t')\rangle \sim \theta(t'-(t+\varepsilon)) \tag{B.2b}$$

and understanding all diagrams in the sense that the limit $\varepsilon \to 0^+$ is taken after evaluating the integrals. Then we indeed have $G_\varepsilon^R(t,t) = G_\varepsilon^A(t,t) \sim \theta(-\varepsilon) = 0$ for every $\varepsilon > 0$, as desired at equal times. After Fourier transform (assuming time-translation invariance) this amounts to the replacement

$$G_\varepsilon^{R/A}(\omega) = e^{\pm i\omega\varepsilon} G_0^{R/A}(\omega) \tag{B.3}$$

in frequency space. The exponential factors $e^{\pm i\omega\varepsilon}$ ensure that the contribution from the large semicircle in the upper (lower) half-planes in integrals like in (B.1) vanishes. Thus the whole integral is zero since the integrand is analytic in the upper (lower) half-plane and vanishes fast enough for $\omega \to \infty$. As such, closed loops over retarded/advanced propagators vanish for every $\varepsilon > 0$, as desired.

We can thus set the Jacobian to $\mathcal{J}[\phi, n] = 1$, but have to keep in mind that this goes hand in hand with the ε-prescription (B.2). Alternative discretizations like the Stratonovich convention can avoid such an ε-prescription (since they correspond to the regularization $\theta(0) = 1/2$ which coincides with the result (B.1) from the 'naive' continuum limit), but there the Jacobian is in general non-zero [257, 258]. Usually, the latter is rewritten as an integral over anti-commuting fields ('ghosts') which otherwise have the same quantum numbers as the original fields. These additional ghost contributions precisely cancel any non-vanishing unphysical contributions from acausal diagrams [194].

B.2 Jacobians and ghosts

The presence of a Jacobian determinant as in (3.26) is not unusual in field-theoretic treatments of classical-statistical systems and can be intuitively understood as follows. The generating functional as formulated in (3.26) can be alternatively derived without ever referring to the non-linear field transformation (3.22), i.e. by just appealing to the standard MSR technique. To see this, first combine the two equations of motion (2.146) into one using vector notation, and rewrite the right-hand side as a field-dependent matrix acting on the (functional) gradient of the free energy (plus a vector containing the contribution from the noises),

$$\frac{\partial}{\partial t}\begin{pmatrix}\phi_a \\ n_{bc}\end{pmatrix} = \tag{B.4}$$

$$-\begin{pmatrix}\delta_{ad}\Gamma_0 & -\frac{g}{2}\{\phi_a, n_{ef}\} \\ -g\{n_{bc},\phi_d\} & -\frac{1}{2}(\delta_{be}\delta_{cf}-\delta_{bf}\delta_{ce})\gamma\boldsymbol{\nabla}^2 - \frac{g}{2}\{n_{bc},n_{ef}\}\end{pmatrix}\begin{pmatrix}\frac{\delta F}{\delta\phi_d} \\ \frac{\delta F}{\delta n_{ef}}\end{pmatrix} + \begin{pmatrix}\theta_a \\ \boldsymbol{\nabla}\cdot\boldsymbol{\zeta}_{bc}\end{pmatrix}$$

In front of the functional gradient of the free energy now stands a (field-dependent) matrix. This matrix is, in fact, the transpose $J^T(\psi)$ of $J(\psi)$ in our non-linear transformation (3.24) of the response fields. The field-dependent matrix $J(\psi)$ and its transpose are invertible for arbitrary field configurations $\psi = \psi(x)$ since the corresponding determinant $\det J(\psi) \neq 0$ does not vanish.[1] Thus we can multiply by ${J^{-1}}^T(\psi)$ on both sides of (B.4) (also using that matrix inversion and transposition commute, $(J^{-1})^T = (J^T)^{-1}$), and rewrite the equations of motion in symbolic superfield notation as

$$\int_{x'} {J_{ij}^{-1}}^T(x,x';\psi)\,\frac{\partial\psi_j(t',\boldsymbol{x}')}{\partial t'} = -\frac{\delta F}{\delta\psi_i(\boldsymbol{x})}\bigg|_t + \int_{x'} {J_{ij}^{-1}}^T(x,x';\psi)\,\xi_j(x') \tag{B.5}$$

with superfield indices i and j, and $\xi = (\xi_i) = (\theta_a, \boldsymbol{\nabla}\cdot\boldsymbol{\zeta}_{bc})$ denoting the noise superfield. We can use this (equivalent) form of the equations of motion now as our starting point for the MSR path integral. Importantly, after the overall multiplication with the field-dependent factor ${J^{-1}}^T(\psi)$, the noise becomes multiplicative. Correspondingly, we have to specify the discretization of the stochastic equations to make them unambiguous. Moreover, we have to include a field-dependent Jacobian as in (3.6) to ensure the overall normalization of the path integral. In Ito discretization, the time derivative in (B.5) becomes a finite backward difference (with finite time step Δt)

$$\frac{\partial\psi_i(t,\boldsymbol{x})}{\partial t} \;\to\; \frac{\Delta^R\psi_i(t,\boldsymbol{x})}{\Delta t} \equiv \frac{\psi_i(t,\boldsymbol{x}) - \psi_i(t-\Delta t,\boldsymbol{x})}{\Delta t}\,. \tag{B.6}$$

The Jacobian matrix $J_{ij}(x,x';\psi)$ is local in time, so we can also write

$${J_{ij}^{-1}}^T(x,x';\psi) \equiv {J_{ij}^{-1}}^T(\boldsymbol{x},\boldsymbol{x}';\psi,t)\,\delta(t-t') \tag{B.7}$$

for its transposed inverse. We can then express the Ito-discretized equations of motion as

$$\begin{aligned}\int_{\boldsymbol{x}'} {J_{ij}^{-1}}^T(\boldsymbol{x},\boldsymbol{x}';\psi,t-\Delta t)\,\frac{\Delta^R\psi_j(t,\boldsymbol{x}')}{\Delta t} = \\ -\frac{\delta F}{\delta\psi_i(\boldsymbol{x})}\bigg|_{t-\Delta t} + \int_{\boldsymbol{x}'} {J_{ij}^{-1}}^T(\boldsymbol{x},\boldsymbol{x}';\psi,t-\Delta t)\,\xi_j(t-\Delta t,\boldsymbol{x}')\,,\end{aligned} \tag{B.8}$$

which involve the fields only at times t and $t-\Delta t$. Note that, as an essential property of Ito discretization, only the first term in the discretized time derivative is evaluated at time t. All other quantities are evaluated at the time before, $t-\Delta t$. We define an operator G as a shorthand notation for these Ito-discretized equations of motions,

$$\begin{aligned}G_i(t,\boldsymbol{x}) \equiv \int_{\boldsymbol{x}'} {J_{ij}^{-1}}^T(\boldsymbol{x},\boldsymbol{x}';\psi,t-\Delta t)\,\frac{\Delta^R\psi_j(t,\boldsymbol{x}')}{\Delta t} \\ + \frac{\delta F}{\delta\psi_i(\boldsymbol{x})}\bigg|_{t-\Delta t} - \int_{\boldsymbol{x}'} {J_{ij}^{-1}}^T(\boldsymbol{x},\boldsymbol{x}';\psi,t-\Delta t)\,\xi_j(t-\Delta t,\boldsymbol{x}')\,.\end{aligned} \tag{B.9}$$

The discretized equations of motion are satisfied if $G = 0$. Its Jacobian matrix can be straightforwardly computed,

$$\frac{\delta G_i(t,\boldsymbol{x})}{\delta\psi_j(t',\boldsymbol{x}')} = {J_{ij}^{-1}}^T(\boldsymbol{x},\boldsymbol{x}';\psi,t-\Delta t)\,\delta(t-t') + (\cdots)\;\delta(t-t'-\Delta t) \tag{B.10}$$

[1] By the inverse function theorem, its inverse can be expressed by the Jacobian matrix of the inverse of the field transformation (3.22),

$$J^{-1}(x,x';\psi) = \frac{\delta\tilde{\psi}(x)}{\delta\tilde{\Psi}(x')}\,.$$

and is a lower triangular block matrix in the discretized time domain. Its determinant can thus be computed as an (infinite) product of the determinants of the blocks at discretized times $t_n = n\Delta t$ along the main diagonal (where the determinants of the blocks are understood with respect to both internal indices i, j and spatial 'indices' $\boldsymbol{x}, \boldsymbol{x}'$),

$$\mathcal{J}'[\psi] = \det \frac{\delta G_i(t, \boldsymbol{x})}{\delta \psi_j(t', \boldsymbol{x}')} = \prod_{t_n} \frac{1}{\Delta t} \det J_{ij}^{-1^T}(\boldsymbol{x}, \boldsymbol{x}'; \psi, t_n - \Delta t)\,. \tag{B.11}$$

This is the same Jacobian as in (3.28). However, in (3.28) it appeared due to the non-linear field transformation of the response field. Remarkably, the determinant does not depend on the noise, even though in the alternative formulation (B.5) of the equations of motion the noise is multiplicative. This is due to the choice of Ito discretization.

By constructing the generating functional using the standard MSR technique, which we have reviewed in Sec. 3.1, we obtain

$$Z[J, \tilde{J}] = \int \mathcal{D}\psi\, \mathcal{D}\tilde{\Psi}\, \mathcal{J}'[\psi] \exp\left\{ iS'[\psi, \tilde{\Psi}] + i \int_x \left(\tilde{J}_i \psi_i + \tilde{\Psi}_i J_i \right) \right\} \tag{B.12}$$

with

$$S'[\psi, \tilde{\Psi}] = -\tilde{\Psi}^T J^{-1^T}(\psi) \frac{\partial \psi}{\partial t} + iT \tilde{\Psi}^T J^{-1^T}(\psi) \tilde{\Psi} - \tilde{\Psi}^T \frac{\delta F}{\delta \psi} \tag{B.13}$$

in compact superfield notation.

As a side remark, note that when one derives $S'[\psi, \tilde{\Psi}]$ by performing the field transformation in the action $S[\psi, \tilde{\psi}]$ for the elementary response fields, the quadratic term in the response fields looks like

$$S[\psi, \tilde{\psi}] = iT \tilde{\psi}^T \hat{\gamma} \tilde{\psi} + \cdots \tag{B.14}$$

(with the superfield matrix $\hat{\gamma} = \mathrm{diag}(\Gamma_0, -\gamma \boldsymbol{\nabla}^2)$ of kinetic coefficients), which translates to

$$S'[\psi, \tilde{\Psi}] = iT \tilde{\Psi}^T J^{-1^T}(\psi) \hat{\gamma} J^{-1}(\psi) \tilde{\Psi} + \cdots \tag{B.15}$$

in the transformed action. This is, in fact, the same quadratic term as in (B.13), which can be seen by using that the symmetric contraction of the antisymmetric Poisson bracket $\{\psi, \psi\}$ with $\tilde{\Psi}^T J^{-1^T}(\psi) = \tilde{\psi}^T$ and $J^{-1}(\psi)\tilde{\Psi} = \tilde{\psi}$ vanishes, and so can add a suitable zero to (B.15),

$$iT \tilde{\Psi}^T J^{-1^T}(\psi) \hat{\gamma} J^{-1}(\psi) \tilde{\Psi} = iT \tilde{\Psi}^T J^{-1^T}(\psi) \underbrace{\left(\hat{\gamma} + g\{\psi, \psi\} \right)}_{J(\psi)} J^{-1}(\psi) \tilde{\Psi} = iT \tilde{\Psi}^T J^{-1^T}(\psi) \tilde{\Psi}\,. \tag{B.16}$$

This shows that the quadratic terms in (B.13) and (B.15) are the same.

The MSR action S' in (B.13) corresponds to the stochastic equations of motion in (B.5). The Jacobian appearing in (3.26) is hence just the standard Jacobian that is always (implicitly) present in the MSR path integral. Its precise value reflects the underlying discretization of the equations of motion. Notice that we can not simply set it to one here by clever choice of discretization, because $J^{-1^T}(\psi)$ appears as a field-dependent factor in front of the time derivative in the equations of motion (B.5). The field-dependent function $J^{-1^T}(\psi)$ thus appears on the diagonal of the Jacobian matrix (B.10). Hence, it will also enter the determinant (B.11).

On a practical level, a field-dependent Jacobian in the MSR formalism can be treated using well-established techniques. For example, by rewriting it using anti-commuting 'ghost' degrees of

freedom. There one expresses the determinant as a Gaussian integral over a pair of Grassmann-valued fields c and $\tilde{c}$,

$$\mathcal{J}'[\psi] = \int \mathcal{D}\tilde{c}\,\mathcal{D}c\, \exp\left\{ -\int_{xx'} \tilde{c}_i(x) \frac{\delta \tilde{\Psi}_i(x)}{\delta \psi_j(x')} c_j(x') \right\}, \tag{B.17}$$

where we have absorbed the infinite factor $\prod_{t_n}(1/\Delta t)$ from the determinant in (B.11) into the definition of the path integral. Rewriting the determinant like this can be interpreted as introducing a ghost part

$$S_{gh} = \int_{xx'} i\tilde{c}_i(x) \frac{\delta \tilde{\Psi}_i(x)}{\delta \tilde{\psi}_j(x')} c_j(x') \tag{B.18}$$

to the total action. We can write down a corresponding generating functional by introducing Grassmann-valued sources η_i, $\tilde{\eta}_j$ for the ghosts $\tilde{c}_i$, c_j,

$$Z[J, \tilde{J}, \eta, \tilde{\eta}] \equiv \int \mathcal{D}[\psi, \tilde{\Psi}, \tilde{c}, c]\, \exp\left\{ iS' + iS_{gh} + i \int_x \left(\tilde{J}_i \psi_i + \tilde{\Psi}_i J_i + \tilde{c}_i \eta_i + \tilde{\eta}_i c_i \right) \right\}. \tag{B.19}$$

The corresponding 1PI effective action is obtained by performing the Legendre transform (3.35) also with respect to the ghost sources.

As we have already stated in Eq. (3.65) in the main text, for $\tilde{J} = \eta = \tilde{\eta} = 0$ but an arbitrary classical source $J \neq 0$ the total action S_J in (B.19) becomes BRST exact. This can be seen as follows. First, we evaluate the BRST variation in (3.65), which yields

$$S_J = Q \left\{ -i\tilde{c}_i \left(J_{ij}^{-1^T}(\psi) \partial_t \psi_j + \frac{\delta F}{\delta \psi_i} - J_i - iT J_{ij}^{-1^T}(\psi) \tilde{\Psi}_j \right) \right\} \tag{B.20}$$

$$= -\tilde{\Psi}_i J_{ij}^{-1^T}(\psi) \partial_t^R \psi_j - \tilde{\Psi}_i \frac{\delta F}{\delta \psi_i} + iT \tilde{\Psi}_i J_{ij}^{-1^T}(\psi) \tilde{\Psi}_j + i\tilde{c}_i J_{ij}^{-1^T}(\psi) \partial_t c_j + \tilde{\Psi}_i J_i + \cdots . \tag{B.21}$$

The terms not spelled out explicitly here (but summarized as '$\cdots$') vanish in Ito regularization, since they only contribute to the off-diagonal elements of the lower triangular matrix in (B.10) and thus do not enter the determinant in (B.11). Moreover, in Ito regularization only the first 'half' of the discretized time derivative $\partial_t c_j \to (c_j(t) - c_j(t - \Delta t))/\Delta t$ effectively enters the determinant (B.11). Hence, one can omit the second half $c_j(t - \Delta t)/\Delta t$ from (B.21). With a field rescaling $c_i(t)/\Delta t \to c_i(t)$ of the first half, and by absorbing the resulting infinite factor $\prod_{t_n}(1/\Delta t)$ again into the definition of the path integral, one arrives at the properly normalized ghost action (B.18). Hence, the expression obtained in (B.21) indeed matches the action in (B.19) (which we have shown here within Ito regularization), so S_J is indeed BRST exact.

The action S_J being BRST symmetric implies the normalization condition (3.61) of the MSR path integral, which can be proven as in Sec. 1.5 of Ref. [192]: A variation $J \to J + \delta J$ in the generating functional (3.26) leads to

$$\begin{aligned} \delta Z[J] &= \int \mathcal{D}[\psi, \tilde{\Psi}, \tilde{c}, c]\, e^{iS_J} i\tilde{\Psi}_i \delta J_i = -\int \mathcal{D}[\psi, \tilde{\Psi}, \tilde{c}, c]\, e^{iS_J} \delta J_i Q\tilde{c}_i \; = \\ &= -\int \mathcal{D}[\psi, \tilde{\Psi}, \tilde{c}, c]\, Q\left\{ e^{iS_J} \delta J_i \tilde{c}_i \right\} = 0 \end{aligned} \tag{B.22}$$

where in the second equality we used that the composite response fields $i\tilde{\Psi}_i = -Q\tilde{c}_i$ are BRST exact, and in the last equality that the integral over a total differential vanishes. Together with the normalization $Z[J = 0] = 1$ we thus have $Z[J] = 1$ for all physical source configurations J on the level of the full path integral.

B.3 Traditional approach of constructing generating functionals

In a traditional approach of constructing a generating functional for correlation functions, one would now go on and introduce source terms as linear couplings to the elementary fields,

$$z[h,\tilde{h},\mathfrak{h},\tilde{\mathfrak{h}}] = \int \mathcal{D}\phi\,\mathcal{D}\tilde{\phi}\,\mathcal{D}n\,\mathcal{D}\tilde{n}\,\exp\Big\{iS + i\int_x \big(h_a(x)\tilde{\phi}_a(x) + \tilde{h}_a(x)\phi_a(x) + \frac{1}{2}\mathfrak{h}_{ab}(x)\tilde{n}_{ab}(x) + \frac{1}{2}\tilde{\mathfrak{h}}_{ab}(x)n_{ab}(x)\big)\Big\} \tag{B.23}$$

However, adding the sources like this has the following disadvantage: Even in the absence of the unphysical response sources $\tilde{h}_a(x)$ and $\tilde{\mathfrak{h}}_{ab}(x)$ the stationary state of the system is no longer a Boltzmann distribution: The equations of motion corresponding to the generating functional (B.23) (for vanishing response sources) read

$$\frac{\partial\phi_a}{\partial t} = -\Gamma_0\frac{\delta F}{\delta\phi_a} + \frac{g}{2}\{\phi_a, n_{bc}\}\frac{\delta F}{\delta n_{bc}} + h_a(x) + \theta_a \tag{B.24}$$

$$\frac{\partial n_{ab}}{\partial t} = \gamma\boldsymbol{\nabla}^2\frac{\delta F}{\delta n_{ab}} + g\{n_{ab},\phi_c\}\frac{\delta F}{\delta\phi_c} + \frac{g}{2}\{n_{ab},n_{cd}\}\frac{\delta F}{\delta n_{cd}} + \mathfrak{h}_{ab}(x) + \boldsymbol{\nabla}\cdot\boldsymbol{\zeta}_{ab} \tag{B.25}$$

which can be reformulated as a shift of the free energy in the dissipative terms,

$$\frac{\partial\phi_a}{\partial t} = -\Gamma_0\frac{\delta}{\delta\phi_a}\Big[F - \int_{x'} h'_a(x')\phi_a(x')\Big] + \frac{g}{2}\{\phi_a, n_{bc}\}\frac{\delta F}{\delta n_{bc}} + \theta_a \tag{B.26}$$

$$\frac{\partial n_{ab}}{\partial t} = \gamma\boldsymbol{\nabla}^2\frac{\delta}{\delta n_{ab}}\Big[F - \frac{1}{2}\int_{x'} \mathfrak{h}'_{ab}(x')n_{ab}(x')\Big] + \frac{g}{2}\{n_{ab},\phi_c\}\frac{\delta F}{\delta\phi_c} + g\{n_{ab},n_{cd}\}\frac{\delta F}{\delta n_{cd}} + \boldsymbol{\nabla}\cdot\boldsymbol{\zeta}_{ab} \tag{B.27}$$

where we have rescaled the source terms by the kinetic coefficients to put them inside the square brackets,

$$\Gamma h'_a(x) = h_a(x)\,, \qquad -\gamma\boldsymbol{\nabla}^2\mathfrak{h}'_{ab}(x) = \mathfrak{h}_{ab}(x)\,. \tag{B.28}$$

This highlights the inconsistency concerning the equilibrium state that arises when the sources couple to the elementary response fields as in (B.23). On the level of the equations of motion, the source terms correspond to shifts in the free energy, but only in the dissipative terms and not in the Poisson-bracket terms. Hence, a Boltzmann distribution $\sim \exp\{-\beta(F - h'\phi - \frac{1}{2}\mathfrak{h}'n)\}$ is no longer a stationary solution to the corresponding Fokker-Planck equation since the mode-coupling terms are no longer divergence-free in presence of the sources, i.e. (2.152) no longer holds. However, when the source terms are added consistently as terms in the free energy (3.3), the reversible mode couplings generate no probability current, i.e. (2.152) is satisfied, and a Boltzmann distribution $\sim \exp\{-\beta(F - H\phi - \frac{1}{2}\mathcal{H}n)\}$ is maintained as a stationary solution.

Appendix C

Thermal-equilibrium symmetry in systems with reversible mode couplings

In this appendix we show that the bare MSR action has the discrete symmetry (3.44), which essentially expresses detailed balance in thermal equilibrium, i.e., we show that $S[\mathcal{T}_\beta(\psi,\tilde{\Psi})] = S[\psi,\tilde{\Psi}]$. The bare MSR action S is in our compact superfield notation given by

$$S = -\tilde{\Psi}^T {J^{-1}}^T(\psi)\partial_t\psi + iT\tilde{\Psi}^T J^{-1}(\psi)\tilde{\Psi} - \tilde{\Psi}^T\frac{\delta F}{\delta\psi} \tag{C.1}$$

where all symbols are interpreted as vectors/matrices with respect to spatial, temporal, and superfield indices. We divide our proof into two steps. In the first step (i), we apply the transformation (where $\dot{\psi}_i \equiv \partial_t\psi_i$)

$$\begin{aligned}\psi_i(t,\boldsymbol{x}) &\to \psi_i(-t,\boldsymbol{x})\,,\\ \tilde{\Psi}_i(t,\boldsymbol{x}) &\to i\beta\dot{\psi}_i(-t,\boldsymbol{x}) + \tilde{\Psi}_i(-t,\boldsymbol{x})\,,\end{aligned} \tag{i}$$

and in the second step (ii), we multiply the fields with their time-reversal parities,

$$\begin{aligned}\psi_i(t,\boldsymbol{x}) &\to \epsilon_i\psi_i(t,\boldsymbol{x})\,,\\ \tilde{\Psi}_i(t,\boldsymbol{x}) &\to \epsilon_i\tilde{\Psi}_i(t,\boldsymbol{x})\,.\end{aligned} \tag{ii}$$

Symbolically, our procedure can be represented by

$$S \xrightarrow{\text{(i)}} S_1 \xrightarrow{\text{(ii)}} S_2 \tag{C.2}$$

where S_2 then equals the transformed MSR action $S_2 = S[\mathcal{T}_\beta(\psi,\tilde{\Psi})]$. After both steps, we will indeed obtain back the original action, $S_2 = S$, so that $\mathcal{T}_\beta$ is indeed a symmetry of S.

1. In step (i) the action transforms as (where we have already replaced $t \to -t$ in the integration)

$$\begin{aligned}S \to S_1 = {}& \tilde{\Psi}^T {J^{-1}}^T(\psi)\dot{\psi} + i\beta\dot{\psi}^T {J^{-1}}^T(\psi)\dot{\psi} + \\ & iT\,\tilde{\Psi}^T {J^{-1}}^T(\psi)\tilde{\Psi} + \underbrace{iT\,i\beta}_{(-)}\,\dot{\psi}^T {J^{-1}}^T(\psi)\tilde{\Psi} + \\ & \underbrace{iT\,i\beta}_{(-)}\,\tilde{\Psi}^T {J^{-1}}^T(\psi)\dot{\psi} + \underbrace{iT\,(i\beta)^2}_{-i\beta}\,\dot{\psi}^T {J^{-1}}^T(\psi)\dot{\psi} + \\ & - \tilde{\Psi}^T\frac{\delta F}{\delta\psi} - i\beta\,\dot{\psi}^T\frac{\delta F}{\delta\psi}\,.\end{aligned} \tag{C.3}$$

Here, the red terms cancel, the violet terms cancel, and the blue term is a total time derivative, so it vanishes upon integrating from $t = -\infty$ to $+\infty$. We thus obtain

$$S_1 = -\dot{\psi}^T J^{-1^T}(\psi)\tilde{\Psi} + iT\,\tilde{\Psi}^T J^{-1^T}(\psi)\tilde{\Psi} - \tilde{\Psi}^T \frac{\delta F}{\delta \psi}\,. \tag{C.4}$$

The first term can be reformulated via (using that the transpose of a (complex) number becomes itself)

$$-\dot{\psi}^T J^{-1^T}(\psi)\tilde{\Psi} = \left(-\dot{\psi}^T J^{-1^T}(\psi)\tilde{\Psi}\right)^T = -\tilde{\Psi}^T J^{-1}(\psi)\dot{\psi} \tag{C.5}$$

such that we finally get

$$S_1 = -\tilde{\Psi}^T J^{-1}(\psi)\dot{\psi} + iT\,\tilde{\Psi}^T J^{-1^T}(\psi)\tilde{\Psi} - \tilde{\Psi}^T \frac{\delta F}{\delta \psi} \tag{C.6}$$

as our result of step (i). Note that in contrast to the original MSR action (C.1) there is $J^{-1}(\psi)$ in the first term, instead of its transpose $J^{-1^T}(\psi)$.[1] If the inverse Jacobian $J^{-1}(\psi)$ would be symmetric (such as in the case of vanishing reversible mode couplings), we would have $J^{-1^T}(\psi) = J^{-1}(\psi)$, and step (i) alone would already constitute a symmetry of our MSR action. To 'change $J^{-1}(\psi)$ back to $J^{-1^T}(\psi)$' is the goal of step (ii).

2. When we multiply the fields with their respective time-reversal parities according to step (ii), the terms in (C.6) change according to

$$-\tilde{\Psi}^T J^{-1}(\psi)\partial_t \psi \to -\tilde{\Psi}^T \epsilon^T J^{-1}(\epsilon\psi)\epsilon\partial_t\psi \tag{C.7a}$$

$$iT\,\tilde{\Psi}^T J^{-1^T}(\psi)\tilde{\Psi} \to iT\,\tilde{\Psi}^T \epsilon^T J^{-1^T}(\epsilon\psi)\epsilon\tilde{\Psi} \tag{C.7b}$$

$$-\tilde{\Psi}^T \frac{\delta F}{\delta\psi}[\psi] \to -\tilde{\Psi}^T \epsilon^T \frac{\delta F}{\delta\psi}[\epsilon\psi] \tag{C.7c}$$

so we need to have

$$\epsilon^T \frac{\delta F}{\delta\psi}[\epsilon\psi] = \frac{\delta F}{\delta\psi}[\psi] \;\text{ and }\; \epsilon^T J^{-1}(\epsilon\psi)\epsilon = J^{-1^T}(\psi) \tag{C.8}$$

to ensure that the MSR action is invariant under the thermal equilibrium symmetry. The first equality in (C.8) is satisfied if the free energy F is invariant under time-reversal, $F[\varepsilon\psi] = F[\psi]$. This means that a Taylor expansion of F may only contain operators that have even parity under time reversal. The second equality in (C.8) can be satisfied by choosing parities $\epsilon_\phi = +1$ and $\epsilon_n = -1$, i.e. the charge densities change sign under time reversal. This is consistent with their interpretation as the iso-vector and iso-axial-vector currents (2.139) in the context of QCD. In matrix notation in $\psi = (\phi, n)$ superfield space, we have

$$\epsilon = \begin{pmatrix} \epsilon_\phi & 0 \\ 0 & \epsilon_n \end{pmatrix} = \begin{pmatrix} +1 & 0 \\ 0 & -1 \end{pmatrix}\,. \tag{C.9}$$

In symbolic shorthand notation, we can expand $J(\psi) = J_0 - \delta J(\psi)$ in a Neumann series in $\delta J(\psi)$ around $\delta J(\psi) = 0$ and apply the transformation individually to each term in the

[1] In the second term this distinction is irrelevant, because due to the symmetric contraction with $\tilde{\Psi}$ from the left and right only the symmetric part of $J^{-1^T}(\psi)$ contributes there.

series,

$$\begin{aligned}\epsilon^T J^{-1}(\epsilon\psi)\epsilon &= \epsilon^T \left(J_0^{-1} + J_0^{-1}\delta J(\epsilon\psi)J_0^{-1} + J_0^{-1}\delta J(\epsilon\psi)J_0^{-1}\delta J(\epsilon\psi)J_0^{-1} + \cdots\right)\epsilon \\ &= \epsilon^T J_0^{-1}\epsilon + \epsilon^T J_0^{-1}(\epsilon\epsilon^T)\,\delta J(\epsilon\psi)\,(\epsilon\epsilon^T)J_0^{-1}\epsilon + \\ &\qquad \epsilon^T J_0^{-1}(\epsilon\epsilon^T)\,\delta J(\epsilon\psi)\,(\epsilon\epsilon^T)J_0^{-1}(\epsilon\epsilon^T)\,\delta J(\epsilon\psi)\,(\epsilon\epsilon^T)J_0^{-1}\epsilon + \cdots \\ &= J_0^{-1} + J_0^{-1}(\epsilon^T\delta J(\epsilon\psi)\epsilon)J_0^{-1} + \\ &\qquad J_0^{-1}(\epsilon^T\delta J(\epsilon\psi)\epsilon)J_0^{-1}(\epsilon^T\delta J(\epsilon\psi)\epsilon)J_0^{-1} + \cdots \end{aligned} \tag{C.10}$$

where we used that $\epsilon^T J_0^{-1}\epsilon = J_0^{-1}$. We calculate

$$\begin{aligned}\epsilon^T\delta J(\epsilon\psi)\epsilon &= -g\begin{pmatrix}+1 & 0\\ 0 & -1\end{pmatrix}\begin{pmatrix}0 & \{\phi,n\}\\ \{n,\phi\} & -\{n,n\}\end{pmatrix}\begin{pmatrix}+1 & 0\\ 0 & -1\end{pmatrix} = \\ &= -g\begin{pmatrix}0 & -\{\phi,n\}\\ -\{n,\phi\} & -\{n,n\}\end{pmatrix} = -\delta J(\psi) = \delta J^T(\psi)\,. \end{aligned} \tag{C.11}$$

We can now resum the series in (C.10) again and find

$$\epsilon^T J^{-1}(\epsilon\psi)\epsilon = {J^{-1}}^T(\psi) \tag{C.12}$$

as anticipated from step (i), such that we finally obtain

$$S_2 = -\tilde{\Psi}^T {J^{-1}}^T(\psi)\dot{\psi} + iT\,\tilde{\Psi}^T {J^{-1}}^T(\psi)\tilde{\Psi} - \tilde{\Psi}^T\frac{\delta F}{\delta\psi} \tag{C.13}$$

as our result of the step (ii). The transformed action S_2 in (C.13) is the same as the original action S in (C.1). This shows that the MSR action (C.1) is indeed invariant under the discrete transformation (3.44) and concludes our proof.

Appendix D

Details on the FRG for systems with reversible mode couplings

In this appendix, we discuss more details about our formulation of the FRG for dynamic systems with reversible mode couplings. In Sec. D.1 we first reiterate the derivation of the flow equation of the effective average action in the spirit of the well-known derivation by Wetterich [72]. A central aspect of our approach is that the regulator couples to the *composite* response fields $\tilde{\Psi} = J(\psi)\tilde{\psi}$, so it is a priori not entirely obvious that the effective average action Γ_k actually converges to the bare MSR action S in the UV limit $k \to \Lambda$. Therefore, we show in Sec. D.2 that the effective average action Γ_k indeed converges to the bare MSR action S, up to an additional logarithm of a field-dependent (Jacobian) determinant, which we identify with the one in (3.26). In Sec. D.3 we discuss how the regulators for the ghosts should be chosen such that the BRST transformation (3.62) is a symmetry of the effective average action at all FRG scales.

D.1 Derivation of the flow equation

For a concise derivation of the flow equation, we first define the effective action $\tilde{\Gamma}_k$ as the (unmodified) Legendre transform (with the sources $J = (H, \mathcal{H})$ and $\tilde{J} = (\tilde{H}, \tilde{\mathcal{H}})$ in superfield space)

$$\tilde{\Gamma}_k[\psi, \tilde{\Psi}] = W_k[J, \tilde{J}] - \int_x J_i(x)\tilde{\Psi}_i(x) - \int_x \tilde{J}_i(x)\psi_i(x) \tag{D.1}$$

such that the effective *average* action Γ_k is given by an additional subtraction of the regulator term, $\Gamma_k = \tilde{\Gamma}_k - \Delta S_k$. By differentiating the Legendre transform (D.1) with respect to the FRG scale k, we calculate

$$\begin{aligned}\partial_k \tilde{\Gamma}_{k|\tilde{\Psi},\psi} &= \partial_k W_{k|J,\tilde{J}} + \int_x \frac{\delta W_k}{\delta J_i(x)} \partial_k J_i(x)_{|\tilde{\Psi},\psi} + \int_x \frac{\delta W_k}{\delta \tilde{J}_i(x)} \partial_k \tilde{J}_i(x)_{|\tilde{\Psi},\psi} \\ &\quad - \int_x \tilde{\Psi}_i(x) \partial_k J_i(x)_{|\tilde{\Psi},\psi} - \int_x \psi_i(x) \partial_k \tilde{J}_i(x)_{|\tilde{\Psi},\psi} \qquad \text{(D.2)} \\ &= \partial_k W_{k|J,\tilde{J}} \qquad \text{(D.3)}\end{aligned}$$

where we used that the field expectation values are given by

$$\psi_i(x) = \frac{\delta W_k}{\delta \tilde{J}_i(x)} \quad \text{and} \quad \tilde{\Psi}_i(x) = \frac{\delta W_k}{\delta J_i(x)} \,. \tag{D.4}$$

Next, we want to show that

$$\partial_k W_k[J,\tilde{J}] = \partial_k \langle \Delta S_k \rangle \tag{D.5}$$

which is straightforward since

$$\begin{aligned}\partial_k W_k[J,\tilde{J}] &= -i\partial_k \log \int \mathcal{D}\psi\, \mathcal{D}\tilde{\Psi}\, \exp\left(iS + i\Delta S_k + i\int_x J_i(x)\tilde{\Psi}_i(x) + i\int_x \tilde{J}_i(x)\psi_i(x)\right) \\ &= \frac{1}{Z_k}\int \mathcal{D}\psi\, \mathcal{D}\tilde{\Psi}\, \exp\left(iS + i\Delta S_k + i\int_x J_i(x)\tilde{\Psi}_i(x) + i\int_x \tilde{J}_i(x)\psi_i(x)\right)\partial_k \Delta S_k \\ &= \partial_k \langle \Delta S_k \rangle\,. \end{aligned} \tag{D.6}$$

Using the superfield notation, the regulator can be written as

$$\Delta S_k = -\frac{1}{2}\int_{xy}\left(\tilde{\Psi}_i(x) R_{ij,k}(x,y)\psi_j(y) + \psi_i(x) R_{ij}(x,y)\tilde{\Psi}_j(y)\right) \tag{D.7}$$

Combining Eq. (D.3) and Eq. (D.5), we find

$$\partial_k \tilde{\Gamma}_k = -\frac{1}{2}\int_{xy}(\partial_k R_{ij,k}(x,y))\left(\langle\tilde{\Psi}_i(x)\psi_j(y)\rangle + \langle\psi_i(x)\tilde{\Psi}_j(y)\rangle\right)\,. \tag{D.8}$$

Using the definitions

$$-iG^R_{ij,k}(x,y) = \langle\psi_i(x)\tilde{\Psi}_j(y)\rangle - \langle\psi_i(x)\rangle\langle\tilde{\Psi}_j(y)\rangle\,, \tag{D.9a}$$

$$-iG^A_{ij,k}(x,y) = \langle\tilde{\Psi}_i(x)\psi_j(y)\rangle - \langle\tilde{\Psi}_i(x)\rangle\langle\psi_j(y)\rangle\,, \tag{D.9b}$$

of the connected retarded and advanced 2-point correlation functions, one can write

$$\begin{aligned}\partial_k \tilde{\Gamma}_k = -\frac{1}{2}\int_{xy}(\partial_k R_{ij,k}(x,y))\big(&- iG^A_{ij,k}(x,y) - iG^R_{ij,k}(x,y) \\ &+ \langle\tilde{\Psi}_i(x)\rangle\langle\psi_j(y)\rangle + \langle\psi_i(x)\rangle\langle\tilde{\Psi}_j(y)\rangle\big)\,. \end{aligned} \tag{D.10}$$

Using $\Gamma_k = \tilde{\Gamma}_k - \Delta S_k$, we obtain

$$\partial_k \Gamma_k = \frac{i}{2}(\partial_k R_{ij,k}(x,y))\left(G^R_{ij,k}(x,y) + G^A_{ij,k}(x,y)\right) \tag{D.11}$$

for the flow of the effective average action. Moreover, using the symmetry relation

$$G^R_{ij,k}(x,y) = G^A_{ji,k}(y,x) \tag{D.12}$$

which can be seen directly from their definition (D.9), and by combining the retarded, advanced, statistical, and anomalous propagators into a 2×2-matrix in the MSR $(\psi,\tilde{\Psi})$ space according to (where the subscript $_c$ denotes the connected part of the correlation function)

$$G_k[\psi,\tilde{\Psi}] = \begin{pmatrix} i\langle\psi_i(x)\psi_j(y)\rangle_c & i\langle\psi_i(x)\tilde{\Psi}_j(y)\rangle_c \\ i\langle\tilde{\Psi}_i(x)\psi_j(y)\rangle_c & i\langle\tilde{\Psi}_i(x)\tilde{\Psi}_j(y)\rangle_c\end{pmatrix} = \begin{pmatrix} iF_{ij,k}(x,y) & G^R_{ij,k}(x,y) \\ G^A_{ij,k}(x,y) & i\widetilde{F}_{ij,k}(x,y)\end{pmatrix}\,, \tag{D.13}$$

and analogously the regulator as a 2×2 matrix in the same MSR space,

$$\hat{R}_k = \begin{pmatrix} 0 & R_{ij,k}(x,y) \\ R_{ij,k}(x,y) & 0\,,\end{pmatrix} \tag{D.14}$$

we can compactly express the flow equation (D.11) as

$$\partial_k \Gamma_k = \frac{i}{2}\,\mathrm{tr}\left\{\partial_k R_k \circ G^R_k + \partial_k R_k \circ G^A_k\right\} = \frac{i}{2}\,\mathrm{tr}\left\{\partial_k \hat{R}_k \circ G_k\right\} \tag{D.15}$$

with the trace

$$\mathrm{tr}\,\{A\circ B\} = \int_{xy} A_{ij}(x,y)B_{ji}(y,x) \tag{D.16}$$

acting in superfield and coordinate space. This finalizes the derivation of the tree-level flow equation (3.71).

D.2 Convergence towards the bare action in the UV limit $k \to \Lambda$

In this section we show that the effective average action Γ_k indeed converges to the bare MSR action S (up to a Jacobian determinant), even if the regulator is coupled to the composite response fields $\tilde{\Psi}$ instead of the usual elementary response fields $\tilde{\psi}$. This is not entirely trivial, since one has to make sure that all fluctuations are properly suppressed in the limit $k \to \Lambda$ [179]. We start from the background field identity,

$$\Gamma_k[\psi, \tilde{\Psi}] = S'[\psi, \tilde{\Psi}] - i \log \Delta Z_k \tag{D.17}$$

with $S'[\psi, \tilde{\Psi}] \equiv S[\psi, \tilde{\psi}]$ and

$$\begin{aligned} \Delta Z_k = \int \mathcal{D}\psi' \, \mathcal{D}\tilde{\psi}' \, \exp\Bigg\{ & i(S[\psi', \tilde{\psi}'] - S[\psi, \tilde{\psi}]) - i\left(\frac{\delta\Gamma_k}{\delta\psi}, \psi' - \psi\right) - i\left(\frac{\delta\Gamma_k}{\delta\tilde{\Psi}}, \tilde{\Psi}' - \tilde{\Psi}\right) \\ & - i\left(\frac{\delta\Delta S_k}{\delta\psi}, \psi' - \psi\right) - i\left(\frac{\delta\Delta S_k}{\delta\tilde{\Psi}}, \tilde{\Psi}' - \tilde{\Psi}\right) + i(\Delta S_k[\psi', \tilde{\Psi}'] - \Delta S_k[\psi, \tilde{\Psi}])\Bigg\} \end{aligned} \tag{D.18}$$

where $(\cdot, \cdot)$ here denotes the inner product

$$(A, B) \equiv \int_x A_i(x) B_i(x) \, . \tag{D.19}$$

We now do a variable substitution in the path integral to the new (composite) response fields, $\tilde{\psi}' \to \tilde{\Psi}'$,

$$\mathcal{D}\tilde{\psi}' = \left| \det \frac{\delta\tilde{\psi}'}{\delta\tilde{\Psi}'} \right| \mathcal{D}\tilde{\Psi}' \tag{D.20}$$

and perform a subsequent shift in the path integral, $\psi' \to \psi + \psi'$, $\tilde{\Psi}' \to \tilde{\Psi} + \tilde{\Psi}'$, such that afterwards ψ' and $\tilde{\Psi}'$ describe the fluctuations around the expectation values ψ and $\tilde{\Psi}$,

$$\begin{aligned} \Delta Z_k = \int \mathcal{D}\psi' \, \mathcal{D}\tilde{\Psi}' \left| \det \frac{\delta\tilde{\psi}'}{\delta\tilde{\Psi}'}(\psi + \psi', \tilde{\Psi} + \tilde{\Psi}') \right| \exp\Bigg\{ & i(S'[\psi + \psi', \tilde{\Psi} + \tilde{\Psi}'] - S'[\psi, \tilde{\Psi}]) \\ & - i\left(\frac{\delta\Gamma_k}{\delta\psi}, \psi'\right) - i\left(\frac{\delta\Gamma_k}{\delta\tilde{\Psi}}, \tilde{\Psi}'\right) + i\Delta S_k[\psi', \tilde{\Psi}']\Bigg\} \end{aligned} \tag{D.21}$$

where we used that the regulator is quadratic in the (composite) fields. We can rewrite (D.21) as

$$\begin{aligned} \Delta Z_k = \exp\Bigg\{ & i\left(S'\left[\psi - i\frac{\delta}{\delta\tilde{j}}, \tilde{\Psi} - i\frac{\delta}{\delta j}\right] - S'[\psi, \tilde{\Psi}]\right) \\ & - \left(\frac{\delta\Gamma_k}{\delta\psi}, \frac{\delta}{\delta\tilde{j}}\right) - \left(\frac{\delta\Gamma_k}{\delta\tilde{\Psi}}, \frac{\delta}{\delta j}\right)\Bigg\} \left| \det \frac{\delta\tilde{\psi}}{\delta\tilde{\Psi}}\left(\psi - i\frac{\delta}{\delta\tilde{j}}, \tilde{\Psi} - i\frac{\delta}{\delta j}\right)\right| \\ & \int \mathcal{D}(\psi', \tilde{\Psi}') \; \exp\left\{ i\Delta S_k[\psi', \tilde{\Psi}'] + i(\tilde{j}, \psi') + i(j, \tilde{\Psi}')\right\}\Bigg|_{j=\tilde{j}=0} . \end{aligned} \tag{D.22}$$

Due to the properties of the regulator term ΔS_k, one can now straightforwardly verify that in the UV limit $k \to \Lambda$ the remaining integral becomes independent of sources $j, \tilde{j}$ in the vicinity of $j = \tilde{j} = 0$ where the functional derivatives are evaluated. By taking the limit $k \to \Lambda$ of (D.22) we finally arrive at

$$\Gamma_k[\psi, \tilde{\Psi}] \xrightarrow{k \to \Lambda} S'[\psi, \tilde{\Psi}] - i \log \left| \det \frac{\delta\tilde{\psi}}{\delta\tilde{\Psi}} \right| + \text{const.} \tag{D.23}$$

which coincides with (3.79). (Because the transformation $\tilde{\Psi} = J(\psi)\tilde{\psi}$ is linear in the usual response fields $\tilde{\psi}$, the remaining determinant actually only depends on the classical fields ψ, not on the response fields $\tilde{\Psi}$.)

This result can be compared with Eq. (3.26), where the non-linear field transformation is performed on the level of the generating functional. In this case, the regulator term is actually quadratic in the *transformed* fields $(\psi, \tilde{\Psi})$, such that the effective average action converges to the 'bare' MSR action $\Gamma_k \to S' - i \log \mathcal{J}'[\psi]$, but the 'bare' MSR action then contains the logarithm of the Jacobian determinant anyway. This highlights the equivalence of the two approaches of either (i) keeping the 'standard' response fields $\tilde{\psi}$ as the fields in the path integral, and coupling the regulator to the composite response fields $\tilde{\Psi} = J(\psi)\tilde{\psi}$ which we followed in the present subsection, or (ii) performing the non-linear field transformation on the level of the path integral, such that the regulator is quadratic in $(\psi, \tilde{\Psi})$. In both cases, one obtains an additional logarithm of a Jacobian determinant in the action, which can be practically handled by rewriting the determinant as an integral over Grassmann-valued ghost fields, as we have already discussed in more detail in Appendix B.2 above.

D.3 Regulators for ghosts

We need to ensure that the normalization condition $Z_k[J] \equiv Z_k[J, \tilde{J} = 0] = 1$ is satisfied at all FRG scales k. A sufficient condition for this is that the BRST transformation (3.62) is a symmetry of the scale-dependent effective average action Γ_k at all FRG scales k. This can be achieved by choosing ΔS_k to be BRST exact,

$$\Delta S_k = -\tilde{\Psi}_i R_{ij,k} \psi_j + i\tilde{c}_i R_{ij,k} c_j = Q\left(-i\tilde{c}_i R_{ij,k}\psi_j\right) , \tag{D.24}$$

which implies $Q(\Delta S_k) = 0$ due to the nilpotency $Q^2 = 0$ of the BRST transformation. In particular, introducing a regulator for the ghost fields ensures that the flow of acausal two-point functions stays zero. Due to causality, two-point functions such as $\Gamma_k^{\psi\psi}$ should be zero at all FRG scales. However, for a general truncation of Γ_k, there might appear non-vanishing diagrams on the right-hand sides of the flow equations for these acausal two-point functions. This will not cause any problem because one can show that diagrams containing ghost fields in the loop will cancel exactly with the appearing acausal diagrams, which ensures that the flow of these acausal two-point functions vanishes. The relation between the ghost fields and causality is also discussed for example in Refs. [82, 191–194]. In fact, the ghosts *solely* appear here to cancel contributions from acausal diagrams. As such, one can simply omit all ghost diagrams and all acausal diagrams, since the two precisely cancel. This is analogous to the cancellation scheme of acausal diagrams known from perturbation theory [82], but here formulated for the FRG flow.

Appendix E

1PI vertex functions of Model G

In this appendix we list the explicit expressions for the 1PI vertex functions that occur in the diagrams in Eqs. (3.114) – (3.120), extracted from our truncation of the effective average action (3.94) by expanding the Jacobian (3.97) in a Neumann series and subsequently evaluating suitable functional derivatives on the expanded terms. We have verified our analytical calculation explicitly using *DoFun* [226] in special cases.

The relevant 'classical' vertices (i.e. those with one response field) are given by:

$$\Gamma_k^{\phi_a\phi_b\tilde{N}_{cd}}(p,q,r) = g_k \frac{iZ^\omega_{\phi,k}(q^0-p^0)}{\gamma_{\phi,k}\,\gamma_{n,k}(\boldsymbol{r})}\,(\delta_{ac}\delta_{bd}-\delta_{ad}\delta_{bc})\,(2\pi)^D\delta(p+q+r) \tag{E.1}$$

$$\Gamma_k^{\phi_a\tilde{\Phi}_b n_{cd}}(p,q,r) = -g_k \frac{iZ^\omega_{n,k}r^0}{\gamma_{\phi,k}\,\gamma_{n,k}(\boldsymbol{r})}\,(\delta_{ac}\delta_{bd}-\delta_{ad}\delta_{bc})\,(2\pi)^D\delta(p+q+r) \tag{E.2}$$

$$\begin{aligned}\Gamma_k^{n_{ab}n_{cd}\tilde{N}_{ef}}(p,q,r) = \frac{g_k}{\gamma_{n,k}(\boldsymbol{r})}\Bigg[&\frac{iZ^\omega_{n,k}p^0}{\gamma_{n,k}(\boldsymbol{p})}(\delta_{ae}\delta_{bc}\delta_{df}-\delta_{af}\delta_{bc}\delta_{de}-\delta_{ac}\delta_{be}\delta_{df}+\delta_{ac}\delta_{bf}\delta_{de}\\ &-\delta_{ae}\delta_{bd}\delta_{cf}+\delta_{af}\delta_{bd}\delta_{ce}+\delta_{ad}\delta_{be}\delta_{cf}-\delta_{ad}\delta_{bf}\delta_{ce})\\ &+\frac{iZ^\omega_{n,k}q^0}{\gamma_{n,k}(\boldsymbol{q})}(\delta_{ad}\delta_{bf}\delta_{ce}-\delta_{ad}\delta_{be}\delta_{cf}-\delta_{ac}\delta_{bf}\delta_{de}+\delta_{ac}\delta_{be}\delta_{df}\\ &-\delta_{bd}\delta_{af}\delta_{ce}+\delta_{bd}\delta_{ae}\delta_{cf}+\delta_{bc}\delta_{af}\delta_{de}-\delta_{bc}\delta_{ae}\delta_{df})\Bigg]\times\\ &(2\pi)^D\delta(p+q+r)\end{aligned} \tag{E.3}$$

The relevant 'anomalous' vertices (i.e. those with two response fields) are given by:

$$\Gamma_k^{\phi_a\tilde{\Phi}_b\tilde{N}_{cd}}(p,q,r) = 0 \quad \text{(by symmetry)} \tag{E.4}$$

$$\Gamma_k^{n_{ab}\tilde{N}_{cd}\tilde{N}_{ef}}(p,q,r) = 0 \quad \text{(by symmetry)} \tag{E.5}$$

$$\begin{aligned}\Gamma_k^{\phi_a\phi_b\tilde{\Phi}_c\tilde{\Phi}_d}(p,q,r,s) = &(2Z^\omega_{\phi,k}-Z^\omega_{n,k})\frac{2g_k^2iT}{\gamma^2_{\phi,k}}\times\\ &\left[\delta_{ac}\delta_{bd}\frac{1}{\gamma_{n,k}(\boldsymbol{p}+\boldsymbol{r})}+\delta_{ad}\delta_{bc}\frac{1}{\gamma_{n,k}(\boldsymbol{p}+\boldsymbol{s})}-\delta_{ab}\delta_{cd}\left(\frac{1}{\gamma_{n,k}(\boldsymbol{p}+\boldsymbol{r})}+\frac{1}{\gamma_{n,k}(\boldsymbol{p}+\boldsymbol{s})}\right)\right]\times\\ &(2\pi)^D\delta(p+q+r+s)\end{aligned} \tag{E.6}$$

$$\Gamma_k^{\phi_a\phi_b\tilde{N}_{cd}\tilde{N}_{ef}}(p,q,r,s) = (2Z^{\omega}_{n,k} - Z^{\omega}_{\phi,k})\frac{2g_k^2 Z^{\omega}_{n,k} iT}{\gamma_{\phi,k}\,\gamma_{n,k}(\boldsymbol{r})\,\gamma_{n,k}(\boldsymbol{s})}\times$$
$$\Big[+\delta_{ad}\delta_{be}\delta_{cf} + \delta_{bd}\delta_{ae}\delta_{cf} - \delta_{ad}\delta_{ce}\delta_{bf} - \delta_{bd}\delta_{ce}\delta_{af}$$
$$- \delta_{ac}\delta_{be}\delta_{df} - \delta_{bc}\delta_{ae}\delta_{df} + \delta_{ac}\delta_{de}\delta_{bf} + \delta_{bc}\delta_{de}\delta_{af}\Big]\times$$
$$(2\pi)^D\delta(p+q+r+s) \tag{E.7}$$

$$\Gamma_k^{n_{gh}n_{ij}\tilde{N}_{kl}\tilde{N}_{mn}}(p,q,r,s) = \frac{2g_k^2 Z^{\omega}_{n,k} iT}{\gamma_{n,k}(\boldsymbol{s})\,\gamma_{n,k}(\boldsymbol{r})}\times$$
$$\Big[\frac{1}{\gamma_{n,k}(\boldsymbol{p}+\boldsymbol{r})}\big(+\delta_{gn}\delta_{hl}\delta_{im}\delta_{jk} - \delta_{gn}\delta_{hk}\delta_{im}\delta_{jl} - \delta_{gn}\delta_{hl}\delta_{ik}\delta_{jm} + \delta_{gn}\delta_{hk}\delta_{il}\delta_{jm}$$
$$- \delta_{gl}\delta_{hn}\delta_{im}\delta_{jk} + \delta_{gk}\delta_{hn}\delta_{im}\delta_{jl} + \delta_{gl}\delta_{hn}\delta_{ik}\delta_{jm} - \delta_{gk}\delta_{hn}\delta_{il}\delta_{jm}$$
$$- \delta_{gm}\delta_{hl}\delta_{in}\delta_{jk} + \delta_{gm}\delta_{hk}\delta_{in}\delta_{jl} + \delta_{gl}\delta_{hm}\delta_{in}\delta_{jk} - \delta_{gk}\delta_{hm}\delta_{in}\delta_{jl}$$
$$- \delta_{gl}\delta_{hj}\delta_{in}\delta_{km} + \delta_{gj}\delta_{hl}\delta_{in}\delta_{km} + \delta_{gk}\delta_{hj}\delta_{in}\delta_{lm} - \delta_{gj}\delta_{hk}\delta_{in}\delta_{lm}$$
$$+ \delta_{gm}\delta_{hl}\delta_{ik}\delta_{jn} - \delta_{gm}\delta_{hk}\delta_{il}\delta_{jn} - \delta_{gl}\delta_{hm}\delta_{ik}\delta_{jn} + \delta_{gk}\delta_{hm}\delta_{il}\delta_{jn}$$
$$+ \delta_{gl}\delta_{hi}\delta_{jn}\delta_{km} - \delta_{gi}\delta_{hl}\delta_{jn}\delta_{km} - \delta_{gk}\delta_{hi}\delta_{jn}\delta_{lm} + \delta_{gi}\delta_{hk}\delta_{jn}\delta_{lm}$$
$$+ \delta_{gl}\delta_{hj}\delta_{im}\delta_{kn} - \delta_{gj}\delta_{hl}\delta_{im}\delta_{kn} - \delta_{gl}\delta_{hi}\delta_{jm}\delta_{kn} + \delta_{gi}\delta_{hl}\delta_{jm}\delta_{kn}$$
$$- \delta_{gk}\delta_{hj}\delta_{im}\delta_{ln} + \delta_{gj}\delta_{hk}\delta_{im}\delta_{ln} + \delta_{gk}\delta_{hi}\delta_{jm}\delta_{ln} - \delta_{gi}\delta_{hk}\delta_{jm}\delta_{ln}\big) +$$
$$\frac{1}{\gamma_{n,k}(\boldsymbol{q}+\boldsymbol{r})}\big(+\delta_{gn}\delta_{hl}\delta_{im}\delta_{jk} - \delta_{gn}\delta_{hk}\delta_{im}\delta_{jl} - \delta_{gn}\delta_{hl}\delta_{ik}\delta_{jm} + \delta_{gn}\delta_{hk}\delta_{il}\delta_{jm}$$
$$- \delta_{gn}\delta_{hj}\delta_{il}\delta_{km} + \delta_{gn}\delta_{hi}\delta_{jl}\delta_{km} + \delta_{gn}\delta_{hj}\delta_{ik}\delta_{lm} - \delta_{gn}\delta_{hi}\delta_{jk}\delta_{lm}$$
$$- \delta_{gl}\delta_{hn}\delta_{im}\delta_{jk} + \delta_{gk}\delta_{hn}\delta_{im}\delta_{jl} + \delta_{gl}\delta_{hn}\delta_{ik}\delta_{jm} - \delta_{gk}\delta_{hn}\delta_{il}\delta_{jm}$$
$$+ \delta_{gj}\delta_{hn}\delta_{il}\delta_{km} - \delta_{gi}\delta_{hn}\delta_{jl}\delta_{km} - \delta_{gj}\delta_{hn}\delta_{ik}\delta_{lm} + \delta_{gi}\delta_{hn}\delta_{jk}\delta_{lm}$$
$$- \delta_{gm}\delta_{hl}\delta_{in}\delta_{jk} + \delta_{gm}\delta_{hk}\delta_{in}\delta_{jl} + \delta_{gl}\delta_{hm}\delta_{in}\delta_{jk} - \delta_{gk}\delta_{hm}\delta_{in}\delta_{jl}$$
$$+ \delta_{gm}\delta_{hl}\delta_{ik}\delta_{jn} - \delta_{gm}\delta_{hk}\delta_{il}\delta_{jn} - \delta_{gl}\delta_{hm}\delta_{ik}\delta_{jn} + \delta_{gk}\delta_{hm}\delta_{il}\delta_{jn}$$
$$+ \delta_{gm}\delta_{hj}\delta_{il}\delta_{kn} - \delta_{gm}\delta_{hi}\delta_{jl}\delta_{kn} - \delta_{gj}\delta_{hm}\delta_{il}\delta_{kn} + \delta_{gi}\delta_{hm}\delta_{jl}\delta_{kn}$$
$$- \delta_{gm}\delta_{hj}\delta_{ik}\delta_{ln} + \delta_{gm}\delta_{hi}\delta_{jk}\delta_{ln} + \delta_{gj}\delta_{hm}\delta_{ik}\delta_{ln} - \delta_{gi}\delta_{hm}\delta_{jk}\delta_{ln}\big)\Big]\times$$
$$(2\pi)^D\delta(p+q+r+s) \tag{E.8}$$

Appendix F

Extraction of the dynamic critical exponent in Model G

To extract the dynamic critical exponent $z_\phi = 2 - \eta_\perp - x_{\Gamma^\phi}$ (with $\eta_\perp = 0$ in our truncation), we consider the functions $f_i(\log k) \equiv k\partial_k \log \Gamma_k^\phi$ for different reduced temperatures τ_i close to the critical point. Each function $f_i(\log k)$ can be seen as a 'flowing' exponent, since in the strict scaling regime where $\Gamma_k^\phi \sim k^{-x_{\Gamma^\phi}}$ it is equal to the critical exponent $-x_{\Gamma^\phi}$. To determine the critical exponent from our data, we first determine the inflection point $\log k_i$ for each $f_i(\log k)$. For illustration, in the case of $d = 3.5$ spatial dimension the inflection points are plotted in the left panel of Fig. F.1. We assume that, near the critical point, the values $f_i(\log k_i)$ at the inflection points depend on the reduced temperatures τ_i as a power law $f_i(\log k_i) = a + b\,\tau_i^c$ with real a, b, and positive $c > 0$, such that for $\tau \to 0$ we would obtain the critical exponent $a = -x_{\Gamma^\phi}$. Introducing the variable $x_i \equiv (\log \tau_i)^{-1}$, we plot the values $f_i(\log k_i)$ against x_i, as shown in the right panel of Fig. F.1. To extrapolate these points to $(\log \tau)^{-1} = 0$ (corresponding to $T = T_c$), we fit these points with $f(x) = a + b\,e^{c/x}$, corresponding to our power-law assumption from above, and then take $f(0) = a$ as the extrapolated value for $-x_{\Gamma^\phi}$. We take the uncertainty σ_a of the coefficient a in the fit as an estimate for the error of our procedure. We employ analogous extractions in $d = 3$ and $d = 2.5$ spatial dimensions.

Similarly, we extract the dynamic critical exponent $z_n = 2 - x_\gamma$ of the charge densities by first determining the minima of the function $f_i(\log k) \equiv k\partial_k \log \gamma_k^n(k)/k^2$ for different reduced temperatures τ_i, since the corresponding values $f_i(\log k_i)$ at the minima $\log k_i$ approach the critical exponent $-x_\gamma$ in the scaling regime. For illustration, in the case of $d = 3$ spatial dimensions the points are plotted for different reduced temperatures in Fig. F.2. In a second step, we plot the values of $f_i(\log k_i)$ at the minima against $(\log \tau_i)^{-1}$, and extrapolate them to $(\log \tau)^{-1} = 0$ using the same method as described above.

In addition, we extract the dynamic critical exponent $z_n = 2 - x_\gamma$ also from the minima of $p\partial_p \log \gamma_{k=0}^n(p)/p^2$ as a function of $\log p$ at $k = 0$ (since one has $\gamma_{k=0}^n(p) \sim p^{-x_\gamma}$ in the scaling regime), as illustrated in Fig. F.3.

The resulting values of a and σ_a from the three extrapolations are listed in Tables F.1, F.2, and F.3 for $d = 2.5, 3, 3.5$ spatial dimensions.

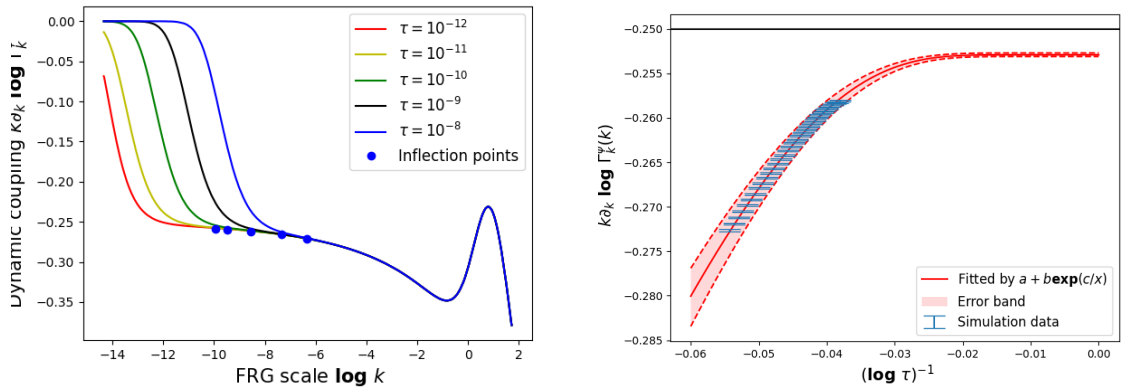

Figure F.1: Extraction of z_ϕ in $d = 3.5$ spatial dimensions. The error band is given by the uncertainty of the parameters a, b and c in the fit.

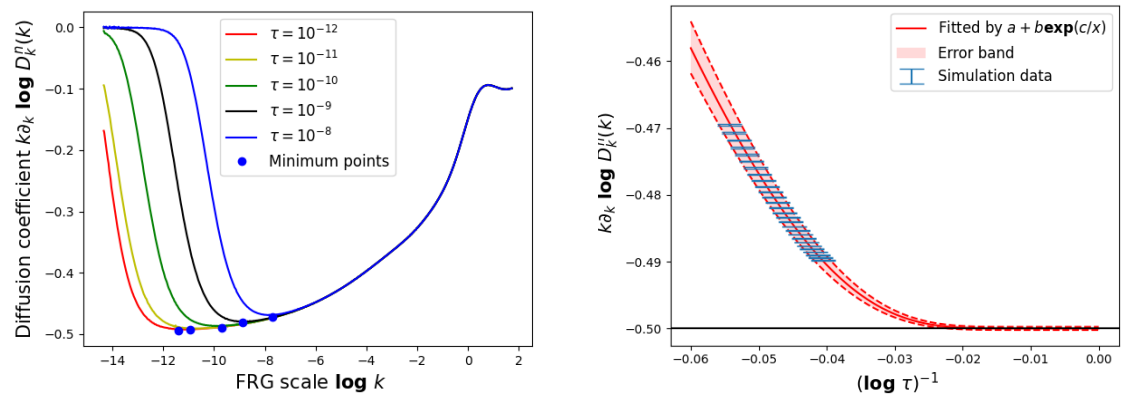

Figure F.2: Extraction of z_n in $d = 3$ spatial dimensions using the minima of the functions $f(k) = k\partial_k \log \gamma^n_k(k)/k^2$ for various reduced temperatures τ_i close to the critical point. The error band is determined from the uncertainty of the parameters a, b and c in the fit.

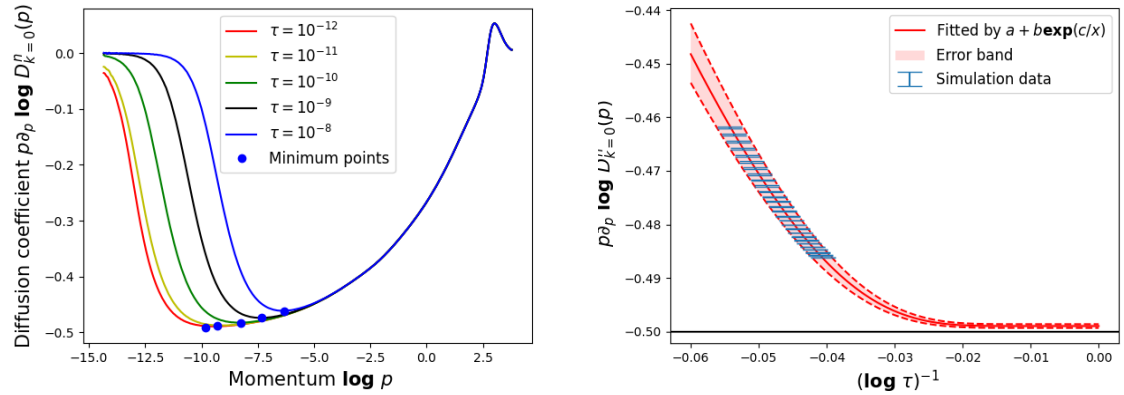

Figure F.3: Extraction of z_n in $d = 3$ spatial dimensions using the minima of the functions $f_i(p) = p\partial_p \log \gamma^n_{k=0}(p)/p^2$ for various reduced temperatures τ_i close to the critical point. The error band is determined by the uncertainty of the parameters a, b and c in the fit.

d	a	σ_a
3.5	-0.253	0.003
3.0	-0.501	0.001
2.5	-0.750	0.000

Table F.1: a and σ_a from fitting the inflection points of $k\partial_k \log \Gamma_k^\phi$ as a function of $\log k$ with $f(x) = a + b\, e^{c/x}$, which gives the result and error of $a = -x_{\Gamma^\phi} = z_\phi + \eta_\perp - 2$ (with $\eta_\perp = 0$ in our truncation).

d	a	σ_a
3.5	-0.246	0.005
3.0	-0.500	0.000
2.5	-0.749	0.001

Table F.2: a and σ_a from fitting the minimum points of $k\partial_k \log \gamma_k^n(k)/k^2$ as a function of $\log k$ with $f(x) = a + b\, e^{c/x}$, which gives the result and error of $a = -x_\gamma = z_n - 2$.

d	a	σ_a
3.5	-0.260	0.010
3.0	-0.499	0.001
2.5	-0.749	0.001

Table F.3: a and σ_a from fitting the minimum points of $p\partial_p \log \gamma_{k=0}^n(p)/p^2$ as a function of $\log p$ with $f(x) = a + b\, e^{c/x}$, which gives the result and error of $a = -x_\gamma = z_n - 2$.

Appendix G

Details on the real-time FRG for the quark-meson model

G.1 Effective Keldysh action

Introducing external sources for the bosonic and fermionic degrees of freedom in the partition function (5.3), one obtains the generating functional for real-time correlation functions,

$$Z[\eta_1,\bar\eta_1,\eta_2,\bar\eta_2,j^q,j^c] \equiv \int \mathcal{D}\bar\psi_1\mathcal{D}\psi_1\mathcal{D}\bar\psi_2\mathcal{D}\psi_2\mathcal{D}\phi^c\mathcal{D}\phi^q \exp\Big\{iS + i\int_x \left[j_a^q\phi_a^c + j_a^c\phi_a^q + \bar\eta_1\psi_2 + \bar\psi_2\eta_1 + \bar\eta_2\psi_1 + \bar\psi_1\eta_2\right]\Big\}. \tag{G.1}$$

Its logarithm, the Schwinger functional W, is the generator of connected correlation functions,

$$W[\eta_1,\bar\eta_1,\eta_2,\bar\eta_2,j^q,j^c] \equiv -i\log Z[\eta_1,\bar\eta_1,\eta_2,\bar\eta_2,j^q,j^c]\,. \tag{G.2}$$

One-point functions (i.e. field expectation values) are obtained from W via functional derivatives

$$\begin{aligned} \phi_a^c &= \frac{\delta W}{\delta j_a^q}\,, & \phi_a^q &= \frac{\delta W}{\delta j_a^c}\,, \\ \psi_1 &= \frac{\delta W}{\delta\bar\eta_2} \equiv \frac{\overrightarrow{\delta}}{\delta\bar\eta_2}W\,, & \bar\psi_1 &= \frac{\delta W}{\delta\bar\eta_2} \equiv W\frac{\overleftarrow{\delta}}{\delta\eta_2}\,, \\ \psi_2 &= \frac{\delta W}{\delta\bar\eta_1} \equiv \frac{\overrightarrow{\delta}}{\delta\bar\eta_1}W\,, & \bar\psi_2 &= \frac{\delta W}{\delta\eta_1} \equiv W\frac{\overleftarrow{\delta}}{\delta\eta_1}\,, \end{aligned} \tag{G.3}$$

where we use the convention that derivatives with respect to the bar fields $\bar\psi,\bar\eta,\ldots$ act from the left, and derivatives with respect to to $\psi,\eta,\ldots$ act from the right.

The effective action Γ, the generator of 1PI vertex functions, is related to the Schwinger functional via a Legendre transform,

$$\Gamma[\bar\psi_1,\psi_1,\bar\psi_2,\psi_2,\phi^c,\phi^q] \equiv W - \int_x \left[j_a^q\phi_a^c + j_a^c\phi_a^q + \bar\eta_1\psi_2 + \bar\psi_2\eta_1 + \bar\eta_2\psi_1 + \bar\psi_1\eta_2\right], \tag{G.4}$$

where the sources on the right-hand side are implicitly given by inverting the relations in (G.3).

G.2 Infinite damping calculation

Let I be a bosonic contribution to the flow of the form

$$I = \frac{k^4}{3\pi^2}\left\{ -\frac{T}{E^2+\gamma^2/4} + \frac{i}{2\pi E}\left[\psi\left(\frac{i\gamma/2+E}{2\pi iT}\right) - \psi\left(\frac{i\gamma/2-E}{2\pi iT}\right)\right]\right\} \tag{G.5}$$

with $E = \sqrt{M^2-\gamma^2/4}$ and $M^2 > 0$. In the limit $\gamma \to \infty$, with M^2 fixed, the energy E behaves as

$$E = \frac{i\gamma}{2} - \frac{iM^2}{\gamma} + \cdots \tag{G.6}$$

such that the arguments of the digamma functions in (G.5) become

$$\frac{i\gamma/2+E}{2\pi iT} = \frac{i\gamma - iM^2/\gamma + \cdots}{2\pi iT} = \frac{\gamma}{2\pi T} + \cdots \tag{G.7}$$

$$\frac{i\gamma/2-E}{2\pi iT} = \frac{iM^2/\gamma + \cdots}{2\pi iT} = \frac{M^2}{2\pi\gamma T} + \cdots \tag{G.8}$$

To evaluate these further, we use the asymptotic expansions

$$\psi(z) = \log z + \mathcal{O}\left(\frac{1}{z}\right) \qquad (z \to \infty) \tag{G.9}$$

$$\psi(z) = -\gamma_E - \frac{1}{z} + \mathcal{O}(z) \qquad (z \to 0) \tag{G.10}$$

where γ_E is the Euler-Mascheroni constant. This yields

$$\psi\left(\frac{\gamma}{2\pi T} + \cdots\right) = \log\left(\frac{\gamma}{2\pi T}\right) + \cdots \tag{G.11}$$

$$\psi\left(\frac{M^2}{2\pi\gamma T} + \cdots\right) = -\gamma_E - \frac{2\pi\gamma T}{M^2} + \cdots \tag{G.12}$$

With this, (G.5) becomes

$$I = \frac{k^4}{3\pi^2}\left\{ -\frac{T}{M^2} + \frac{i}{2\pi E}\left[\log\left(\frac{\gamma}{2\pi T}\right) + \gamma_E + \frac{2\pi\gamma T}{M^2} + \cdots\right]\right\} \tag{G.13}$$

where we also used that $E^2 + \gamma^2/4 = M^2$ is independent of γ. Expanding

$$\frac{i}{2\pi E} = \frac{1}{\pi\gamma} + \cdots \tag{G.14}$$

further yields

$$I = \frac{k^4}{3\pi^2}\left\{ -\frac{T}{M^2} + \frac{1}{\pi\gamma}\left[\log\left(\frac{\gamma}{2\pi T}\right) + \gamma_E + \frac{2\pi\gamma T}{M^2}\right] + \cdots\right\}. \tag{G.15}$$

We see that in the infinite-damping limit $\gamma \to \infty$ both the $(1/\gamma)\log(\gamma/2\pi T)$ and the γ_E/γ terms vanish, such that only the one survives where the two γ's in the numerator and the denominator cancel, which finally yields

$$I \to \frac{k^4 T}{3\pi^2 M^2} \qquad (\gamma \to \infty)\,. \tag{G.16}$$

Appendix H

Temperature dependence of the pion damping

The two models $\gamma_1(T)$ and $\gamma_2(T)$ for the temperature dependence of the pion damping defined in Eqs. (5.91) and (5.92) are plotted in Fig. H.1 against the damping factor exponents of Ref. [117] that were obtained using spectral reconstruction of lattice-QCD data. The trend of the black data points in Fig. H.1 suggests a linear dependence of the damping factor exponents at high temperatures, which is incorporated in both models $\gamma_1(T)$ and $\gamma_2(T)$. However, one can see in Fig. H.1 that the first model $\gamma_1(T)$ underestimates the size of the pion damping at higher temperatures. These rather large values for the pion damping are taken into account with $\gamma_2(T)$ in our second model (cf. Eq. (5.92)). As written in the main text, we choose the two parameters α and T_{**} to reproduce the qualitative shape of the reconstructed damping factor of exponents of Ref. [117], which leads to the values $\alpha \approx 5.5$ and $T_{**} \approx 200$ MeV.

There are, however, important caveats in this naive identification. In the spectral reconstruction of Ref. [117] a form for the spectral function is used that is different from our Breit-Wigner form of the present work. (The Breit-Wigner form originates from the Ohmic spectral distribution of the heat bath.) This means that, strictly speaking, the damping factor exponents of Ref. [117] can not be directly identified with our damping constant $\gamma(T)$. Nevertheless, we consider it to be important to study the situation where the pion damping is as large as the data from Ref. [117] suggests. Hence, for the scope of this work, we assume that at least the order of magnitude of our pion damping roughly matches to the damping-factor exponents of Ref. [117]. For the future it would be interesting to incorporate the thermoparticle assumption into the quark-meson model consistently, and study its effects both on the static equilibrium properties and the dynamical properties.

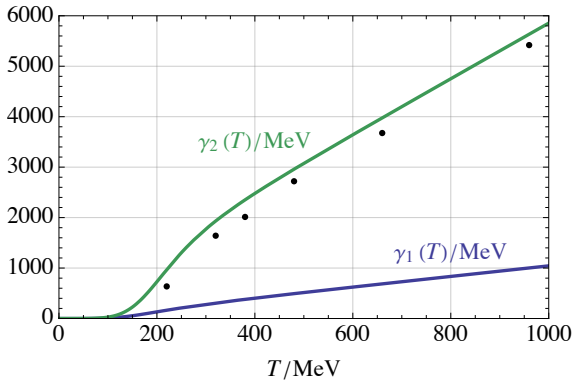

Figure H.1: The two models $\gamma_1(T)$ (blue) and $\gamma_2(T)$ (green) for the temperature dependence of the pion damping from Eqs. (5.91) and (5.92) plotted against the reconstructed damping-factor exponents of Ref. [117] (black).

Bibliography

[1] J.V. Roth and L. von Smekal, *Critical dynamics in a real-time formulation of the functional renormalization group*, *JHEP* **10** (2023) 065 [2303.11817].

[2] J.V. Roth, Y. Ye, S. Schlichting and L. von Smekal, *Dynamic critical behavior of the chiral phase transition from the real-time functional renormalization group*, *JHEP* (2025) 118 [2403.04573].

[3] J.V. Roth, Y. Ye, S. Schlichting and L. von Smekal, *Universal critical dynamics near the chiral phase transition and the QCD critical point*, *Phys. Rev. D* **111** (2025) L111901 [2409.14470].

[4] J.V. Roth, Y. Ye, S. Schlichting and L. von Smekal, *Effects of dissipation on phase diagram and bosonic excitations in the quark-meson model*, 2503.21746.

[5] D.J. Gross and F. Wilczek, *Ultraviolet Behavior of Nonabelian Gauge Theories*, *Phys. Rev. Lett.* **30** (1973) 1343.

[6] H.D. Politzer, *Reliable Perturbative Results for Strong Interactions?*, *Phys. Rev. Lett.* **30** (1973) 1346.

[7] HotQCD collaboration, *Chiral crossover in QCD at zero and non-zero chemical potentials*, *Phys. Lett. B* **795** (2019) 15 [1812.08235].

[8] F. Özel and P. Freire, *Masses, Radii, and the Equation of State of Neutron Stars*, *Ann. Rev. Astron. Astrophys.* **54** (2016) 401 [1603.02698].

[9] A.M. Halasz, A.D. Jackson, R.E. Shrock, M.A. Stephanov and J.J.M. Verbaarschot, *On the phase diagram of QCD*, *Phys. Rev. D* **58** (1998) 096007 [hep-ph/9804290].

[10] J. Berges and K. Rajagopal, *Color superconductivity and chiral symmetry restoration at nonzero baryon density and temperature*, *Nucl. Phys. B* **538** (1999) 215 [hep-ph/9804233].

[11] F. Karsch, *Critical behavior and net-charge fluctuations from lattice QCD*, *PoS* **CORFU2018** (2019) 163 [1905.03936].

[12] M. Asakawa and K. Yazaki, *Chiral Restoration at Finite Density and Temperature*, *Nucl. Phys. A* **504** (1989) 668.

[13] M. Buballa, *NJL model analysis of quark matter at large density*, *Phys. Rept.* **407** (2005) 205 [hep-ph/0402234].

[14] B.-J. Schaefer and J. Wambach, *The Phase diagram of the quark meson model*, *Nucl. Phys. A* **757** (2005) 479 [nucl-th/0403039].

[15] R.-A. Tripolt, C. Jung, L. von Smekal and J. Wambach, *Vector and axial-vector mesons in nuclear matter*, *Phys. Rev. D* **104** (2021) 054005 [2105.00861].

[16] Y. Aoki, G. Endrodi, Z. Fodor, S.D. Katz and K.K. Szabo, *The Order of the quantum chromodynamics transition predicted by the standard model of particle physics*, *Nature* **443** (2006) 675 [hep-lat/0611014].

[17] W.-j. Fu, J.M. Pawlowski and F. Rennecke, *QCD phase structure at finite temperature and density*, *Phys. Rev. D* **101** (2020) 054032 [1909.02991].

[18] F. Gao and J.M. Pawlowski, *Chiral phase structure and critical end point in QCD*, *Phys. Lett. B* **820** (2021) 136584 [2010.13705].

[19] P.J. Gunkel and C.S. Fischer, *Locating the critical endpoint of QCD: Mesonic backcoupling effects*, *Phys. Rev. D* **104** (2021) 054022 [2106.08356].

[20] J. Bernhardt and C.S. Fischer, *From imaginary to real chemical potential QCD with functional methods*, *Eur. Phys. J. A* **59** (2023) 181 [2305.01434].

[21] G. Basar, *QCD critical point, Lee-Yang edge singularities, and Padé resummations*, *Phys. Rev. C* **110** (2024) 015203 [2312.06952].

[22] D.A. Clarke, P. Dimopoulos, F. Di Renzo, J. Goswami, C. Schmidt, S. Singh et al., *Searching for the QCD critical endpoint using multi-point Padé approximations*, 2405.10196.

[23] O. DeWolfe, S.S. Gubser and C. Rosen, *A holographic critical point*, *Phys. Rev. D* **83** (2011) 086005 [1012.1864].

[24] M. Hippert, J. Grefa, T.A. Manning, J. Noronha, J. Noronha-Hostler, I. Portillo Vazquez et al., *Bayesian location of the QCD critical point from a holographic perspective*, *Phys. Rev. D* **110** (2024) 094006 [2309.00579].

[25] W. Busza, K. Rajagopal and W. van der Schee, *Heavy Ion Collisions: The Big Picture, and the Big Questions*, *Ann. Rev. Nucl. Part. Sci.* **68** (2018) 339 [1802.04801].

[26] P. Kovtun, D.T. Son and A.O. Starinets, *Viscosity in strongly interacting quantum field theories from black hole physics*, *Phys. Rev. Lett.* **94** (2005) 111601 [hep-th/0405231].

[27] BRAHMS collaboration, *Quark gluon plasma and color glass condensate at RHIC? The Perspective from the BRAHMS experiment*, *Nucl. Phys. A* **757** (2005) 1 [nucl-ex/0410020].

[28] PHENIX collaboration, *Formation of dense partonic matter in relativistic nucleus-nucleus collisions at RHIC: Experimental evaluation by the PHENIX collaboration*, *Nucl. Phys. A* **757** (2005) 184 [nucl-ex/0410003].

[29] PHOBOS collaboration, *The PHOBOS perspective on discoveries at RHIC*, *Nucl. Phys. A* **757** (2005) 28 [nucl-ex/0410022].

[30] STAR collaboration, *Experimental and theoretical challenges in the search for the quark gluon plasma: The STAR Collaboration's critical assessment of the evidence from RHIC collisions*, *Nucl. Phys. A* **757** (2005) 102 [nucl-ex/0501009].

[31] A. Pelissetto and E. Vicari, *Critical phenomena and renormalization group theory*, *Phys. Rept.* **368** (2002) 549 [cond-mat/0012164].

[32] F. Karsch, M. Neumann and M. Sarkar, *Scaling functions of the three-dimensional Z(2), O(2), and O(4) models and their finite-size dependence in an external field*, *Phys. Rev. D* **108** (2023) 014505 [2304.01710].

[33] P. Parotto, M. Bluhm, D. Mroczek, M. Nahrgang, J. Noronha-Hostler, K. Rajagopal et al., *QCD equation of state matched to lattice data and exhibiting a critical point singularity*, *Phys. Rev. C* **101** (2020) 034901 [1805.05249].

[34] M.S. Pradeep and M. Stephanov, *Universality of the critical point mapping between Ising model and QCD at small quark mass*, *Phys. Rev. D* **100** (2019) 056003 [1905.13247].

[35] M.A. Stephanov, *Non-Gaussian fluctuations near the QCD critical point*, *Phys. Rev. Lett.* **102** (2009) 032301 [0809.3450].

[36] M.A. Stephanov, *On the sign of kurtosis near the QCD critical point*, *Phys. Rev. Lett.* **107** (2011) 052301 [1104.1627].

[37] Y. Hatta and M.A. Stephanov, *Proton number fluctuation as a signal of the QCD critical endpoint*, *Phys. Rev. Lett.* **91** (2003) 102003 [hep-ph/0302002].

[38] STAR collaboration, *Nonmonotonic Energy Dependence of Net-Proton Number Fluctuations*, *Phys. Rev. Lett.* **126** (2021) 092301 [2001.02852].

[39] STAR collaboration, *Measurements of Proton High Order Cumulants in $\sqrt{s_{\rm NN}} = 3$ GeV Au+Au Collisions and Implications for the QCD Critical Point*, *Phys. Rev. Lett.* **128** (2022) 202303 [2112.00240].

[40] STAR collaboration, *Precision Measurement of (Net-)proton Number Fluctuations in Au+Au Collisions at RHIC*, 2504.00817.

[41] B. Friman, C. Hohne, J. Knoll, S. Leupold, J. Randrup, R. Rapp et al., eds., *The CBM physics book: Compressed baryonic matter in laboratory experiments*, vol. 814 (2011), 10.1007/978-3-642-13293-3.

[42] B. Berdnikov and K. Rajagopal, *Slowing out-of-equilibrium near the QCD critical point*, *Phys. Rev. D* **61** (2000) 105017 [hep-ph/9912274].

[43] S. Mukherjee, R. Venugopalan and Y. Yin, *Real time evolution of non-Gaussian cumulants in the QCD critical regime*, *Phys. Rev. C* **92** (2015) 034912 [1506.00645].

[44] M. Stephanov and Y. Yin, *Hydrodynamics with parametric slowing down and fluctuations near the critical point*, *Phys. Rev. D* **98** (2018) 036006 [1712.10305].

[45] M. Pradeep, K. Rajagopal, M. Stephanov and Y. Yin, *Freezing out fluctuations in Hydro+ near the QCD critical point*, *Phys. Rev. D* **106** (2022) 036017 [2204.00639].

[46] P.C. Hohenberg and B.I. Halperin, *Theory of dynamic critical phenomena*, *Rev. Mod. Phys.* **49** (1977) 435.

[47] D.T. Son and M.A. Stephanov, *Dynamic universality class of the QCD critical point*, *Phys. Rev. D* **70** (2004) 056001 [hep-ph/0401052].

[48] C. Chattopadhyay, J. Ott, T. Schaefer and V. Skokov, *Dynamic scaling of order parameter fluctuations in model B*, *Phys. Rev. D* **108** (2023) 074004 [2304.07279].

[49] L.J. Sieke, M. Harhoff, S. Schlichting and L. von Smekal, *Universal non-equilibrium scaling of cumulants across a critical point*, *Nucl. Phys. B* **1011** (2025) 116808 [2411.10266].

[50] C. Chattopadhyay, J. Ott, T. Schaefer and V.V. Skokov, *Simulations of Stochastic Fluid Dynamics near a Critical Point in the Phase Diagram*, *Phys. Rev. Lett.* **133** (2024) 032301 [2403.10608].

[51] C. Chattopadhyay, J. Ott, T. Schaefer and V.V. Skokov, *Critical fluid dynamics in two and three dimensions*, *Phys. Rev. D* **111** (2025) 034026 [2411.15994].

[52] G. Başar, J. Bhambure, R. Singh and D. Teaney, *Stochastic relativistic advection diffusion equation from the Metropolis algorithm*, *Phys. Rev. C* **110** (2024) 044903 [2403.04185].

[53] J. Bhambure, A. Mazeliauskas, J.-F. Paquet, R. Singh, M. Singh, D. Teaney et al., *Relativistic Viscous Hydrodynamics in the Density Frame: Numerical Tests and Comparisons*, 2412.10303.

[54] J. Bhambure, R. Singh and D. Teaney, *Stochastic relativistic viscous hydrodynamics from the Metropolis algorithm*, 2412.10306.

[55] HotQCD collaboration, *Chiral Phase Transition Temperature in (2+1)-Flavor QCD*, *Phys. Rev. Lett.* **123** (2019) 062002 [1903.04801].

[56] F. Cuteri, O. Philipsen and A. Sciarra, *On the order of the QCD chiral phase transition for different numbers of quark flavours*, *JHEP* **11** (2021) 141 [2107.12739].

[57] J. Braun, W.-j. Fu, J.M. Pawlowski, F. Rennecke, D. Rosenblüh and S. Yin, *Chiral susceptibility in (2+1)-flavor QCD*, *Phys. Rev. D* **102** (2020) 056010 [2003.13112].

[58] J. Bernhardt and C.S. Fischer, *QCD phase transitions in the light quark chiral limit*, *Phys. Rev. D* **108** (2023) 114018 [2309.06737].

[59] R.D. Pisarski and F. Wilczek, *Remarks on the Chiral Phase Transition in Chromodynamics*, *Phys. Rev. D* **29** (1984) 338.

[60] Particle Data Group Collaboration collaboration, *Review of particle physics*, *Phys. Rev. D* **110** (2024) 030001.

[61] E. Grossi, A. Soloviev, D. Teaney and F. Yan, *Soft pions and transport near the chiral critical point*, *Phys. Rev. D* **104** (2021) 034025 [2101.10847].

[62] K. Rajagopal and F. Wilczek, *Static and dynamic critical phenomena at a second order QCD phase transition*, *Nucl. Phys. B* **399** (1993) 395 [hep-ph/9210253].

[63] D. Devetak, A. Dubla, S. Floerchinger, E. Grossi, S. Masciocchi, A. Mazeliauskas et al., *Global fluid fits to identified particle transverse momentum spectra from heavy-ion collisions at the Large Hadron Collider*, *JHEP* **06** (2020) 044 [1909.10485].

[64] P. Lu, R. Kavak, A. Dubla, S. Masciocchi and I. Selyuzhenkov, *Quantification of the low-p_{T} pion excess in heavy-ion collisions at the LHC and top RHIC energy*, 2407.09207.

[65] E. Grossi, A. Soloviev, D. Teaney and F. Yan, *Transport and hydrodynamics in the chiral limit*, *Phys. Rev. D* **102** (2020) 014042 [2005.02885].

[66] A. Florio, E. Grossi, A. Soloviev and D. Teaney, *Dynamics of the $O(4)$ critical point in QCD*, 2111.03640.

[67] A. Florio, E. Grossi and D. Teaney, *Dynamics of the $O(4)$ critical point in QCD: critical pions and diffusion in Model G*, 2306.06887.

[68] A. Florio, E. Grossi, A. Mazeliauskas, A. Soloviev and D. Teaney, *Supercooled Goldstones at the QCD chiral phase transition*, 2504.03516.

[69] A. Florio, E. Grossi, A. Mazeliauskas, A. Soloviev and D. Teaney, *Quenching through the QCD chiral phase transition*, 2504.03514.

[70] A.Y. Kotov, M.P. Lombardo and A. Trunin, *QCD transition at the physical point, and its scaling window from twisted mass Wilson fermions*, *Phys. Lett. B* **823** (2021) 136749 [2105.09842].

[71] J. Braun et al., *Soft modes in hot QCD matter*, 2310.19853.

[72] C. Wetterich, *Exact evolution equation for the effective potential*, *Phys. Lett. B* **301** (1993) 90 [1710.05815].

[73] J. Berges, N. Tetradis and C. Wetterich, *Nonperturbative renormalization flow in quantum field theory and statistical physics*, *Phys. Rept.* **363** (2002) 223 [hep-ph/0005122].

[74] N. Dupuis, L. Canet, A. Eichhorn, W. Metzner, J.M. Pawlowski, M. Tissier et al., *The nonperturbative functional renormalization group and its applications*, *Phys. Rept.* **910** (2021) 1 [2006.04853].

[75] N. Tetradis and C. Wetterich, *Critical exponents from effective average action*, *Nucl. Phys. B* **422** (1994) 541 [hep-ph/9308214].

[76] D.F. Litim, *Critical exponents from optimized renormalization group flows*, *Nucl. Phys. B* **631** (2002) 128 [hep-th/0203006].

[77] I. Balog, H. Chaté, B. Delamotte, M. Marohnic and N. Wschebor, *Convergence of Nonperturbative Approximations to the Renormalization Group*, *Phys. Rev. Lett.* **123** (2019) 240604 [1907.01829].

[78] G. De Polsi, I. Balog, M. Tissier and N. Wschebor, *Precision calculation of critical exponents in the $O(N)$ universality classes with the nonperturbative renormalization group*, *Phys. Rev. E* **101** (2020) 042113 [2001.07525].

[79] G. De Polsi, G. Hernández-Chifflet and N. Wschebor, *Precision calculation of universal amplitude ratios in O(N) universality classes: Derivative expansion results at order O(∂4)*, *Phys. Rev. E* **104** (2021) 064101 [2109.14731].

[80] G. De Polsi and N. Wschebor, *Regulator dependence in the functional renormalization group: A quantitative explanation*, *Phys. Rev. E* **106** (2022) 024111 [2204.09170].

[81] L. Canet and H. Chate, *Non-perturbative Approach to Critical Dynamics*, *J. Phys.* **40** (2007) 1937 [cond-mat/0610468].

[82] L. Canet, H. Chate and B. Delamotte, *General framework of the non-perturbative renormalization group for non-equilibrium steady states*, *J. Phys. A* **44** (2011) 495001 [1106.4129].

[83] D. Mesterházy, J.H. Stockemer, L.F. Palhares and J. Berges, *Dynamic universality class of Model C from the functional renormalization group*, *Phys. Rev. B* **88** (2013) 174301 [1307.1700].

[84] C. Duclut and B. Delamotte, *Frequency regulators for the nonperturbative renormalization group: A general study and the model A as a benchmark*, *Phys. Rev. E* **95** (2017) 012107 [1611.07301].

[85] G. Aarts, *Spectral function at high temperature in the classical approximation*, *Phys. Lett. B* **518** (2001) 315 [hep-ph/0108125].

[86] J. Berges, S. Schlichting and D. Sexty, *Dynamic critical phenomena from spectral functions on the lattice*, *Nucl. Phys. B* **832** (2010) 228 [0912.3135].

[87] S. Schlichting, D. Smith and L. von Smekal, *Spectral functions and critical dynamics of the $O(4)$ model from classical-statistical lattice simulations*, *Nucl. Phys. B* **950** (2020) 114868 [1908.00912].

[88] D. Schweitzer, S. Schlichting and L. von Smekal, *Spectral functions and dynamic critical behavior of relativistic Z_2 theories*, *Nucl. Phys. B* **960** (2020) 115165 [2007.03374].

[89] D. Schweitzer, S. Schlichting and L. von Smekal, *Critical dynamics of relativistic diffusion*, *Nucl. Phys. B* **984** (2022) 115944 [2110.01696].

[90] J.V. Roth, D. Schweitzer, L.J. Sieke and L. von Smekal, *Real-time methods for spectral functions*, *Phys. Rev. D* **105** (2022) 116017.

[91] P. Buividovich, M. Hanada and A. Schäfer, *Real-time dynamics of matrix quantum mechanics beyond the classical approximation*, *EPJ Web Conf.* **175** (2018) 08006 [1711.05556].

[92] P.V. Buividovich, M. Hanada and A. Schäfer, *Quantum chaos, thermalization, and entanglement generation in real-time simulations of the Banks-Fischler-Shenker-Susskind matrix model*, *Phys. Rev. D* **99** (2019) 046011 [1810.03378].

[93] K. Maeda, M. Natsuume and T. Okamura, *Dynamic critical phenomena in the AdS/CFT duality*, *Phys. Rev. D* **78** (2008) 106007 [0809.4074].

[94] M. Edalati, J.I. Jottar and R.G. Leigh, *Shear Modes, Criticality and Extremal Black Holes*, *JHEP* **04** (2010) 075 [1001.0779].

[95] A. Buchel, *Critical phenomena in N=4 SYM plasma*, *Nucl. Phys. B* **841** (2010) 59 [1005.0819].

[96] M. Natsuume and T. Okamura, *Dynamic universality class of large-N gauge theories*, *Phys. Rev. D* **83** (2011) 046008 [1012.0575].

[97] S. Janiszewski and M. Kaminski, *Quasinormal modes of magnetic and electric black branes versus far from equilibrium anisotropic fluids*, *Phys. Rev. D* **93** (2016) 025006 [1508.06993].

[98] S. Huelsmann, S. Schlichting and P. Scior, *Spectral functions from the real-time functional renormalization group*, *Phys. Rev. D* **102** (2020) 096004 [2009.04194].

[99] R.-A. Tripolt, N. Strodthoff, L. von Smekal and J. Wambach, *Spectral Functions for the Quark-Meson Model Phase Diagram from the Functional Renormalization Group*, *Phys. Rev. D* **89** (2014) 034010 [1311.0630].

[100] P.C. Martin, E.D. Siggia and H.A. Rose, *Statistical Dynamics of Classical Systems*, *Phys. Rev. A* **8** (1973) 423.

[101] C. De Dominicis, *Techniques de renormalisation de la théorie des champs et dynamique des phénomènes critiques*, *J. Phys. Colloques* **37** (1976) C1.

[102] H.-K. Janssen, *On a lagrangean for classical field dynamics and renormalization group calculations of dynamical critical properties*, *Z. Phys. B* **23** (1976) 377.

[103] A. Onuki, *Phase Transition Dynamics*, Cambridge University Press (2002).

[104] U.C. Täuber, *Critical Dynamics: A Field Theory Approach to Equilibrium and Non-Equilibrium Scaling Behavior*, Cambridge University Press (2014), 10.1017/CBO9781139046213.

[105] L. Canet, B. Delamotte, O. Deloubriere and N. Wschebor, *Nonperturbative renormalization group study of reaction diffusion processes and directed percolation*, *Phys. Rev. Lett.* **92** (2004) 195703 [cond-mat/0309504].

[106] J. Berges and D. Mesterhazy, *Introduction to the nonequilibrium functional renormalization group*, *Nucl. Phys. B Proc. Suppl.* **228** (2012) 37 [1204.1489].

[107] L.M. Sieberer, A. Chiocchetta, A. Gambassi, U.C. Täuber and S. Diehl, *Thermodynamic Equilibrium as a Symmetry of the Schwinger-Keldysh Action*, *Phys. Rev. B* **92** (2015) 134307 [1505.00912].

[108] L. Canet, B. Delamotte and N. Wschebor, *Fully developed isotropic turbulence: symmetries and exact identities*, *Phys. Rev. E* **91** (2015) 053004 [1411.7778].

[109] S. Floerchinger and E. Grossi, *Conserved and nonconserved Noether currents from the quantum effective action*, *Phys. Rev. D* **105** (2022) 085015 [2102.11098].

[110] U.C. Täuber and Z. Rácz, *Critical behavior of O(n)-symmetric systems with reversible mode-coupling terms: Stability against detailed-balance violation*, *Phys. Rev. E* **55** (1997) 4120.

[111] E.D. Siggia, B.I. Halperin and P.C. Hohenberg, *Renormalization-group treatment of the critical dynamics of the binary-fluid and gas-liquid transitions*, *Phys. Rev. B* **13** (1976) 2110.

[112] L.T. Adzhemyan, A.N. Vasiliev, Y.S. Kabrits and M.V. Kompaniets, *H-model of critical dynamics: Two-loop calculations of rg functions and critical indices*, *Theoretical and Mathematical Physics* **119** (1999) 454.

[113] A. Altland, M. Fleischhauer and S. Diehl, *Symmetry classes of open fermionic quantum matter*, *Phys. Rev. X* **11** (2021) 021037 [2007.10448].

[114] A. Caldeira and A. Leggett, *Path integral approach to quantum brownian motion*, *Physica A: Statistical Mechanics and its Applications* **121** (1983) 587 .

[115] J.R. Pelaez, *From controversy to precision on the sigma meson: a review on the status of the non-ordinary $f_0(500)$ resonance*, *Phys. Rept.* **658** (2016) 1 [1510.00653].

[116] J.L. Goity and H. Leutwyler, *On the mean free path of pions in hot matter*, *Phys. Lett. B* **228** (1989) 517.

[117] P. Lowdon and O. Philipsen, *Pion spectral properties above the chiral crossover of QCD*, *JHEP* **10** (2022) 161 [2207.14718].

[118] A. Kamenev, *Field Theory of Non-Equilibrium Systems*, Cambridge University Press (2011), 10.1017/CBO9781139003667.

[119] A.K. Das, *Finite Temperature Field Theory*, World Scientific, New York (1997).

[120] K. Kamikado, N. Strodthoff, L. von Smekal and J. Wambach, *Real-time correlation functions in the $O(N)$ model from the functional renormalization group*, *Eur. Phys. J. C* **74** (2014) 2806 [1302.6199].

[121] J.M. Pawlowski and N. Strodthoff, *Real time correlation functions and the functional renormalization group*, *Phys. Rev. D* **92** (2015) 094009 [1508.01160].

[122] R.-A. Tripolt, P. Gubler, M. Ulybyshev and L. Von Smekal, *Numerical analytic continuation of Euclidean data*, *Comput. Phys. Commun.* **237** (2019) 129 [1801.10348].

[123] J. Horak, J.M. Pawlowski, J. Rodríguez-Quintero, J. Turnwald, J.M. Urban, N. Wink et al., *Reconstructing QCD spectral functions with Gaussian processes*, *Phys. Rev. D* **105** (2022) 036014 [2107.13464].

[124] J.M. Pawlowski, C.S. Schneider, J. Turnwald, J.M. Urban and N. Wink, *Yang-Mills glueball masses from spectral reconstruction*, *Phys. Rev. D* **108** (2023) 076018 [2212.01113].

[125] HotQCD collaboration, *Lattice QCD estimates of thermal photon production from the QGP*, *Phys. Rev. D* **110** (2024) 054518 [2403.11647].

[126] J.S. Schwinger, *Brownian motion of a quantum oscillator*, *J. Math. Phys.* **2** (1961) 407.

[127] L.V. Keldysh, *Diagram technique for nonequilibrium processes*, *Zh. Eksp. Teor. Fiz.* **47** (1964) 1515.

[128] L. Kadanoff and G. Baym, *Quantum Statistical Mechanics: Green's Function Methods in Equilibrium and Nonequilibrium Problems*, Frontiers in Physics: Lecture note and reprint series, A, W.A. Benjamin (1962).

[129] M. Gell-Mann and F. Low, *Bound states in quantum field theory*, *Phys. Rev.* **84** (1951) 350.

[130] R. Kubo, *Statistical-mechanical theory of irreversible processes. i. general theory and simple applications to magnetic and conduction problems*, *Journal of the Physical Society of Japan* **12** (1957) 570 [https://doi.org/10.1143/JPSJ.12.570].

[131] P.C. Martin and J. Schwinger, *Theory of many-particle systems. i*, *Phys. Rev.* **115** (1959) 1342.

[132] G.-L. Ingold, *Path integrals and their application to dissipative quantum systems*, *Lecture Notes in Physics* (2002) 1–53.

[133] U. Weiss, *Quantum Dissipative Systems*, WORLD SCIENTIFIC, 4th ed. (2012), 10.1142/8334, [https://www.worldscientific.com/doi/pdf/10.1142/8334].

[134] T. Schaefer and V. Skokov, *Dynamics of non-Gaussian fluctuations in model A*, *Phys. Rev. D* **106** (2022) 014006 [2204.02433].

[135] L.D. Landau and E.M. Lifshitz, *Statistical Physics, Part 1*, vol. 5 of *Course of Theoretical Physics*, Butterworth-Heinemann, Oxford (1980).

[136] N. Goldenfeld, *Lectures on phase transitions and the renormalization group (1st ed.)*, CRC Press (1992), 10.1201/9780429493492.

[137] J. Zinn-Justin, *Quantum field theory and critical phenomena*, *Int. Ser. Monogr. Phys.* **113** (2002) 1.

[138] K.G. Wilson and J.B. Kogut, *The Renormalization group and the epsilon expansion*, *Phys. Rept.* **12** (1974) 75.

[139] L.P. Kadanoff, *Scaling laws for Ising models near T(c)*, *Physics Physique Fizika* **2** (1966) 263.

[140] I. Dzyaloshinskii and G. Volovick, *Poisson brackets in condensed matter physics*, *Annals of Physics* **125** (1980) 67.

[141] D.T. Son, *Hydrodynamics of nuclear matter in the chiral limit*, *Phys. Rev. Lett.* **84** (2000) 3771 [hep-ph/9912267].

[142] R. Zwanzig, *Memory Effects in Irreversible Thermodynamics*, *Phys. Rev.* **124** (1961) 983.

[143] H. Mori, *Transport, Collective Motion, and Brownian Motion*, *Prog. Theor. Phys.* **33** (1965) 423.

[144] P. Hotzy, K. Boguslavski and D.I. Müller, *Advancing real-time Yang-Mills: towards real-time observables from first principles*, *PoS* **LATTICE2023** (2024) 194 [2401.05723].

[145] V. Prudnikov, A. Ivanov and A. Fedorenko, *Critical dynamics of spin systems in the four-loop approximation*, *Journal of Experimental and Theoretical Physics Letters* **66** (1997) 835.

[146] M.J. Dunlavy and D. Venus, *Critical slowing down in the two-dimensional ising model measured using ferromagnetic ultrathin films*, *Phys. Rev. B* **71** (2005) 144406.

[147] W. Zhong, G.T. Barkema, D. Panja and R.C. Ball, *Critical dynamical exponent of the two-dimensional scalar ϕ^4 model with local moves*, *Physical Review E* **98** (2018) 062128.

[148] M.P. Nightingale and H.W.J. Blöte, *Monte carlo computation of correlation times of independent relaxation modes at criticality*, *Phys. Rev. B* **62** (2000) 1089.

[149] L. Canet and H. Chaté, *A non-perturbative approach to critical dynamics*, *Journal of Physics A: Mathematical and Theoretical* **40** (2007) 1937–1949.

[150] L.T. Adzhemyan, D.A. Evdokimov, M. Hnatič, E.V. Ivanova, M.V. Kompaniets, A. Kudlis et al., *The dynamic critical exponent z for 2d and 3d Ising models from five-loop ε expansion*, *Phys. Lett. A* **425** (2022) 127870 [2111.04719].

[151] D. Mesterházy, J.H. Stockemer and Y. Tanizaki, *From quantum to classical dynamics: The relativistic $O(N)$ model in the framework of the real-time functional renormalization group*, *Phys. Rev. D* **92** (2015) 076001 [1504.07268].

[152] M. Hasenbusch, *Dynamic critical exponent z of the three-dimensional ising universality class: Monte carlo simulations of the improved blume-capel model*, *Phys. Rev. E* **101** (2020) 022126.

[153] L. Onsager, *Crystal statistics. i. a two-dimensional model with an order-disorder transition*, *Phys. Rev.* **65** (1944) 117.

[154] L. Batini, E. Grossi and N. Wink, *Dissipation dynamics of a scalar field*, *Phys. Rev. D* **108** (2023) 125021 [2309.06586].

[155] L. Canet, B. Delamotte, D. Mouhanna and J. Vidal, *Optimization of the derivative expansion in the nonperturbative renormalization group*, *Phys. Rev. D* **67** (2003) 065004 [hep-th/0211055].

[156] L. Canet, B. Delamotte, D. Mouhanna and J. Vidal, *Nonperturbative renormalization group approach to the Ising model: A Derivative expansion at order partial**4*, *Phys. Rev. B* **68** (2003) 064421 [hep-th/0302227].

[157] F. Kos, D. Poland, D. Simmons-Duffin and A. Vichi, *Precision Islands in the Ising and $O(N)$ Models*, *JHEP* **08** (2016) 036 [1603.04436].

[158] Z. Komargodski and D. Simmons-Duffin, *The Random-Bond Ising Model in 2.01 and 3 Dimensions*, *J. Phys. A* **50** (2017) 154001 [1603.04444].

[159] M. Haensch, F. Rennecke and L. von Smekal, *Medium induced mixing, spatial modulations, and critical modes in QCD*, *Phys. Rev. D* **110** (2024) 036018 [2308.16244].

[160] S. Jeon and U. Heinz, *Introduction to Hydrodynamics*, *Int. J. Mod. Phys. E* **24** (2015) 1530010 [1503.03931].

[161] B.I. Halperin, P.C. Hohenberg and S.-k. Ma, *Renormalization-group methods for critical dynamics: 1. Recursion relations and effects of energy conservation*, *Phys. Rev. B* **10** (1974) 139.

[162] R. Guida and J. Zinn-Justin, *Critical exponents of the N vector model*, *J. Phys. A* **31** (1998) 8103 [cond-mat/9803240].

[163] E. Nakano, V. Skokov and B. Friman, *Transport coefficients of O(N) scalar field theories close to the critical point*, *Phys. Rev. D* **85** (2012) 096007 [1109.6822].

[164] M. Stephanov, *QCD Critical Point and Hydrodynamic Fluctuations in Relativistic Fluids*, *Acta Phys. Polon. B* **55** (2024) 5 [2403.03255].

[165] P. Kovtun, *Lectures on hydrodynamic fluctuations in relativistic theories*, *J. Phys. A* **45** (2012) 473001 [1205.5040].

[166] Y. Akamatsu, D. Teaney, F. Yan and Y. Yin, *Transits of the QCD critical point*, *Phys. Rev. C* **100** (2019) 044901 [1811.05081].

[167] E.M. Lifshitz and L.P. Pitaevskii, *Statistical Physics, Part 2*, vol. 9 of *Course of Theoretical Physics*, Butterworth-Heinemann, Oxford (1980).

[168] B.I. Halperin, P.C. Hohenberg and E.D. Siggia, *Renormalization-group treatment of the critical dynamics of superfluid helium, the isotropic antiferromagnet, and the easy-plane ferromagnet*, *Phys. Rev. B* **13** (1976) 1299.

[169] L.D. Landau and E.M. Lifshitz, *Fluid Mechanics*, vol. 6 of *Course of Theoretical Physics*, Pergamon Press, Oxford (1987).

[170] L. Sasvári, F. Schwabl and P. Szépfalusy, *Hydrodynamics of an n-component phonon system*, *Physica A: Statistical Mechanics and its Applications* **81** (1975) 108.

[171] H.-K. Janssen, *Renormalized field theory of the critical dynamics of O(n)-symmetric systems*, *Z. Phys. B* **26** (1977) 187.

[172] C. De Dominicis and L. Peliti, *Field-theory renormalization and critical dynamics above T_c: Helium, antiferromagnets, and liquid-gas systems*, *Phys. Rev. B* **18** (1978) 353.

[173] C. De Dominicis and L. Peliti, *Deviations from dynamic scaling in helium and antiferromagnets*, *Phys. Rev. Lett.* **38** (1977) 505.

[174] L.H. Yao and U.C. Täuber, *Critical dynamics of the antiferromagnetic O(3) nonlinear sigma model with conserved magnetization*, *Phys. Rev. E* **105** (2022) 064128 [2204.11145].

[175] F. Wilczek, *Application of the renormalization group to a second order QCD phase transition*, *Int. J. Mod. Phys. A* **7** (1992) 3911.

[176] A. Pelissetto and E. Vicari, *Relevance of the axial anomaly at the finite-temperature chiral transition in QCD*, *Phys. Rev. D* **88** (2013) 105018 [1309.5446].

[177] M. Grahl, *$U(2)_A \times U(2)_V$-symmetric fixed point from the functional renormalization group*, *Phys. Rev. D* **90** (2014) 117904 [1410.0985].

[178] D.T. Son and M.A. Stephanov, *Pion propagation near the QCD chiral phase transition*, *Phys. Rev. Lett.* **88** (2002) 202302 [hep-ph/0111100].

[179] J.M. Pawlowski, *Aspects of the functional renormalisation group*, *Annals Phys.* **322** (2007) 2831 [hep-th/0512261].

[180] H. Gies, *Introduction to the functional RG and applications to gauge theories*, *Lect. Notes Phys.* **852** (2012) 287 [hep-ph/0611146].

[181] G. Aarts and J. Smit, *Finiteness of hot classical scalar field theory and the plasmon damping rate*, *Phys. Lett. B* **393** (1997) 395 [hep-ph/9610415].

[182] S. Weinberg, *The quantum theory of fields. Vol. 2: Modern applications*, Cambridge University Press (8, 2013), 10.1017/CBO9781139644174.

[183] J.M. Pawlowski, N. Strodthoff and N. Wink, *Finite temperature spectral functions in the O(N)-model*, *Phys. Rev. D* **98** (2018) 074008 [1711.07444].

[184] J. Braun et al., *Renormalised spectral flows*, *SciPost Phys. Core* **6** (2023) 061 [2206.10232].

[185] S. Floerchinger, *Analytic Continuation of Functional Renormalization Group Equations*, *JHEP* **05** (2012) 021 [1112.4374].

[186] J. Bjorken and S. Drell, *Relativistic Quantum Fields*, McGraw-Hill (1965).

[187] A.K. Cyrol, J.M. Pawlowski, A. Rothkopf and N. Wink, *Reconstructing the gluon*, *SciPost Phys.* **5** (2018) 065 [1804.00945].

[188] J. Fehre, D.F. Litim, J.M. Pawlowski and M. Reichert, *Lorentzian Quantum Gravity and the Graviton Spectral Function*, *Phys. Rev. Lett.* **130** (2023) 081501 [2111.13232].

[189] J. Horak, F. Ihssen, J.M. Pawlowski, J. Wessely and N. Wink, *Scalar spectral functions from the spectral functional renormalization group*, *Phys. Rev. D* **110** (2024) 056009 [2303.16719].

[190] S. Töpfel, J.M. Pawlowski and J. Braun, *Phase structure of quark matter and in-medium properties of mesons from Callan-Symanzik flows*, 2412.16059.

[191] B. Marguet, E. Agoritsas, L. Canet and V. Lecomte, *Supersymmetries in nonequilibrium Langevin dynamics*, *Phys. Rev. E* **104** (2021) 044120 [2101.08766].

[192] M. Crossley, P. Glorioso and H. Liu, *Effective field theory of dissipative fluids*, *JHEP* **09** (2017) 095 [1511.03646].

[193] P. Glorioso, M. Crossley and H. Liu, *Effective field theory of dissipative fluids (II): classical limit, dynamical KMS symmetry and entropy current*, *JHEP* **09** (2017) 096 [1701.07817].

[194] P. Gao, P. Glorioso and H. Liu, *Ghostbusters: Unitarity and Causality of Non-equilibrium Effective Field Theories*, *JHEP* **03** (2020) 040 [1803.10778].

[195] O. Kaczmarek, F. Karsch, A. Lahiri, L. Mazur and C. Schmidt, *QCD phase transition in the chiral limit*, 3, 2020 [2003.07920].

[196] J. Braun, B. Klein and P. Piasecki, *On the scaling behavior of the chiral phase transition in QCD in finite and infinite volume*, *Eur. Phys. J. C* **71** (2011) 1576 [1008.2155].

[197] Y.-r. Chen, R. Wen and W.-j. Fu, *Critical behaviors of the O(4) and Z(2) symmetries in the QCD phase diagram*, *Phys. Rev. D* **104** (2021) 054009 [2101.08484].

[198] F. Gao and J.M. Pawlowski, *Phase structure of (2+1)-flavor QCD and the magnetic equation of state*, *Phys. Rev. D* **105** (2022) 094020 [2112.01395].

[199] Y.-y. Tan, Y.-r. Chen and W.-j. Fu, *Real-time dynamics of the $O(4)$ scalar theory within the fRG approach*, *SciPost Phys.* **12** (2022) 026 [2107.06482].

[200] M. Harder, P. Kovtun and A. Ritz, *On thermal fluctuations and the generating functional in relativistic hydrodynamics*, *JHEP* **07** (2015) 025 [1502.03076].

[201] H.-K. Janssen, *Field-theoretic method applied to critical dynamics*, in *Dynamical Critical Phenomena and Related Topics*, C.P. Enz, ed., vol. 104 of *Lecture Notes in Physics*, (Heidelberg), pp. 25–47, Springer Berlin (1979).

[202] N. Nakanishi and I. Ojima, *Covariant operator formalism of gauge theories and quantum gravity*, vol. 27, World Sci. Lect. Notes Phys. (1990).

[203] R. Alkofer and L. von Smekal, *The Infrared behavior of QCD Green's functions: Confinement dynamical symmetry breaking, and hadrons as relativistic bound states*, *Phys. Rept.* **353** (2001) 281 [hep-ph/0007355].

[204] F. Lenz, J.W. Negele, L. O'Raifeartaigh and M. Thies, *Phases and residual gauge symmetries of Higgs models*, *Annals Phys.* **285** (2000) 25 [hep-th/0004200].

[205] F. Lenz, H.W.L. Naus, K. Ohta and M. Thies, *Zero modes and displacement symmetry in electrodynamics*, *Annals Phys.* **233** (1994) 51.

[206] M. Tarpin, L. Canet and N. Wschebor, *Breaking of scale invariance in the time dependence of correlation functions in isotropic and homogeneous turbulence*, *Phys. Fluids* **30** (2018) 055102 [1707.06809].

[207] M. Tarpin, L. Canet, C. Pagani and N. Wschebor, *Stationary, isotropic and homogeneous two-dimensional turbulence: a first non-perturbative renormalization group approach*, *J. Phys. A* **52** (2019) 085501 [1809.00909].

[208] L.M. Sieberer, M. Buchhold and S. Diehl, *Keldysh field theory for driven open quantum systems*, *Reports on Progress in Physics* **79** (2016) 096001.

[209] D. Birmingham, M. Blau, M. Rakowski and G. Thompson, *Topological field theory*, *Phys. Rept.* **209** (1991) 129.

[210] E. Wang and U.W. Heinz, *A Generalized fluctuation dissipation theorem for nonlinear response functions*, *Phys. Rev. D* **66** (2002) 025008 [hep-th/9809016].

[211] D.F. Litim, *Derivative expansion and renormalization group flows*, *JHEP* **11** (2001) 059 [hep-th/0111159].

[212] A. Connelly, G. Johnson, F. Rennecke and V. Skokov, *Universal Location of the Yang-Lee Edge Singularity in $O(N)$ Theories*, *Phys. Rev. Lett.* **125** (2020) 191602 [2006.12541].

[213] F. Rennecke and V.V. Skokov, *Universal location of Yang–Lee edge singularity for a one-component field theory in 1≤d≤4*, *Annals Phys.* **444** (2022) 169010 [2203.16651].

[214] G. Johnson, F. Rennecke and V.V. Skokov, *Universal location of Yang-Lee edge singularity in classic O(N) universality classes*, *Phys. Rev. D* **107** (2023) 116013 [2211.00710].

[215] D. Binosi, J. Collins, C. Kaufhold and L. Theussl, *JaxoDraw: A Graphical user interface for drawing Feynman diagrams. Version 2.0 release notes*, *Comput. Phys. Commun.* **180** (2009) 1709 [0811.4113].

[216] M. Galassi, J. Davies, J. Theiler, B. Gough and G. Jungman, *GNU Scientific Library - Reference Manual, Third Edition, for GSL Version 1.12 (3. ed.)*. (01, 2009).

[217] T. Hahn, *Cuba—a library for multidimensional numerical integration*, *Computer Physics Communications* **168** (2005) 78–95.

[218] J. Engels and F. Karsch, *Finite size dependence of scaling functions of the three-dimensional O(4) model in an external field*, *Phys. Rev. D* **90** (2014) 014501 [1402.5302].

[219] M.A. Stephanov, K. Rajagopal and E.V. Shuryak, *Signatures of the tricritical point in QCD*, *Phys. Rev. Lett.* **81** (1998) 4816 [hep-ph/9806219].

[220] K. Kawasaki, *Kinetic equations and time correlation functions of critical fluctuations*, *Annals Phys.* **61** (1970) 1.

[221] Y. Akamatsu, M. Asakawa, M. Hongo, M. Stephanov and H.-U. Yee, *Enhancement of photon emission rate near QCD critical point*, 2505.07169.

[222] L. Canet, *Functional renormalisation group for turbulence*, *J. Fluid Mech.* **950** (2022) 1 [2205.01427].

[223] Y.-r. Chen, Y.-y. Tan and W.-j. Fu, *Critical dynamics of Model H within the real-time fRG approach*, 2406.00679.

[224] D.F. Litim, *Optimized renormalization group flows*, *Phys. Rev. D* **64** (2001) 105007 [hep-th/0103195].

[225] A. Wipf, *Statistical Approach to Quantum Field Theory*, vol. 864 (01, 2013), 10.1007/978-3-642-33105-3.

[226] M.Q. Huber, A.K. Cyrol and J.M. Pawlowski, *DoFun 3.0: Functional equations in Mathematica*, *Comput. Phys. Commun.* **248** (2020) 107058 [1908.02760].

[227] T. Ohta and K. Kawasaki, *Mode Coupling Theory of Dynamic Critical Phenomena for Classical Liquids. I: Dynamic Critical Exponents*, *Prog. Theor. Phys.* **55** (1976) 1384.

[228] C.S. Fischer, *QCD at finite temperature and chemical potential from Dyson–Schwinger equations*, *Prog. Part. Nucl. Phys.* **105** (2019) 1 [1810.12938].

[229] F. Gao and J.M. Pawlowski, *QCD phase structure from functional methods*, *Phys. Rev. D* **102** (2020) 034027 [2002.07500].

[230] J. Braun, A. Geißel and B. Schallmo, *Speed of sound in dense strong-interaction matter*, *SciPost Phys. Core* **7** (2024) 015 [2206.06328].

[231] R.-A. Tripolt, L. von Smekal and J. Wambach, *Flow equations for spectral functions at finite external momenta*, *Phys. Rev. D* **90** (2014) 074031 [1408.3512].

[232] C. Jung, F. Rennecke, R.-A. Tripolt, L. von Smekal and J. Wambach, *In-Medium Spectral Functions of Vector- and Axial-Vector Mesons from the Functional Renormalization Group*, *Phys. Rev. D* **95** (2017) 036020 [1610.08754].

[233] R.-A. Tripolt, J. Weyrich, L. von Smekal and J. Wambach, *Fermionic spectral functions with the Functional Renormalization Group*, *Phys. Rev. D* **98** (2018) 094002 [1807.11708].

[234] R.-A. Tripolt, D.H. Rischke, L. von Smekal and J. Wambach, *Fermionic excitations at finite temperature and density*, *Phys. Rev. D* **101** (2020) 094010 [2003.11871].

[235] J. Horak, J.M. Pawlowski and N. Wink, *Spectral functions in the ϕ^4-theory from the spectral DSE*, *Phys. Rev. D* **102** (2020) 125016 [2006.09778].

[236] J. Horak, J.M. Pawlowski and N. Wink, *On the quark spectral function in QCD*, 2210.07597.

[237] J. Horak, J.M. Pawlowski and N. Wink, *On the complex structure of Yang-Mills theory*, 2202.09333.

[238] J. Horak, J.M. Pawlowski, J. Turnwald, J.M. Urban, N. Wink and S. Zafeiropoulos, *Nonperturbative strong coupling at timelike momenta*, *Phys. Rev. D* **107** (2023) 076019 [2301.07785].

[239] G. Eichmann, A. Gómez, J. Horak, J.M. Pawlowski, J. Wessely and N. Wink, *Bound states from the spectral Bethe-Salpeter equation*, *Phys. Rev. D* **109** (2024) 096024 [2310.16353].

[240] L. Shen, J. Berges, J.M. Pawlowski and A. Rothkopf, *Thermalization and dynamical spectral properties in the quark-meson model*, *Phys. Rev. D* **102** (2020) 016012 [2003.03270].

[241] A. Meistrenko, H. van Hees and C. Greiner, *Kinetics of the chiral phase transition in a quark–meson σ-model*, *Annals Phys.* **431** (2021) 168555 [2007.09929].

[242] F. Schwabl, R. Hilton and A. Lahee, *Advanced Quantum Mechanics*, Springer Berlin Heidelberg (2008).

[243] J. Berges, D.U. Jungnickel and C. Wetterich, *Two flavor chiral phase transition from nonperturbative flow equations*, *Phys. Rev. D* **59** (1999) 034010 [hep-ph/9705474].

[244] N. Strodthoff, B.-J. Schaefer and L. von Smekal, *Quark-meson-diquark model for two-color QCD*, *Phys. Rev. D* **85** (2012) 074007 [1112.5401].

[245] R.-A. Tripolt, B.-J. Schaefer, L. von Smekal and J. Wambach, *Low-temperature behavior of the quark-meson model*, *Phys. Rev. D* **97** (2018) 034022 [1709.05991].

[246] S. Resch, F. Rennecke and B.-J. Schaefer, *Mass sensitivity of the three-flavor chiral phase transition*, *Phys. Rev. D* **99** (2019) 076005 [1712.07961].

[247] E. Grossi, F.J. Ihssen, J.M. Pawlowski and N. Wink, *Shocks and quark-meson scatterings at large density*, *Phys. Rev. D* **104** (2021) 016028 [2102.01602].

[248] K. Otto, C. Busch and B.-J. Schaefer, *Regulator scheme dependence of the chiral phase transition at high densities*, 2206.13067.

[249] F. Ihssen, J.M. Pawlowski, F.R. Sattler and N. Wink, *Towards quantitative precision for QCD at large densities*, 2309.07335.

[250] E. Grossi and N. Wink, *Resolving phase transitions with Discontinuous Galerkin methods*, 1903.09503.

[251] F. Ihssen, F.R. Sattler and N. Wink, *Numerical RG-time integration of the effective potential: Analysis and Benchmark*, 2302.04736.

[252] H. Leutwyler and A.V. Smilga, *Nucleons at finite temperature*, *Nucl. Phys. B* **342** (1990) 302.

[253] J. Braun, M. Leonhardt and J.M. Pawlowski, *Renormalization group consistency and low-energy effective theories*, *SciPost Phys.* **6** (2019) 056 [1806.04432].

[254] P. Kovtun, G.D. Moore and P. Romatschke, *The stickiness of sound: An absolute lower limit on viscosity and the breakdown of second order relativistic hydrodynamics*, *Phys. Rev. D* **84** (2011) 025006 [1104.1586].

[255] H. Fujii and M. Ohtani, *Soft modes at the critical end point in the chiral effective models*, *Prog. Theor. Phys. Suppl.* **153** (2004) 157 [hep-ph/0401028].

[256] C. Jung and L. von Smekal, *Fluctuating vector mesons in analytically continued functional RG flow equations*, *Phys. Rev. D* **100** (2019) 116009 [1909.13712].

[257] R. Bausch, H.K. Janssen and H. Wagner, *Renormalized field theory of critical dynamics*, *Zeitschrift fur Physik B Condensed Matter* **24** (1976) 113.

[258] C. De Dominicis and L. Peliti, *Field Theory Renormalization and Critical Dynamics Above t(c): Helium, Antiferromagnets and Liquid Gas Systems*, *Phys. Rev. B* **18** (1978) 353.

Selbstständigkeitserklärung

Ich erkläre: Ich habe die vorgelegte Dissertation selbstständig und ohne unerlaubte fremde Hilfe und nur mit den Hilfen angefertigt, die ich in der Dissertation angegeben habe. Alle Textstellen, die wörtlich oder sinngemäß aus veröffentlichten Schriften entnommen sind, und alle Angaben, die auf mündlichen Auskünften beruhen, sind als solche kenntlich gemacht. Ich stimme einer evtl. Überprüfung meiner Dissertation durch eine Antiplagiat-Software zu. Bei den von mir durchgeführten und in der Dissertation erwähnten Untersuchungen habe ich die Grundsätze guter wissenschaftlicher Praxis, wie sie in der „Satzung der Justus-Liebig-Universität Gießen zur Sicherung guter wissenschaftlicher Praxis" niedergelegt sind, eingehalten.

Gießen, den 08.07.2025

.....

(Johannes Vincent Manfred Roth)